QATAR UNIVERSITY

COLLEGE OF ENGINEERING

INVESTIGATION OF HYBRID EFFECTS OF CNT AND NANOCLAY IN TAILROING MECHANICAL AND ELECTRICAL PROPERTIES OF EPOXY

BY

ALI ESMAEILI

A Dissertation Submitted to

the College of Engineering

in Partial Fulfillment of the Requirements for the Degree of

Doctorate of Philosophy in Materials Science and Engineering

June 2020

COMMITTEE PAGE

The members of the Committee approve the Dissertation of
Ali Esmaeili defended on 07/05/2020.

Prof. Abdel Magid Hamouda
Thesis/Dissertation Supervisor

Prof. Ramesh Singh
Committee Member

Prof. Faris Tarlochan
Committee Member

Prof. Asan Gani Bin Abdul Muthalif
Committee Member

Approved:

Khalid Kamal Naji, Dean, College of Engineering

ABSTRACT

ESMAEILI, ALI, Doctorate: June: 2020,

Doctorate of Philosophy in Materials Science and E

Title: Investigation of Hybrid Effects of CNT and Nanoclay in Tailoring Mechanical and Electrical Properties of Epoxy

Supervisor of Dissertation: Prof. Abdel, Magid, Hamouda.

Many studies performed on multifunctional properties of epoxy-based nanocomposites reinforced with CNTs and nanoclay whereas synergetic effects of CNTs and nanoclay on mechanical and piezoresistive behavior of ternary state nanocomposites still remains unaddressed. Therefore, the hybrid effects of CNTs and Montmorillonite platelets on the mechanical, electrical and piezoresistive performances of the epoxy are addressed in this study. The project was divided into two main phases. In the first phase, different CNTs morphologies (SWCNTs and DWCNTs) and weight concentrations were used. For the second phase, CNT content was kept constant while two different nanoclay loadings were used for the ternary states. In fact, the nanocomposites were prepared in two different states, i.e. the binary state, including 0.1wt.% CNTs, and the ternary states, including 0.1wt.% CNT and two levels of NC (0.5wt.% and 1wt.%). SEM, FESEM, and XRD were used for the microstructural analysis of the materials while tensile and mode I fracture tests were performed for mechanical and piezoresistive characterizations. In overall, by taking into consideration of multifunctional properties including tensile strength, fracture toughness, electrical conductivity and sensitivity, it was stated out that the ternary nanocomposites

developed in phase 2 demonstrated better performance compared to the ones produced in phase 1. In fact, low tensile strength along with high variations observed in phase1, raised questions for the effective exploitation of CNTs in multifunctional properties enhancement. On the other hand, highly monotonous outcomes especially for tensile strength without sacrificing other properties indicated the effective exploitation of nanofillers in tailoring material performances in phase 2. The addition of nanoclay to CNTs doped epoxy resulted in better CNTs dispersion, hindering CNTs re-agglomeration. Significant increase in critical stress intensity factor and critical strain energy release rate compared to the neat epoxy was obtained for the hybrid nanocomposites developed in phase 2 due to crack bridging and crack deflection mechanisms. The electrical conductivity of the ternary state materials increased substantially with respect to the binary nanocomposite. The hybrid nanocomposites also manifested higher piezoresistive sensitivity and a more robust signal in tensile and fracture tests, respectively.

DEDICATION

To my family.

ACKNOWLEDGMENTS

First, I would like to express my sincere appreciation to my PhD supervisor Prof. Abdel Magid Hamouda, for his permanent support and contribution toward completion of my thesis. I am also so grateful to Prof. Claudio Sbarufatti in Polytechnic University of Milan for his amazing excellent guidance and contribution in completion of my PhD thesis. I would like to also thank "Prof. Alberto Jiménez-Suárez" from Rey Juan Carlos University for his extreme help in providing facilitates during the experimental aspect of this thesis.

In addition, I am very grateful for all Polimi staffs especially for Ludovica Rovatti for her enormous help during SEM analysis and materials characterization.

Many thanks to my colleges Thomas Oggioni and Dayou Ma who assisted me in performing the laboratory tests.

Finally, I would like to thank my parent for their loves and permanent supports in the past year.

TABLE OF CONTENTS

LIST OF TABLES

LIST OF FIGURES

CHAPTER 1: INTRODUCTION

1.1. Advanced composite materials

The persistent interests of the aerospace industry to increase the efficiency of the military and commercial airplanes have been continuously stimulated the researchers and engineers across the world to create high performance structural materials. In this context, composite materials were taken into account as one of the most significant materials used in aircraft industries due to their excellent mechanical properties including high strength, high stiffness to density ratio and premiere physical characteristics [1].

Advanced Composite materials also referred as advanced polymer matrix composites were typically produced by incorporation of two or more constituent materials with various properties, one as matrix and the others as the filler, when incorporated, develop a novel material manifesting new characteristics with improved strength, toughness, stiffness and low density that cannot be achieved individually.
In this context, of particular interests, has been made on carbon fiber reinforced polymers (CFRPs) due to their numerous applications in many industries including aerospace and automobile industries [2].

In general, CFRPs are composed of two distinguished parts including the reinforcements (very stiff and strong) that can be found in various shapes such as long or short fibers, and the matrix itself (tough but brittle), typically epoxy. The former was led to enhancing mechanical properties of the materials such as tensile strength, Young's modulus, low weight, appropriate fatigue strength and fracture toughness resulting from outstanding mechanical properties of the fibers, whereas the latter acted

as a medium for load transfer between fibers and matrix [3].

In the last decades, the CFRPs have been extensively used in aerospace industries i.e. for military and commercial aircrafts as shown in Figure 1. 1a and b respectively. In fact, replacing conventional metallic materials such as aluminum and steel with modern CRFRPs resulted in significant reduction of aircraft weight, thus, reducing the fuel consumption and fuel costs. In other words, CFRPs were taken into account as an alternative to conventional alloys for structural purposes.

It was pointed out that almost 50% of the constituent materials in an aircraft were made of CRFPs and this trend has being rapidly growing for further usage of CFRPs in high performance structural composites to meet the new engineering demands in terms of appropriate mechanical properties, good fatigue life, high corrosion resistance, and low weight. This was attributed to low density of the CFRPs in the range of 1.5 g/cm3, which is dramatically lower than 2.7 g/cm3 for aluminum, and high modulus of CFRPs over twice conventional aluminum alloys [3].

Apart from numerous benefits of CFRPs compared with classic martials, fibers delamination resulting from poor bonding between fiber and epoxy was the most important challenge in manufacturing CFRP industry [4]. In addition, the growing demand in industry in terms of creating novel-engineered composite materials such as conductive polymer composites has led to numerous research in effective exploitation of nanoreinforcements in tailoring multifunctional properties of epoxy, thus, epoxy based nanocomposites was introduced which is the main scope of this study [5,6].

It is worth noting that the main scope of this study is investigation of multifunctional properties of epoxy reinforced by CNTs and Nanoclay NC at bulk materials i.e. at macroscopic scale. However, the developed bulk nanocomposites could be thoroughly used as the enhanced matrix for further modification of CRPPs

performance. Taking into account the previous explanation in situ numerous applications of CFRPs in aerospace and automobile industries, tailoring multifunctional properties of the epoxy, which is typical matrix for CFRPs industry, is crucial for future aspects in CFRPs industry. As a result, this necessitates further investigations on the extending performance of the epoxy by using nanomaterials, which are discussed in the next sections.

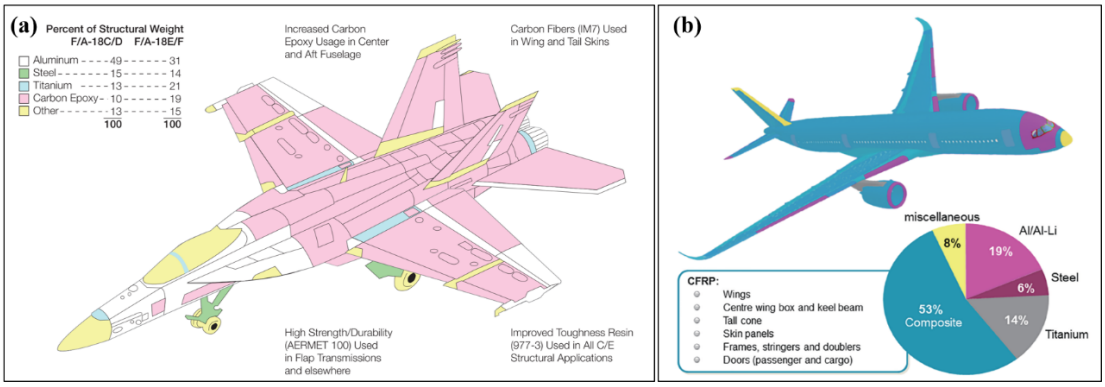

Figure 1. 1. CFRPs usage in aircraft: (a) Military aircraft [1], (b) commercial aircraft-Airbus A350 [7,8].

1.2. Epoxy based nanocomposites

The advent of nanomaterials along with their superior characteristics has made significant improvements in tailoring multifunctional properties of epoxy based nanocomposites including mechanical, electrical, and electromechanical properties of polymer [9,10]. Since the main objective of this study is to improve multifunctional properties of epoxy by means of CNTs and nannoclay, thus, a detailed discussion are made for each of the constituent materials including epoxy, CNTs and nanoclay in the following sections.

1.2.1. Epoxy

Epoxy is one of the most commonly thermosetting polymers used in different industrial sectors because of its outstanding characteristics including low shrinkage, low density, high tensile strength, and high thermal stability and chemical resistance [9,11]. Owing to these remarkable properties, epoxy has been widely employed as the main matrix in advanced structural composites for aerospace applications [12] such as CFRPs as well as being extensively used as preliminary resin in electronic industries for printed circuit boards and transistors [13], adhesive bonding [14], renewable energy [15], and civil infrastructures [16].

Epoxy is generally two parts i.e. part A the epoxy monomer and part B the hardener. Epoxy monomer is typically composed of an oxirane or a glycidyl group as shown in Figure 1. 2a. Various curing agents (also known as hardener) including aromatic amines, amidoamines, and polyamides were treated with the oxirane group resulting in formation of solid thermosetting products [17]. Amongst different epoxy resins existed in the market, the diglycidyl ether of bisphenol A (DGEBA), the one used in this study, introduced in 1960, is the most typical epoxy used for different purposes including high performance materials as well as adhesive joints [6,17]. DGEBA was synthetized via condensation reaction of bisphenol A and epichlorohydrin in the presence of sodium hydroxide catalyst [18] as shown in Figure 1. 2b.

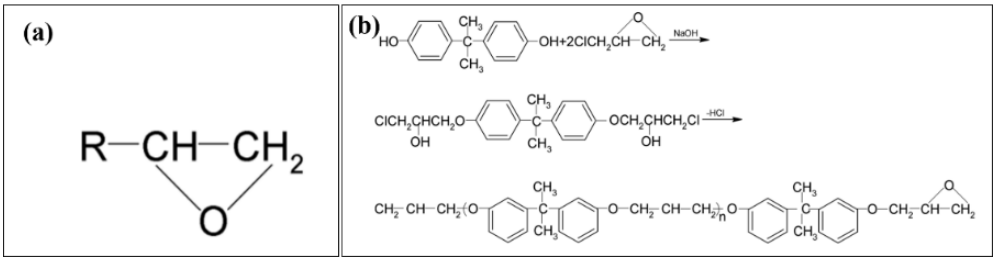

Figure 1. 2. (a) Epoxide ring, (b) condensation reaction of bisphenol A and epichlorohydrin [18].

Apart from many benefits of pure epoxy i.e. superior thermal and mechanical characteristics [19], high crosslink density of the epoxy during curing made it very susceptible to crack initiation as well as shock and impact loadings, which are typical loading conditions in aerospace industries. Therefore, pristine epoxy generally manifested relatively low fracture toughness which was the main drawback of epoxy against its many advantageous [11]. Its high crosslink density resulted in formation of internal residual stresses caused by curing which accounted for lowering its fracture toughness [20]. This limited its application in many industrial fields; thus, further efforts are required to improve its toughness. In this context, many efforts have been conducted on improving mechanical properties of the epoxy using nanomaterials resulting from activation of various toughening mechanisms, depending on the nanofiller used, which will are discussed later in details.

There are many nanomaterials currently being used by researchers for polymer based nanocomposites including CNTs, graphene nanoplatelets (GNPs), nanoclay, nesosilicate, nanofibers, and so on. Since the scope of this study is about CNTs and nanoclay, hereinafter, the discussion are made on CNTs and nanoclay. It should be noted that any materials that has at least one dimension in the range of 1-100 nm is considered as nanomaterials. Apart from that, nanomaterial can be distinguished in

three different categories based on their dimensional conditions as follow:

- 0D nanomaterial: all three dimensions are in the range of 1-100 nm i.e. nanoparticles such as fullerene as shown in Figure 1. 3e-f.
- 1D nanomaterials: one dimension in the scale of micron and two dimensions in scale of nanometer such as CNTs as shown in Figure 1. 3h.
- 2D nanomaterials: two dimensions in the scale of micron and one dimension in the nanometer scale such as GNPs and nanoclay as shown in Figure 1. 3b.

1.2.2. CNTs

CNTs, as one of the most promising reinforcements in nanotechnology, has engrossed wide attentions of scientists and industries due to their superior properties [21,22].

In the last decade, of particular interest has been made on fabrication of multifunctional nanocomposites using CNTs, owing to their outstanding mechanical and electrical properties including tensile strength up to 100 GPa, Young's modulus up to 1 TPa and electrical conductivity up to 106 S/m [23]. In fact, high electrical conductivity of CNTs along with their low electrically percolated thresholds, the region where a significant increase in electrical conductivity can be obtained, by addition of CNTs resulting in transformation of an electrically insulating material to electrically conductive one.

In addition, introduction of CNTs induced strain sensitivity capability to the epoxy, hereinafter called piezoresistive material, which can be used for structural health monitoring (SHM) [24–26]. In this context, incorporation of only small amount of CNTs to the epoxy manifested excellent performance in tailoring electromechanical properties of the epoxy i.e. inducing strain sensing capability to the matrix [23,27–31].

This was mainly attributed to the breakage of electrical pathway formed in the matrix due to strain increase, resulting mainly from a combination of tunneling effect and loss of electrical contacts amongst neighboring CNTs which was severely related to the state of CNT dispersion [32–37].

1.2.2.1.History

Carbon with the symbol “C” has been considered as the most versatile element which was appeared in different forms based on the arrangement of carbon atoms (Figure 1. 3) including graphite, diamonds, fullerenes, and CNTs [38]. The first two types of carbon i.e. graphite and diamond were discovered in 1779 and 1789 respectively. Kroto et al. [39] have discovered fullerenes in 1985, and finally Iijima et al. [40] made one of the most important discoveries on carbon based nanomaterials in the form of tubes called CNTs in 1991.

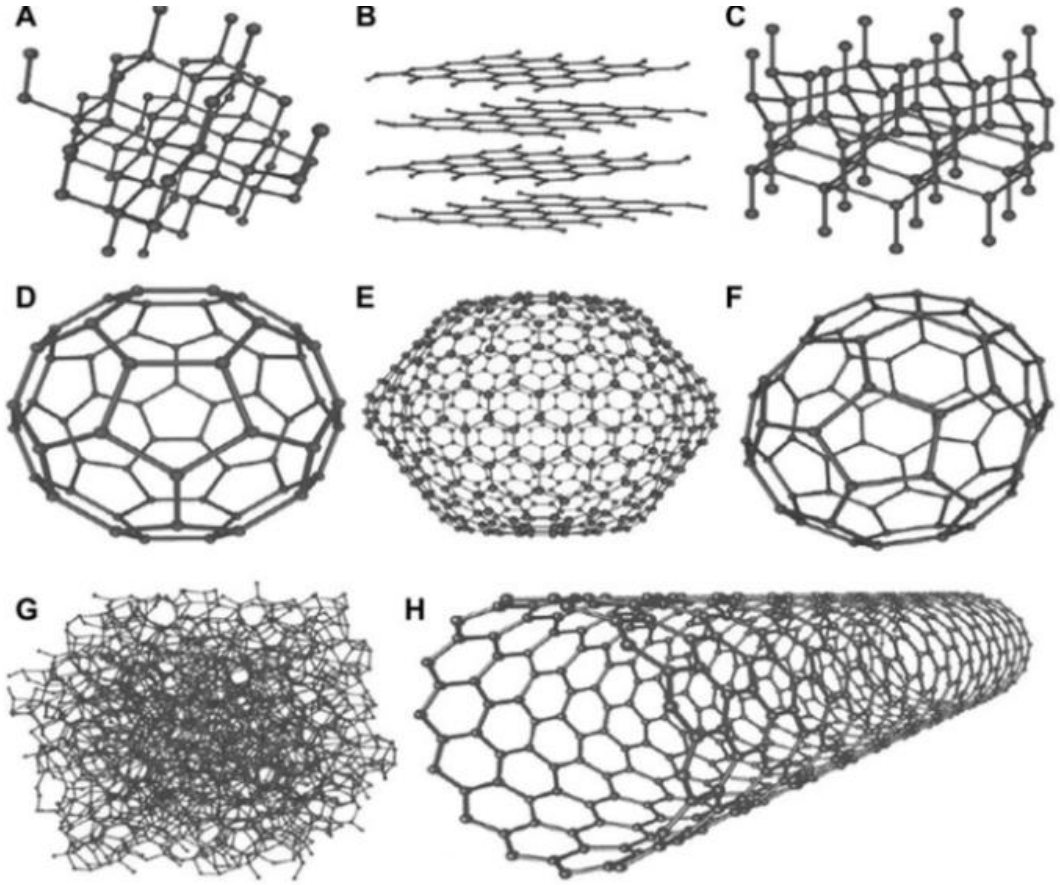

Figure 1. 3. Carbon allotropes: (a) Diamond, (b) Graphite (graphene is a single of graphite), (c) Lonsdaleite, (d) C60- Buckminsterfullerene or bukyball, (E) C540 Fullerene, (F) C70 Fullerene, (G) Amorphous carbon, (H) Single-walled carbon nanotube [38].

1.2.2.2.CNTs types

Based on the numbers of concentric cylinders or tubes involved, three main types of CNTs were found including SWCNTs, DWCNTs, and MWCNTs. The SWCNTs was taken into account by rolling up a single layer of graphene into a seamless cylinder, whilst MWCNTs contained multi-layer of graphene sheet, with inter-layer distance in the range of 0.34nm [41], manifesting internal diameter in the range of SWCNTs and external diameter relatively larger than SWCNTs as shown in

Figure 1. 4 DWCNTs are considered as distinctive case of MWCNTs where only two concentric layers of graphene rolled into seamless hollow core. In fact, these variations observed for different types of CNTs in terms of the arrangement of layer and aspect ratio, the ratio of length over diameter, resulted in different physical and mechanical properties for different types of CNTs. Regardless of CNTs morphology, they are taken into consideration as 1D nanomaterials due to their large aspect ratio [38].

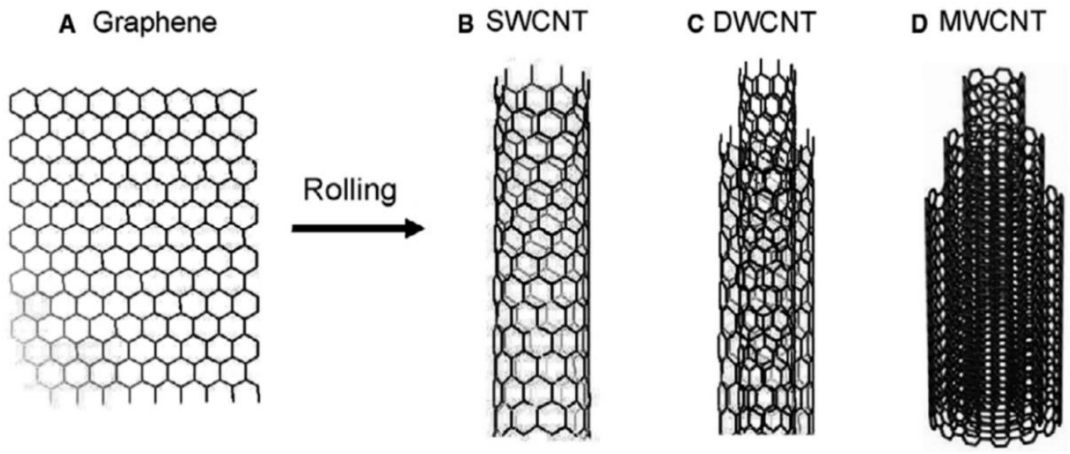

Figure 1. 4. Schematic illustration of rolling single graphene layer into seamless CNTs: (a) graphene, (b) SWCNTs, (c) DWCNTs (d) MWCNTs [42].

1.2.2.3.CNTs mechanical and physical properties

Table 1. 1 summarizes some physical and mechanical properties of intrinsic CNTs. As shown in Table 1. 1, CNTs manifested extraordinary mechanical properties resulting from strong sp2 bond between carbon atoms i.e. a Young's modulus of 1TPa which is five time bigger than steel, and electrical conductivity in the range of 106 (S/M) which is comparable with copper could be obtained for CNTs. It is worth noting that due to larger specific surface srea (SSA) and aspect ratio of SWCNTs, they were

most likely tend to form aggregates with respect to DWCNTs and MWCNTs. In fact, an SSA of 1300 m2/g was reported for SWCNTs whereas SSA in the range of 600-800 m2/g and 200 m2/g were obtained for DWCNTs and MWCNTs respectively [43]. For thermal conductivity, CNTs also possessed excellent conductivity arisen from strong sp2 C-C bond that made them even better than diamond along their axis, though no conductivity could be reached in diagonal axis.

Table 1. 1. Physical and Mechanical Properties of CNTs. The Data are Extracted from [22,43].

Properties	SWCNTs	DWCNTS	MWCNTs
Tensile Strength (GPa)	50-100	23-63	10-60
Elastic Modulus (TPa)	1	--	0.3-1
Elongation (%)	5.8	28	--
Density (g/cm^3)	1.3.-1.5	1.5	1.8-2
Total ETDs	211	100	
Electrical conductivity (S/m)	106	106	106
Thermal conductivity (W/m-k)	6000	3000	2000
Thermal stability	>700	>700	>700
Thermal diameter (nm)	1	5	20
Specific surface area (m^2/g)	1200	600-800	200

It is worth noting that two types of CNTs i.e. SWCNTs and DWCNTs, with varied aspect ratios were used in this study in order to truthfully compare their effects on final microstructure, mechanical and electromechanical characteristics of the epoxy

that are discussed later in details.

1.2.2.4.Quantum mechanical tunneling theory

Due to high electrical conductivity of CNTs, they have been widely used in conductive polymer composites. In this section, theory of converting an insulating material to electrically conductive material using CNTs is explained. The concept behind converting an electrically insulating polymer to electrically conductive material is arisen from mechanical quantum tunneling [44] as shown in Figure 1. 5 where E, U, and L represent the particle energy i.e. electron energy, potential energy of the barrier and distance between two adjacent conductive particles called tunneling distance respectively. According to the classic physic, particle (electron) with energy E cannot pass through the barrier with energy U if E<U (Figure 1. 5a) and it is transmitted back by the barrier. On the other hand, based on quantum mechanical tunneling theory, electron can tunnel through insulting material (epoxy) under certain conditions resulting in transmitting the electron (particle from the barrier (Figure 1. 5b). The probability of tunneling can be explained by equation 1.1:

$$T = Ge^{-2kL} \quad , \quad G = 16\frac{E}{U}\left(1-\frac{E}{U}\right) \; and \; k = \sqrt{\frac{2m(U-E)}{h^2}} \qquad (1.1)$$

Where E is electron energy (eV), U potential barrier energy (eV), m electron mass, h plank's constant, and L tunneling distance.

From equation 1.1, it can be seen that the tunneling probability of electron exponentially inversely correlated to the tunneling distance. Thus, the insulating matrix (epoxy) between two neighboring CNTs plays the role of barrier (U). Increasing L (tunneling distance), i.e. CNTs become far away from each other accounts for

decreasing the conductivity because electron has less probability to tunnel through the epoxy. As a result, it is important to avoid of agglomeration of CNTs since it leads to increasing the distance between adjacent CNTs resulting in less probability for the electron to tunnel from the barrier.

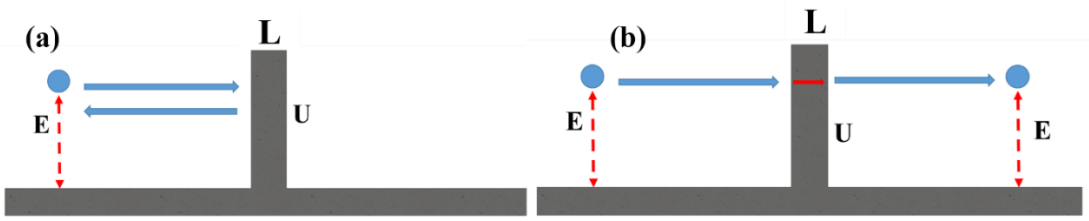

Figure 1. 5. Quantum mechanical tunneling theory: (a) classis physic (b) quantum physic.

Electrical conductivities of the composites at different CNTs contents can be explained by the different mechanisms contributing in formation of electrically conductive paths throughout the matrix including electrical contact amongst CNTs and tunneling effect as shown in Figure 1. 6 [45]. When CNTs content is low, the main mechanism is tunneling effect as shown by red circle in Figure 1. 6a. The effect of electrical contact, shown by blue circle in Figure 1. 6a, in gaining conductivity is less evident since it is difficult to obtain a homogenous distribution of CNTs with no aggregates i.e. it is possible to find some area in the matrix that CNTs have no contact known as CNTs-poor regions. In fact, agglomerations is inevitable phenomenon even at low CNT concentration due to their inherent tendency to aggregate [46].

As a result, tunneling effect plays the dominant role in enhancement of electrical conductivity on insulating polymer matrix at low weight concentration near percolation threshold [37]. In contrast, at high CNT contents (Figure 1. 6b), both mechanisms

contribute in formation of electrical networks, though the effect of tunneling is less evidence due to huge amount of electrical pathway arisen from mechanical contact.

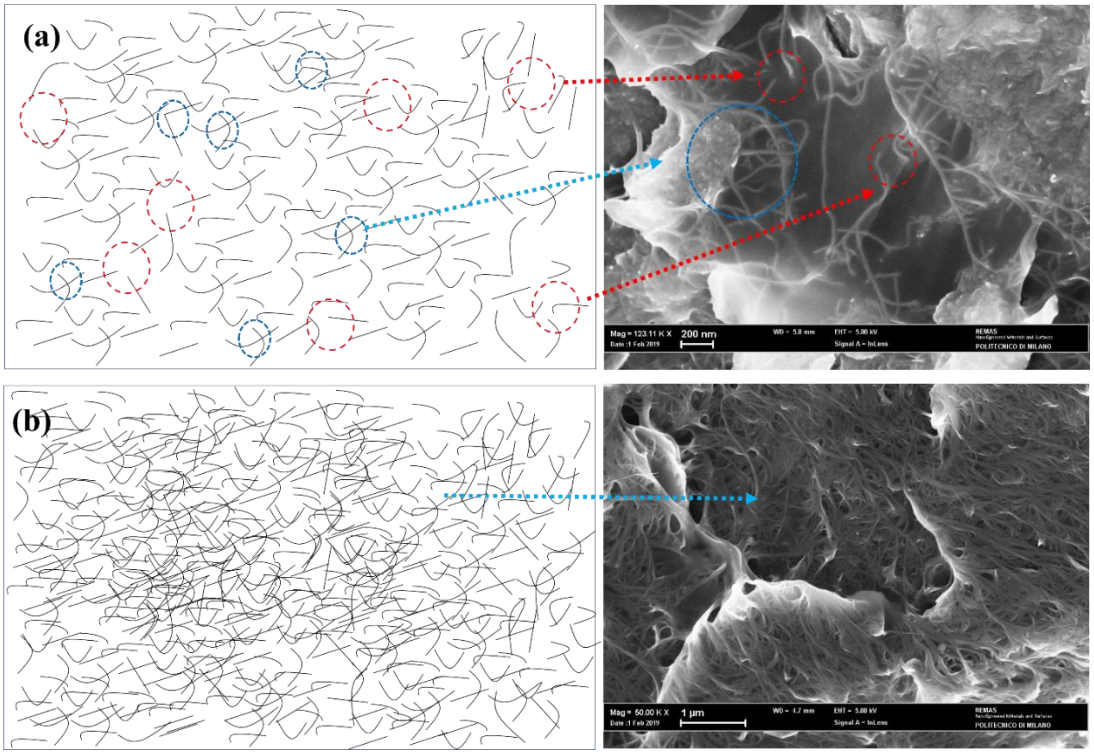

Figure 1. 6. Formation of electrically conductive pathway throughout the epoxy: (a) low CNTs loading, (b) High CNTs loading

1.2.3. Nanoclay

Layered silicate nanoclay has been another widely used nanofillers to create high performance composite materials due to its low cost, easy access and its excellence performance in improvement of fracture toughness, flame retardancy and thermal stability of the epoxy based nanocomposites [47–52]. Recently, Zabihi et al [53] conducted a comprehsive review on clay doped epoxy materials indicating that nanoclay manifested many advantages including mechanical properties improvement, appropriate transparency, high recyclability, high thermal resistance, thus, flame

retardancy and good transport properties. This excellent performance in advanced composite materials was mainly attributed to its 2D morphology i.e. large surface area and high absorption capacity resulted in extensive usage of nanoclay in many commercial applications such as automobile industry[54].

1.2.3.1.History

Nanoclay as an additive in polymer nanocomposites was primarily used by researchers in fabrication of nylon-6 reinforced by montmorillonite (MMT) in 1987 where low weight concentration of intercalated nanoclay resulted in remarkable enhancement in mechanical characteristics [55]. One can say that the great attention in using nanoclay for polymer based nanocomposites was started in 1993 when a well-known Japanese automobile manufacturer, Toyota company, has used, for the first time, an exfoliated nanoclay in tailoring thermal and mechanical characteristics of nylon6 [56]. Upon this great discovery, many studies were conducted on tailoring thermal and mechanical properties of polymer-based nanocomposites [49,52]. According to a literary review, the effect of nanoclay in enhancing facture toughness properties were much more noticeable rather than tensile strength [6].

1.2.3.2.Nanoclay types

Clay is considered in the category of aluminosilicates or silicates that are comprised of aluminum, silicon, oxygen, magnesium along with hydroxyl group containing different cations [52]. They have also known as layered-silicates resulting from their 1nm thick aluminosilicates layered structures. Generally, they can be divided

into three groups according to ratio of aluminum and silica sheets in clay galleries [57]. The first type comprises of a total two numbers of mineral sheets, one for aluminum and one for silica i.e. 1:1 ratio. This type of clay is also known as two-sheet mineral or dimorphic where hydrogen bonds amongst –OH groups are responsible for holding the layered-clay. The second type of clay consists of two silica sheets and one alumina sheet placed between silica sheets i.e. 2:1 ratio, thus, based on this structure it named three-sheet minerals or trimorphic. The last type comprises of two sheets for both silica and alumina i.e. 2:2 ratio, call four-sheet minerals or metamorphic.

Montmorillonite, a type 2 clay, is the most typical nanoclay used in polymer nanocomposites. This was attributed to its excellent capability in expansion of clay interlayer resulting from its complicated structures as depicted in Figure 1. 7. As already discussed for the clay type 2, it consists of an alumina layers sandwiched between two silica layers. These layers , each layer thickness of 1nm (Figure 1. 7), are accumulated on top of each other through their thickness directions, forming an intercalated clay structures which is typical clay structure for as –received clays. Arrangement of these silicate layers on top of each other in order to form aggregates along with a van der Waals gap amongst them referred as clay galleries or interlayer. It is worth noting that the total of an individual layer in addition to interlayer distance is known as basal distance or d-spacing a shown in Figure 1. 7. The d- spacing is an important clay-structure related properties which defines the final structure of clay doped polymer i.e. intercalated and exfoliated structures. The basal distance can be identified using x ray diffraction (XRD).

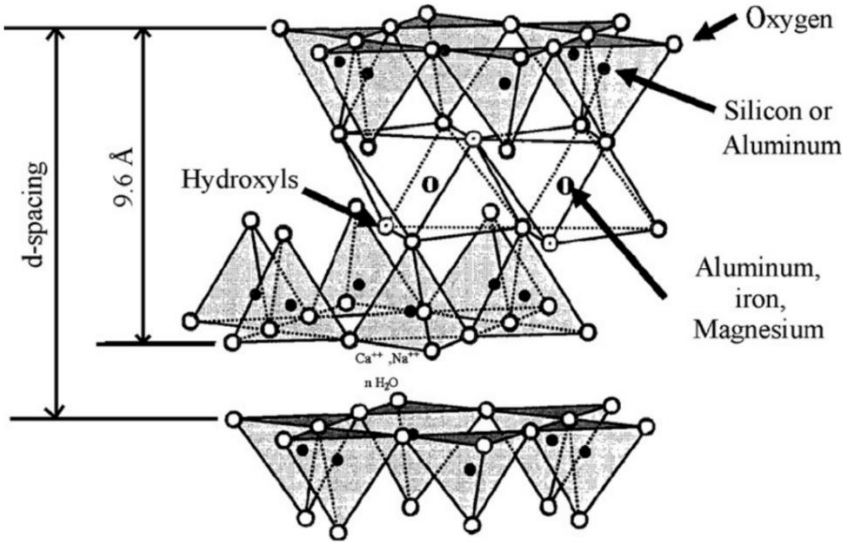

Figure 1. 7. Montmorillonite structures [52]

1.2.3.3.Clay composite structures

Polymers reinforced by nanoclay divide into three groups depending on the nanoclay gallery configuration including phase separated, intercalated and exfoliated as shown in Figure 1. 8a-c respectively [49]. The first structure (Figure 1. 8a) is a typical pattern for the conventional composites in which the nanoclay sheets are appeared in their primary states (as-received) i.e. without any resin penetration between the layers as shown in Figure 1. 8a. Thus, they show the same d-spacing or basal spacing like as-received clay, the distance between clay galleries, which can be detected by XRD.

The intercalated structure (Figure 1. 8b) is also quite similar to the first one, but the distance between clay galleries expands due to small resin penetration. This expansion can be also proven by XRD, showing smaller 2θ angle compared to as-received clay. Finally, in exfoliated clay, the individual nanoclay interlayer completely separate from each other, manifesting no 2θ angle by XRD (Figure 1. 8c).

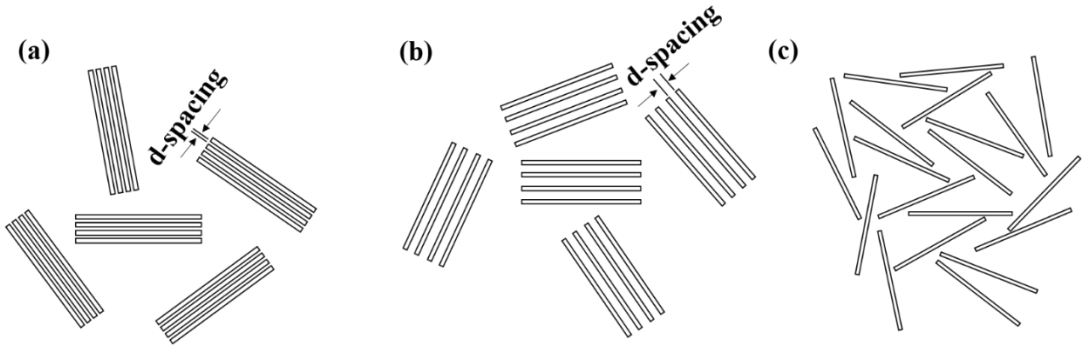

Figure 1. 8. Different nanoclay structures: (a) Conventional composite, (b) intercalated structure, (c) exfoliated structure

1.2.3.4.Clay composite flame retardancy

One of the main applications of clay as an additive was its high potential as flame retardancy. This was well described in the literature indicating that nanoclay could successfully improve thermal stability and heat resistance temperature of the polymer composites [47,51,58,59]. As mentioned before, one of the main applications of epoxy was its usage in electronic industry for printed board circuit. This along with weak performance of the pristine epoxy when exposed to fire has led to numerous research on flame retardancy of nanoclay-doped epoxy. This was related to presence of thick char yield on the surface exposed to the fire [60]. This char yield acted as a thermal barrier, thus, isolating the materials from further diffusion of oxygen into burning materials as shown in Figure 1. 9a.

This was also proven by formation of char yield acting as insulating thermal barrier on the surface of the epoxy reinforced with nanoclay (Figure 1. 9c-d) compared to the neat epoxy (Figure 1. 9b) . Formation of many cracks on the surface of the pristine epoxy (Figure 1. 9b) was quite noticeable whereas nanocomposites (Figure 1. 9c-d) manifested a relatively finer surface with small crack. It was concluded that nanoclay

introduction to epoxy could successfully improve it flame retardancy.

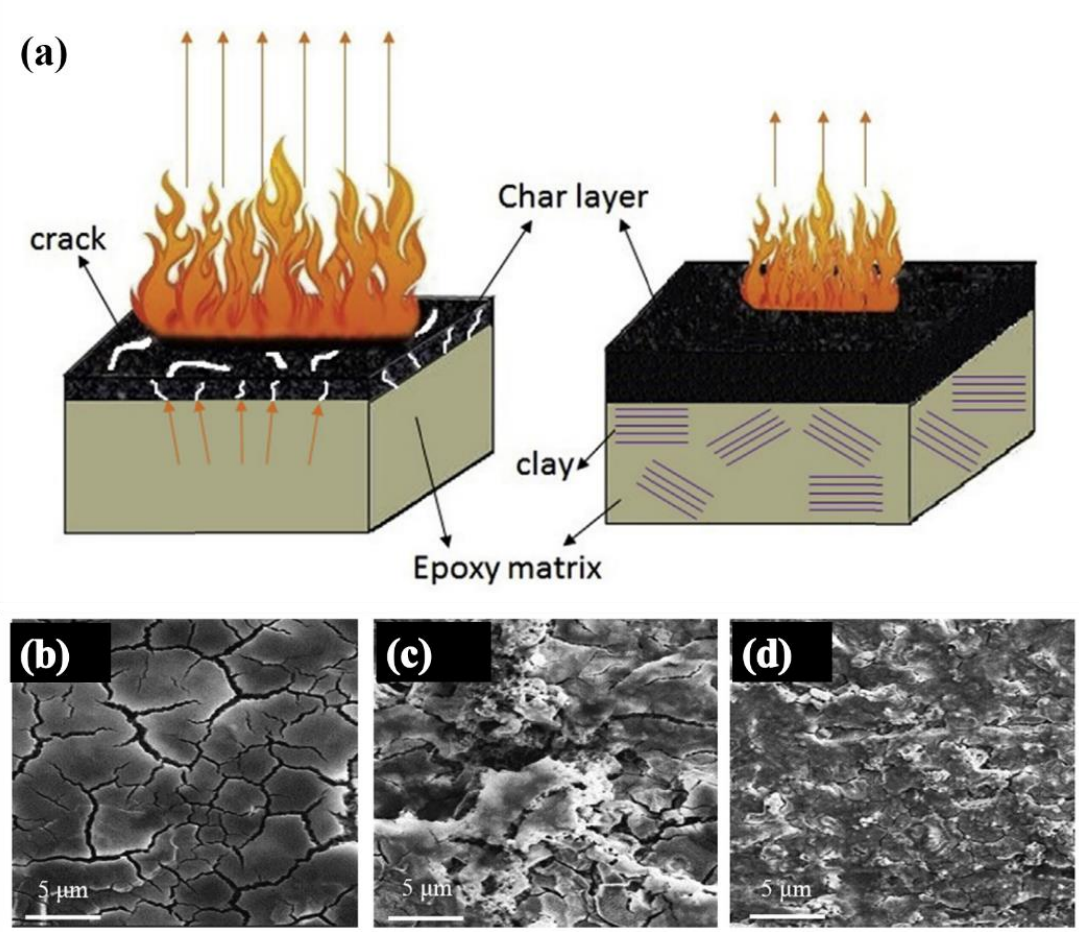

Figure 1. 9. (a) Flame retardancy mechanism [49], (b-c) char residues after cone calorimetry test for pure epoxy, epoxy/2.5 wt.% Nanomer I.28E, and epoxy/2.5 wt.% deoxyribonucleic acid (DNA) modified clay respectively [61].

1.3. Literature review

In the previous sections, some basic information about advanced composite, epoxy, CNTs, and nanoclay were provided. In this section, more focuses are made on the previous attempts that have been performed on epoxy based nanocomposite reinforced with CNTs and nanoclay. In this context, mechanical and electromechanical

properties in terms of tensile strength, fracture toughness, impact strength, electrical conductivity and piezoresistive sensitivity performance of the epoxy composite are reviewed. Due to importance of electrical conductivity and piezoresistivity, that are one of the main focuses of this study, they are reviewed independently from mechanical point of view. Thus, this section is divided into two subsections including multifunctional properties in terms of mechanical and thermal properties, and piezoresistive sensitivity performance.

1.3.1. Multifunctional properties

This section is divided into three subsections including CNTs/epoxy, nanoclay/epoxy and hybrid CNTs-nanoclay/epoxy in which a literary review on mechanical characteristics of the aforementioned nanocomposites in both binary and ternary states are made. This is quite important in order to find out the performance of the individual CNTs and nanoclay in their binary states, followed by their performance in the hybrid states. This will provide a better guideline for the current study in terms of what have been done in the past and what challenges still exist and need to be addressed.

1.3.1.1.CNTs/epoxy

Carbon Nanotubes (CNTs) have been taken into account as one of the most promising nanofillers in tailoring mechanical properties of nanocomposites owing to their outstanding mechanical properties, high surface area, high aspect ratio and low density [62]. Low weight, cost-effectiveness, high fatigue strength, good stiffness,

excellent performance in highly harsh environment, i.e. appropriate chemical resistance and high thermal and dimensional stability, are some advantages of the CNTs in modification of the mechanical properties of the polymer based nanocomposites [16]. In the past decade, numerous attempts have been carried out on improving mechanical properties of epoxy based nanocomposites embedded with CNTs including enhancement of tensile strength and Young's modulus [63–67], fracture toughness [43,68–76] as well as impact strength using CNTs [77–79]. In a study made by Wernik et al. [67], mechanical properties of a DGEBA epoxy reinforced with different MWCNT contents from 0.5wt.% to 3 wt.% in increments of 0.5 wt.% were investigated. Based on their results, tensile strength and stiffness increased by 25 % at CNT loading of 1.5 wt.% and 2 wt.% respectively (Figure 1. 10). In addition, they pointed out that high CNT contents resulted in degradation of mechanical properties due to presence of aggregates.

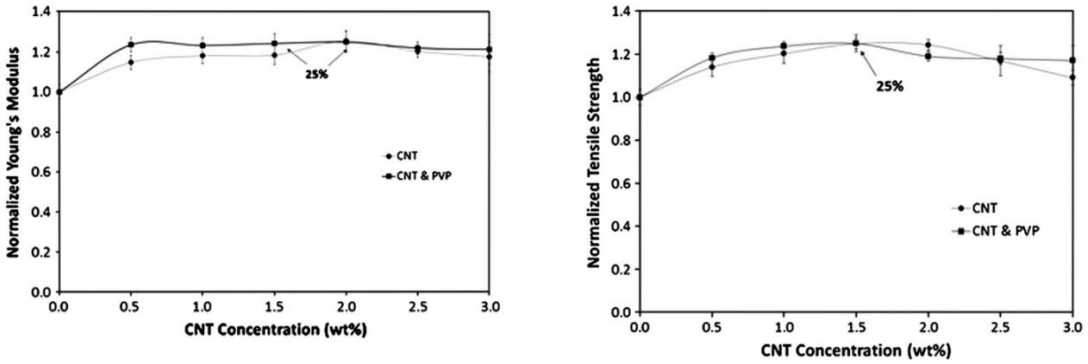

Figure 1. 10. The effect of MWCNTs addition on mechanical properties: (a) Young's modulus, (b) tensile strength [67].

Manotazeri et al. [64], investigated the incorporation effect of different MWCNT loadings, in the range of 0.1wt.% to 3wt.%, on Young's modulus and ultimate tensile strength of Araldite epoxy i.e. Ly564 resin and Hy560 hardener. In addition,

they have also utilized some acid-treated CNTs to compare their effects on mechanical properties with untreated CNTs. Tensile strength and stiffness were increased for all CNTs contents regardless of the CNTs surface modification used. The treated CNTs manifested better performance in tensile strength whereas the untreated CNTs showed better Young's modulus. These opposite behaviours of the untreated and treated CNTs in stiffness and tensile strength were attributed to the CNTs dispersion states.

In fact, a homogenous CNT dispersion was obtained for the former (Figure 1. 11c-d) whereas presences of CNT aggregates were quite notable for the untreated CNTs (Figure 1. 11a-b). In other words, better CNTs/epoxy interfacial bonding along with low aspect ratio for the treated CNTs resulting from the surface modification caused better performance with respect to the untreated CNTs. The lower tensile strength for the untreated CNTs compared to treated CNTs was related to CNTs agglomeration acting as large particles, thus, resulting in tensile strength reduction. In summary, tensile strength increased by 10 % and 25 % for untreated and treated CNTs, respectively, while an increase of 27 % and 22 % in Young's modulus were achieved for untreated and treated CNTs respectively (at 3 wt.%).

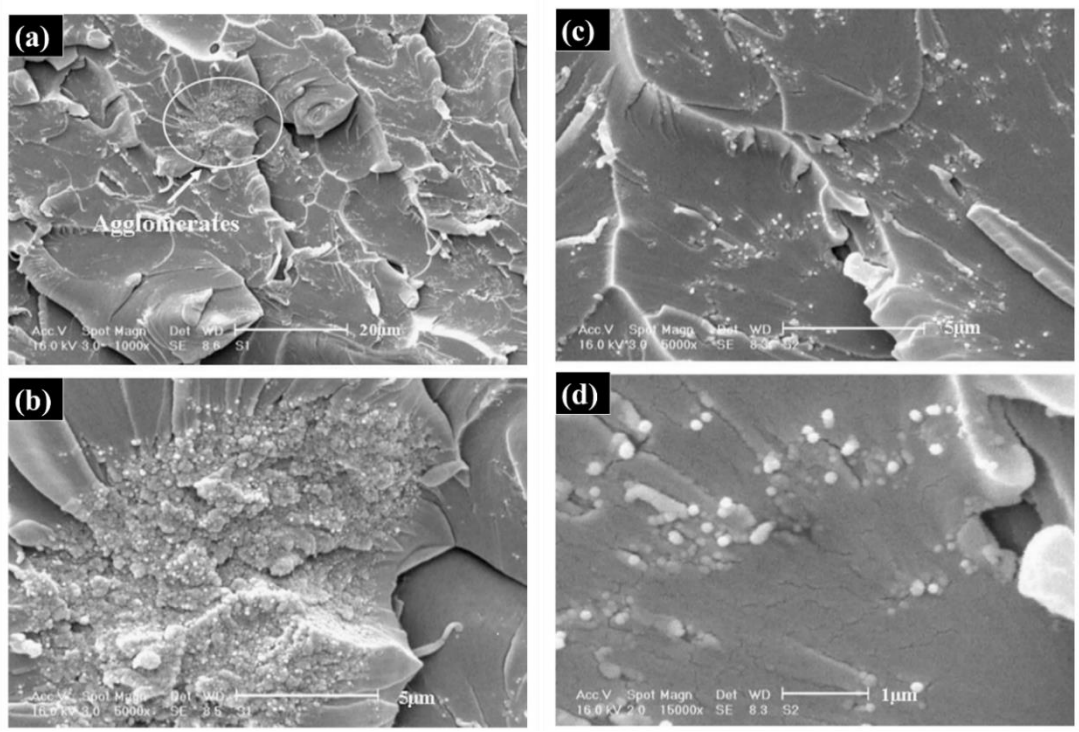

Figure 1. 11. Better CNT dispersion for treated CNT compared to untreated CNTs: (a-b) untreated CNTs, (c-d) acid treated CNTs[64]

Electrical and mechanical characteristics of the epoxy reinforced with MWCNTs was evaluated by Allaoui et al. [65] . The electrical conductivity of the nanocomposite substantially increased compared to the pristine epoxy by addition of MWCNTs where a percolation threshold region around 0.5 wt.% was achieved (Figure 1. 12a). Large aspect ratio of CNT along with its high electrical conductivity were accounted for converting insulating epoxy to conductive polymers [65]. In addition, stiffness and tensile strength were also enhanced by addition of MWCNTs i.e. an increase of 200 % and 400 % were obtained for Young's modulus and yield strength, respectively, as shown in Figure 1. 12b.

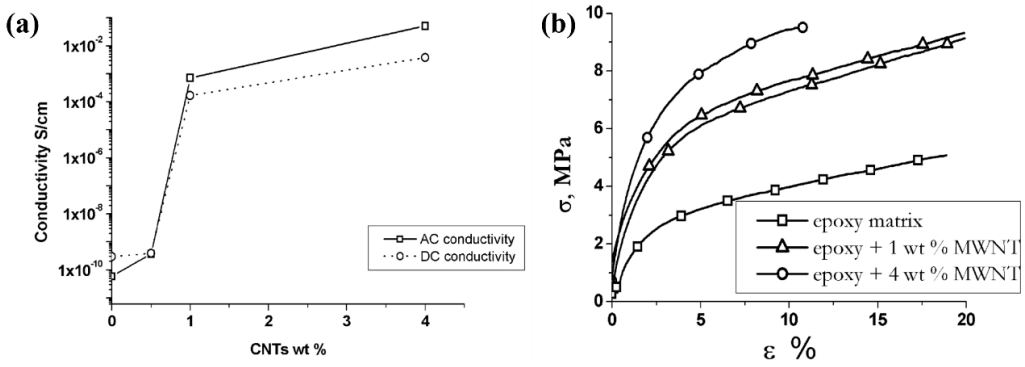

Figure 1. 12. MWCNTS doped epoxy: (a) electrical properties, (b) stress-strain curves [65]

The effect of SWCNTs alignment on electrical conductivity and mechanical properties of the epoxy was analyzed in a study performed by Wang et al. [66]. As it is shown in Figure 1. 13a, the nanocomposites manifested better performance along the alignment of the CNTs with respect to perpendicular to the CNTs alignment. Similar behaviour was also noticed for the mechanical properties i.e. the Young's modulus and tensile strength are higher parallel to CNT alignment whereas lower mechanical properties were obtained perpendicular to the CNTs alignment (Figure 1. 13b-c). High SWCNT content resulted in mechanical properties degradation, in particular for tensile strength, which was attributed to formation of CNT aggregates arisen from high viscosity of the CNTs/epoxy mixture.

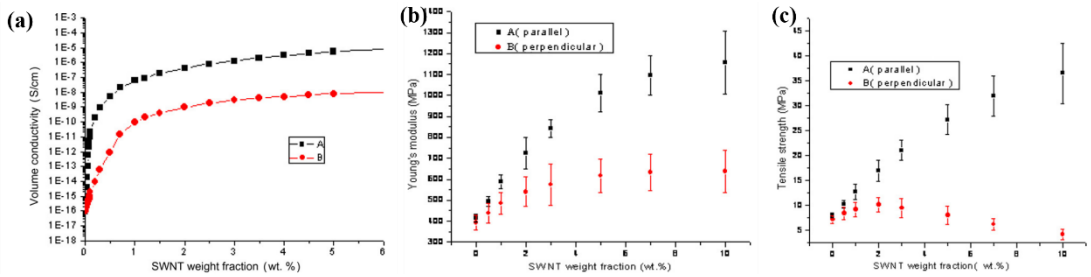

Figure 1. 13. The effect of CNTs alignment on (a) electrical conductivity, (b) stiffness, (c) tensile strength [66].

In another study made by Cha et al. [68], mechanical properties of epoxy resin MY0510 were enhanced by incorporation of two different types of MWCNTs including melamine-functionalized and non-functionalized MWCNTs. According to their results, melamine-functionalized CNTs exhibited better performance in tailoring mechanical properties with respect to the pristine CNTs/epoxy (Figure 1. 14a-c). In fact, the best performance was achieved at 2 wt.% where Young's modulus, tensile strength and fracture toughness enhanced by 64 %, 22 %, and 95 %, respectively, compared with the neat epoxy.

In addition, the functionalized CNTs showed better dispersing state (Figure 1. 14e-f) compared with pristine CNTs where presence of CNTs aggregates are notable (Figure 1. 14d), indicating appropriate performance of the functionalization in improving CNT dispersion. In summary, they have concluded that excellent CNT dispersion as well as appropriate interfacial bonding between functionalized CNTs and matrix accounted for the mechanical properties enhancement while crack bridging taken into consideration as the toughening mechanism in significant increase in fracture toughness.

The enhancement effect of MWCNTs in tensile strength and fracture toughness properties (mode I and II) of resin ML-506 epoxy were investigated by Ayatollahi et

al. [76]. Mode I and II refer to opening mode (a tensile stress normal to the plane of the crack) and sliding mode (a shear stress acting parallel to the plane of the crack and perpendicular to the crack front respectively. Apart from CNT loading, a negligible increase in tensile strength was obtained whiles an increase of 17% in stiffness was observed at 1wt.% CNTs content (Figure 1. 14g). On the other hand, fracture toughness showed greater enhancement by CNT addition, in particular for mode II (Figure 1. 14h). In fact, mode II of fracture toughness increased by increasing CNT content (Figure 1. 14h) while the maximum increase was 47 % at 1 wt.%. Mode I fracture toughness increased by 27 % at 0.5 wt.%, then reduced at higher CNT loading. This indicated that mode I fracture toughness was more susceptible to CNTs aggregates compared to mode II.

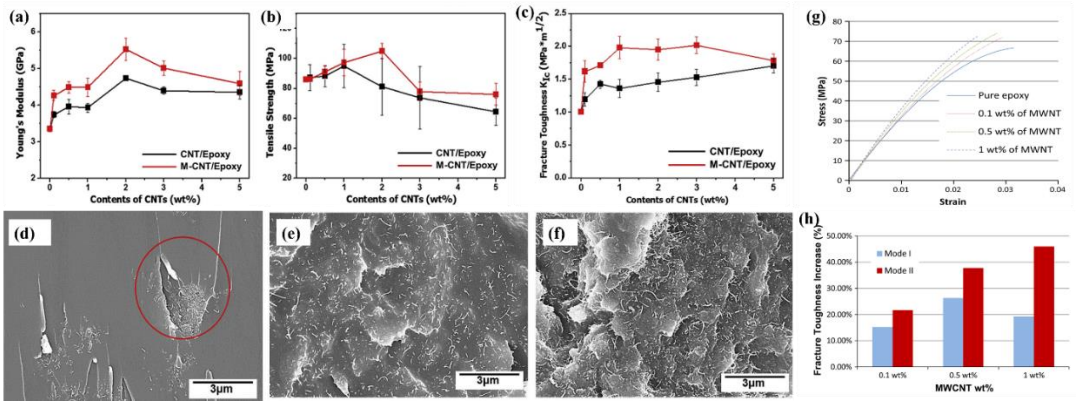

Figure 1. 14. (a-c) stiffness, tensile strength and mode I fracture toughness of MWCNTs doped epoxy, respectively, CNTs dispersion at (d) 2 wt.% nonfunctional MWCNTs while red circle points to CNT aggregates, (e-f) melamine-melamine functionalized MWCNTs at 2 wt.% and 3 wt.% respectively [68]; (g-h) stress-strain curves and fracture toughness properties of MWCNTs doped epoxy respectively [76].

In another study, improvement of tensile strength and fracture toughness of

epoxy resin MGSL135i with an amine hardener H137i using DWCNTs was evaluated [69]. Young's modulus and fracture toughness enhanced by increasing DWCNT loading as shown in Figure 1. 15b and d respectively. On the other hand, tensile strength initially reduced when low DWCNT content was used (0.1 wt.%), then increased at higher weight concentration (Figure 1. 15c).No justification was provided in their study for the reduction of tensile strength at low CNT content while crack bridging was taken into account as the toughening mechanism for the fracture toughness.

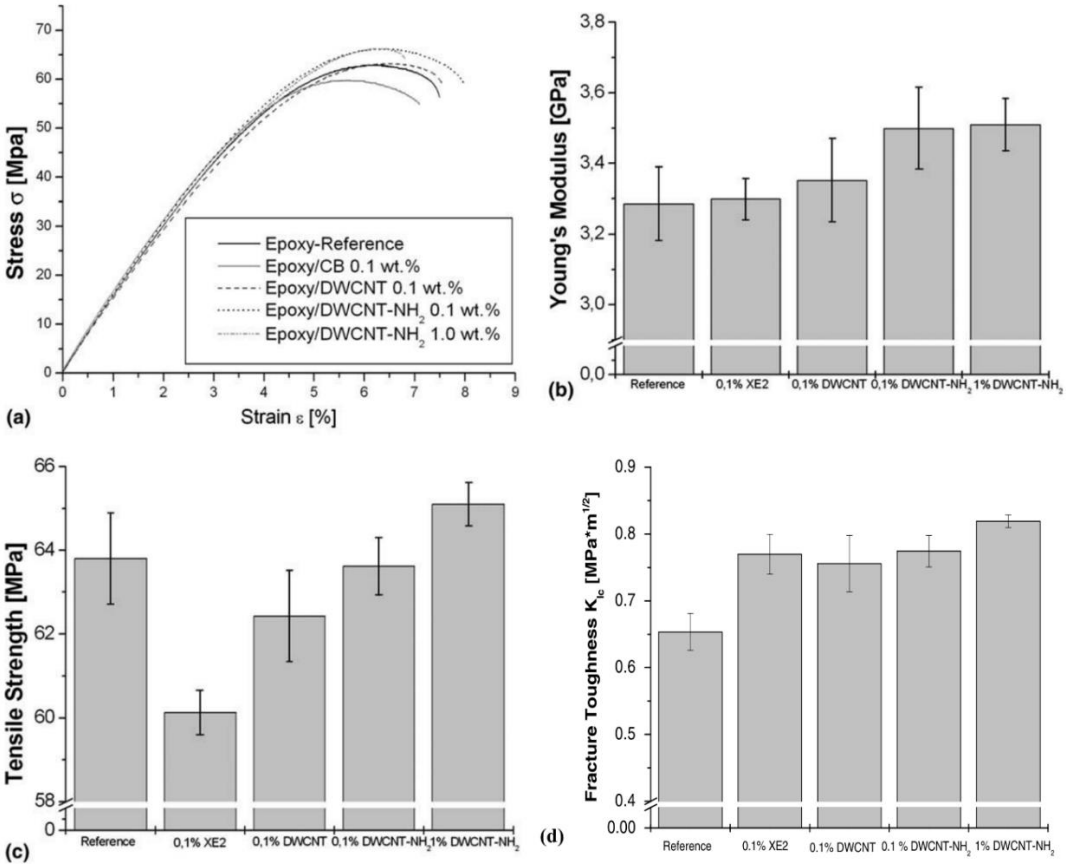

Figure 1. 15. DWCNTs/epoxy: (a) stress-strain curves, (b) Stiffness, (c) Tensile strength, (d) Fracture toughness (K_{IC}) [69].

A comprehensive examination was carried by Gojny et al. [43] in which they investigated the influence of adding different types of CNTs, including SWCNTs,

DWCNTs and MWCNTs, on tensile strength, Young's modulus and fracture toughness (Figure 1. 16). According to their results, the enhancement effect of CNTs on fracture toughness was more notable compared with tensile strength and Young's modulus. As it is shown in Figure 1. 16b-c, regardless of CNT content and morphology used, Young's modulus and fracture toughness (K_{IC}), respectively, increased for all nanocomposites where a maximum increase of 11 % and 30 % in stiffness and K_{IC} were obtained at 0.3 wt.% DWCNTs . Crack bridging, CNTs pullout, and CNTs rupturing were accounted for the fracture toughness enhancement (Figure 1. 16d-e).

On the other hand, tensile strength was varied depending on the CNT content and morphology used (Figure 1. 16a). MWCNTs showed the weakest performance in tensile strength with respect to SWCNTs and DWCNTs which was attributed to lack of appropriate shear loading transfer through the internal layer of MWCNTs. It was concluded that 0.3 wt.% DWCNTs manifested better performance in terms of tensile strength, stiffness and K_{IC} as illustrated in Figure 1. 16a-c respectively.

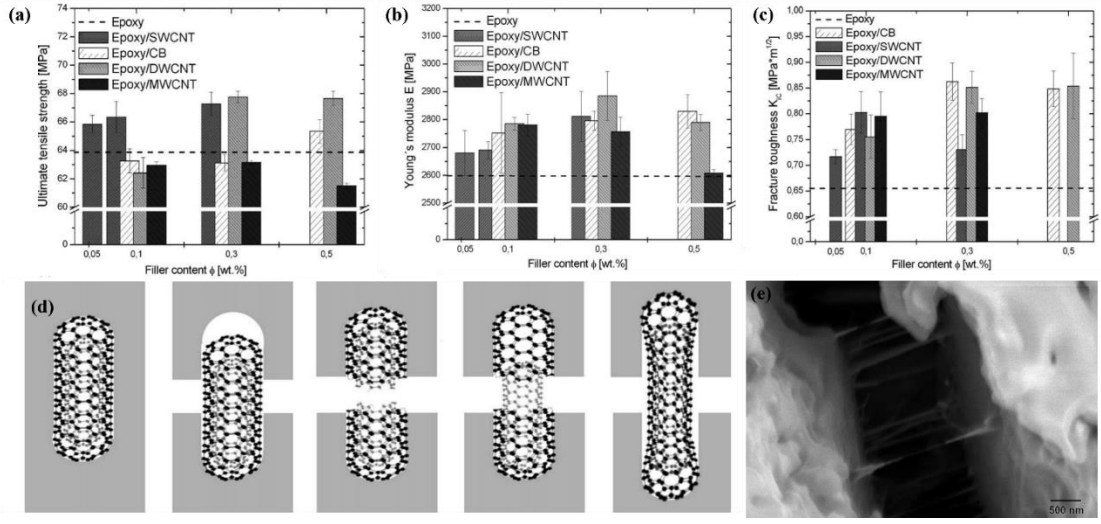

Figure 1. 16. The effect of different CNTs morphologies and wt.% on : (a) tensile strength, (b) stiffness, (c) fracture toughness, (d) schematic illustration of crack

bridging and CNT rupturing mechanisms, (e) TEM image of crack bridging as the main toughening mechanism for CNT doped epoxy [43].

The effect of MWCNT aspect ratio on tensile and impact strengths and fracture toughness properties of Bisphenol A epoxy was studied [79]. According to their results, MWCNTs with larger aspect ratio resulted in higher impact strength and fracture toughness with respect to the one with small aspect ratio. In fact, impact strength was improved by 84 % and 63 % for epoxy reinforced with 1 wt.% of large and small aspect ratios of MWCNTs respectively. Fracture toughness enhanced by 12 % for the MWCNTs with larger aspect ratio whilst no improvement was noticed for the CNTs with smaller aspect ratio. Tensile strength did not change significantly compared with the neat epoxy whilst stiffness reduced for both types of MWCNTs, which was attributed to lack of functionalization in MWCNTs.

According to the aforementioned studies, high variations can be identified in mechanical properties especially in tensile strength which can be attributed to manufacturing defects such as voids and porosities as well as agglomerations. Agglomeration and weak interfacial bonding between CNTs and the epoxy were well addressed in the above literature as the main challenges in achieving proper mechanical properties, resulting from high surface area and high surface energy of individual CNTs.

1.3.1.2.Nanoclay/epoxy

Mechanical properties of a DGEBA epoxy resin reinforced with different types of nanoclay including MMT-Na+, MMT-I.30E, MMT-30B and MMT- cetylpyridinium

chloride (CPC) at three different weight concentrations, 1 wt.%, 5 wt.% and 10 wt.%, were examined in a study made by Qi et al. [80]. According to their results, stiffness was improved for all nanocomposites i.e. an increase of 27%, 13%, 15% and 3% was achieved for MMT-Na+, MMT-I.30E, MMT-30B and MMT-CPC respectively. This was attributed to higher stiffness of the nanoclay in comparison to the epoxy.

On the other hand, tensile strength and strain at fracture were remarkably reduced compared to the neat epoxy. This was attributed to poor dispersion of the nanoclay along with presence of voids and pores left in the specimen after degassing due to higher viscosity of the nanoclay/epoxy mixture. In fact, these defects, pores and clay agglomeration, acted as stress concentrator, thus, premature failure took place.
In addition, fracture toughness (K_{IC}) was also enhanced by 59 %, 54 %, 25 %, and 57 % for MMT-Na+, MMT-I.30E, MMT-30B and MMT-CPC respectively.

They (Qi et al. [80]) have pointed out that higher fracture toughness of the clay nanocomposites compared to the neat epoxy could be related to deviation of crack opening when confronted to the intercalated clay [80]. This phenomenon was known as crack deflection considered as the main toughening mechanism in the clay composites. This was also endorsed by higher surface roughness of the nanocomposites with respect to the pristine epoxy as shown in Figure 1. 17.

In fact, presence of many tiny cracks on the fracture surface of the specimens while they were inclined to curve around intercalated clay (Figure 1. 17b-c) was accounted for the increasing energy, thus, enhancing fracture toughness properties. It was pointed out that although the clay aggregates had detrimental influences on tensile strength, they could thoroughly improve fracture toughness.

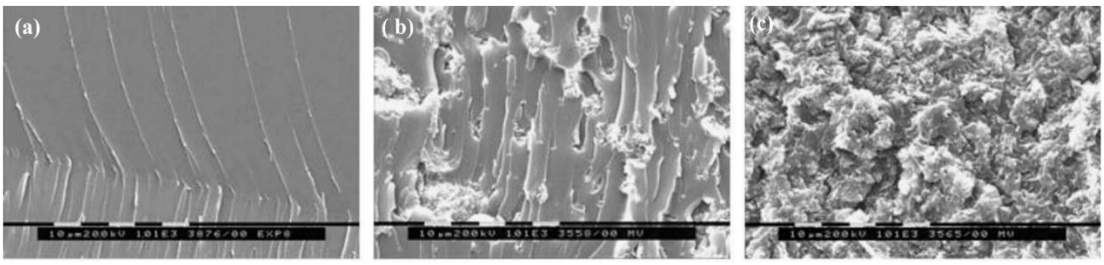

Figure 1. 17. SEM image of the fracture surface after fracture test showing higher surface roughness for the reinforced epoxy compared to the neat epoxy: (a) neat epoxy, (b) 2wt.% MMT-I.30E/epoxy, (c)) 10wt.% MMT-I.30E/epoxy[80].

In another study made by Wang et al. [51], mechanical properties of bisphenol A epoxy reinforced by silane-modified clay (SMC), including 1 wt.%, 2 wt.% and 3 wt.%, were examined. They could reach a complete exfoliated nanoclay structure in the nanocomposites using organic modifier which was used an as auxiliary media for better nanoclay dispersion (Figure 1. 18a). This can be proven from the XRD analysis (Figure 1. 18a) where no peak was found for the nanocomposites whereas a peak at 4˚ and 7˚ were identified for the modified and unmodified nanoclay respectively. This was led to better exploitation of nanoclay in enhancement of tensile strength, stiffness and fracture toughens (K_{IC} and G_{IC}) as shown in Figure 1. 18b-d respectively. As it is shown in the XRD results (Figure 1. 18a), the peak for the modified nanoclay, SWC, was at lower angle (4˚) with respect to the peak for the pristine nanoclay (7˚). This indicated that the silane modifier could successfully enhance the basal distance of the nanoclay, thus, some epoxy could penetrate amongst nanoclay layers.

In addition, no specific peak was seen for the nanocomposites; demonstrating clay nanocomposites possess a complete exfoliated structure as shown by TEM image of the nanocomposites in Figure 1. 18e. As a result of the exfoliated clay structures, they could successfully improve mechanical properties i.e. stiffness increased by 13 %

at 3 wt.%, tensile strength 25 % at 2 wt.%, K_{IC} and the critical strain energy release rate (G_{IC}) increased by 77 % and 190 % at 2 wt.%, respectively.

The higher modulus of the nanoclay was accounted for the linear increase in stiffness as a function of nanoclay content increase (Figure 1. 18). On the other hands, for tensile strength and fracture toughness properties, the aforementioned properties dropped at higher nanoclay content (3wt.%) which was attributed to the presence of clay aggregates resulting from higher viscosity of the nanoclay/epoxy mixture.

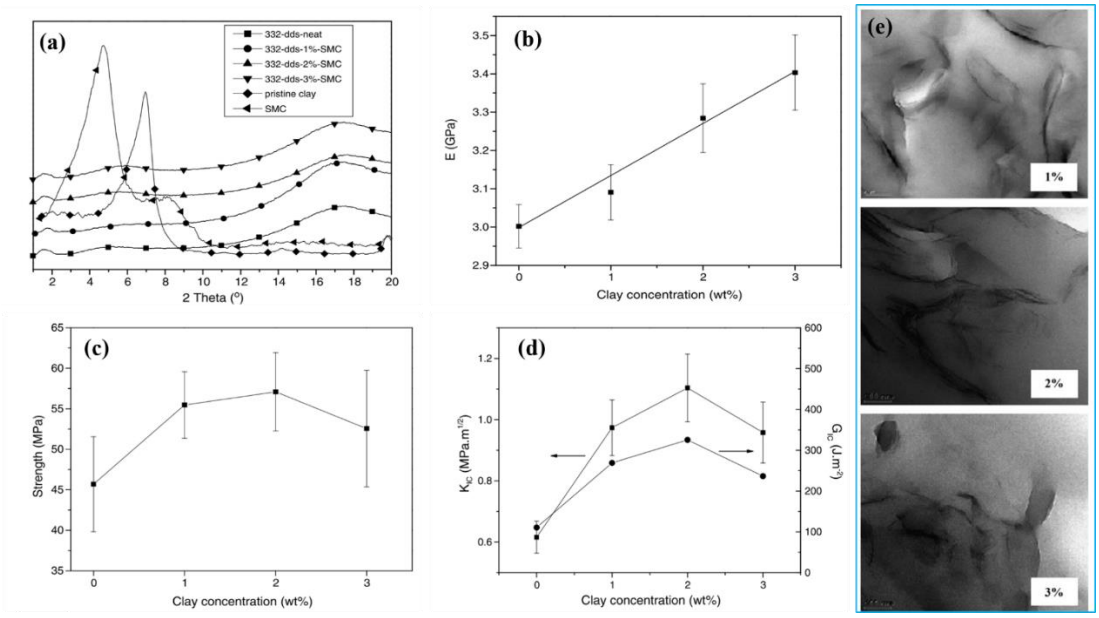

Figure 1. 18. Silane modified clay doped epoxy: (a) XRD analysis, (b) stiffness, (c) tensile strength, (d) K_{IC} and G_{IC}, (e) TEM image [51].

Mechanical properties of DGEBA epoxy contained sodium montmorillonite at different weight concentrations including 1 wt.%, 2.5 wt.%, 3.5 wt.% and 5 wt.% were investigated by Wang et al. [81]. They reached a complete exfoliated clay structures using slurry-compounding process as shown in Figure 1. 19a. Because of the nanoclay addition, the Young's modulus enhanced with increasing nanoclay content (Figure 1. 19b). On the other hand, tensile strength of the clay nanocomposites reduced by

incorporation of nanoclay to epoxy which was attributed to presence of flaws in the matrix resulting from weak interfacial bonding between epoxy and nanoclay (Figure 1. 19c).

The fracture energy i.e. the critical strain energy release rate (G_{IC}) was increased up to 2.5 wt.%, then reduced at higher nanoclay loadings due to presence of aggregates at high nanoclay loading (Figure 1. 19d). Formation of large numbers of micro-crack inside and outside of clay galleries and increasing fracture surface area (Figure 1. 19e), because of crack deflection, were taken into account as the main toughening mechanisms of the material. This was also proven by high TEM magnification image (Figure 1. 19f), showing formation of crack between the clay interlayer i.e. the micro-cracks were formed inside the clay galleries due to the weak bonding amongst silicate layers. This phenomenon was followed by merging all of the micro-crack, thus, transforming to a macro-crack which resulted in the specimen failure. In summary, formation of many tiny cracks between internal layers of clay galleries accounted for the significant improvement of the fracture toughness. This phenomenon is also called crack branching or crack tailing which account for the fracture toughness enhancement in clay doped epoxy nanocomposites.

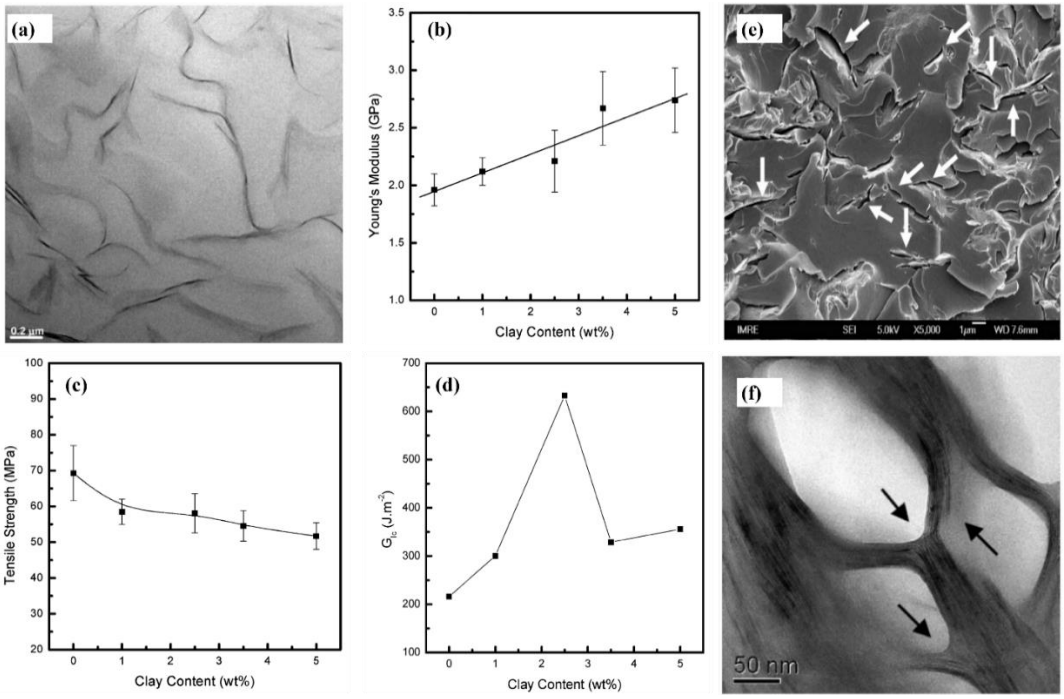

Figure 1. 19. DGEBA epoxy containing sodium montmorillonite: (a) exfoliated clay microstructure, (b) stiffness, (c) tensile strength, (d) G_{IC}, (e-f) SEM and ITEM image of the formation of many micro-crack between interlayer clay galleries respectively [81].

Lu et al. [82] investigated different dispersion methods, including magnetic stirrer, vigorously stirred by high-speed emulsifying and homogenizing mixer called HEHM, and ball milling method, on final structure of clay nanocomposites, impact and flexural strength (Figure 1. 20). It is worth noting that in Figure 1. 20b-c, A, B, C, and D point to the neat epoxy, MMT/epoxy produced by magnetic stirrer, HEHM, and ball milling respectively. They could achieve a complete exfoliated nanoclay structure using ball milling technique whereas other methods mostly contained an intercalated nanoclay structure as shown in Figure 1. 20a. The intercalated and exfoliated nanoclay structures were clearly identified in the XRD analysis where a peak at $2\theta = 5^{\circ}$ was identified for the as-received nanoclay while no peak was seen for the clay

nanocomposite obtained using ball milling method (Figure 1. 20a left).

As a consequence of exfoliated clay structure obtained by ball milling methods, the impact and flexural strengths were increased by 50 % and 8 % (at 3 wt.%), respectively, whereas those produced by mechanical dispersing technique manifested slight decrease with respect to the neat epoxy (Figure 1. 20b-c). The improvement in impact and flexural strengths was attributed to pulverization of clay aggregates by ball milling methods, thus, more homogenous and exfoliated nanoclay was obtained which effectively reinforced the matrix.

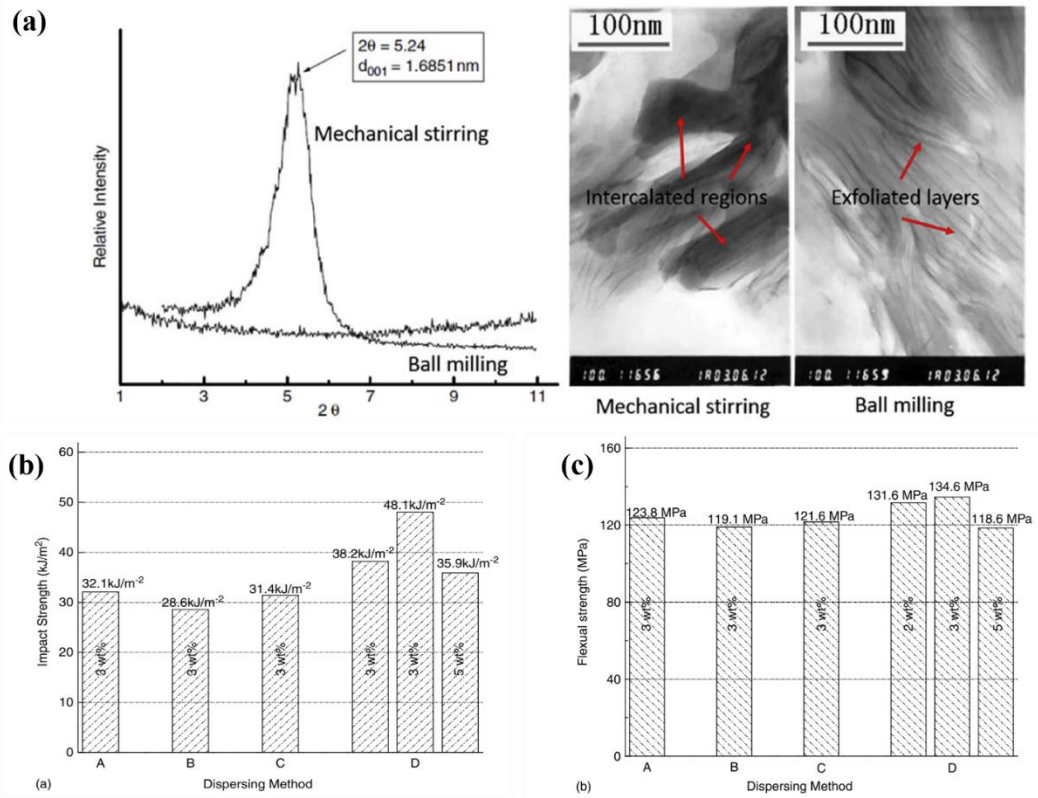

Figure 1. 20. MMT/ epoxy produced by mechanical stirring and ball milling methods: (a) XRD analysis and TEM images [49], (b) Impact strength, (c) flexural strength [82].

The effect of different modifiers on dispersion states i.e. intercalated and

exfoliated structures, mechanical and thermomechanical characteristics of the sodium montmorillonite incorporated to bisphenol A epoxy was evaluated in an attempt by Zaman et al. [83]. The modifiers were XTJ502 (XTJ), M2070 (M27), and ethanolamine (ETH). As it is shown in Figure 1. 21a, the modifier could successfully increase the d-spacing since the peak was shifted to lower angles for the modified clay. This indicated that effective grafting of the surfactant to the interlayer of clay resulting in clay swelling. In fact, a d-spacing of 16.5 Å, 16.5 Å, 12.4 Å, and 12 Å were obtained for the XTJ-clay, M27-clay, ETH-clay and sodium clay respectively. The higher d-spacing for the XTJ and M27 was related to their longer chains with respect to smaller chain in ETH-clay and pristine clay.

It is worth noting that the modifiers not only increased the basal distance, but also led to better clay structure when mixed into epoxy (Figure 1. 21b). In fact, the sodium clay showed the same peak before and after dispersion, indicating that an interrelated clay structure was achieved. On the other hand, for the modified clays, although the peaks appeared almost at the same angle i.e. before and after mixing into epoxy, their densities were much lower than the ones obtained before dispersion technique applied. This indicated that an exfoliated clay nanocomposite was obtained for the modified clays whereas the unmodified nanocomposite (sodium clay/epoxy) manifested an intercalated structures.

In addition to dispersion states of the nanoclay, the mechanical properties in terms of Young's modulus, tensile strength, and K_{IC} and G_{IC} were also studied. Regardless of the type of nanoclay used, stiffness, K_{IC} and G_{IC} were enhanced by introduction of nanoclay where the maximum enhancement of 16 %, 58 % and 114 % in stiffness, K_{IC} and G_{IC}, respectively, were achieved for XTJ-clay nanocomposite. In contrast, tensile strength for the clay nanocomposites reduced by addition of nanoclay

while no justification was provided in their investigations.

It is worth noting that although the highest tensile strength of 59 MPa was obtained for XTJ-clay nanocomposites, it was still lower than the neat epoxy showing tensile strength of 64 MPa. The glass transient temperature denoted Tg, defined as the temperature where polymers transferred from its glassy and rigid state to a most-likely rubbery and viscous state, was also examined in their study (Figure 1. 21c). According to their results, the Tg for the XTJ-clay and M27-clay composites were 99.7 ˚C and 96.2 ˚C, respectively, whilst a Tg of 93.7 ˚C was found for the neat epoxy. This enhancement in Tg was related to penetration of epoxy into interlayer of exfoliated clays, and due to their high surface area, they acted as a thermal barrier resulting in improvement of Tg.

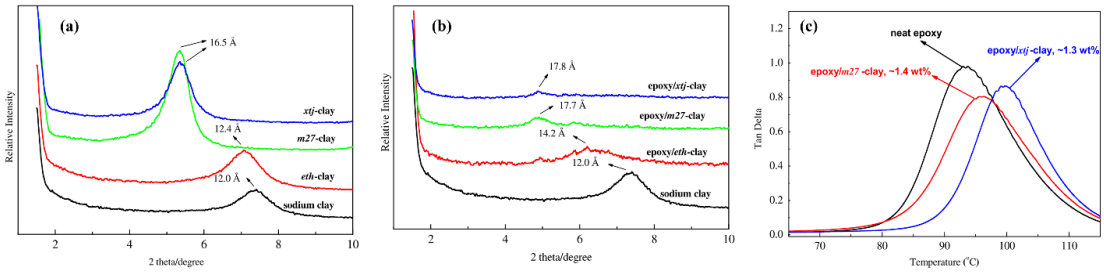

Figure 1. 21. Unmodified and modified sodium clay clays: (a) XRD for the powder, (b) XRD for clay nanocomposites at 2.5 wt.%, (c) Tg for the neat and clay nanocomposites [83].

1.3.1.3.Hybrid CNTs-nanoclay/epoxy

Throughout this section, a literary review of epoxy base nanocomposites reinforced by simultaneous additions of CNTs and nanoclay is carried out. In this context, the mechanical and thermomechanical properties of the materials are

investigated. Although many studies have been conducted at binary state i.e. CNT/epoxy and NC/epoxy as discussed before, the synergistic effects of CNTs and nanoclay in creating high performance materials have been investigated to a much lower extent [54,58,59,84–86].

Aradhana et al. [54] investigated the concurrent effect of nanoclay (Cloisite30B) and MWCNTs on mechanical and thermomechanical characteristics of adhesive bonding with aluminum substrates. In order to achieve proper dispersion of CNTs and nanoclay, a combination of mechanical stirrer and sonication was employed while the resin was initially preheated at 100 ˚C for 1 hr to remove the entrapped air (Figure 1. 22a). According to their results, shear strength was increased for all nanocomposites where a significant increase of 48 % and 52 % for CNTs/epoxy and clay/epoxy was obtained (Figure 1. 22b). Large aspect ratio of CNTs and good adhesive bonding between nanoclay and epoxy were accounted for the shear strength improvement for CNTs/epoxy and nanoclay/epoxy composites. On the other hand, negligible increase (~4 %) in shear strength was obtained in hybrid state CNTs-nanoclay/epoxy compared to the neat epoxy (Figure 1. 22b). This was attributed to poor dispersion of CNTs and nanoclay, especially agglomeration, due to high viscosity of the mixture. The thermal stability of the composite was also studied using thermogravimetric analysis (TGA) (Figure 1. 22c). Apart from the type of the nanofiller, the activation energy for thermal degradation was improved by 9.7 %, 6.4 % and 57.3 % for CNTs/epoxy, nanoclay/epoxy, and hybrid CNTs-nanoclay/epoxy, indicating appropriate thermal stability for all nanocomposites with respect to the neat epoxy.

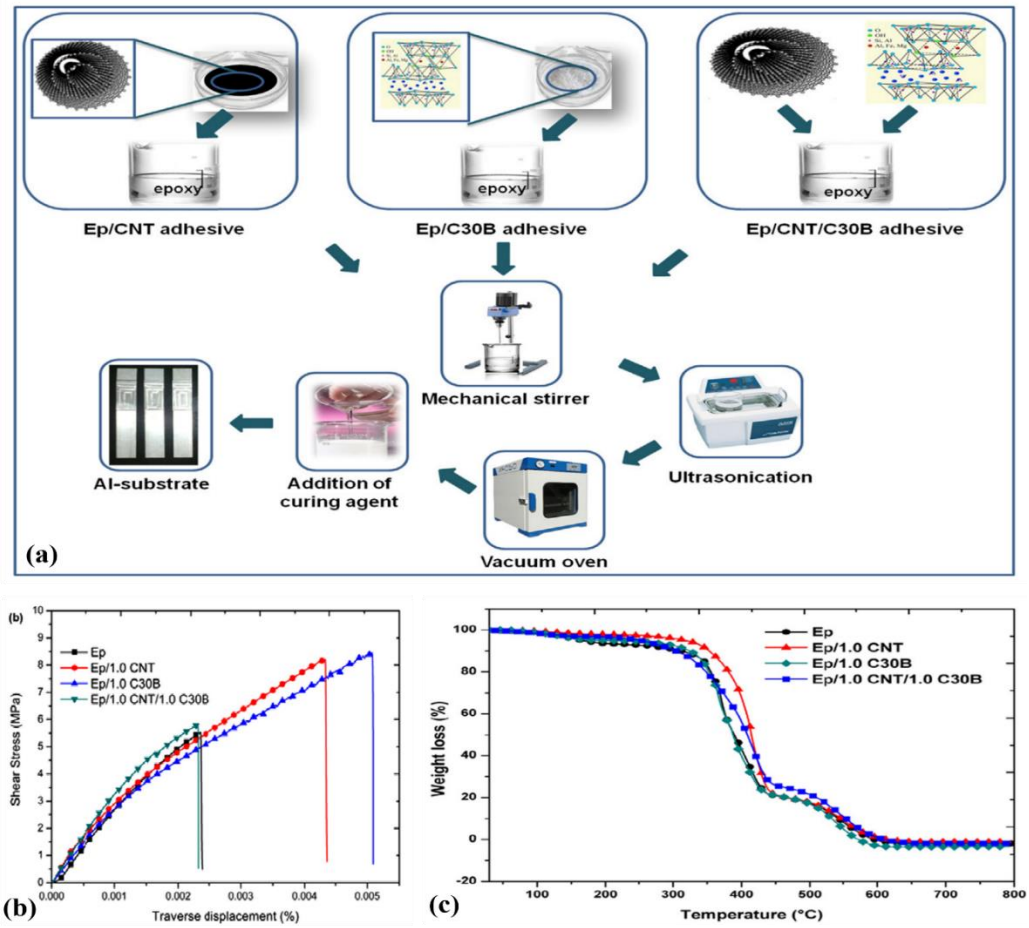

Figure 1. 22. Synergetic effect of CNTs and nanoclay: (a) manufacturing procedure, (b) shear strength, (c) TGA analysis [54].

Nguyen et al. [84] investigated hybrid effects of MWCNTs and nanoclay I.30E in tailoring mechanical and flame retardancy of epoxy Epikote 240. A combination of mechanical stirrer and probe-sonication was used to achieve homogenous dispersion of the nanomaterials. Different weight concentrations of nanoclay (1 wt.% to 3 wt.% in 1 wt.% increments) and MWCNTs (0.01 wt.% to 0.04 wt.% in 0.01 wt.% increments) were employed. Based on their results, the most homogenous CNTs and nanoclay dispersion was achieved at 0.02 wt.% and 2 wt.% for CNTs and nanoclay contents ,respectively, in which a proper mutual interaction between CNTs and nanoclay was also obtained (Figure 1. 23a).

Apart from the nanofiller loadings and types used for the nanocomposite fabrication, all nanocomposites manifested an exfoliated clay structures based on the XRD analysis i.e. no particular peak was obtained for the nanocomposites whereas several peaks were observed for the as-received nanoclay (Figure 1. 23b). EP4 to EP6 in Figure 1. 23b denoted as 0.01 wt.% to 0.03 wt.% MWCNT loadings, respectively, while a constant nanoclay content (2 wt.%) was used.

In addition, tensile strength, flexural strength, compressive strength, and impact strength were enhanced by 72 %, 33 %, 40 %, and 214 % respectively. Finally, they could successfully improve thermal characteristics of the nanocomposites in which limiting oxygen index (LOI) increased from 20.6 (neat epoxy) to 25 (EP5 nanocomposites), respectively, and combustion rate decreased from 28.41 mm/min (neat epoxy) to 20.5 mm/min (EP5 nanocomposites), respectively. This was also proven by SEM image of residues after the Horizontal Burning tests (UL-94HB) as shown in Figure 1. 23c-d, where many tiny cracks formed on burned surface of the neat epoxy (Figure 1. 23c) whilst no crack was identified for the nanocomposites (Figure 1. 23d) i.e. the nanocomposites showed improvement in flame retardancy.

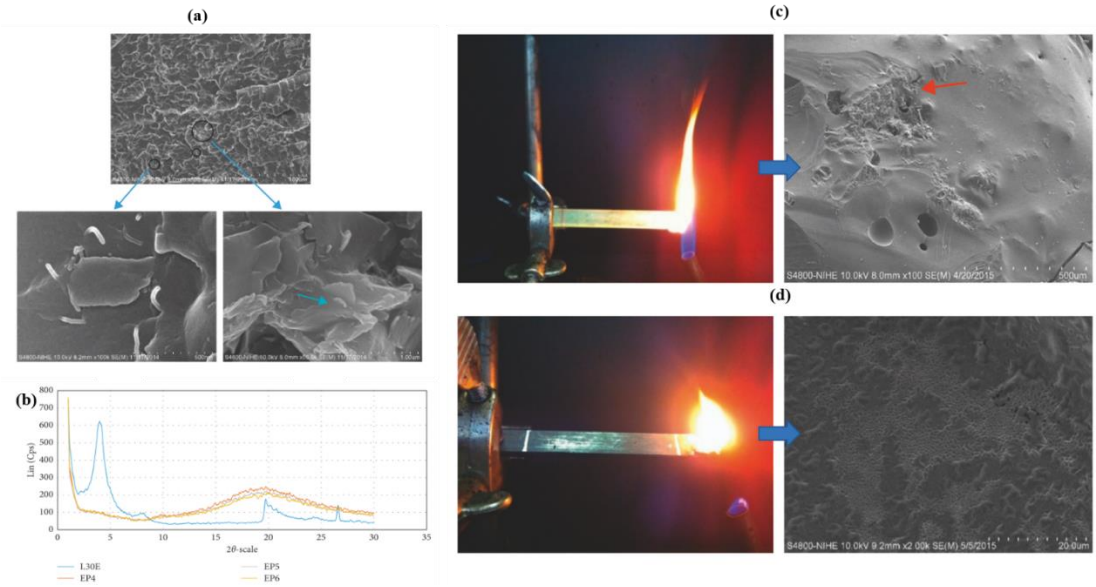

Figure 1. 23. MWCNTs and I.30E doped into epoxy: (a) FESEM image of the fracture surface, (b) XRD analysis, (c-d) SEM image of the burned surface after UL-94HB for the neat and nanocomposite respectively [84].

Zeng at al. [85] studied mechanical and thermomechanical characteristics of the Araldite LY 1564 with amine-hardener Aradur 3486 reinforced with MWCNTs anchored on MMT wherein different mass ratios of MWCNTs and MMT including MWCNT–Mt(0.05:1), MWCNT–Mt(0.1:1) and MWCNT–Mt(0.2:1) were used. In fact, they have used MWCNTs as an auxiliary filler to achieve more exfoliated MMT structures, thus, resulting in better performance in terms of mechanical and thermomechanical properties. First, the self-assembled CNTs-MMT in the form of dried powders were produced, then they dispersed into the epoxy using (i) magnetic stirrer (400 rpm-24 hr), (ii) probe-sonication (600 W-30 min), (iii) calendaring method (gap size of 20 µm, 10 µm, and 5 µm) for nanocomposite fabrication.

According to their results, they could successfully increase d-spacing of the MMT by means of the amino-functionalized CNTs i.e. a peak at $2\theta = 7.07^{\circ}$ was obtained for untreated MMT whilst it was shifted to smaller angles for the MWCNT-

MMT (Figure 1. 24a). This was attributed to insertion of triethylenetetramine (TETA) between MMT interlayers resulted in further expansion of the clay sheets. This was also validated by TEM analysis where a transparent exfoliated MMT layer at MWCNT–Mt (0.1:1) shown by black arrow in Figure 1. 24b was obtained whereas a stacked clay galleries was identified for MWCNT–Mt (0.05:1) as shown by white arrow in Figure 1. 24b.

Apart from the dried powders, when varied mass ratio of MWCNT-MMT combined to the epoxy, a complete exfoliated structure was archived for all MWCNT-MMT hybrid composites whilst an intercalated structure was observed for untreated MMT/epoxy (Figure 1. 24c). This was also proven by TEM image (Figure 1. 24d) wherein an exfoliated and interacted MMT structure was obtained for MWCNT-MMT hybrid composites and MMT/epoxy respectively. It is worth noting that presence of stacked MMT and bundles of CNTs at low (0.05 wt.%) and high (0.2 wt.%) MWCNTs loadings were notable respectively (Figure 1. 24d).

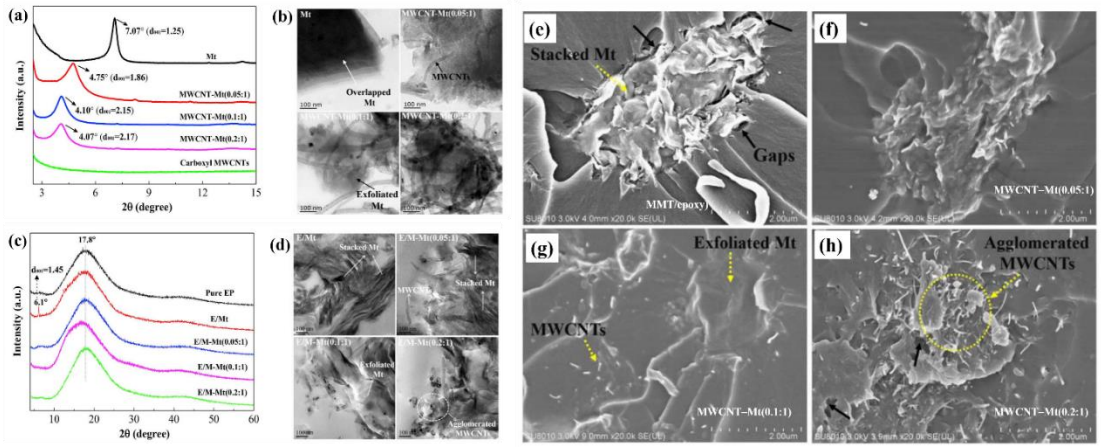

Figure 1. 24. MWCNTs-MMT hybrid at varied loadings: (a) XRD analysis of the dried powders, (b) TEM image of the powder ,(c) XRD analysis for the composites,

(d) TEM image of the composites, (e-f) SEM image of fracture surface of the tensile specimen [85].

This dispersion state and interfacial bonding of CNTs and MMT were also analyzed using SEM image of the fracture surface of the tensile specimens as shown in Figure 1. 24e-h. For untreated MMT/epoxy, formation of stacked clays accompanied with weak interfacial bonding to epoxy resulted in formation of defects in their vicinity such as voids, was notable as shown by black arrows in Figure 1. 24e. On the other hand, an appropriate interfacial bonding took place between MWCNT-MMT and epoxy since no defect was found. In addition, as mentioned before, at low and high CNT loadings (Figure 1. 24f and h respectively), presence of some intercalated clays and agglomeration of CNTs were also remarkable.

As a consequence of proper dispersion states of CNTs and nanoclay, mechanical and thermomechanical properties were enhanced with respect to the neat epoxy and untreated MMT/epoxy composite (Figure 1. 25). For the mechanical properties, similar trend was noticed in tensile and flexural tests i.e. the aforementioned properties enhanced up to MWCNT–Mt (0.1:1), then reduced at MWCNT–Mt(0.2:1) due to agglomeration of CNTs. In fact, tensile strength, Young's modulus, elongation at break, tensile toughness, flexural strength and flexural modulus at MWCNT–Mt (0.1:1) were increased by 26.8 %,18.8 %, 19.7 %, 92 %, 20.4 %, and 22.3 % , respectively, compared with untreated MMT/epoxy (Figure 1. 25a-f).

The thermomechanical behaviour of the nanocomposites in terms of storage modulus (E′), loss factor ($tan\delta$), the glass transition temperature (Tg), and the temperature that E′ becomes stable (Tr) were also studied using the dynamic mechanical thermal analysis (DMTA) as shown in Figure 1. 25g-h. Similar to

mechanical properties, same trend was identified in thermomechanical properties i.e. an increase up to MWCNT–Mt (0.1:1), followed by an slight reduction at 0.2 wt.% CNTs. All MWCNT-MMT contents manifested higher thermomechanical properties with respect to the neat epoxy and untreated MMT/epoxy, indicating grafting CNTs on the surface of MMT could successfully improve CNT dispersion as well as exfoliated clay structure, thus, improving multifunctional properties of the epoxy. In fact, storage modulus enhanced by 15.8 % at MWCNT–Mt (0.1:1) whereas the loss factor decreased to 29.3 % compared with untreated MMT/epoxy.

In addition, Tg and Tr increased from 76.99 ˚C to 83.97 ˚C and 87.92 ˚C to 98.21 ˚C respectively. This was attributed to positive effect of simultaneous addition of MWCNTs-MMT resulting in declining the epoxy molecules chain in vicinity the CNT-MMT. This behavior was explained by proper dispersion of CNTs, mechanical interlocking of polymer chain due to high aspect ratio and large surface area of CNTs, strong covalent bond amongst CNTs and epoxy, and finally efficient barrier impact of exfoliated nanoclay.

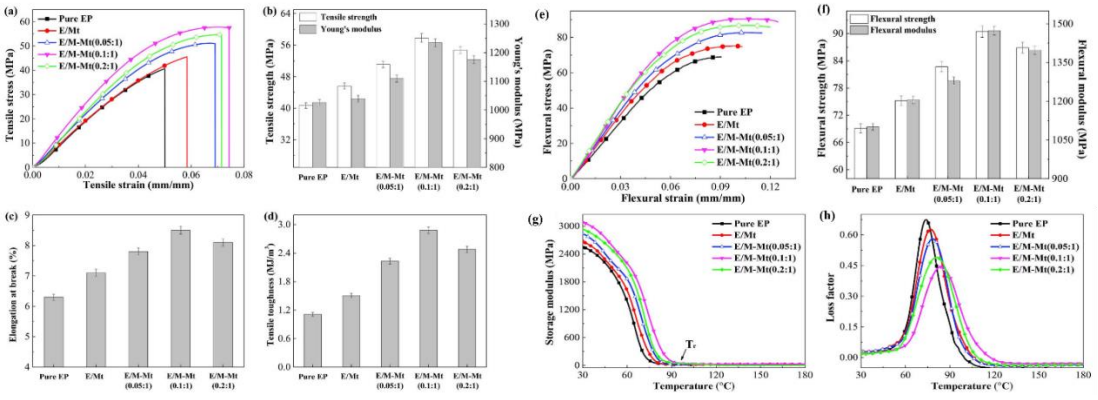

Figure 1. 25. MWCNTs-MMT hybrid at varied loadings: (a-d) tensile test, (e-f) flexural test, (g-h) DMTA) test [85].

Wang et al. [87] could successfully develop an exfoliated clay-CNTs structure incorporated into DGEBA epoxy using CNT growth on the surface of the nanoclay by chemical vapor deposition (CVD). The Vickers microhardness and impact tests were performed in which an increase of 26 % and 110 %, respectively, were obtained for the clay-CNTs/epoxy composites with respect to the neat epoxy. This was attributed to CNT growth on the surface of nanoclay that led to an exfoliated clay structures in addition to interlocking of epoxy chains by CNTs. Finally, the clay-CNTs/epoxy nanocomposites manifested higher surface roughness compared with the neat epoxy, resulted from deviation of the crack between clays, thus, making the crack propagation more difficult. This was led to significant increase in impact strength of the CNT-clay hybrid composites with respect to the neat epoxy.

Some studies focused on improving thermal stability and flame retardant characteristics of the epoxy using hybrid CNTs and nanoclay [58,59]. According to their results, MWCNTs could reduce the degradation rate of the epoxy and simultaneously increased the chare yield and LOI, indicating CNTs behaved as an effective thermal barrier and heat insulator. Nanoclay played as an ambient for energy storage and hampered heat transfer within the matrix resulting from their great heat specific.

1.3.2. Electrical conductivity and piezoresistivity

Structural Health Monitoring (SHM) has attracted attention of many researchers to assure safety of the structural composites for many industrial applications, especially for aerospace applications as shown in Figure 1. 26a [88]. Structural composites are typically subjected to a variety of loading situations such as shock-loading, impact,

fatigue, crack initiation, delamination etc. Therefore, it is necessary to monitor the health of the whole structure during its operation to avoid potentially catastrophic failures.

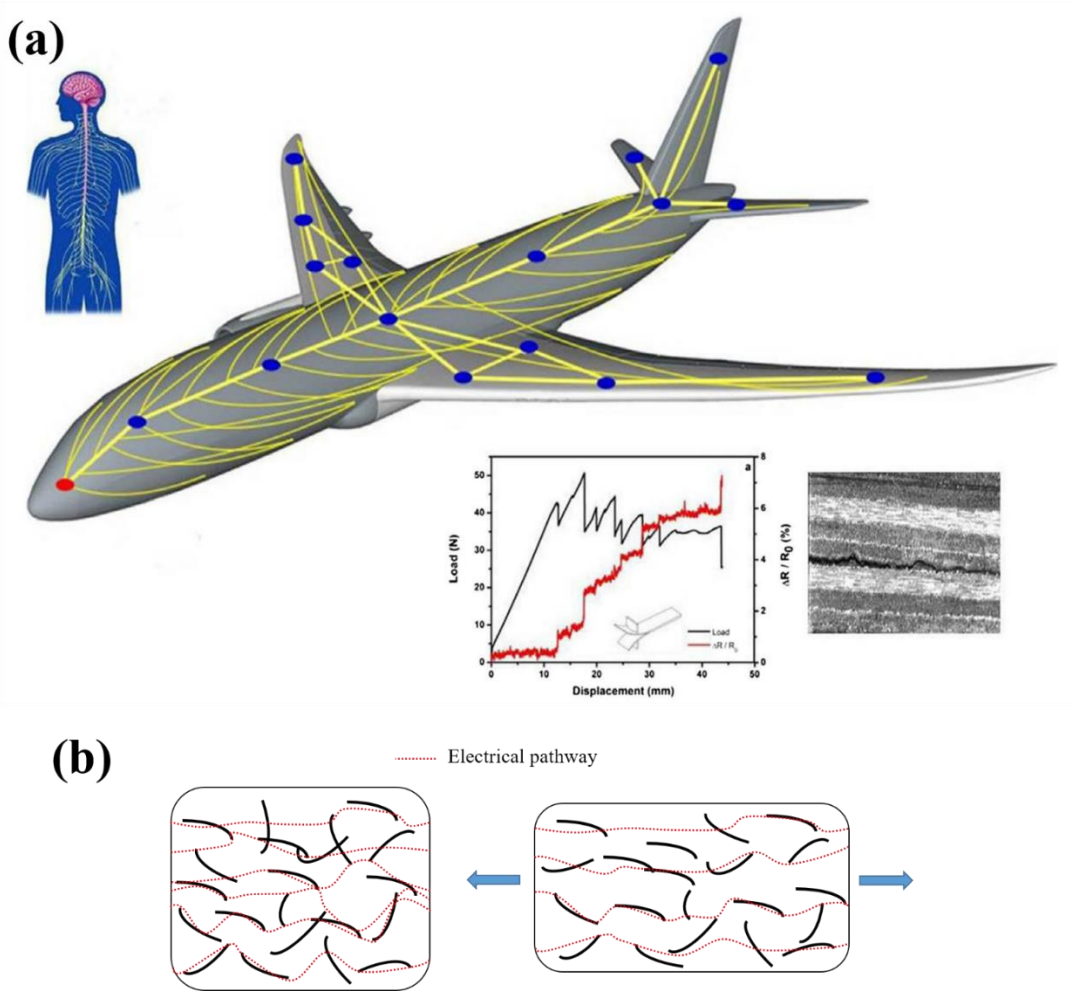

Figure 1. 26. (a) illustration of SHM system used for aircraft industry, enabling self-sensing strain increase and damage initiation[89], (b) simple illustration of the mechanism of piezoresisitve sensitivity in response of strain increase.

In this context, many authors have demonstrated advantages over the traditional strain sensors since they could detect damage initiation globally i.e. at bulk scale while the traditional sensors were mainly localized [28]. Early detection of the

aforementioned defects is challenging using old technologies such as non-destructive tests i.e. X-ray [90], ultrasonic [91] and eddy current [92]. However, some of these technologies require the disassembly of parts at a high cost and prevent real-time monitoring implementation. Many attempts are present in the literature for distributed ultrasonic real-time monitoring leveraging on piezoelectric transducers to generate and acquire guided waves, potentially detecting any deviation from a baseline condition [93]. Localized strain sensing is another widely studied technique for real-time SHM, often leveraging on embedded optical fiber sensors, however limited in monitoring only small areas in the vicinity of the strain gauges [94]. Both methods induce stress concentrations and potential crack initiation when sensors are embedded into the composite [95,96] and often require costly equipment for signal acquisition.

The excellent electrical conductivity of CNTs opened alternatives to scientists to create multifunctional materials in which CNTs assign self-sensing capacity to the host material, often exploited for damage detection [97–101]. This was mainly attributed to the high aspect ratio and low density of CNTs which brought about numerous studies on tailoring electromechanical characteristics of polymer based nanocomposites[5,6,9,21]. Specifically, many researches addressed the piezoresistive characteristics of the bulk nanocomposites for strain sensing applications [26,102,103]. The concept behind using them as a strain sensor was related to change in normalized electrical resistance in presence of strain as shown in Figure 1. 26b. In fact, the number of electrical pathway, illustrated by dashed red lines in Fig.26b, reduced as function of strain increase, thus, adjacent CNTs become far away from each other resulting in further breakage of electrical network in the system.

Many efforts have been conducted on demonstrating the self-sensing performance of CNT-based epoxy, monitoring the strain variation under different

loading configurations, most of the time referring to tensile and three point bending tests [27,30,111–113,45,104–110]. Under the applied load, normalized resistance change versus strain manifested itself as different trends, either linear [104] or nonlinear [30] amongst the current literature. In addition, the specimen sensitivity to strain was varying depending on CNT contents used, CNT dispersion [30,37] – uncontrolled dispersion can induce formation of CNT agglomeration and entangles which deteriorate the robustness of the measure [23] – and the presence of additional defects into the material, such as voids, porosity and imperfect adhesion between the CNTs and the resin.

It is worth noting that although there are other conductive nanomaterials in suit SHM such as nanoparticle[114], GNPs [28], carbon black[115], Carbon Nanofibers (CNFs) [108], and nanowire [116], the scope of this thesis is investigation of inducing peizoresistivity to the epoxy using CNTs. Thus, in the following sections, some of the previous studies on electrical conductivity and piezoresistivity performance of the CNTs doped epoxy in binary (CNTs/epoxy) and ternary states (CNTs-nanoclay/epoxy) will reviewed in detail.

1.3.2.1.CNTs/epoxy

Electrical and electromechanical properties of epoxy reinforced by MWCNTs was investigated by Vertuccio et al. [104,111]wherein the piezoresistive-sensitivity of the developed nanocomposites were analyzed in two different conditions including tensile an flexural tests. Different CNT contents were used to find out the percolation threshold region along with the suitable CNTs loading for the piezoresistivity test. The volume electrical conductivity of the nanocomposites manifested a percolation

threshold region between 0.1-0.4wt.% CNTs as shown in Figure 1. 27a. In fact, the electrical conductivity substantially increased up to 11 orders of magnitude at 0.3wt.% of CNTs resulting from tunneling effect amongst neighboring CNTs as shown in Figure 1. 27b. It is worth noting that based on percolation theory [117], electrical conductivity increases with increasing filler content (equation 1.2).

$$\sigma = \sigma_0(\vartheta - \vartheta_c)^t \qquad (1.2)$$

Where σ is volumetric electrical conductivity of the nanocomposite (S/m), σ_0 the intrinsic electrical conductivity of the filler (S/m) i.e. in this study CNTs, ϑ_c the weight concentration corresponding to percolation threshold (wt.%), ϑ the weight concentration (wt.%), and t the critical exponent. The critical exponent of 2.2 was obtained in their study by linear interpolation of the slope of the inset of the Figure 1. 27a, which is typically between 0.7-3 for CNTs doped nanocomposites [118].

In addition, the nanocomposite manifested appropriate strain-sensing capability in tensile test where a linear trend was observed in normalized resistance corresponding to the elastic region, followed by a nonlinear trend in normalized resistance at high strain which was attributed to formation of micro-crack in the specimens (Figure 1. 27c). A sensitivity of 0.43, the slope of the normalized resistance-strain curve, was obtained throughout tensile test where tunneling resistance was taken into account as the predominant mechanism, governing piezoresistive-sensitivity of the nanocomposite.

The reliability and reversibility of the developed sensors was examined using cyclic tensile loading at different strain level i.e. low, middle and high strain value (Figure 1. 27d). It was concluded that the strain sensor was reversible and repetitive in response of the cyclic loading when low and medium strain values, corresponding to the elastic region, applied to the specimen. On other hand, at high strain values

corresponding to the plastic region upon the removal of applied cyclic loading, the normalized resistance manifested irreversible behaviour where it did not go back to its initial states i.e. “normalized resistance=0”.

For the flexural test, similar to tensile test, the developed sensor was capable of monitoring strain increase, however a nonlinear trend was found in normalized resistance versus strain (Figure 1. 27e). In addition, the sensor could trace on-off loading in a reliable and repetitive manner as shown in Figure 1. 27f. Unlike the tensile test, lower change in normalized resistance in response of strain increase was obtained throughout flexural test compared to tensile test. This was attributed to loading condition where a complete axial load was applied to the tensile specimen whereas a combination of tension-compression loading was applied to the specimen in flexural test. As a result, throughout flexural test, simultaneous formation and destruction of conductive pathways in the compression and tension sides, respectively, neutralized their effects on piezoresistivity, thus, less change in normalized resistance as a function of strain increase was identified (Figure 1. 27g). On the other hand, in tensile test, simultaneous breakage of the electrical networks in the system manifested positive increase in piezoresistivity as a function of strain increase. In addition, the nonlinearity observed in bending test indicated that the effect of breakage of electrical networks dominated the piezoresistivity, thus, a nonlinear trend was observed.

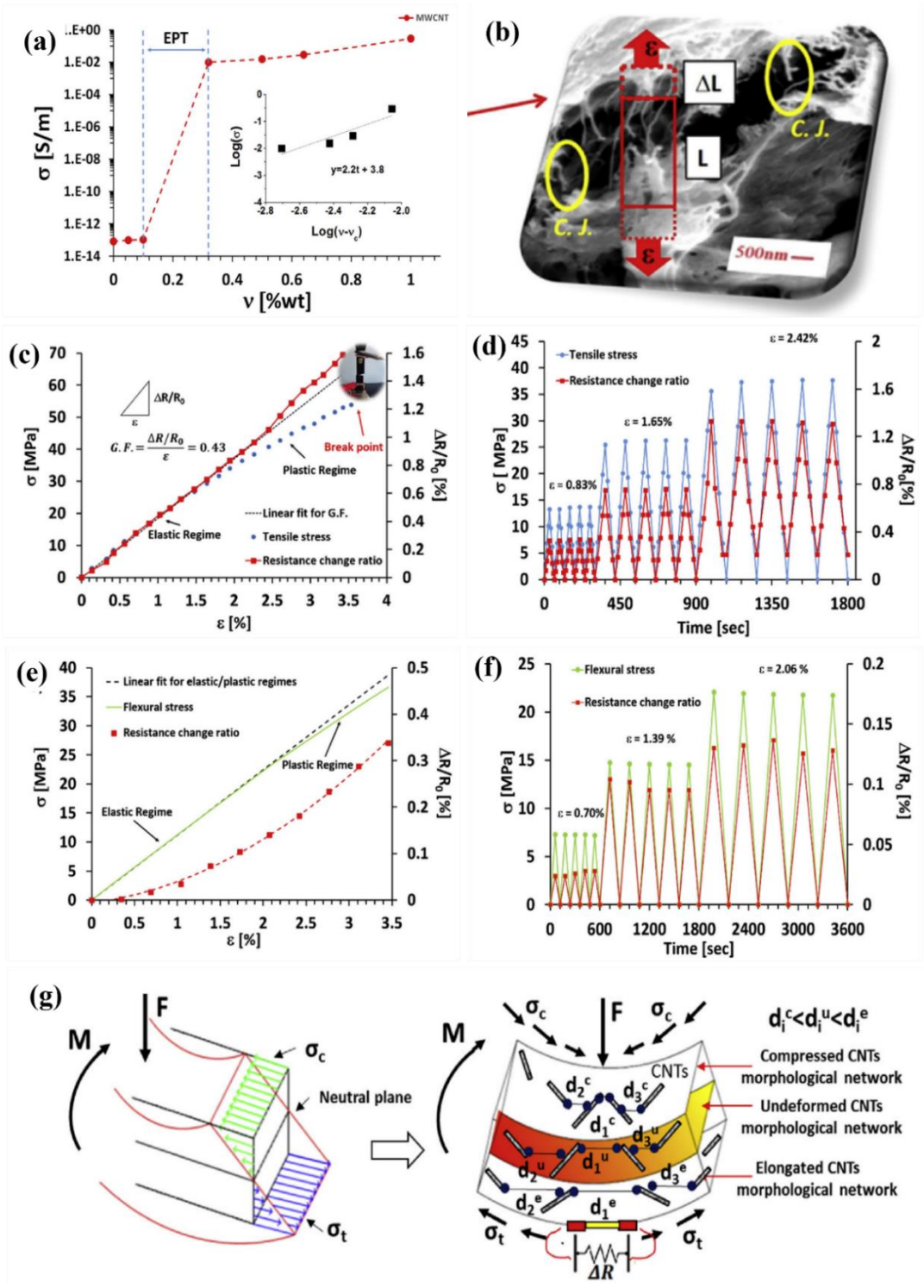

Figure 1. 27. MWCNTs doped epoxy: (a) Electrical conductivity, (b) conjunction bond, (c-d) piezoresistivity in tensile test subjected to static and cyclic loadings respectively, (e-f)piezoresistivity in flexural test subjected to static and cyclic

loadings respectively, (g) schematic illustration of piezoresistivity during flexural test [104].

However, different piezoresistivity behaviours were noticed in a study made by Gao et al. [45] where strain-sensing capability of MWCNTs doped epoxy subjected to quasi-static and cyclic tensile loadings were analyzed (Figure 1. 28). The electrical conductivity (Figure 1. 28a) increased by seven orders of magnitude at CNT loading above 0.025 vol % where a critical exponent t=4 was achieved, indicating the validity of measured percolation threshold region. For the strain monitoring, however, the normalized resistance increased by strain increase up to critical strain denoted ε_c, then reduced at higher strain values. The linearity was associated to synchronization of decrease of electrical contact points between neighbouring CNTs and increasing tunneling distance. This was further proven by equation 1.3 where a linear relation between strain and resiatcne changed was identified [119].

$$\frac{\Delta R}{R_0} = \exp[\gamma \delta_0 (cos^2\theta - \vartheta sin^2\theta)\varepsilon] - 1 \qquad (1.3)$$

$$\gamma = \frac{4\pi}{h}\sqrt{2m\emptyset}$$

Where ΔR is relative resiatcne change, R_0 the initial resistance, δ_0 the average inter-particle distance at zero strain, θ load angle with respect to the CNTs alignment, ε strain, $\emptyset$ potential barrier height, m electron mass, h Plank's constant.

By increasing strain up to critical strain, a balance took place between formation and breakage of electrical pathways, thus, a platform was observed (Figure 1. 28b). Then, the trend reversed where a nonlinearity observed at high stain, up to final failure resulted from reorientation of CNTs which was led to creation of more electrical pathways instead of electrical breakage, thus, in total normalized resistance decreased.

It is worth noting that this behaviour i.e. reduced piezoresistivity was not in agreement with majority of studies conducted on piezoresistivity performance of the CNTs doped epoxy nanocomposites where a monotonous increase in piezoresistivity until failure was obtained throughout tensile test [107,120–122].

Finally, the performance of the developed sensors were ascertained in cyclic loading (10 cycles) at different strain amplitudes (Figure 1. 28c), where the normalized resistance value could not go back to its initial states (zero) due to permanent damage and deformation in the system. Thus, the sensor could thoroughly predict residual damage in the system by showing nonzero normalized resistance after load relaxation.

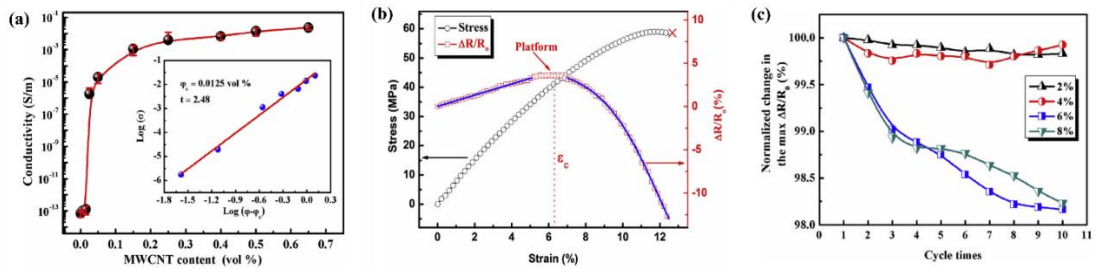

Figure 1. 28. MWCNTs/epoxy:: (a) electrical conductivity, (b-c) piezoresistivity performance in Quasi-static and cyclic tensile test respectively [45].

Piezoresistive behavior of CNTs doped epoxy was compared at bulk nanocomposite and thin film coating during tensile and bending tests as shown in Figure 1. 29 [106]. In tensile test, the thin film manifested higher sensitivity compared with bulk composite while a nonlinear and linear trend in piezoresisitivity were obtained respectively (Figure 1. 29a). In fact, a sensitivity of 5 and 1 at strain of 0.005 (mm/mm) were obtained for thin film and bulk nanocomposite during tensile test, respectively, which was attributed to higher impact of electrical breakage during loading on thin film with respect to the bulk nanocomposite.

In addition, both thin film and bulk nanocomposite showed much lower sensitivity throughout flexural text (Figure 1. 29b-c) with respect to tensile test (Figure 1. 29a) which was ascribed to simultaneous formation and breakage of electrical pathways in the compression and tension sides respectively. Interestingly, the thin film was capable of detecting type of stress applied to the specimen as two different trends in compression and tension sides were obtained (Figure 1. 29c) whereas a same trend was identified for bulk nanocomposite at both compression and tension sides (Figure 1. 29b).

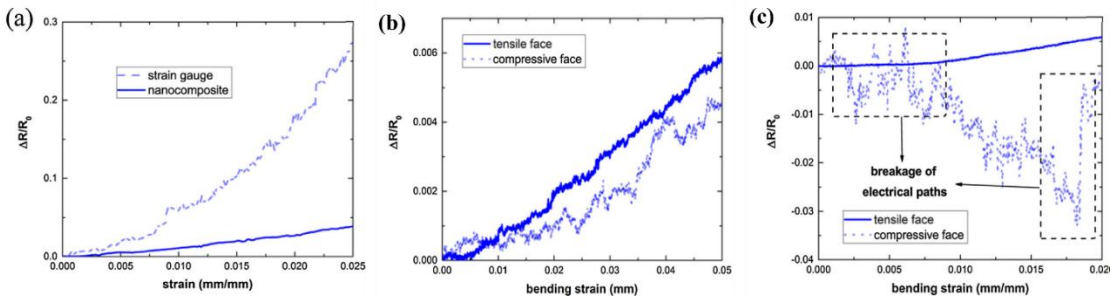

Figure 1. 29. Piezoresistivity of MWCNTs/epoxy at bulk composite and thin film coating: (a) tensile test, (b-c) bending test for the bulk material and thin film respectively [106].

In another study made by Sanli et al. [112], the piezoresistive performance of the MWCNTs/epoxy and conventional strain gauge, both connected to a cantilever beam subjected to cyclic tension and compression loading, were compared in terms of sensitivity, durability, stability, mechanical creep, response and recovery time, hysteresis, and temperature-sensitivity. Based on their results, the nanocomposite film manifested much better performance with respect to conventional strain gauge in terms of sensitivity of 78, appropriate stability of 0.26 % and durability of -0.08 % upon removal of cyclic loading.

In addition, it was also demonstrated better creep properties i.e. little creep of ± 0.26 %, quicker response and recovery times, and low hysteresis. Confinement impact of CNTs manifested in reducing the mobility of epoxy chain by CNTs accounted for improved stability of the MWCNTs/epoxy composite in creep properties. Higher response and recovery times were attributed to prompt rearrangement of CNT pathways within the matrix. Finally, the nanocomposite could successfully monitor the temperature variation when the specimen subjected to heating/cooling cycles, manifested negative and positive changes in relative resistance respectively.

Rams et al. [107] investigated strain sensing capability of AralditeLY556 epoxy with amine hardener XB3473 reinforce with MWCNTs (0.1wt.% and 0.3wt.%) where a calendering method was used for the CNT dispersion. The nanocomposite loaded at 0.3wt.% manifested higher sensitivity compared to 0.1wt.%, though both sensors showed linear trend in piezoresistivity. In fact, it has been challenging to scientists to find out the optimum weight concertation of conductive fillers in which the maximum piezoresisitivity performance was obtained. This i.e. the change in sensitivity with respect to CNT content was broadly investigated by scholars in which they showed the maximum piezoresistive-sensitivity was obtained near percolation threshold region (at upper bound) [30,37,119,123,124].

Sanli et al.[30] investigated the piezoresistive behaviour of epoxy thin film when different MWCNT loadings were used (Figure 1. 30a). According to their results, the sensitivity of the thin film decreased by increasing CNT contents. In fact, sensitivity of 15.39, 8.37, 3.85, 3.04, and 2.86 were obtained for 0.3 wt.%-1 wt.% CNT content, respectively, which were much higher than traditional strain gauge with gauge factor around 2. In addition, the normalized resistance trend was also changed as a function of CNT loading i.e. a nonlinear piezoresistivity was identified at low CNT

concentration whereas the nonlinearity decreased by increasing CNT contents as shown in Figure 1. 30a.

Similar behaviour was also noticed in another study in which deferent MWCNTs (1wt.%-5wt.%) were used as thin film coating applied on the surface of a cantilever beam subject to an axial tension loading (Figure 1. 30b)[37]. For comparison, they have also plotted the piezoresistive performance of a traditional strain gauge. It was concluded that sensitivity of the composites decreased at high CNT loading whereas low CNT content manifested the highest gauge factor along with higher nonlinearity. In fact, a sensitivity of 16 was detected for the thin film coating at 1 wt.% which is 8 times bigger than the sensitivity of a traditional strain gauge.

The variations in piezoresistivity trend and sensitivity as a function of CNT content were related to different mechanisms ruling electromechanical properties. In fact, at low CNT contents, especially near the percolation threshold, tunneling effect was the predominant mechanism in governing the piezoresistivity due to less amount of CNTs, thus, less content of electrical networks throughout the matrix.

On the other hand, by increasing CNT content, the number of electrical pathways gradually increased in which the loss of electrical contact amongst neighbouring CNTs accounted for the reduced sensitivity. As a result, in order to reach higher piezoresistive-sensitivity performance, a CNT content near percolation threshold should be used. It is worth noting that other factors including CNT dispersion, aspect ratio of CNTs as well as the potential barrier of the matrix are also important in gaining the maximum sensitivity.

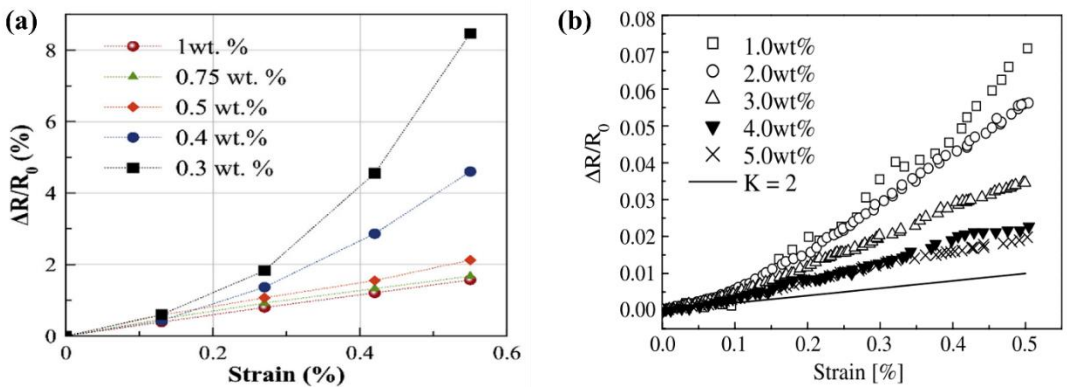

Figure 1. 30. Piezoresistivity performance as a function of CNTs loading: (a) [30], (b) [37]

1.3.2.2.Hybrid CNTs-nanoclay/epoxy

This section concentrates on electrical conductivity and piezoresistivity performance of the epoxy based nanocomposite in ternary state i.e. synergetic addition of CNTs and nanoclay. In spite of numerous works on mechanical and thermomechanical properties of hybrid CNTs and nanoclay nanocomposites, as discussed in section 1.3.1.3, less number of works has been conducted on their electromechanical properties[125,126]. Indeed, all of the aforementioned studies mainly concentrated on electrical conductivity of the CNT-nanoclay hybrid nanocomposites whereas no report about their piezoresistivity performance in ternary states was found in the literature.

Ayatollahi et al. [125] investigated mechanical and electrical properties of epoxy reinforced with hybrid MWCNTs and nanoclay. As it is shown in Figure 1. 31a, the as-received nanoclay manifested a peak at 5˚ whereas a broader peak at smaller angle was identified for both binary and hybrid nanocomposites, thus, nanoclay composite demonstrated larger d-spacing with respect to the as-received nanoclay. In

addition, the binary state i.e. MWCNTs/epoxy, manifested a conductivity of 10-5 S/m whereas introduction of nanoclay into the CNTs doped epoxy i.e. at ternary state substantially reduced the electrical conductivity (Figure 1. 31b). This was related to lack of conductivity of nanoclay that hindered formation of electrical networks within the matrix upon their addition to CNTs doped epoxy.

On the other hand, in another study made by Liu et al. [126], introduction of nanoclay resulted in improving CNTs dispersion, thus, better mechanical and electrical properties were achieved. Based on their result, addition of 2 wt.% nanoclay could substantially increase electrical conductivity of CNTs doped epoxy, in particular at low CNT loading (Figure 1. 31c). It is worth noting that not only electrical conductivity was improved, but also lower percolation threshold was obtained in ternary state (CNTs-nanoclay/epoxy) with respect to the binary state (CNTs/epoxy). In fact, a percolation threshold of 0.01 wt.% was achieved for ternary nanocomposite whereas 0.5 wt.% was the percolation threshold for binary state. In order to find out the optimum nanoclay loading in tailoring electrical conductivity, CNT content was kept constant at 0.05 wt.% while nanoclay loading was varied (Figure 1. 31). It was found out that the 0.2 wt% nanoclay loading showed higher electrical conductivity with respect to 2 wt.% and 5 wt.%. The reduction of electrical conductivity at high nanoclay content was attributed to weak CNT dispersion arisen from high viscosity of the mixture, thus, deteriorating the formation of electrical networks within the matrix. Furthermore, introduction of nanoclay to CNTs/epoxy caused further improvement in storage modulus with respect to the binary state, though the glass transition temperature slightly reduced at ternary state compared with binary composite.

Serval reasons were accounted for enhancing CNT dispersing and electrical conductivity in ternary composite. First, introduction of nanoclay resulted in further

increase in viscosity, thus, hindering CNTs re-agglomeration during nanocomposite manufacturing. Second, micro-scale lateral size of nanoclay efficiently formed isolated CNTs regions. Finally, CNTs were inclined to create strong interaction with nanoclay rather than the epoxy due to negative surface charge of the nanoclay. In totals, they indicated that nanoclay could be successfully used as a novel method in improving CNTs dispersion in which other method such as CNTs functionalization and chemical surfactant manifested some disadvantages.

As it was shown, different results in terms of electrical conductivity in ternary epoxy nanocomposite reinforced with CNTs and nanoclay make it more complicated to thoroughly interpret the multifunctional properties of the hybrid CNTs-nanoclay epoxy composite. Indeed, the discrepancy observed in ternary states in addition to no report on piezoresistive characteristics of the ternary nanocomposite necessitate further investigations on the electromechanical properties of CNTs and nanoclay hybrid states. This is one of the focuses of this thesis that are explained well in the next sections.

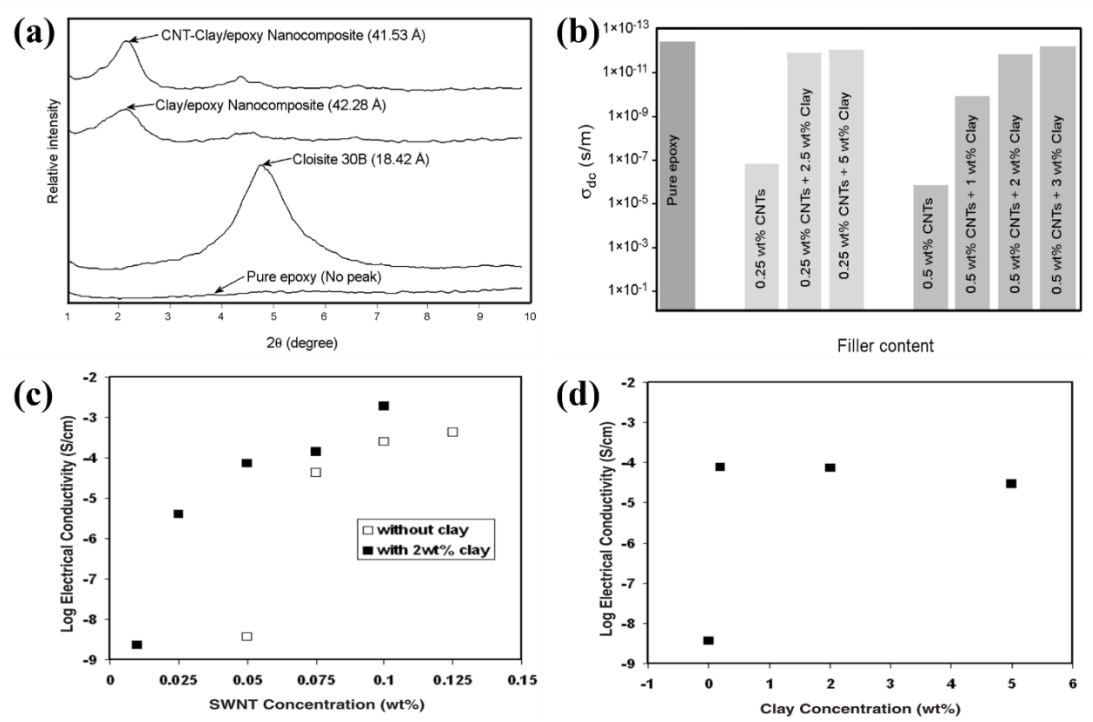

Figure 1. 31. Ternary epoxy nanocomposite using CNTs and nanoclay: (a-b) XRD analysis and electrical conductivity respectively [125], (c-d) improving electrical conductivity by addition on nanoclay into CNTs doped epoxy [126].

1.4. Challenges

As discussed in section 1.3.2, large discrepancies were notified for the epoxy based nanocomposites at both binary and ternary states in terms of mechanical, electromechanical and thermomechanical properties. This was mainly attributed to presence of some manufacturing defects including agglomeration, in particular for CNTs, and void and bubbles entrapped in the epoxy mixture due to improper degassing. In fact, most of the heterogeneities were related to poor dispersion of the nanofiller that played a significant role in effective exploitation of nanofillers in tailoring multifunctional properties of epoxy doped nanocomposites. As a result, in the following section, the typical dispersion methods used for polymer nanocomposites are compared.

Finally, the importance of degassing on final mechanical properties of the nanocomposites is explored.

1.4.1. Nanofiller dispersion

Figure 1. 32 shows the most common mechanical dispersing methods used for polymer nanocomposites. Sonication also known as ultrasonic homogenizer was most likely the most typical dispersion method used in nanocomposite due to minimum waste as its main advantage compared to other methods in addition to its high user-friendly. Nanofillers damage especially when high sonication time and power used was the main drawback of probe-sonication [127]. It is worth noting that selecting appropriate sonication parameters including time and power was case specific due to the damage that sonication might induce into nanofiller. This was also studied by researchers to find out the effect of different sonication parameters on final mechanical and electromechanical properties of epoxy nanocomposites [32,128].

Three roll mill method also known as calendering method was another typical procedure used for nanofiller dispersion in which shear forces exerted by the rollers caused dispersion of nanofillers. This method was taken into account as the most efficient method in breaking CNTs aggregates into smaller pieces especially when viscosity was high [69]. On the other hands, nanofillers wastes and the gap size limitation (1-5 μm) made some concerns for effective usage of this method for some purposes [129]. It is worth noting that the feeding materials must possess appropriate viscosity, therefore, calendering method might not be an appropriate method for low viscous material such as thermoplastics [129].

Another methods used in polymer nanocomposite is ball milling where the

nanomaterials grinded into smaller pieces like powders by applied pressure from rotating balls. This methods was typically used to transform nanofillers to smaller size such as CNTs to nanoparticles [130]. In addition, ball milling has also being used for breaking the intercalated clay galleries and converting them to exfoliated clay structure [82]. It is worth noting that this method was less attractive as dispersion technique due to the fact that it changed the nanofiller aspect ratio and morphology, thus, it was used as a pre-dispersion tool in order to change the nanomaterial into desired forms [129].

Finally, high shear mixing method also called toroidal method was another technique used for polymer nanocomposites. The shape and size of mixing blade along with the rotational speed and temperature were the main parameters affecting the dispersion states of the nanofiller. In fact, as shown in in Figure 1. 32, throughout this method, degassing under controlled temperature could be carried out, which is very helpful in efficient removal of air bubbles, in particular, when high viscos materials are treated. This method was one of the most common methods for clay based nanocomposites due to its cost-effectiveness, and easy procedure [53]. The homogenization effect of this method was also demonstrated by Sánchez-Romate et al. [23] in which an effective breakage of large CNT aggregates into tiny pieces took place i.e. toroidal could successfully reduce the CNT aggregates and reduced them homogeneously in the matrix. This was related to 3-D shear forces excreted by propeller leading to better homogenization effect. Apart from mechanical dispersion methods, chemical surface functionalization was another widely used method in order to improve their dispersion as well as their interfacial reaction with epoxy.

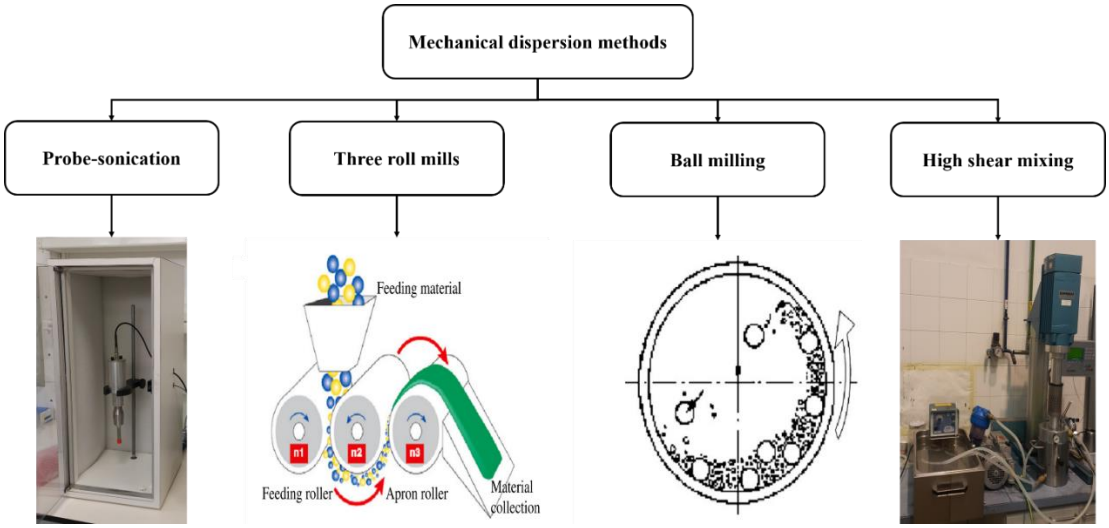

Figure 1. 32. Mechanical dispersion techniques used for polymer nanocomposite, the schematic illustrations of three roll mill and ball milling were reprinted from [129].

1.4.2. Degassing

Few studies showed some reductions in tensile strength by introducing nanofillers to the epoxy matrix whilst fracture toughness increased [43,131–133]. This was mainly attributed to presence of aggregates, formation of voids and ineffective load transfer between the CNTs and the epoxy, especially when high CNT loading were used. In fact, the brittleness of the epoxy caused the material to be very susceptible to imperfections, particularly in the form of bubbles and voids, resulted in significant reduction of the mechanical properties. The detrimental effects of voids over the mechanical properties were well addressed in the literature, concluding that degassing was a critical step to be carried out in order to minimize the void contents [134–138].

Ashir et al. [135], investigated harmful effect of remaining voids on mechanical properties of CFRP composites. Tensile strength dropped by 10 % at 2 % void contents. Flexural and impact strengths also decreased by 4 %and 26 %, respectively, at 6 % void content. Similar behaviours were also observed in a study performed by Liu et al. [138]

in which tensile, shear and flexural strengths substantially reduced by increasing void contents i.e. a reduction of 18 %, 22 %, and 28 % were distinguished for tensile, shear and flexural strengths respectively. This indicated that mechanical properties dramatically dropped by presence of void content. Significant reduction in electrical conductivity in response of air bubbles was also reported in the literature i.e. a reduction of 580 % was seen in a sample with high amount of voids with respect to the sound sample [137].

In summary, agglomeration and presence of voids are still the main challenges for epoxy-based composites. Although many attempts have been performed to overcome aforementioned issues as discussed above, further investigations are needed in order to achieve better results in terms of multifunctional properties.

1.5. Application

As discussed in the previous sections, epoxy was the main matrix for CFRPs and GFRPs manufacturing industry in which they mostly used in aerospace applications as shown in Figure 1. 1 [1,12,139]. In contrast, the growing developments in such state of the art technology necessitated creating highly advanced composite materials to meet customer's demands. Therefore, to create superior materials for such applications, it is important to developed novel materials in which they possess not only proper mechanical properties, but they can also improve the electrical conductivities of the bulk composite.

This improvement in electrical conductivities of epoxy nanocomposites and its consequences piezoresistive-sensitivity have shown to provide self-sensing capability to the host materials, such as epoxy in the case of CFRP and GFRP composites, which

can be used for SHM [88,89]. In other words, CNTs/epoxy composites can be used as an embedded sensor in the composite materials used for aircraft industry, and thus save people's life and cost by earlier detection of damage and failure in the system. In this context, CNTs doped epoxy materials, were employed in different ways including bulk materials [45,103], thin film coating [120,140], CNTs coated fibers embedded in CFRPs and GFRP composites [109,110] as shown in Figure 1. 33a-c respectively.

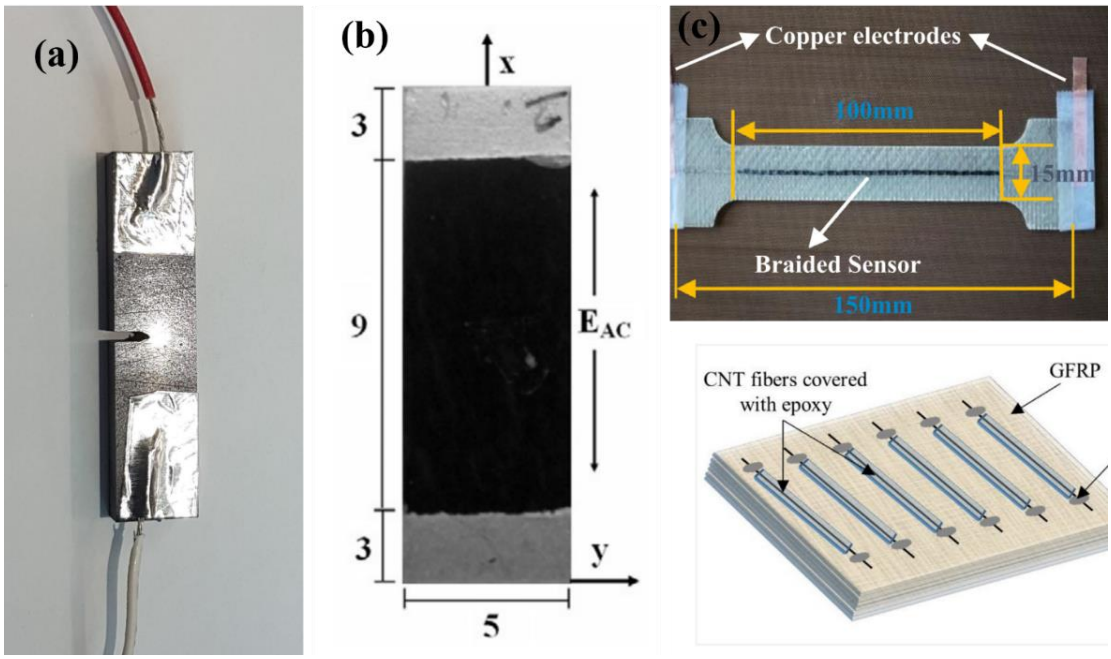

Figure 1. 33. Different types of sensor based epoxy reinforced with CNTs: (a) bulk materials, (b) thin film coating applied on aluminum substrate[120], (c) CNTs coated fibers embedded into GFRPs upper and lower image were taken from [109,110] respectively.

Moreover, conductive adhesive i.e. CNTs doped epoxy demonstrated appropriate performance in traditional soldering methods used to joint silicon wafers in solar cells [141]. Wearable technology is another application of CNTs based composites where physical performance of the human body can be monitored for

medical and athletics purposes [142]. High thermal and mechanical properties of nanoclay also led to numerous usages of epoxy based nanocomposites reinforced with nanoclay such as automobile, electronic, aerospace industries. In summary, many applications can be achieved by combining CNTs and nanoclay into epoxy as shown in Figure 1. 34 at their binary states. Thus, synergetic addition of nanoclay and CNTs may provide much more alternatives for growing demand in highly sate of are technologies, in particular, for aerospace and biomedical applications.

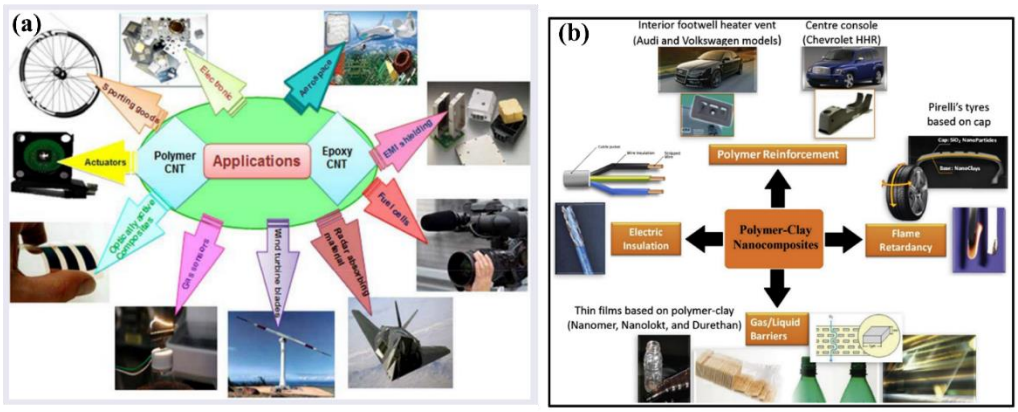

Figure 1. 34. Application of epoxy based nanocomposite: (a) CNTs [143], (b) nanoclay [49].

1.6. Novelty

As discussed in previous sections, epoxy is one of the most commonly thermosetting polymers used in different industrial sectors because of its outstanding characteristics including low shrinkage, high tensile strength, and appropriate thermal and chemical resistance [9]. However, some drawbacks of epoxy including high crosslink density manifested epoxy as highly brittle materials; besides the growing demands in industry in terms of creating novel-engineered composite materials such as

conductive polymer composites has led to numerous research in exploitation of nanoreinforcement, particularly for hybrid nanocomposites, in tailoring multifunctional properties of epoxy, thus epoxy based nanocomposites is introduced [5,6]. In addition, since structural composites are typically subjected to a variety of loading situations such as shock-loading and impact, it is necessary to monitor the health of the whole structure during its operation to avoid potentially catastrophic failures.

CNTs have outstanding electrical conductivity and mechanical property along with high aspect ratio and low density which brought about extensive research on tailoring properties of polymer based composites. CNTs doped epoxy nanocomposites has been widely used as a smart material for real-time monitoring of deformation and damage initiations in a system i.e. introduction of CNTs to the epoxy assigns a strain sensing capability to the bulk composite itself, which can be used as a damage-detecting sensor capable of self-monitoring defect initiation throughout the whole structure [33]. Moreover, nanoclay has the potential to toughen the epoxy resulting from its excellent performance in acting as crack barrier as well as flame retardancy [49]. They have high surface energy and high aspect ratio, low cost in which make it a good candidate to be used for advanced composites.

Many works have been done on multifunctional properties of CNTs based epoxy and nanoclay based epoxy, however, less attempts have been carried out on their hybrid effects in multifunctional properties. In addition, piezoresistive characteristics of CNTs/epoxy under tensile and bending tests were well reported in the literature whilst the piezoresistive behaviour of the CNTs/epoxy under fracture test has not been addressed.

Although many studies have been conducted at binary state i.e. CNT/epoxy and nanoclay/epoxy as discussed before, the synergistic effects of CNTs and nanoclay in

creating high performance materials have been investigated to a much lower extent [54,58,59,84–86]. However, most of the aforementioned studies have focused on the exploitation of the concurrent effects of both nanofillers in tailoring mechanical, thermal and flame retardancy of the epoxy based nanocomposites. Electrical conductivity of the hybrid epoxy nanocomposite using CNTs and nanoclay has also been studied by Liu et al. [126] and Ayatollahi et al. [125] and contradictory behaviour in electrical conductivity was observed. In other words, the former could increase electrical conductivity at hybrid state (CNTs-nanoclay/epoxy) with respect to the binary state (CNT/epoxy) whereas the latter showed a decrease in electrical conductivity. This necessitates further investigation of the electrical properties at hybrid state to examine the effect of nanoclay addition on the electrical performance of CNTs doped epoxy. To the best of our knowledge, no study has been performed on the piezoresistive characterization of hybrid CNTs-nanoclay doped epoxy.

1.7. The purpose of this study

As a result, this study is aimed to investigate synergetic effects of addition of CNTs and nanoclay on multifunctional properties of epoxy based nanocomposites in terms of tensile strength, fracture toughness, electrical conductivity and piezoresistive characteristics in order to meet the requirements of the industrial applications. It is worth noting that the effect of using various types of CNTs i.e. SWCNTs and DWCNTs at both binary state (CNTs/epoxy) and ternary state (CNT/nanoclay/epoxy) is one innovative part of this study because less research was conducted on comparison of the effect of using different CNTs on electromechanical properties of the epoxy. Based on the above-mentioned problems, the aim of this work can be summarized as following:

- Finding the optimum weight concentrations of CNTs and nanoclay in order to achieve a balanced mechanical and electromechanical property.
- Identifying the appropriate manufacturing method to achieve homogenous dispersion of nanofiller in both binary and ternary states.
- Investigation of the effect of using different CNTs, various aspect ratios, and various morphologies i.e. SWCNTs and DWCNTs on final mechanical and electrical properties.
- Creating a novel method in improving CNTs dispersion using nanoclay, thus, enhancing mechanical and electromechanical properties in ternary state compared with the binary composite.

1.8. Structure of the thesis

This thesis summarizes the main experimental findings obtained in the nanocomposites produced in both binary and ternary states in terms of mechanical properties, electrical conductivity and piezoresistivity performance of the nanocomposite. Chapter 2 discusses the experimental approaches employed along with a detail of the electromechanical tests performed for the analysis. Chapter 3 to 7 are a summary of either the related papers published or currently under review i.e. chapter 3-5 are related to the phase 1 of the project while chapter 6-7 are associated to phase 2. Chapter 3 deals with mechanical and electromechanical properties of SWCNTs/epoxy produced in phase 1 in which the results already published in a highly prestigious journal [46]. Similarly, chapter 4 investigates the piezoresistivity performance of DWCNTs/epoxy created in phase 1 in which the results recently accepted to be published in journal of "Polymer Composite". Chapter 5 mostly focuses on mechanical

performance of the SWCNTs/epoxy and DWCNTs/epoxy, both produced in phase 1 because the previous chapters i.e. chapter 3 and 4 mainly concentrate on electromechanical properties.

Chapter 6 examines mechanical, electrical and piezoresistive characteristics of the DWCNTs-nanoclay/epoxy fabricated in phase 2. Chapter 7 is the same analysis, however for SWCNTs-nanoclay/epoxy. Chapter 8 presents all data obtained in this study in a more global way to ease the comparison between different types of the nanocomposite produced in this study. In this content, chapter 8 is divided into three main subsections i.e. phase 1, phase 2, and phase 1&2 together. Finally, the most important outcomes of this thesis are summarized in the conclusion.

CHAPTER 2: EXPERIMENTAL METHODOLOGY

Throughout this chapter, the materials and the experimental approaches are explained in details. Taking into account the main purposes of this study, developing an enhanced epoxy based nanocomposites using hybrid CNTs and nanoclay in terms of mechanical, electrical, and electromechanical characteristics.

Therefore, two different phases are defined in this study in situ sample productions i.e. phase 1 and 2. The former mostly focuses on multifunctional properties of binary composite i.e. CNTs/epoxy whereas the latter concentrates in ternary states i.e. CNTs-nanoclay/epoxy.

2.1. Materials

Araldite LY556 resin and amine based hardener XB3473 provided by Hunstman were used for the matrix. It is an aerospace epoxy grade with low viscosity, ideal candidate for CNTs dispersion. Electrical conductivity, tensile strength and fracture toughness of the pristine epoxy (K_{IC}) were 10 -11 S/m, 46 MPa and $0.77MPa\sqrt{m}$ respectively.

For the nanomaterials, different kinds of nanomaterials including SWCNTs, DWCNTS, and Shelsite 30B Montmorillonite also known as nanoclay were used in this study. Their detailed information can be found in Table 2. 1. It is worth noting that DWCNTs contained a mixture of SWCNTs and DWCNTs, hereinafter called DWCNTs.

Table 2. 1. The Materials Specifications

Martial	Specifications
Epoxy	Araldite LY556 and amine hardener XB3473
SWCNT-OH	Outer diameter: 1-2 nm, Length: 10-30 µm, Purity > 99 wt%, functional content: 3.96 wt. %, Ash< 1.5 wt. %)
SWCNT/DWCNT	Outer diameter: 1-2 nm, Length: 3-30 µm, Purity: >99wt%, Ash: 0wt %
Nanoclay	Shelsite 30B Montmorillonite Nanopowder, (Purity: 99%, APS: <80nm

Figure 2. 1 shows field emission scanning electron microscopy (FESEM) image of the nanomaterials used in this study. As discussed previously, different CNT morphologies i.e. SWCNTs and DWCNTs were used to compare their effects on mechanical and electromechanical properties of the epoxy based nanocomposites. From Figure 2. 1 and Table 2. 1, it can be concluded that SWCNTs have higher aspect ratio compared to DWCNT. This along with larger SSA of SWCNTs with respect to the DWCNTs lead to higher CNT agglomeration in the former. An intercalated structure can be seen for the as-received nanoclay as shown in Figure 2. 1 in which its platelet morphology with respect to cylindrical shape of CNTs can be easily detected.

High amount of agglomerations, appeared for both CNTs and nanoclay in their pristine states, necessitate using appropriate dispersion technique for nanocomposites manufacturing, in particular in the ternary states, where two different fillers are expected to incorporate into epoxy. In this context, a comprehensive trial and error

experiment was performed during dispersion of nanofiller into epoxy in binary state that are discussed later in detail. Consequently, a modified dispersion approach was used for the phase 2 based on the performance obtained in phase 1.

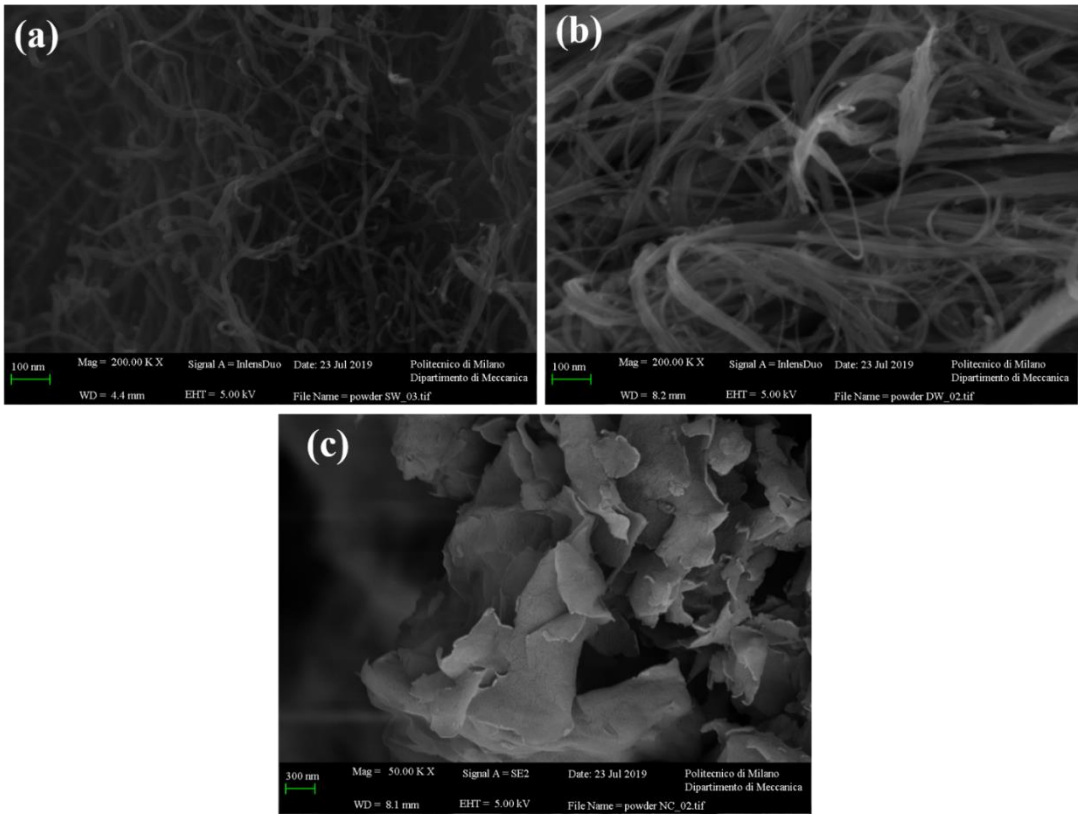

Figure 2. 1. Nanomaterial: (a) SWCNTs, (b) DWCNTs, (c) nanoclay.

2.2. Nanocomposite manufacturing

As mentioned in the previous section, this project was divided into two main phases (Figure 2. 2). In the first phase, different CNTs morphologies and weight concentrations (0.25, 0.5 and 0.75 wt.%) were used. This was important to find out the appropriate CNT loading along with identifying the optimum manufacturing procedure, being used in phase 2. As a result, methodological approaches used in phase 2 were selected based on the performance in phase 1. For the phase 2, CNTs

content was kept constant while two different nanoclay loadings were used for the ternary states. It is worth nothing that a binary state composite containing 0.1 wt.% CNTs was also produced in the second phase along with the ternary composites as a reference material.

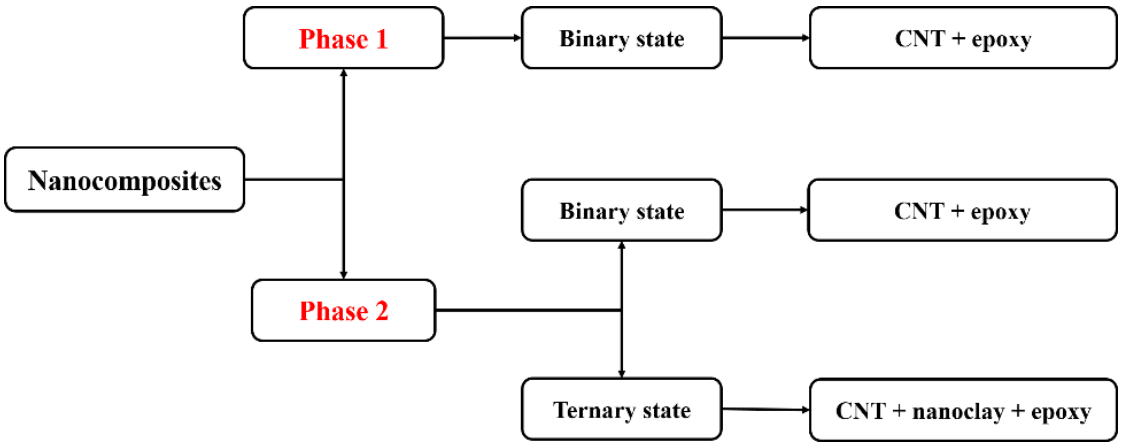

Figure 2. 2. Different phases of the project.

2.2.1. Phase 1

In the first phase, a comprehensive study was performed to compare the effect of introduction of different CNTs morphology (SWCNTs and DWCNTs) and weight concentrations on mechanical and electromechanical properties. It should be noted that manufacturing procedures as well as the CNTs loading used in phase 2 were selected based on the outcomes of this phase. Figure 2. 3 shows the manufacturing details used in phase 1.

Varying CNTs weight concentrations of 0.25 wt.%, 0.5 wt.%, and 0.75 wt.% were used to compare their mechanical, electrical and piezoresistive behaviour and to correlate the microstructures obtained at each weight concentration to the electromechanical properties of the specimen. A releasing agent named Frekote 700-

NC purchased from Henkel was applied to the mold surfaces to ease the plate separation after final curing.

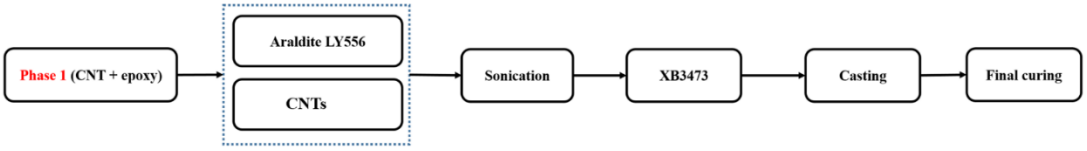

Row	Filler	Wt.%	Manufacturing methodology	Number of specimen		
				Tensile	fracture	impact
Neat epoxy	----	----	(i) Sonication for 30 min (400 W and 24KHz), (ii) degassing at 70 C° for 30 min, (iii) adding hardener, (iv) casting into an open mold at 140 C° for 8 hrs	6	10	9
Phase 1	SWCNTs	0.25		3	3	9
		0.5		3	3	9
		0.75		3	3	9
	DWCNTs	0.25		3	3	9
		0.5		3	3	9
		0.75		3	3	9
Total test performed				24	28	63

Figure 2. 3. Manufacturing procedure for phase 1.

It is worth noting that regardless of CNTs morphology and content, same manufacturing procedure was used for all nanocomposites in order to thoroughly compare the effect of only one parameters, CNTs morphology and content, on final mechanical and electromechanical properties, not other factors such as manufacturing parameters. In situ manufacturing, first, the resin and CNTs were mixed together manually followed by sonication (Hielscher UP400S) for 30 min to break the aggregates (maximum 50 C° temperature was recorded during sonication). The sonication was carried out using 50 % of amplitude and a cycle of 0.5 s (the maximum power and frequency were 400 W and 24 kHz). As mentioned in the introduction, due to CNT damage resulting from high sonication time, constant sonication parameters were used at all CNT loadings to assure the same amount of CNT damage manifested in all the specimens, thus, without additional detrimental effect on the piezoresistive behaviour.

A high number of air bubbles were entrapped in the epoxy as shown in Figure

2. 4a. Due to high viscosity of the mixture upon addition of the CNTs, a degasification was carried out to evacuate air bubbles entrapped in the resin. The resin was degassed at an elevated temperature of 70 C˚ for 30 minutes, as the viscosity of the epoxy is low at higher temperature. Then, amine hardener was added to the mixture at a weight ratio of 100:23 g i.e. Araldite LY556: XB3473, and cast into an open mold of 196×145× 5 mm dimension (Figure 2. 4b). Finally, the nanocomposite was cured in an oven at 140 C˚ for 8 hr. Top surface of the plates was machined in order to prepare flat samples and remove any remaining voids after curing.

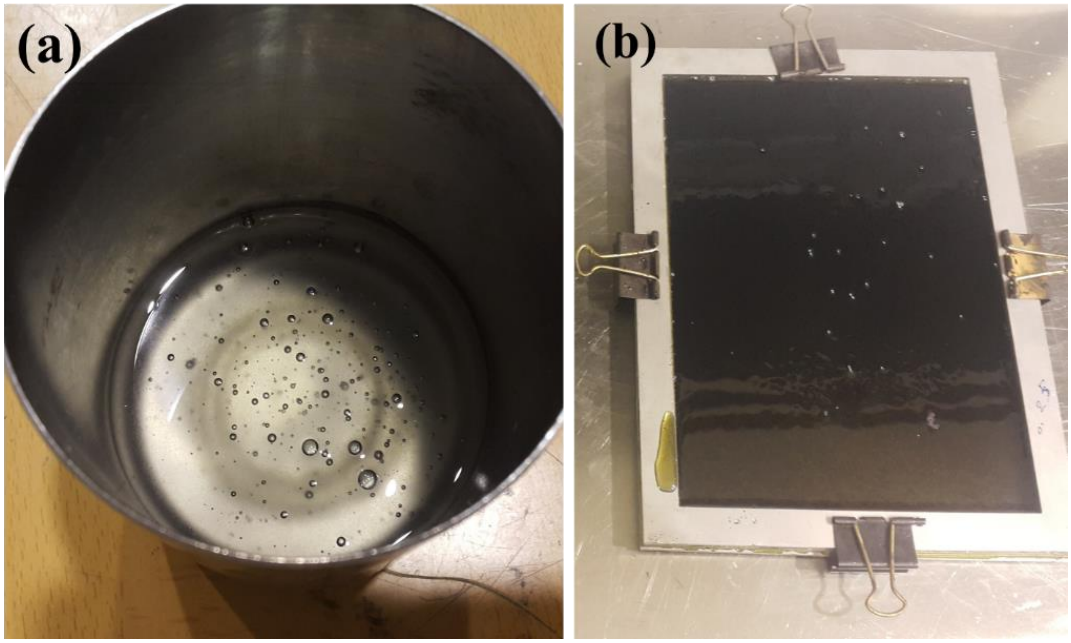

Figure 2. 4. (a) Presence of air bubbles within the resin, (b) casting CNTs/ epoxy mixture into open mold.

2.2.2. Phase 2

Figure 2. 5 illustrates the manufacturing details used in phase 2. It is worth noting that two different nanocomposites including binary and ternary states were

produced while same manufacturing methodology was employed. The former was produced as a reference for the results comparison. In fact, CNTs were used to induce electrical conductivity and piezoresistive characteristics to the epoxy while nanoclay was employed to further improve fracture toughness and CNT dispersion. Therefore, a constant CNT content (0.1 wt.%) was used for the hybrid composites whereas the weight concentration of the nanoclay was varied i.e. 0.5 wt.% and 1 wt.%. The CNT loading used in this study (0.1 wt.%) was selected based on the percolation threshold region reported in the literature for similar CNTs doped epoxy based materials, showing a percolation threshold region around 0.1 wt.% [25].

Although most of the literature used high nanoclay loading (1-5 wt.%) to achieve appropriate mechanical properties, some restrictions in this study such as proper electrical conductivity and appropriate piezoresistivity in the hybrid states, caused to use relatively low amount of nanoclay in this study (0.5 and 1 wt.%). In addition, due to high viscosity at hybrid states and in order to facilitate the fabrication process, a CNT loading of 0.1 wt.% was used in phase . It is worth mentioning that a percolation threshold region around 0.1-0.3 wt.% was found for CNT doped epoxy based materials [25]. This was also in agreement with the experimental results in phase 1 in which percolation threshold region between 0.1 to 0.3 wt.% was obtained. As a result, it can be stated out that the nanofiller contents (CNT and nanoclay) were selected by taking into consideration of the performance of the materials developed in phase 1 as well as the manufacturing difficulties at hybrid states. . Same approach was used to optimize manufacturing process in phase 2.

The main steps of the nanocomposite fabrication are shown in Figure 2. 5. A more homogeneous dispersion of nanofillers and a minimum void content was achieved by a combination of toroidal stirring using Dispermat dissolver and ultra-sonication by

Hielscher UP400S at 50 % amplitude and 0.5 sec cycle. The mixture was simultaneously degassed during toroidal stirring at a constant temperature of 60 ˚C throughout the entire manufacturing process.

The combined dispersion method was conducted as follow: (i) the CNTs/epoxy mixture was stirred using high shear mixing method also called toroidal method at 5500 rpm for 10 min, (ii) sonication for 15 min, (iii) toroidal stirring at 2000 rpm for 10 min, (iv) sonication for 15 min and (v) toroidal stirring at 50 rpm for 30 min. Upon the completion of nanoparticles dispersion, the hardener was added to the mixture and cast into an open mold of 196×145×5 mm dimension. Finally, the samples were cured at 140 ˚C for 8 hours. It should be noted that nanoclay was added to the CNTs doped epoxy mixture at stage (iii).

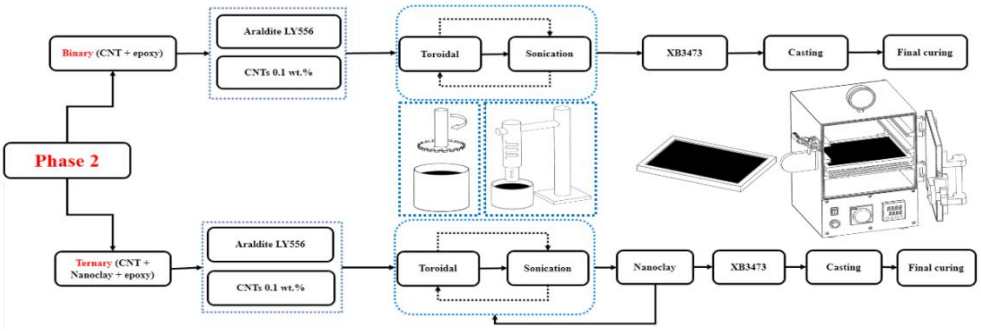

Row	Filler	Wt.%	Manufacturing methodology	Number of specimen	
				Tensile	fracture
Binary 2	SWCNTs	0.1	(i) toroidal stirring at 5500 rpm using a Dispermat dissolver for 10 min, (ii) probe sonication using Hielscher UP400S at 50% of amplitude and a cycle of 0.5 s for 15 min, (iii) toroidal stirring at 2000 rpm for 10 min, (iv) sonication for 15 min, (v) (v) toroidal at 50 rpm for 30 min.	6	5
	DWCNTs	0.1		6	5
Ternary*	SWCNTs/NC	0.5		6	5
		1		6	5
	DWCNTs/NC	0.5		6	5
		1		6	5
Total test performed				36	30
* CNT content was kept constant (0.1wt.%) for all ternary nanocomposites whereas two different nanoclay loading, 0.5-1wt.% were used.					

Figure 2. 5. Manufacturing procedure for phase 2.

2.3. Sample preparation

Upon curing the specimen, the top surface of the cured plates was subjected to machining to provide more flat surface and to remove possible voids left in the specimen (Figure 2. 6a). Tensile, impact and fracture specimens were cut from the casted plate using waterjet (Figure 2. 6b), according to ASTM D638, ASTM D4812, and ASTM D5045, respectively (Figure 2. 6c-e). Six, nine and five specimens were prepared for tensile, impact and fracture tests, respectively.

It is worth noting that the impact test were performed only in phase 1. For the fracture test, a tiny crack (Figure 2. 6g-h) was introduced into the single-edge notch bending (SENB) specimens using a new razor blade each time to assure minimum fracture toughness i.e. to obtain the critical stress intensity factor (K_{IC}) and critical strain energy release rate (G_{IC}). To improve repeatability, the pre-crack was created with a machine holding the razor blade (Figure 2. 6f) and sliding the specimen while a constant load of 50 N was applied. The method allowed providing pre-cracks with 80 µm to 150 µm length dispersion (measured with optical microscope as in Figure 2. 6h).

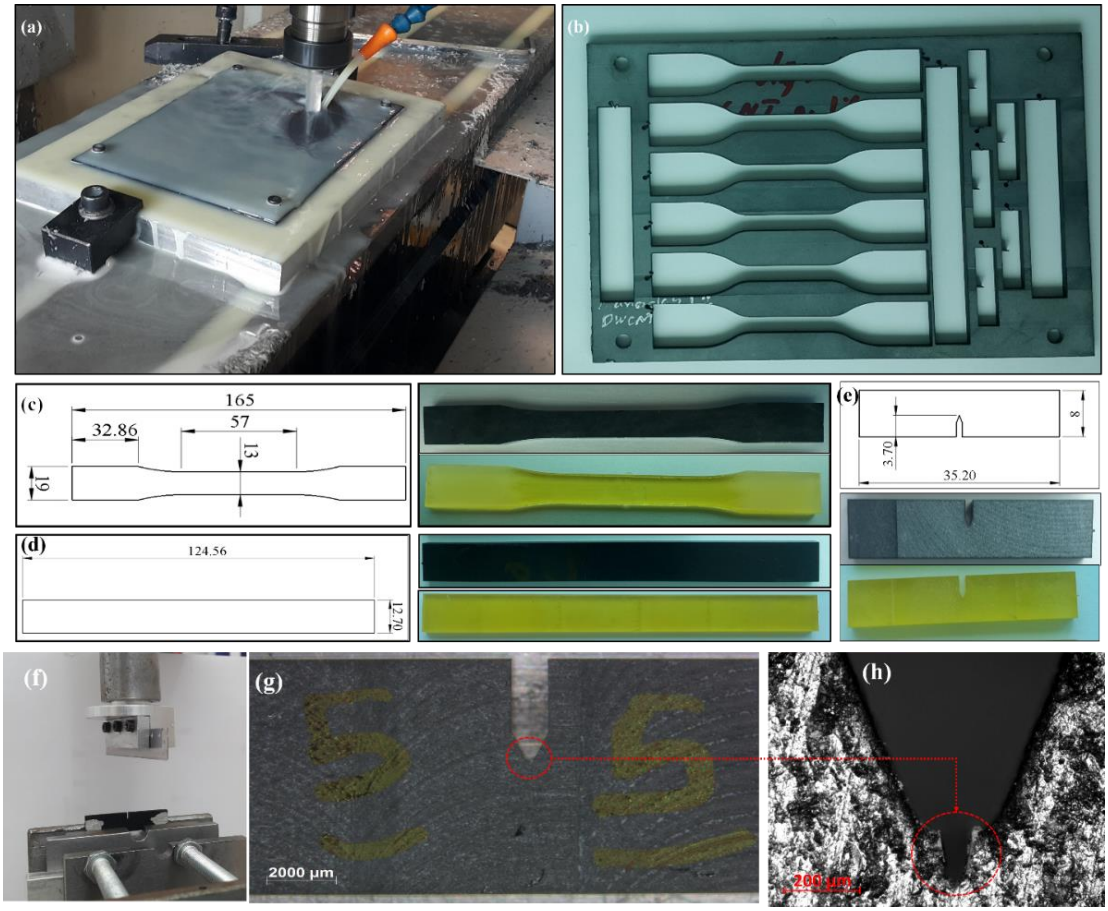

Figure 2. 6. (a) Machining top surface of the plates, (b) specimen extraction by waterjet, (c-e)tensile, impact and SENB specimens respectively , (f) machined used for creation of the pre-crack, (g-h) tiny pre-crack made into the notch.

2.4. Electrical conductivity measurement

The electrical conductivity of the nanocomposites was measured to compare the effect of the addition of nanofillers on the electrical conductivity. According to ASTM D257, three square specimens with parallel sides and a dimension of 10 × 10 × 1 mm were prepared for each nanocomposite to achieve reliable results. A resistivity chamber Keithley 8009 connected to a source-meter Keithley 2410 was employed for the measurement of volumetric electrical conductivity using two parallel circular electrodes placed on each side of the specimen. A steady pressure was applied over the

specimen using a fixture to guarantee that appropriate and consistent contact was obtained between the specimen and the electrodes. Voltage from 1 to 100 V, depending on the sample conductivity, was applied to the specimen, and followed by the measurement of the current intensity.

Electrical resistance (R) was calculated by the Ohm's law (equation 2.1), and the resistivity of the specimen (ρ) was subsequently obtained from equation 2.2, considering the specimens geometry (L, A). Finally, the inverse of the resistivity (equation 2.3) was considered as the specimen conductivity (σ).

$$R = \frac{V}{I} \qquad (2.1)$$

$$R = \rho \frac{L}{A} \qquad (2.2)$$

$$\sigma = \frac{1}{\rho} \qquad (2.3)$$

V is the voltage (V), I the current (A), L the specimen length, A the specimen cross-section area, ρ the resistivity (Ω) and σ the conductivity (S/m).

2.5. Mechanical and microstructural characterization

Figure 2. 7 shows the mechanical and electromechanical tests carried out in this study. Tensile (Figure 2. 7a-c) and fracture (Figure 2. 7d-f) tests were performed to measure the tensile strength and fracture toughness properties, K_{IC} and G_{IC} of the nanocomposites and the pristine epoxy. MTS Alliance RF150 and MTS Synergie 200 electromechanical testing machines with a crosshead speed of 0.5 mm/min were used for the tensile and fracture tests respectively. The strain was truthfully measured using a 634.12F-54 MTS extensometer during the tensile test, recording the applied force and the displacement, the latter measured by a 634.12F-54 MTS extensometer (Figure 2.

7c), to avoid errors due to machine deformation. In addition, the displacement throughout fracture tests was evaluated from the grips displacement, taking into account negligible effects of machine deformation caused by a low applied load.

Specifically for the measurement of K_{IC} and G_{IC}, a three point bending tests was conducted on the SENB specimen (Figure 2. 7d-f) with the span length of 32mm. Equations 2.4 and 2.5 were used to obtain K_{IC} and G_{IC}, respectively, following the specimen size criterion (equation 2.6) and the validity test (equation 2.7) recommended in the ASTM D5045.

$$K_Q = \left(\frac{P_Q}{BW^{\frac{1}{2}}}\right) f(x) \tag{2.4}$$

$$G_Q = \frac{U}{(BW\emptyset)} \tag{2.5}$$

$$x = \frac{a}{w} 0.45 < x < 0.55 \tag{2.6}$$

$$B, a, (W - a) > 2.5 \left(\frac{K_Q}{\sigma_y}\right)^2 \tag{2.7}$$

Where K_Q is the conditional fracture toughness [MPa.m0.5], G_Q the conditional fracture energy [KJ/m2], P_Q the maximum load [N], U the corrected energy (KJ), B the thickness [mm], W the width [mm], a the total crack length i.e. the pre-crack length plus notch depth [mm], and σ_y yield strength [MPa]. $f(x)$ and $\emptyset$ were obtained using an interpolation from the values given in the ASTM D5045.

It is worth noting that the test machine compliance and indentation effect were considered negligible in the load range applied during the tests; thus, the energy U was calculated through the integrated area of the force-displacement curve obtained from the test. A cantilever beam (Izod-Type) impact machine with 4 J impact energy was used for the impact test (Figure 2. 7g). The calibration was carried out by running few

tests without specimen. The specimen was clamped using a fixture where 30.75 mm of its length were outside the fixture. After releasing the pendulum, the excess energy left after breaking the specimen was recorded. The impact strength was obtained by dividing the absorbed energy to the cross-section area. The impact strength reported in this study was the average of 9 tested specimens.

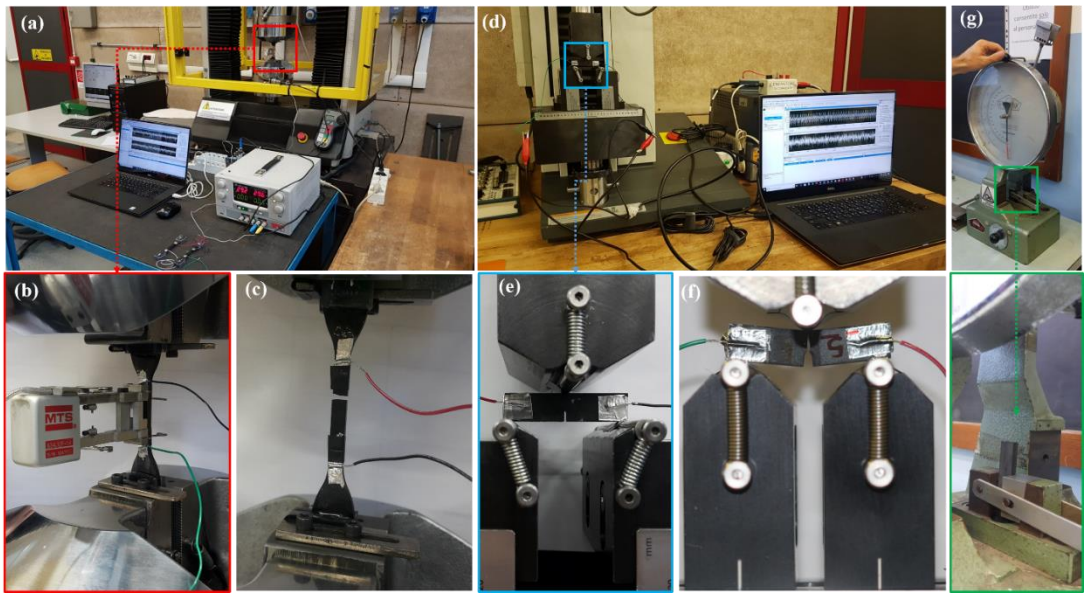

Figure 2. 7. Mechanical test: (a-c) tensile test, (d-f) fracture test, (g) Izod impact test.

SEM (ZEISS –EVO 50) and FESEM (ZEISS-SUPRA40) along with optical microscope were employed for the microstructural analysis. SEM was mainly used for the fractography whereas the FESEM was employed for the dispersion analysis of the nanofillers. It is worth noting that the fracture surfaces were coated by gold for better imaging. XRD was also performed to truthfully compare the microstructure of the nanoclay (intercalated or exfoliated [50] before and after the dispersion into the epoxy. Finally, Optical profilometry analysis was performed to obtain the surface roughness of the fractured specimens for some of the specimen.

2.6. Piezoresistive characterization

For the piezoresistive sensitivity characterization, a two probe techniques (Figure 2. 8 and Figure 2. 9) was used to simultaneously monitor the normalized resistance change as a function of strain and displacement during tensile and fracture tests respectively. The electrodes were located on the specimens at a distance of 30 and 25 mm for tensile and SENB specimen, respectively, connected by silver paste to enhance the conductivity of the joints. A silver paint was applied to the surface to increase the conductivity of the joints. The crack extension throughout the fracture test was measured by post processing of the video taken during the test, in case of gradual crack propagation.

It is worth noting that the tensile and SENB specimens were isolated from the machine using PMMA tabs and insulating tape during tensile and fracture tests, respectively, in order to reduce the noise imposed by contact with the conductive machine parts. Thus, to assure than minimum noise interruption occurred during the piezoresistivity test, several initial test were carried out in order to measure the noise and reduced its value in case of high amount of noise.

Two different methods were used to measure normalized resistance change as a function of strain increase for phase 1 and 2 as shown in Figure 2. 8 and Figure 2. 9 respectively. . For the phase 1, constant current was flowed throughout the specimens while the change in output voltage was registered. On the other hand, for phase 2, a constant voltage was flowed throughout the specimen whereas the output currents were monitored. It is worth noting that this did not have any impact of final piezoresistivity. In fact, it was done to make the experimental setup easier. In the following sections, the detail about the piezoresistivity measurement during phase 1 and 2 are explained.

2.6.1. Phase 1

The monitoring scheme was based on a current generator and a potential measurement employing two probe techniques (Figure 2. 8a). The current generator consisted in a power supply STAB AR60, an in-house-built active potentiometer maintaining the current stationary and a FLUKE-8846A multimeter for the current visualization. Voltage measurement was performed in real-time during the tests with a NI9234 acquisition board connected to a laptop running Ni Labview software. A constant current of 0.200 mA was applied between two probes in all the tests. A general view of the system setup during tensile tests is shown in Figure 2. 8b.

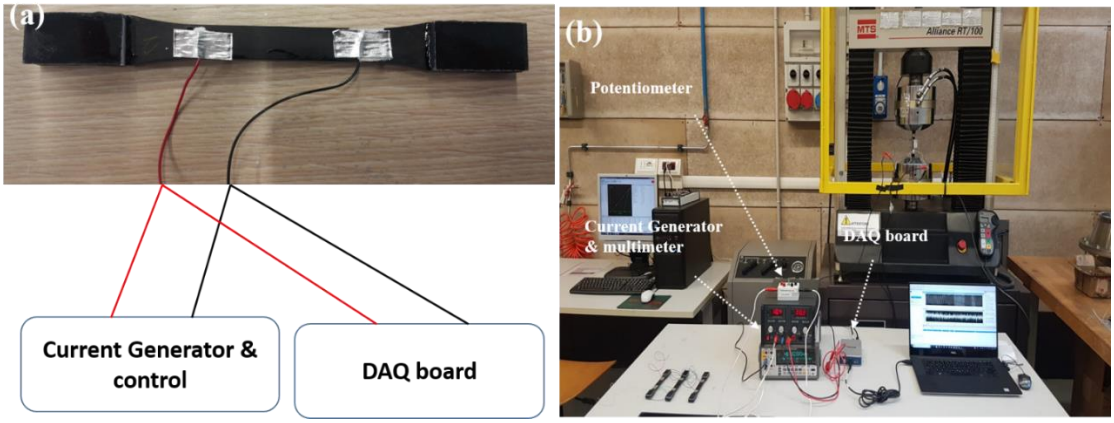

Figure 2. 8. Schematic view of the tests set up (a) voltage acquisition setup for strain monitoring characterization, (b) tensile test setup.

2.6.2. Phase 2

A constant voltage of 30 V was applied to the specimen by the power supply STAB AR60 while the current (mA) was monitored in a real-time manner throughout

the test using NI9234 Data Acquisition (DAQ) connected to a laptop, running Ni Labview. A schematic view of the setup can be seen in Figure 2. 9. The advantage of this method with respect to the previous method is its easier installation due to less wiring required.

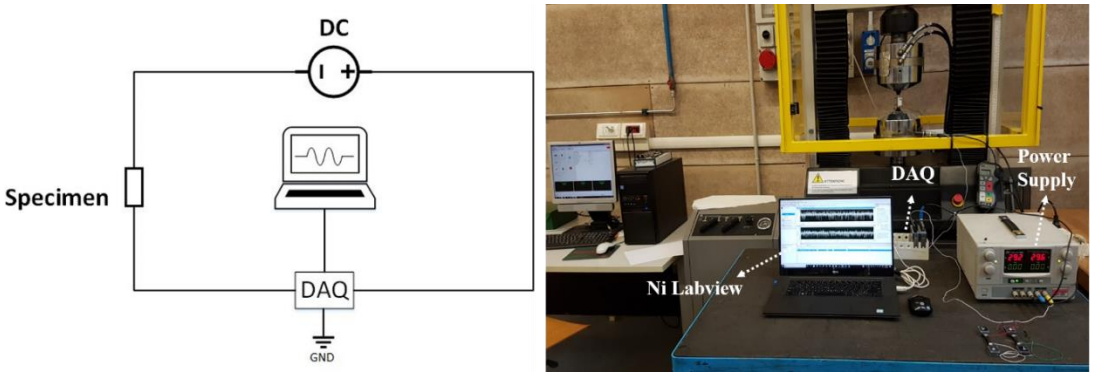

Figure 2. 9. Schematic presentation of the two probe techniques used for the piezoresistive characterization.

CHAPTER 3: MULTIFUNCTIONAL PROPERTIES OF SWCNTS/EPOXY

In this chapters, the piezoresistive characteristics of different SWCNTs contents incorporated into epoxy matrix were investigated and compared under tensile and fracture tests. Sonication method with constant parameters was adopted at each CNT loading in order to guarantee that no difference in CNT damages occur among the specimens, however resulting in different dispersion states as a function of the CNT loading.

The effect of different dispersion states on the electrical conductivity and sensitivity along with the related mechanisms behind the piezoresistive behaviours of the nanocomposite corresponding to different SWCNT loadings are deeply discussed with reference to SEM and FESEM analyses. The self-sensing performance, in terms of strain sensitivity, was measured at different SWCNTs concentrations to compare the piezoresistivity and sensitivity of SWCNTs/epoxy nanocomposites at different contents and to evaluate the sensitivity of the specimen at weight concentrations close and above the percolation threshold.

The target is to show how different microstructures obtained at different CNT concentrations (thus related to different types and level of defects) relate to different electromechanical properties. Finally, the performance of the developed nanocomposites during fracture tests before and after crack propagation were compared and discussed, aiming to identify potential precursors of damage initiation.

3.1. Microstructural analysis

Figure 3. 1a-c shows low magnification of FESEM image of the tensile

specimens with different CNTs loading after failure. Thanks to the features of the FESEM analysis, and the use of an inlens detector, the dark regions are representing high electrically conductive areas. Varying CNTs contents from 0.25 to 0.75 wt.% results in increasing number of the micrometric conducting domains as shown by yellow arrows in Figure 3. 1b-c. A high-resolution FESEM investigation (Figure 3. 1d) allows us to conclude that the domains are constituted by agglomerates of CNTs. In particular, 0.75 wt.% contains higher numbers of large agglomerates whereas a better dispersion can be seen at 0.25 and 0.5 wt.%. In other words, sonication was capable to successfully break the agglomerates when low CNTs contents used while high viscosity of CNTs/epoxy mixture at high CNTs loading resulted in improper dispersion.

In order to properly compare the CNTs dispersion and the interfacial CNTs/epoxy bonding, high magnification images are shown in Figure 3. 2. A homogenous dispersion of CNTs as well as a lack of aggregates and entanglements is clearly visible at 0.25 and 0.5 wt.% (Figure 3. 2a-b and c-d respectively), indicating proper interfacial bonding between the CNTs and matrix. This leads to appropriate shear-loading transfer between CNTs and matrix, thus CNTs can successfully play their roles in matrix reinforcement. It is worth noting that presence of tiny aggregates is visible at 0.5 wt.% (yellow arrow in Figure 3. 1b), but it is not sufficiently large to entangle together due to the fact that there is a consistent cohesion between aggregates and epoxy as shown in Figure 3. 2d.

On the other hand, a CNTs-weak interface inside the agglomerated-CNTs can be distinguished at 0.75 wt.% where CNTs are severely twisted and entangled together resulting in loss of cohesion between entangled CNTs and the epoxy resin (Figure 3. 2e-f). These weak-interface regions cause rearrangement of the CNTs, due to improper interfacial bonding inside the aggregates, resulting in aligning them parallel to shear-

loading transfer during the test as shown in Figure 3. 2e.

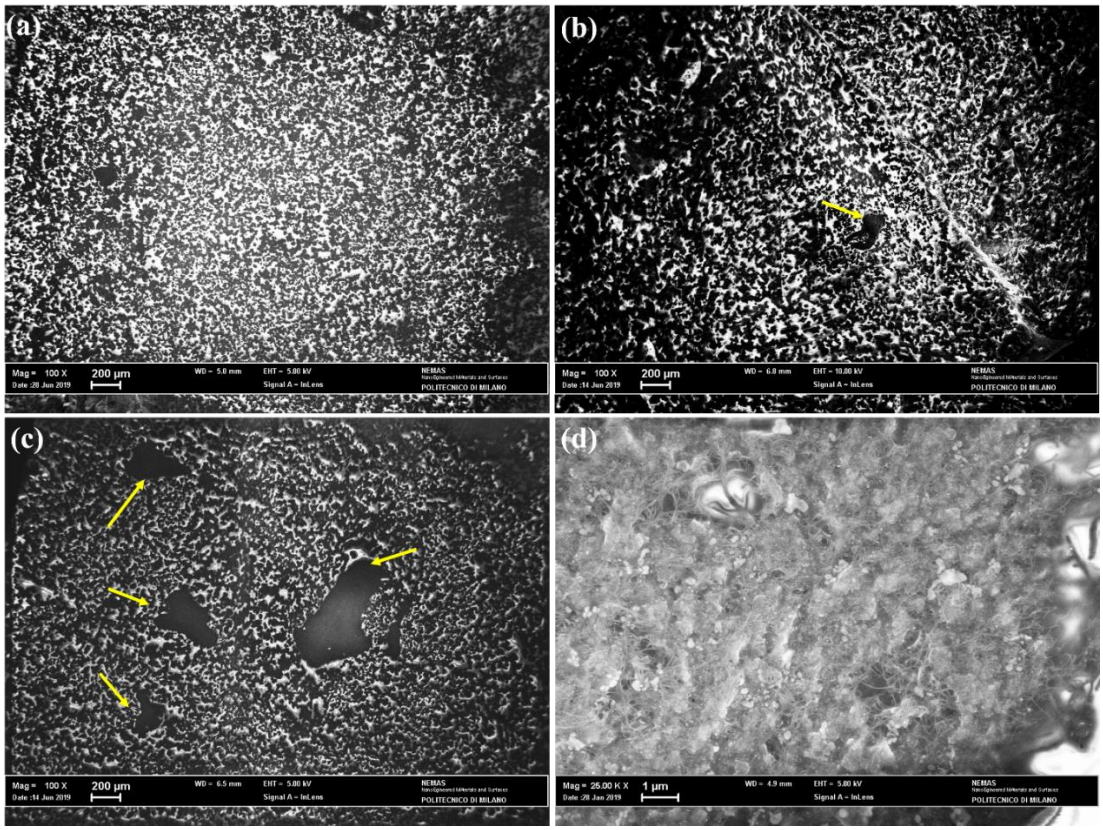

Figure 3. 1. CNTs dispersion- low magnification FESEM images of the dog-bone specimens after failure: (a) 0.25 wt.%, (b) 0.5 wt.%, (c) 0.75 wt.%, (d) .Higher magnification FESEM image of the aggregates regions at 0.75 wt.%.

As a matter of fact, the weak bonding resulting from poor-wettability of CNT aggregates with epoxy facilitates separation of CNTs inside the aggregates, thus no effective shear loading transfer occurs at 0.75 wt.% as shown by white arrows in Figure 3. 2e. The poor wettability of the CNTs within the aggregates manifests as fragile inclusion which initiates the fracture [144]. This leads to substantial reduction of mechanical properties when a high CNT loading is used, that are discussed in the following sections. Considering the manufacturing factors used in this study, it can be stated out that a uniformly dispersion of CNTs and appropriate cohesive bonding at the

CNTs/epoxy interface are observed at CNTs of 0.25 and 0.5 wt.% whilst excessive amounts of agglomerated CNTs showing weak CNTs/epoxy bonding are noticed at 0.75 wt.%. These different dispersion states will influence the piezoresistivity of the material. As a result, an accurate comparison can be made in terms of the relation of the different microstructures, including well-dispersed CNTs and entanglements, and the electromechanical properties.

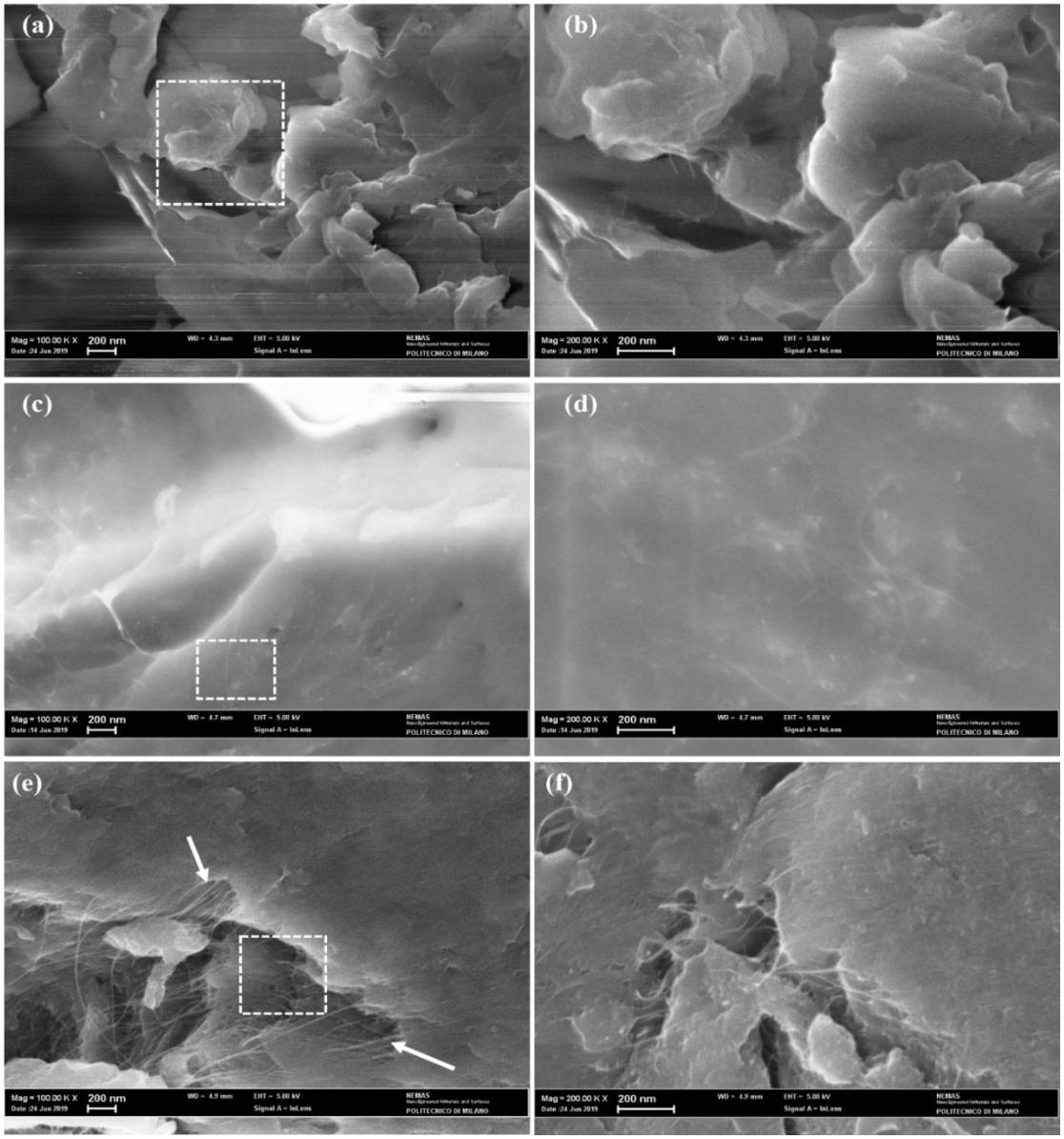

Figure 3. 2. High magnification FESEM images of epoxy resin with different CNTs loading: (a-b) 0.25 wt.%, (c-d) 0.5 wt.%, (e-f) 0.75 wt.%. Dashed rectangle indicate the area investigated at larger magnification and reported in the right column.

3.2. Electrical conductivity

Due to the inherent electrical conductivity of CNTs, incorporating CNTs into epoxy leads to a significant improvement of the electrical conductivity of the epoxy [25]. Figure 3. 3 shows the electrical conductivity of the SWCNT/epoxy at different

weight concentrations. Electrical conductivity dramatically increases up to 9 orders of magnitude after the addition of only 0.25 wt.% of SWCNTs i.e. the percolation threshold is quite low which is consistent with the literature [25]. This significant enhancement is mainly attributed to the tunneling effect [35]. According to the classic physic, particle (electron) with energy E cannot pass through the barrier with energy U if E<U and it is transmitted back by the barrier. On the other hand, based on quantum mechanical tunneling theory, electron can tunnel through insulting material (epoxy) under certain conditions resulting in transmitting the electron (particle from the barrier.

Moreover, a further increase of the CNTs content from 0.25 wt.% to 0.5 wt.% results in negligible enhancement of conductivity. Specifically, 0.5 wt.% is quite above the percolation threshold resulting in less improvement of electrical conductivity, while a slight decrement of conductivity is found at CNTs contents of 0.75 wt.%, which can be attributed to the presence of large aggregates and entanglements caused by the high CNTs content as shown in Figure 3. 2e-f. This is in good agreement with the literature indicating that presence of aggregates induces negligible enhancement in electrical conductivity [23].

It should be mentioned that, in theory, the electrical conductivity should increase with an increase of the CNTs content while, in reality, a proper dispersion at high CNTs content is difficult to achieve; in fact, in our tests, CNTs tend to bundle together resulting in a slight decrease of the electrical conductivity.

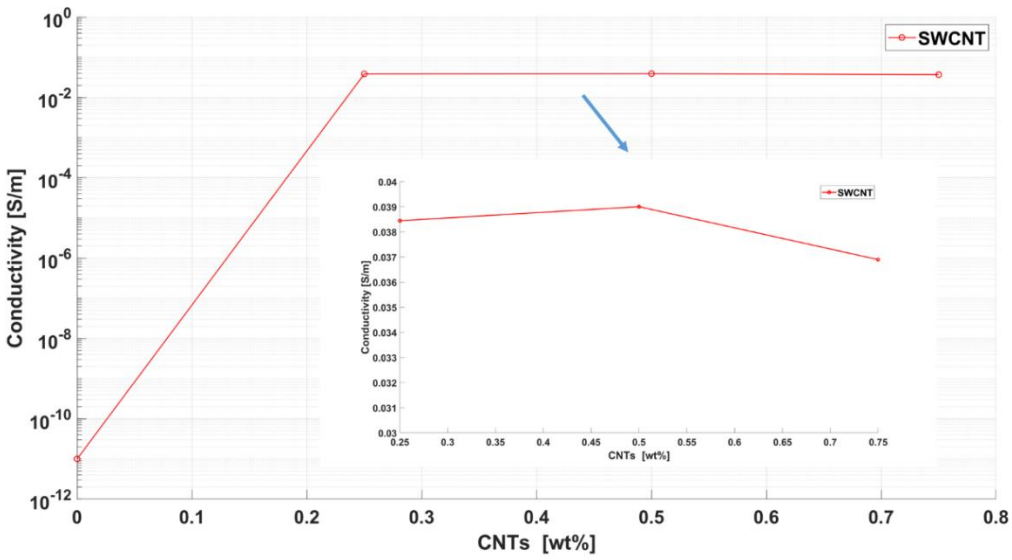

Figure 3. 3. Electrical conductivity versus CNTs content.

3.3. Piezoresistive behaviour

The piezoresistive behaviour of the nanocomposite during tensile and fracture toughness tests were investigated hereafter. Figure 3. 4 illustrates a normalized resistance change at different CNT loadings as a function of the axial strain increase under tensile tests. Axial strain was calculated based on the measure of the specimen axial displacement taken by the extensometer. Hereafter, the normalized resistance change ΔR_n is expressed as equation 3.1:

$$\Delta R_n = \frac{\Delta R}{R_0} = \frac{R(t)-R_0}{R_0} = \frac{V(t)-V_0}{V_0} \qquad (3.1)$$

Where $V(t)$ is the measured voltage as a function of time, V_0 is the reference voltage, $R(t)$ is the time dependent resistance, influenced by the strain level and potentially by any damage modifying the electrical paths and R_0 is the reference electrical resistance. It is worth noticing that proportionality between voltage and electrical resistance is guaranteed by a constant current flowing into the specimen.

3.3.1. Tensile test

As widely discussed in the literature [30,107], specimens loaded with different CNT contents can simultaneously trace strain change i.e. the normalized resistance change increases in real time with the strain . Specifically, CNTs contents of 0.25 and 0.5 wt.% (Figure 3. 4a-b) show a nonlinear behaviour resulting from a tunneling effect, which plays the dominant role in the electrical characterization of the nanocomposite [37].

According to quantum mechanical tunneling theory, electrons can tunnel through the insulting material under certain conditions, thus resulting in the electron transmission between two electrically conductive fillers [44]. Tunneling resistance can be calculated according to equation 3.2 [44]:

$$R_{tunnel} = \frac{V}{AJ} = \frac{h^2 d}{Ae^2\sqrt{2m\lambda}} exp\left(\frac{4\pi d}{h}\sqrt{2m\lambda}\right) \qquad (3.2)$$

Where V is the electrical potential difference, A the cross section, J the tunneling current density, h the Plank's constant, d the tunneling distance between two neighboring CNTs, e the quantum of electricity, m the electron mass, and λ the barrier height around 0.5 to 2.5 eV for the epoxy [30].

According to equation (3.2), tunneling resistance exponentially increases as a function of the tunneling distance, with a validity of the relation up to approximately $d = 1.8\,nm$ [35]. As a result, the nonlinear piezoresistive behaviour of the nanocomposite at 0.25 and 0.5 wt.% can be mainly attributed to the tunneling effect as there is nonlinear relation between tunneling distance and tunneling resistance based on equation 3.2.

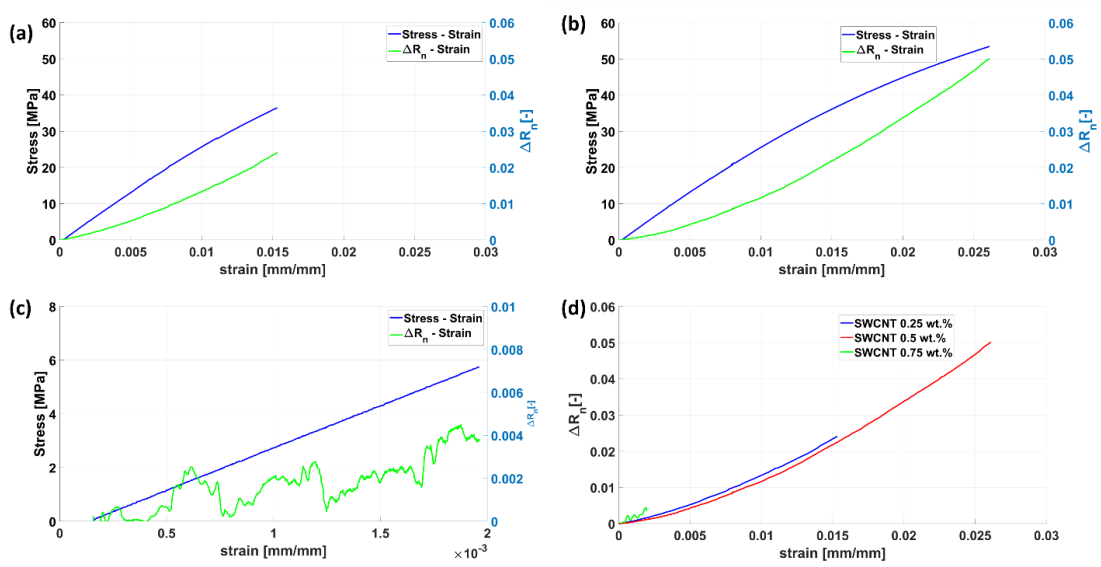

Figure 3. 4. ΔR_n and stress versus strain under tensile test :(a) SWCNT 0.25 wt.%, (b) SWCNT0.5 wt.%, (c) SWCNT0.75 %, (d) ΔR_n versus strain for all CNTs contents. Notice a different scale has been used in (c).

Focusing on the strain region below 0.015, the SWCNTs content of 0.25 wt.% displays higher ΔR_n with respect to 0.5 wt.% (Figure 3. 4d) since it is closer to the percolation threshold of the composite, thus in good agreement with the literature stating that proper electromechanical characteristics can be obtained near the percolation threshold [30].

In the case of the SWCNTs at 0.75 wt.%, a non-steady state growth of ΔR_n is visible in Figure 3. 4c which can be ascribed to the early creation of internal damages resulting from high entanglement (as shown in Figure 3. 2e-f) acting as a stress concentrator during the tensile test and manifesting itself as a premature unexpected failure of the specimens in correspondence of a stress level of approximately 6 MPa. Therefore, not only the high weight concentrations of SWCNTs above the percolation threshold may not be appropriate for increasing conductivity, but they will also induce a lower tensile strength if no action is taken to guarantee sufficient dispersion and high

oscillations in the measures of normalized resistance, thus leading to a misinterpretation of the piezoresistive behaviour of the nanocomposite.

An important factor of a sensor is its sensitivity, referred to as Gauge Factor (GF) and defined as in equation 3.3:

$$GF = \frac{\Delta R_n}{\varepsilon} \tag{3.3}$$

Where ε is the strain in correspondence of ΔR_n. If a nonlinear sensitivity is found, the GF can be approximated by numerically calculating the slopes of the curves in Figure 3. 4d for discrete intervals. Results are reported in Figure 3. 5 for two different weight concentrations, i.e. 0.25 and 0.5 wt.%, as a function of strain.

Figure 3. 5 shows sensitivity increases with an increasing strain. When the strain is low (less than 0.01 in the tests performed), increasing the strain leads to larger distance amongst neighboring CNTs (inter-particles distance) at nanoscale, hence, tunneling effect can be taken into account as the dominant mechanism governing piezoresistivity and resulting in increasing sensitivity by strain [37]. Variation in resistance caused by loss of contact between neighboring CNTs can be neglected when strain is low because CNTs are highly contacted [30].

On the other hand, the breakage of electrical networks resulting from the formation of internal damages governs the piezoresistivity at higher strain (larger than 0.01 in the test performed). It is worth noting that even at high strain the tunneling effect plays a role in piezoresistivity because CNTs start separating and, thus, promoting new tunneling links which result in a further GF increase.

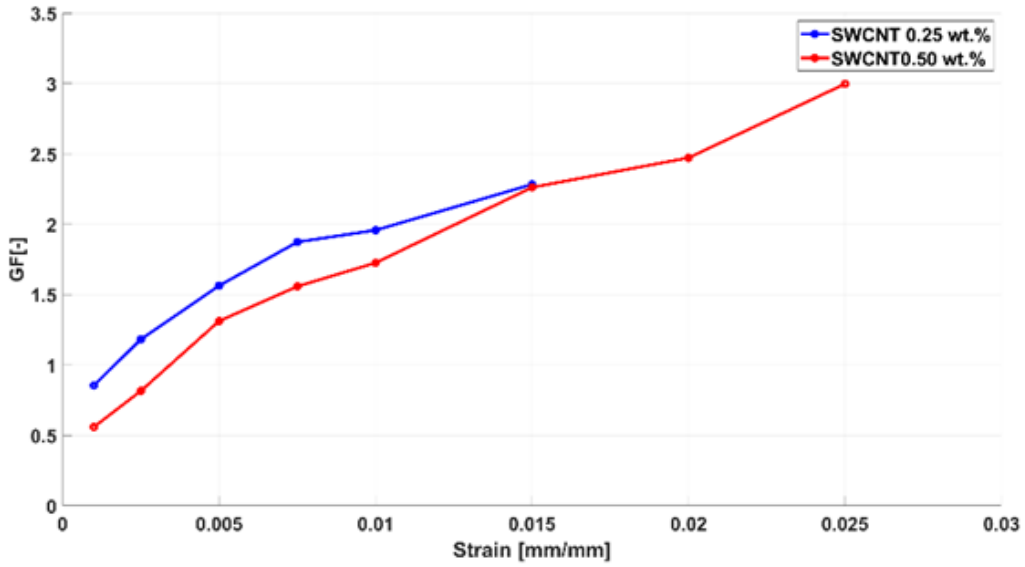

Figure 3. 5. GF versus strain for 0.25 and 0.5 wt.% of SWCNTs.

Regardless of the amount of strain, the GF of SWCNT with 0.25 wt.% is higher than 0.5 wt.%, in agreement with the literature indicating that the GF is higher near the percolation threshold due to a more pronounced tunneling effect [28,30,145]. This can be attributed to the proper dispersion of CNTs as well as the lack of large clusters of CNTs in the former compared to the latter [23]. It is also worth noticing how the distance between the two curves remains constant before damage initiation occurs.

Although the highest GF (around 3) was obtained for the specimen loaded at 0.5 wt.% CNTs loading, the tensile strength of this specimen is higher than 0.25 wt.% due to high content of CNTs in the matrix. It can be concluded that 0.5 wt.% shows better performance with respect to 0.25 and 0.75 wt.% in terms of tensile strength and piezoresistivity, however, strictly dependent on the manufacturing parameters used in this study.

3.3.2. Fracture test

The piezoresistive behaviour of the nanocomposites before and after crack onset was investigated during fracture toughness tests (Figure 3. 6and Figure 3. 8), to compare sensitivity of the specimens corresponding to deformation and crack growth respectively. In the first test phase (Figure 3. 6), the specimen is mainly subjected to localized deformation under three-points bending load, thus enabling to compare the sensitivity of different CNTs loadings. Subsequently, in the second phase, the piezoresistivity associated to macroscopic fracture was studied (Figure 3. 8), the latter manifesting as a sudden failure of the specimen or as a macroscopic crack evolution, depending on the material microstructure.

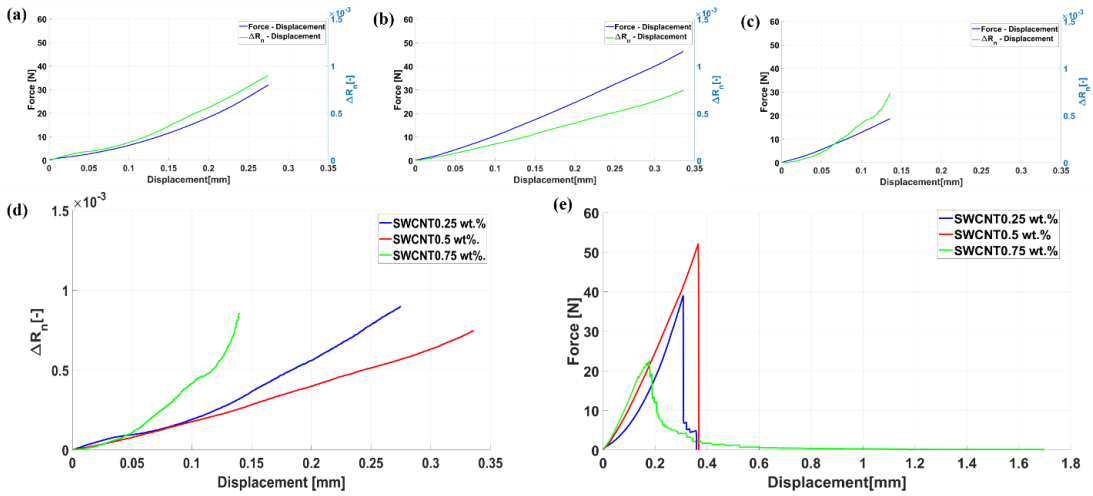

Figure 3. 6. Normalized resistance and force versus displacement under fracture test: (a) SWCNT 0.25 wt.%, (b) SWCNT 0.5 wt.%, (c) SWCNT 0.75 wt.%, (d) resistivity change versus displacement of all CNTs contents, (e) force- displacement for all CNTs content.

Focusing on Phase 1, results in Figure 3. 6 show a piezoresistive behaviour

similar to the tensile tests, i.e. a resistance increase in relation to displacement. Herein, ΔR_n is shown as a function of displacement due to the nonuniform strain field between the electrodes. In can be noticed that ΔR_n is significantly lower than it was for tensile tests. Specifically, the maximum change in normalized resistance are 0.0009 and 0.0007 for CNT contents of 0.25 wt.% and 0.5 wt.% respectively during fracture toughness test (Phase 1), whereas in the case of the tensile test, they are 0.025 and 0.05 for CNT loading of 0.25 and 0.5 wt.% respectively. First, this difference is related to the fact that the whole specimen is subjected to an axial strain during the tensile test with a uniform strain on the specimen section whilst the strain is more localized in the case of the fracture test.

Second, bending force creates both tension and compression throughout the SENB specimen, thus it is reasonable to expect CNTs reorientations at the compression side, i.e. the CNTs bend and change their orientations, thus, resulting in the creation of new electrical paths, and an increase of the tunneling distance at the tension side, with additional possibility for breakage of the electrical networks [28]. A combination effect of these phenomena accounts for the lower normalized resistance change during the fracture toughness test (before the macroscopic crack growth).

Furthermore, different ΔR_ntrends are observed depending on the CNT contents used, i.e. an almost linear trend can be seen in the case of CNTs content of 0.5 wt.% (Figure 3. 6b) whereas a nonlinear behaviour can be distinguished in the case of 0.25 (Figure 3. 6a) and 0.75 wt.% (Figure 3. 6c). This variation in piezoresistivity can be related to the CNT contents, which define the mechanism driving the electromechanical characteristics along with the specimen stiffness.

As discussed for tensile test, CNTs loading of 0.25 wt.% showed higher strain sensitivity than 0.5 wt.%, being closer to percolation threshold, i.e. the tunneling effect

plays the dominant role in the piezoresistive behaviour of the specimen. In addition, focusing on Figure 3. 6e, it can be seen that higher displacement, thus deformation, can be seen at 0.25 wt.% compared with 0.5 wt.%, for a given level of force. Therefore, the nonlinearity appeared in the former can be attributed to the predominant effect of tunneling (non-linear) resistance along with the higher deformation of the specimen.

On the other hand, higher amount of CNTs as well as less deformation (at the same level of force) at 0.5 wt.% soften the normalized resistance increase, thus a linear-like ΔR_n- displacement trend was observed. In practice, at 0.5 wt.% the loss of contact between CNTs, which typically appears at high CNT content, drives the piezoresistive characteristics of the specimen [37].

The justification for nonlinearity at 0.75 wt.% is different. Figure 3. 7a-b provide an insight on how CNTs aggregates lead to nonlinear piezoresistivity at 0.75 wt.%. While applying bending load during fracture test, the CNTs inside the aggregate change their orientation due to the weak CNTs/epoxy interface (related to poor wettability of agglomerated CNTs) i.e. they elongate parallel to the shear loading transfer (Figure 3. 7c-d). This leads to damage evolution in their vicinity (Figure 3. 7e-f), resulting in high amount of electrical breakages and manifesting as a significant nonlinearity even before the specimen failure (displacement < 0.14 mm).

In fact, damage evolution arisen from aggregates does not indicate failure if the aggregate is far from the notch, while the crack front developed from the notch acts as the most critical stress concentrator. Therefore, failure does not take place by formation of micro-damage near aggregates but the latter will facilitate the failure once the notch crack tip passes through them. As a conclusion, the augmented but highly nonlinear sensitivity of ΔR_n versus displacement at 0.75 wt.% is related to the damage evolution in the vicinity of the aggregates.

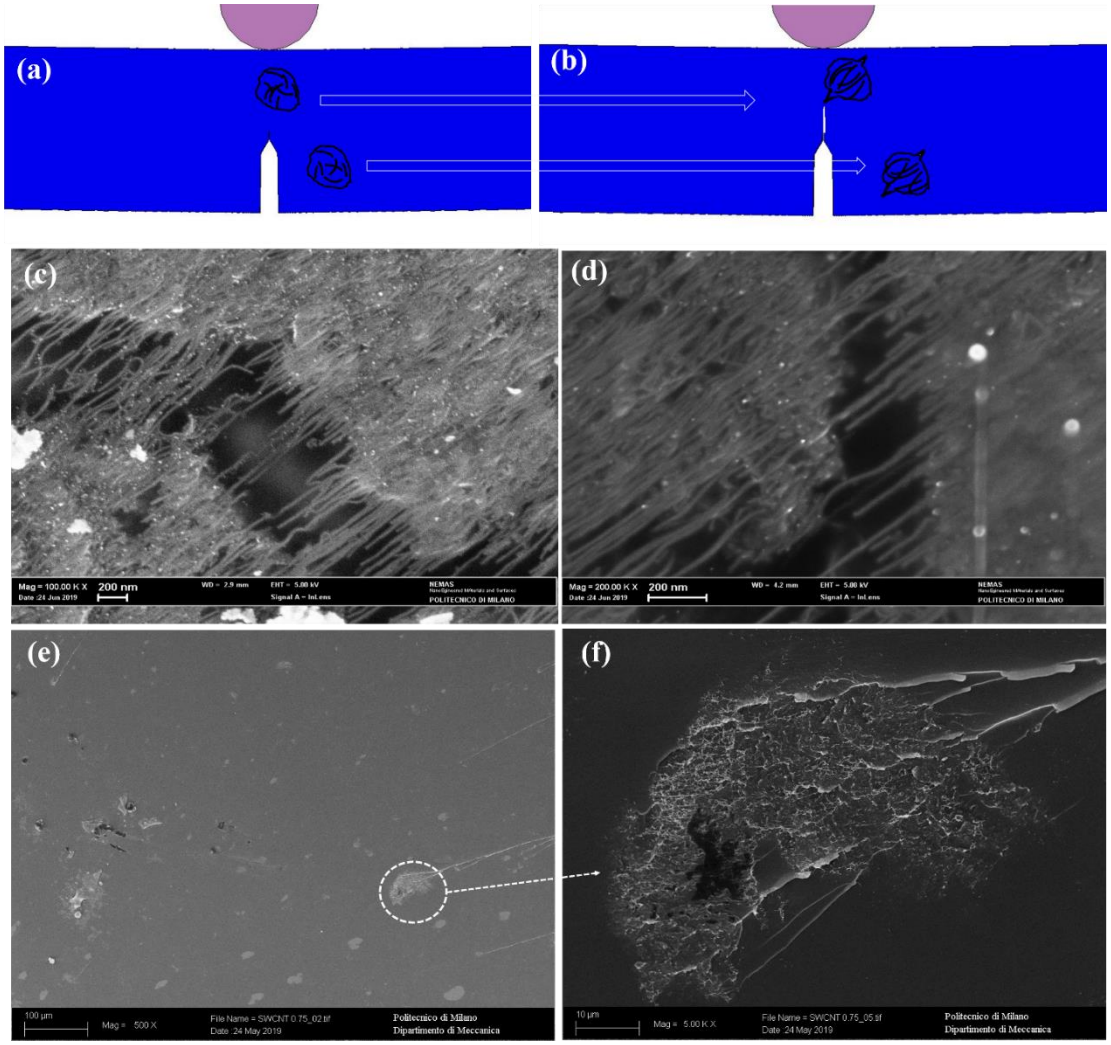

Figure 3. 7. The effect of aggregates on piezoresistivity at 0.75 wt.% in fracture test: (a-b) changing the aggregates orientation and shape, (c-d) elongation of CNTs parallel to shear loading transfer, (e-f) Micro-damage evolution in vicinity of CNT cluster along with presence of void inside the aggregate.

Focusing on Phase 2, the sensitivity to macro-crack propagation is visible in Figure 3. 8. Three different behaviour patterns were observed depending on the CNTs concentration including (i) step by step crack propagation, (ii) abrupt failure under high force, and (iii) continuous extension of the crack at CNTs contents of 0.25, 0.5 and 0.75 wt.% respectively (Figure 3. 8a-c).

The specimen containing 0.5 wt.% of CNTs showed higher fracture toughness ($1.26\ MPa\sqrt{m}$) compared with the CNTs content of 0.25 wt.% ($0.88\ MPa\sqrt{m}$) and 0.75 wt.% ($0.67\ MPa\sqrt{m}$). This leads to the highest force and displacement before failure for 0.5 wt.% case, i.e. the nanocomposite is tough enough to resist against crack growth up to the failure limit (Figure 3. 8b). However, although the size criterion in equation (2.7) was met for 0.25 and 0.5 wt.% specimens, the K_{IC} was not validated for 0.75 wt.%, mainly due to the low tensile strength of the material, nevertheless without hampering the investigation on piezoresistivity.

Although the specimen containing 0.25 wt.% CNTs failed at 39 N, it did not break completely in correspondence of the maximum load, showing a step by step pattern of macroscopic crack propagation in Figure 3. 8a. The onset of macro-crack propagation was marked by an abrupt increase of ΔR_n up to 0.18 i.e. at step number one shown in Figure 3. 8a. In fact, at stage one, the crack abruptly extends from its initial length (approximately 50 μm shown in Figure 3. 8j) to almost 2 mm, causing a large drop of the force measured by the load cell of the test machine. Then, the crack stops propagating resulting in a little force increase until the second step propagation appears, step number 2 in Figure 3. 8a, correspondingly showing another jump in ΔR_n (approximately 0.07 increase). This behaviour repeats itself up to the last step when the specimen fails. Figure 3. 8k shows the crack extension before the final failure step 4.

A continuous extension of the crack takes place in the case of CNT loading of 0.75 wt.% as shown in Figure 3. 8c. This can be mainly attributed to the lower fracture toughness of the specimens compared to those at 0.25 wt.% arisen from large CNTs clusters showing a weak interface with the epoxy matrix as mentioned before. As a result, the crack extension shows a gradual pattern instead of a step by step extension as shown in Figure 3. 8c.

A detailed analysis of the crack growth is shown in Figure 3. 8d-i, using different scales for ΔR_n at different time instants. An abrupt increase up to 0.0037 is visible in normalized resistance before the peak force is reached (Figure 3. 8d), specifically in correspondence of a little indentation in the force-displacement curve. In correspondence of the next force drops, ΔR_n increases up to 0.0072 and 0.05 respectively (Figure 3. 8e-f). This gradual increase in resistivity continues up to final failure where the maximum ΔR_n is 1.35 (Figure 3. 8c).

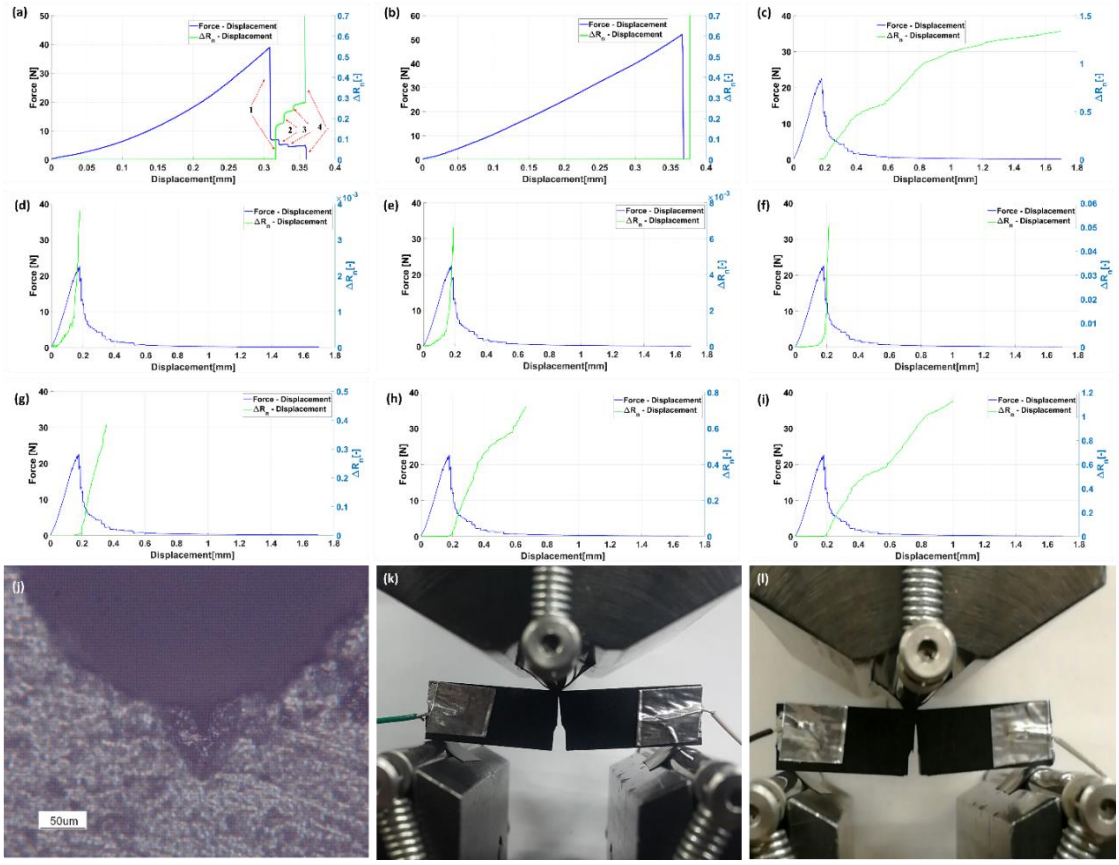

Figure 3. 8. (a-c): Piezoresistive behavior patterns during macro-crack propagation for CNT loading of 0.25, 0.5 and 0.75 wt.% respectively, (d-i) detailed analysis of crack growth at 0.75 wt.% (j) initial pre-crack made by a razor blade in the notch, (k-l) crack extension before complete fracture at 0.25 and 0.75 wt.% respectively.

3.4. Fractography and toughening mechanism

SEM images of the fracture surface upon tensile test is shown in Figure 3. 9. A river-like surface, cleavage pattern, can be seen at weight concentration of 0.25 and 0.5 wt.%(Figure 3. 9 a and b respectively) whereas a flat smooth surface, mirror-like pattern, appear at CNT content of 0.75 wt.% (Figure 3. 9c). In addition, surface roughness at 0.5 wt.% (Figure 3. 9b) is quite larger than the one at 0.25 wt.% (Figure 3. 9a). This can be attributed to higher tensile strength of the former with respect to the latter resulting in more deformation before failure. As a result, higher surface roughness indicates higher tensile strength whereas a smooth surface (Figure 3. 9c) refers to weak tensile strength.

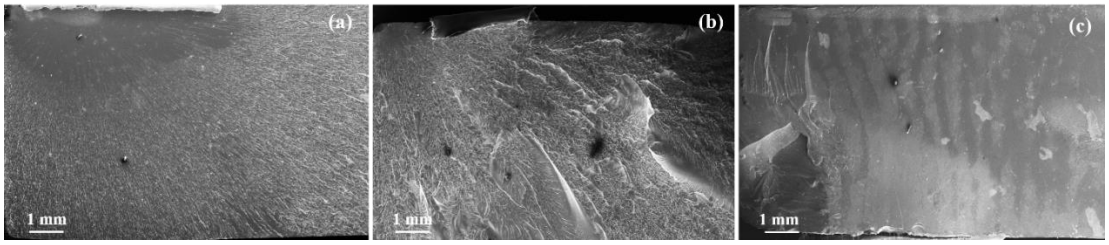

Figure 3. 9. SEM image of the fracture surface of the dog-bone specimens: (a) 0.25 wt.%, (b) 0.5 wt.%, (c) 0.75 wt.%.

SEM images of the SENB specimen upon fracture test demonstrate the aforementioned failure patterns (Figure 3. 10). Green dashed line and yellow dashed rectangle illustrate the initial crack propagation and the waviness regions respectively. A very shiny and smooth surface i.e. a mirror-like surface can be seen at 0.5 wt.% SWCNTs manifesting abrupt failure (Figure 3. 10d-f) whilst a waviness can be revealed at 0.25 and 0.75 wt.% presenting step by step and gradual failure (Figure 3. 10a-c and g-i).

Presence of large SWCNTs cluster at 0.75 wt.% (Figure 3. 10g-i) is also noticeable resulting in earlier failure of the specimen compared with 0.25 and 0.5 wt.%. On other hand, a better dispersion of CNTs can be observed at 0.25 and 0.5 wt.% as shown in Figure 3. 10a-f, presenting higher K_{IC} in comparison with 0.75 wt.%.

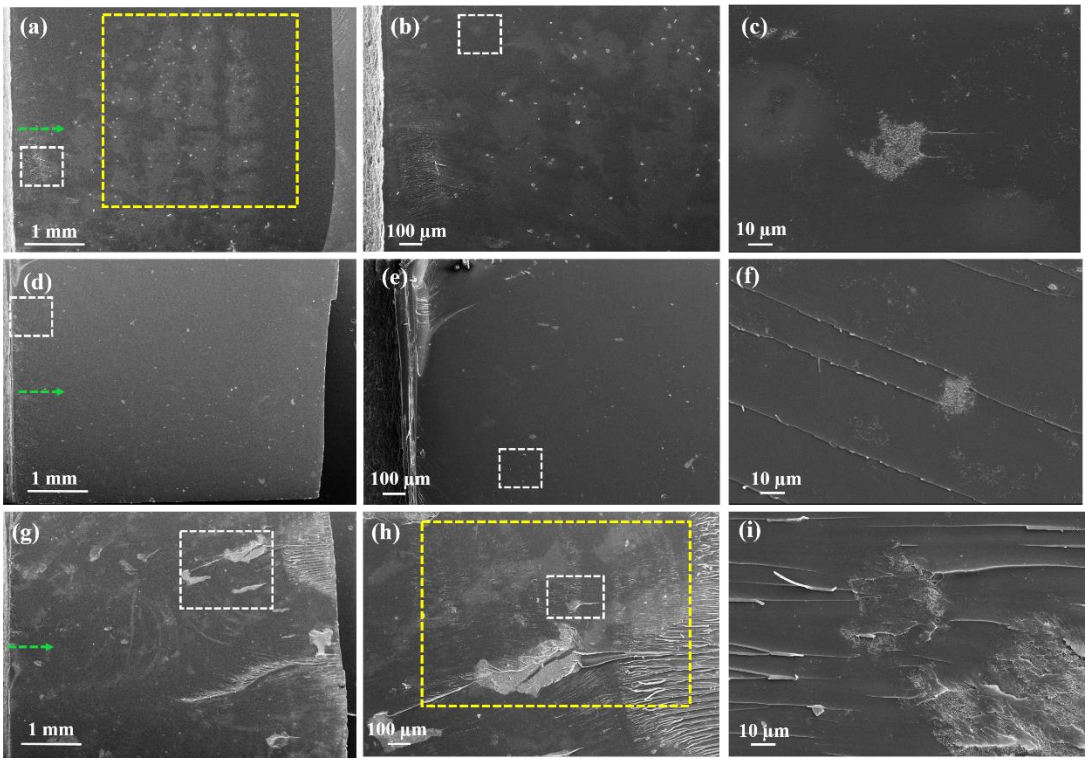

Figure 3. 10. SEM images of the fracture surface of the SENB specimens: (a-c) 0.25 wt.%, (d-f) 0.5 wt.%, (g-i) 0.75 wt.% (white dashed rectangles represent the region magnified on the right side.

It is worth noting that different toughening mechanisms were addressed in the literature for polymer base nanocomposites including crack deflection, crack pinning, crack bridging and CNT pull out [70,146]. In the case of CNTs reinforced polymers, crack-bridging mechanism is more likely to take place when the crack front encounters into the CNT region, carrying the entire load (Figure 3. 11). As a result, the crack-bridging mechanism accounts for the predominant toughening mechanism in CNT

based nanocomposites in case of good CNT dispersion, i.e. at 0.25 and 0.5 wt.%.

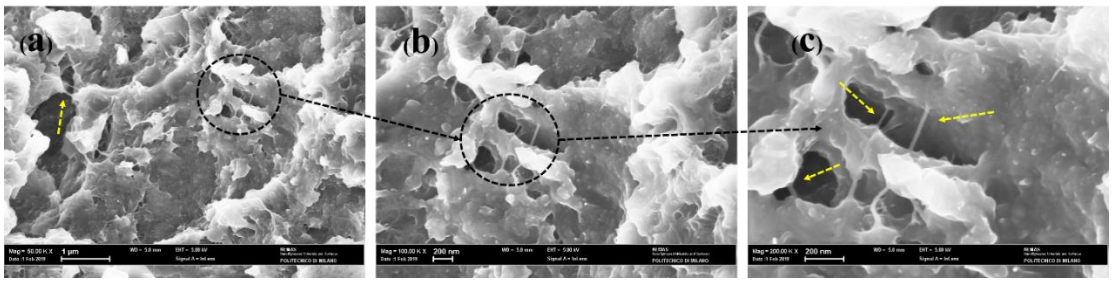

Figure 3. 11. Bridging mechanism of SWCNTs/epoxy.

However, in the case of CNTs aggregates, as discussed before, due to poor wettability of them with epoxy, CNTs align in a way parallel to shear-loading transfer as shown in Figure 3. 12. In fact, the interfacial bonding between CNTs entrapped in the aggregates with epoxy is poor, resulting in formation of aligned CNT bundles during the test. This causes lower fracture toughness of the specimen at 0.75 wt.% with respect to other CNT loadings due to the fact that they act as imperfections, thus reducing mechanical properties.

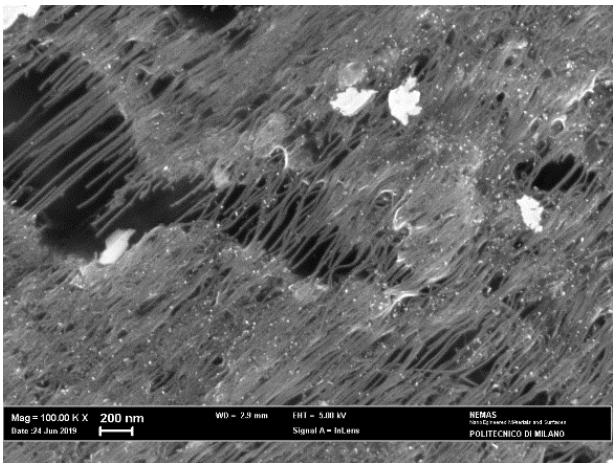

Figure 3. 12. Alignment of CNTs parallel to shear-loading transfer inside the aggregate - SENB specimen at 0.75 wt.%.

3.5. CNTs agglomeration on electromechanical properties

Introduction of CNTs into the epoxy matrix leaded to remarkable increase of electrical conductivity, thus conferring piezoresistive properties to the material, being able to self-sense the strain increase and the damage initiation in a real-time manner. However, piezoresistivity was severely related to the state of CNTs dispersion in the epoxy matrix, which defines the mechanism governing piezoresistivty of the material and influences the gauge factor. It was found that the possibility for generation of aggregates increases by augmenting the CNTs concentration.

It is clear from Figure 3. 1 and Figure 3. 2 that specimens loaded at 0.25 and 0.5 wt.% demonstrated better CNTs dispersion in terms of number of aggregates, aggregates size and interfacial bonding, as proved by SEM and FESEM imaging. Comparing Figure 3. 1b and c for CNT loading of 0.5 and 0.75 wt.%, respectively, the largest aggregate size in the former was approximately 200 μm whereas an aggregate size of 800 μm was observed in the latter. These variations in microstructure drive the different electromechanical behaviours discussed in this study.

A schematic view of electrical pathways formation in the epoxy matrix is provided in Figure 3. 13 for two different unloading-loading scenarios, i.e. without and with aggregates (left and right, respectively). Specifically, top and bottom subfigures represent change in electrical networks before and after deformation due to load, respectively. From Figure 3. 13a and c, it can be concluded that presence of aggregates substantially reduces the amount of electrical pathways formed throughout the matrix (red dotted lines) because a part of the CNTs contributes in the aggregates, thus leaving CNTs-poor regions in their vicinity (blue dotted rectangles). As a result, reduced

electrical conductivity was measured at 0.75 wt.% in comparison with 0.5 wt.% in this study (Figure 3. 13).

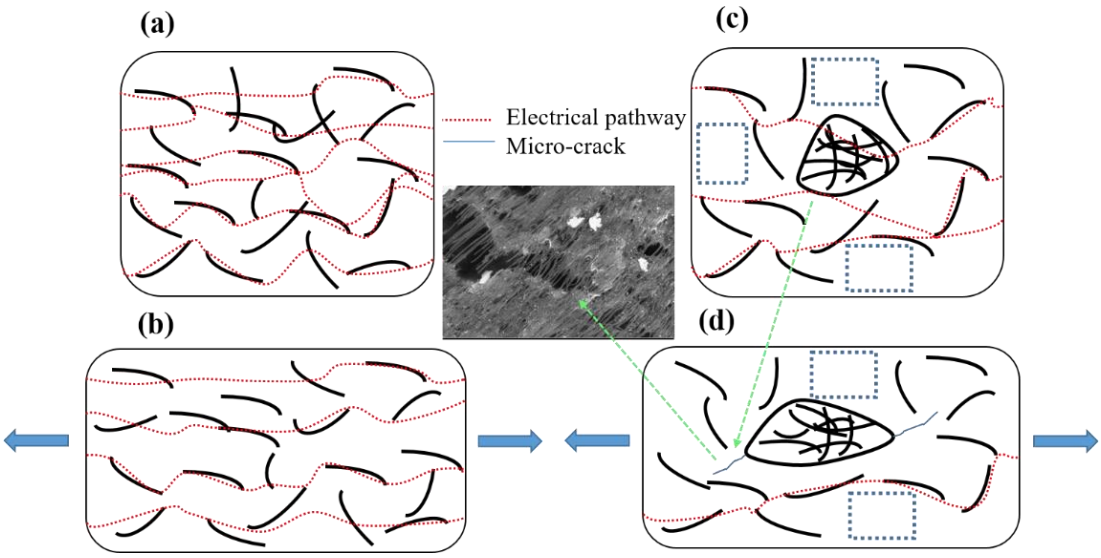

Figure 3. 13. The effect of well-dispersed CNTs and agglomeration on electrical pathways (red dotted lines) in unloaded-loaded scenarios: (a-b) well-dispersed CNTs, (c-d) presence of CNT aggregates. Blue dotted rectangles indicate CNTs-poor regions.

The effect of agglomeration on piezoresistivity and sensitivity during deformation is more complicated and can be appreciated in Figure 3. 13c-d. As discussed before, specimens with 0.75 wt.% CNT loading manifested higher sensitivity of normalized resistance, although with high non-linear fluctuations, during deformation in both tensile and fracture tests (Figure 3. 4d and Figure 3. 6d). This increase can be related to damage evolution in vicinity of aggregates, resulting in

destruction of higher numbers of electrical networks as shown in the schematics of Figure 3. 13c-d and experimentally appreciated in Figure 3. 7.

In fact, formation of micro-cracks near the aggregates, arisen from their weak-interfacial bonding with the epoxy, leads to breakage of more electrical pathways during the test, thus inducing higher increase in normalized resistance and manifesting a higher sensitivity. However, although 0.75 wt.% CNT loading manifests higher sensitivity in both tensile and fracture tests (compared to 0.25 and 0.5 wt.%), the mechanical performance results strongly reduced, the CNT aggregates and porosity acting as failure initiation regions.

3.6. Summary

Throughout this study, the self-sensing capability of epoxy composites reinforced by SWCNT was investigated. SWCNTs with different weight concentrations including 0.25, 0.5, and 0.75 wt.% were used in order to compare the electrical conductivities and self-sensing performance of the specimens under tensile and fracture toughness tests. In summary, the following results were achieved:

1. A uniform dispersion of CNTs and appropriate CNTs/epoxy interfacial bonding was found at CNTs content of 0.25 and 0.5 wt.% whereas highly entangled CNTs accompanied with weak interfacial bonding was obtain at 0.75 wt.%. Moreover, the electrical conductivity was increased up to 9 orders of magnitude with the addition of 0.25 wt.% of CNTs resulting from a tunneling effect and electrical contact among neighboring CNTs.
2. A nonlinear pattern in piezoresistivity of the nanocomposite subjected to tensile load was observed as a function of the strain value. At lower strain, the

nonlinearity was related to the tunneling effect whereas formation of internal damages within the matrix at high strain was taken into account for the appearance of additional nonlinearity. Higher sensitivity was achieved in the case of the CNT content of 0.25 wt.% compared with 0.5 wt.% at lower strain. Gage Factors were around 2 and 1.7 at a strain of 0.01 [-] for CNTs loading of 0.25 and 0.5 wt.% respectively. The highest GF around 3 was achieved at SWCNT loading of 0.5 wt.% at a strain of 0.025 [-].

3. The piezoresistive behaviour during fracture tests were depending on the CNTs loading and the specimen compliance, i.e. a linear trend in ΔR_n versus displacement was noticed at 0.5 wt.%, whilst CNT loading of 0.25 and 0.75 wt.% manifested a nonlinear trend. Tunnelling effect and loss of mechanical contacts amongst neighboring CNTs were accounted for while explaining the observed nonlinearity and linearity at 0.25 and 0.5 wt.% as well as the different displacements on the two sets of specimens at a given level of force. For 0.75 wt.%, reorientation of aggregates and damage evolution in their vicinity resulting from weak CNTs/epoxy interface caused the high nonlinearity in normalized resistance versus displacement. In addition, different failures were encountered at three different SWCNT loadings during fracture toughness test, the normalised resistance parameter being able to track the different trends in the force-displacement curve.
4. Two different fracture morphologies were noticed on the fracture surfaces of dog-bone specimens including river-like and mirror-like patterns. This was attributed to tensile strength of the specimens i.e. higher surface roughness related to larger tensile strength whilst a shiny flat surface was referred to weak tensile strength. In addition, fracture surface of the SENB specimens showed

different morphologies i.e. waviness was observed in the case of step by step failure whereas a shiny flat surface, mirror-like surface, appeared at 0.5 wt.%, characterized by sudden brittle failure.

5. Bridging mechanism was considered as the main toughening mechanism in SWCNTs reinforced epoxy at CNT content of 0.25 and 0.5 wt.% whereas the weak interfacial bonding between CNTs aggregates and the epoxy resulted in alignment of CNTs parallel to shear loading transfer, inducing the degradation of mechanical properties at 0.75 wt.% .
6. Presence of aggregates hampered the mechanical performance and the piezoresistive reliability of the 0.75 wt.% loaded specimens, the latter as a result from the destruction of higher number of electrical pathways during deformation which was attributed to micro-crack evolution in their vicinity. On the other hand, CNTs contents of 0.25 and 0.5 wt.% showed better strain monitoring performance due to the fact that their piezoresistive properties were mainly driven by deformation of the electrical networks as a function of strain increase, especially before damage evolution.

CHAPTER 4: MULTIFUNCTIONAL PROPERTIES OF DWCNTS/EPOXY

The purpose of the current chapter is to investigate the effect of the addition of SWCNTs-DWCNTs on electromechanical properties of the nanocomposites subjected to both tensile and mode I of fracture tests. Different weight concentrations including 0.25, 0.5 and 0.75 wt.% are adopted to compare and correlate the microstructures achieved at each CNT content to the mechanical properties, the tensile strength and the fracture toughness (K_{IC}), as well as the piezoresistive behaviour of the developed nanocomposites. Finally, the CNT weight concentration for achieving a compromise between mechanical properties, strain and crack growth-sensing capabilities are discussed in relation with the levels of CNT dispersion homogeneity obtained at different CNT contents.

4.1. Microstructural characterization

Figure 4. 1 exhibits SEM images of the fracture surfaces after fracture toughness test failure for different CNT contents. As indicated by yellow arrows, presence of aggregates within the matrix is noticeable at all CNT contents, i.e. agglomeration is typically manifesting even at low content due to intrinsic tendency of CNTs to aggregate, as a consequence of their high surface energy. In the specimens containing 0.25wt.% of CNTs, less and smaller agglomerations compared with those at 0.5 and 0.75 wt.% can be noticed from Figure 4. 1a-d.

In addition, areas that are not properly filled with CNTs i.e. CNTs-poor regions are more apparent in the case of 0.25 wt.% (Figure 4. 1d) in comparison with 0.5 and 0.75 wt.%, due to CNT tendency to bundle. CNT bundling in addition to less content

of CNTs result in appearance of CNT poor-regions within the matrix at 0.25 wt.%. On the other hand, this regions cannot be seen at 0.5 and 0.75 wt.% since the content of CNTs is sufficiently high to properly disperse across the matrix, though the number of agglomerations as well as their size are quite larger.

A proper dispersion of CNTs as well as CNT-aggregates within the matrix can be seen at 0.5 wt.% from Figure 4. 1e-h. In fact, sonication could successfully break the large clusters into smaller fragments and disperse them homogenously inside the matrix as shown in Figure 4. 1e. In contrast, high amount of large agglomerations can be noticed in the case of 0.75 wt.% (Figure 4. 1i-l) compared with 0.5 wt.%. This happens because the viscosity is very high at high CNT content, and sonication may not be very effective in breaking the aggregates, thus, resulting in formation of large cluster of CNTs inside the matrix.

It is worth noting that large aggregates are often accompanied with the formation of micro crack in their vicinity, as shown in Figure 4. 1k, due to weak interface between clusters of CNTs and the epoxy matrix. This week interface impacts on the electromechanical characteristics of the sensor, as will be discussed later in detail. It can be concluded that CNT loading of 0.5 wt.% presents better dispersion state of CNTs and CNT-aggregates along the matrix compared with 0.25 and 0.75 wt.%.

It is thus clear that the electrical and mechanical performances of the nanocomposites are strongly dependent on the efficiency of the manufacturing process and the capability to derive a sufficiently homogeneous microstructure. As this requirement is not sufficiently met for all CNT loadings, the results reported hereafter will try to explain how these defects in general will affect mechanical performances and electrical signals through the CNTs paths.

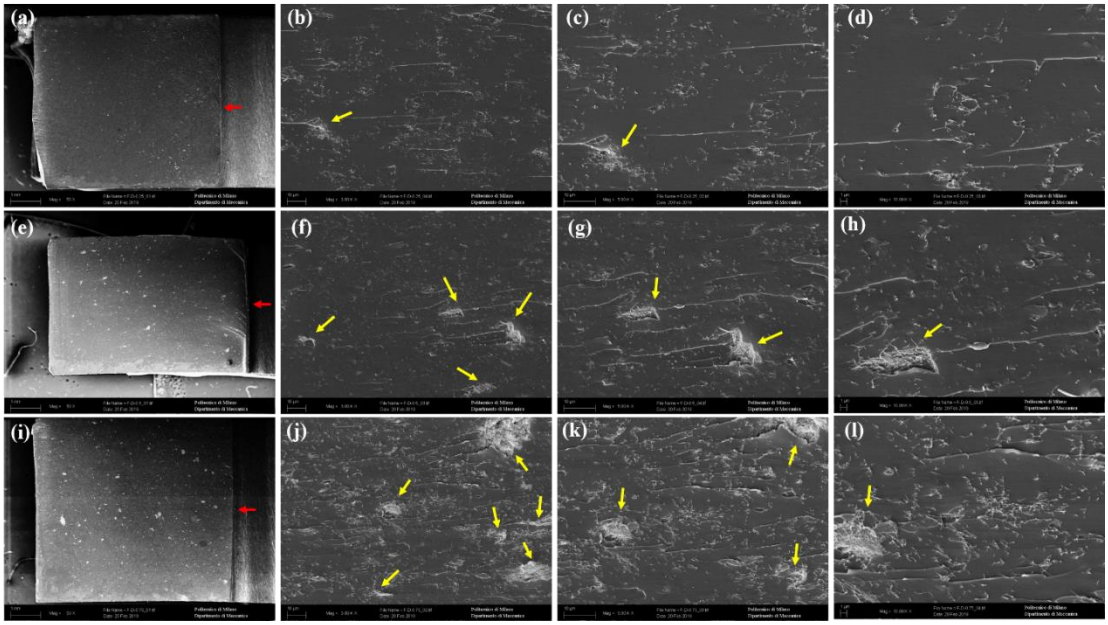

Figure 4. 1. Microstructural characteristics at different CNTs loading: (a-d) 0.25 wt.%, (e-h) 0.5 wt.%, (i-l) 0.75 wt.% (red and yellow arrows indicate direction of crack propagation and CNTs aggregates respectively).

4.2. Electrical conductivity

Figure 4. 2 illustrates electrical conductivity of the nanocomposite in relation to different CNT loadings. It can be noticed that the electrical conductivity significantly improves up to 10 orders of magnitude with addition of a low amount of CNTs i.e. 0.25 wt.%. In other words, the nanocomposite converts from electrically insulating polymer to a conductive polymer. In fact, a combination of electrical contact between CNTs, tunneling effect and intrinsic conductivity of the CNTs account for this remarkable enhancement in electrical conductivity [147]. A minor increase of electrical conductivity can be noticed at CNTs content of 0.5 wt.% compared with 0.25 wt.%. The maximum conductivity (0.1 S/m) was achieved at 0.75 wt.% concentration, resulting from large amounts of electrically conductive paths within the matrix (Figure

4. 1i-l).

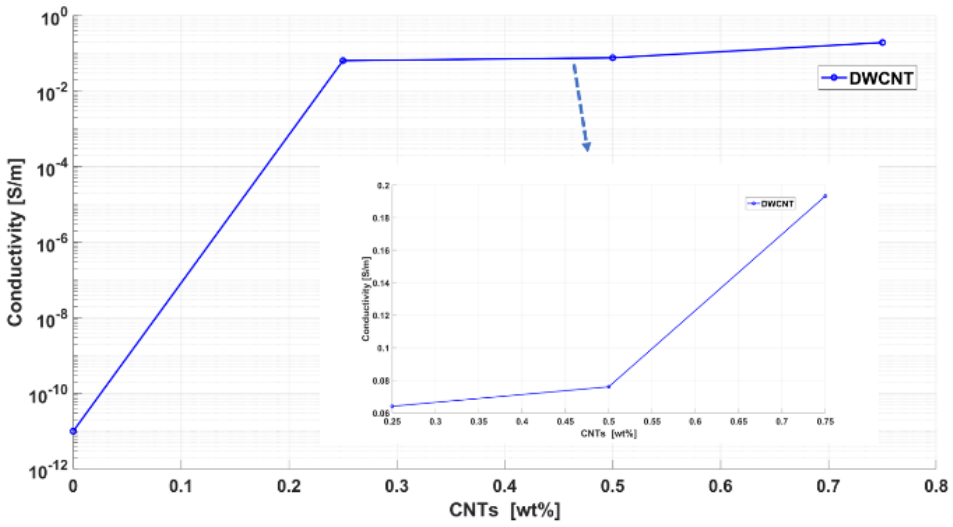

Figure 4. 2. Electrical conductivity versus CNTs content.

4.3. Piezoresistive characteristics

Strain and crack growth sensing capability of the nanocomposites are investigated under tensile and mode I fracture tests. Herein, the behaviors of the nanocomposites subjected to the aforementioned tests are investigated.

4.3.1. Tensile test

Increasing strain results in resistivity growth for all the CNTs concentrations during axial tension loading (Figure 4. 3a-i). In fact, CNT-based sensors can successfully monitor strain increase as well as damage initiation inside the matrix in real-time. Furthermore, specimens loaded with 0.5 wt.% induce higher change in electrical resistance compared with 0.25 and 0.75 wt.%, arisen from a more homogeneous dispersion of the nano-filler as shown in Figure 4. 1e-h.

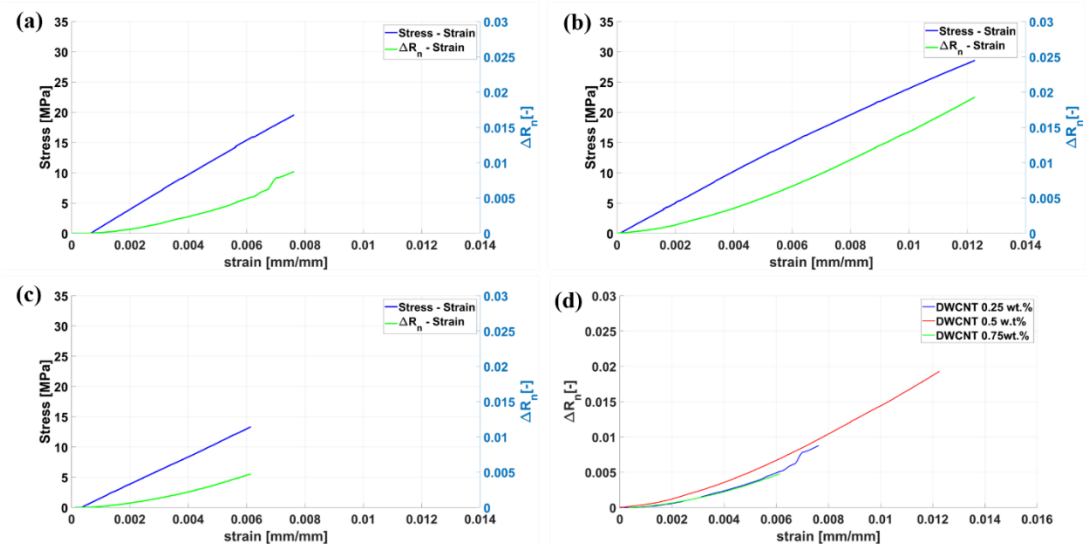

Figure 4. 3. Normalized resistance-strain and stress-strain curve: (a) 0.25 wt.%, (b) 0.5 wt.%, (c) 0.75 wt.%, (d) normalized resistance versus strain for all CNTs wt.%.

Piezoresistive characteristics at 0.25 and 0.75 wt.% show approximately the same trend, though a slight increase manifested for 0.25 wt.%, with respect to 0.75 wt.%, at strain values above 0.006 (Figure 4. 3d). This can be attributed to presence of larger agglomerations in the latter, leading to a softening effect in resistance growth in relation to strain [23]. Moreover, from Figure 4. 3d, it can be noticed that CNTs content of 0.5 wt.% possesses higher tensile strength compared with 0.25 and 0.75 wt.%. Although these results are affected by the state of CNTs dispersion, it can be concluded that 0.5 wt.% of CNTs shows better compromise between piezoresistivity and mechanical properties throughout this study, due to proper dispersion and lower amount of voids and aggregates related to manufacturing.

It is worth noting that all CNT contents demonstrate a nonlinear trend in normalized resistance at the beginning of test, when the strain is low, whereas the nonlinearity reduces at the end of the test, when the strain is high, as shown in Figure 4. 3; and also confirmed later in Figure 4. 4. These variations in piezoresistivity versus

strain can be attributed to different mechanisms driving the electromechanical properties in tensile tests. When the strain is low, tunneling resistance plays the dominant role in piezoresistivity [30], whereas the loss of contact between neighboring CNTs at higher strains mitigates the change in resistance, thus reducing the nonlinearity [148].

Figure 4. 4 illustrates sensitivity versus strain for different CNT contents. Sensitivity increases by strain increment regardless of the CNT content, then its increment rate decreases at higher strain. The increase of sensitivity during the test corresponded to 84 % , 86 % and 66 % for CNT loadings of 0.25, 0.5 and 0.75 wt.% respectively. From Figure 4. 4, it can be concluded that CNTs loading of 0.5 wt.% manifests higher sensitivity compared with 0.25 wt.%. This can be related to improper dispersion of CNTs within the matrix, as shown in Figure 4. 4d. In fact, the existence of CNTs-poor regions along the matrix at 0.25 wt.% compared with 0.5 wt.% causes less contribution of the tunneling effect.

Moreover, sensitivity at 0.75 wt.% is also less than that at 0.5 wt.%, which is in line with the literature mentioning that above the percolation threshold the sensitivity decreases by increase of the CNT content [30,112]. In practice, due to increasing CNTs contents above the percolation threshold, the tunneling effect on piezoresistivity reduces, favoring the formation of contact resistances, thus resulting in a lower sensitivity. Referring to Figure 4. 1j-l, formation of a large numbers of electrical contacts throughout the matrix at 0.75 wt.% resulting from high CNTs content soften the tunneling effect between neighboring CNTs.

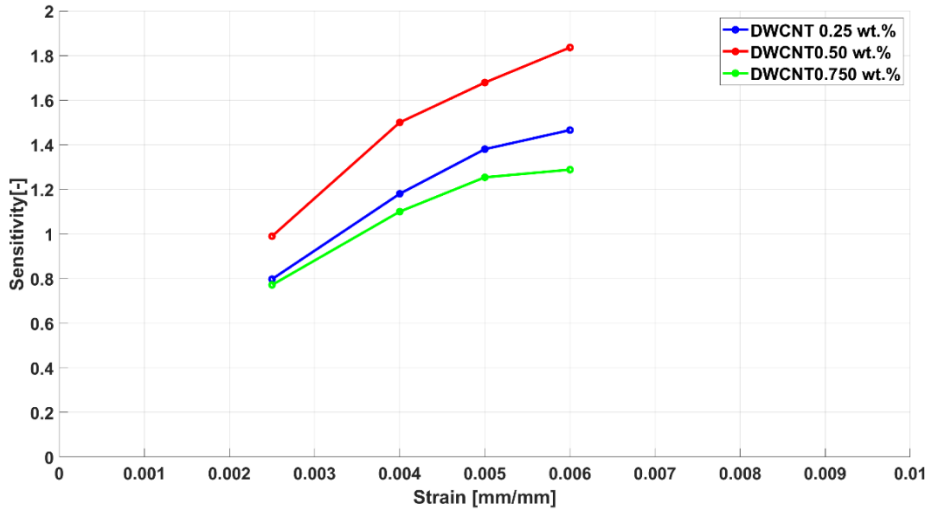

Figure 4. 4. Sensitivity versus strain

4.3.2. Fracture test

Two different stages, prior and during crack evolution, were taken into account for fracture toughness investigations. First, the piezoresistive response of SENB specimens prior to macro-crack propagation is studied in Figure 4. 5, i.e. only including the effect of localized strain on the piezoresistivity of the specimens. Then, the normalized resistance change due to the macroscopic failure associated to crack propagation is investigated (Figure 4. 6). The force-displacement curves associated to all the specimens are presented in Figure 4. 5 in order to ease the comparison in terms of electromechanical properties variation.

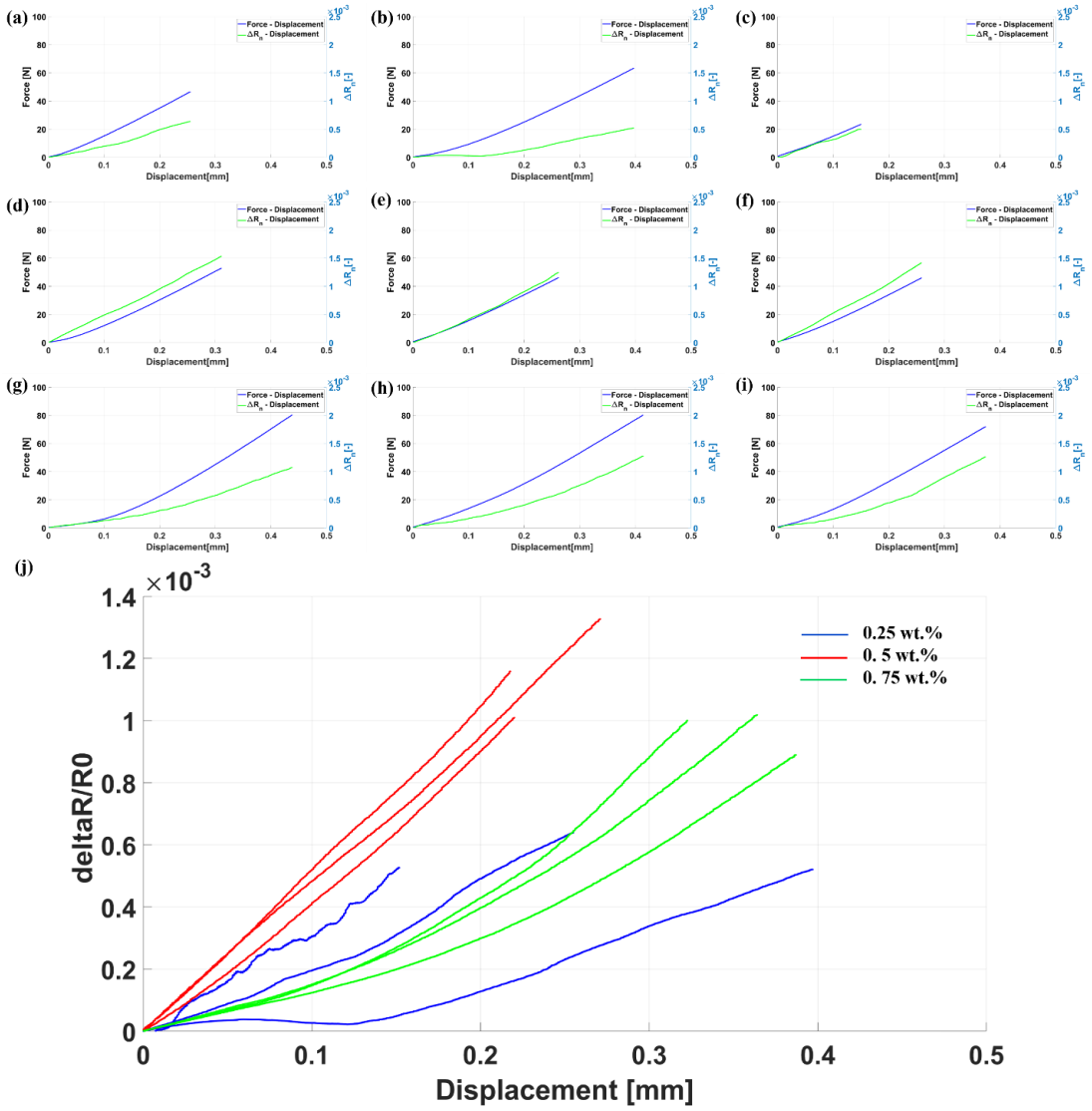

Figure 4. 5. Normalized resistance-displacment and force-displacment curve for three repetitions at each CNT wt.%, before macro-crack propagation: (a-c) 0.25 wt.%, (d-f) 0.5 wt.%, (g-i) 0.75 wt.%, (j) normalized resistance versus displacment for all the specimens(Specimen 1 to 3 from left to right at each CNTs loading).

Focusing on stage one (Figure 4. 5), normalized resistance versus mid-span displacement shows an augmented dispersion for specimens with 0.25 wt.% of CNT in comparison with CNT loadings of 0.5 and 0.75 (Figure 4. 5a-c and j), which again can be ascribed to insufficient CNTs content, i.e. inducing the CNTs-poor regions. This is in accordance with the tensile test results for CNT content of 0.25 wt.%. In contrast,

less deviations or more repetitiveness and homogeneity can be seen in the case of nanocomposites reinforced at 0.5 and 0.75 wt.% as depicted in Figure 4. 5d-j. In addition, nanocomposites containing 0.5 wt.% present higher sensitivity, here intended as the variation of ΔR_n with respect to the applied displacement, than those at 0.25 and 0.75 wt.% as clearly visible in Figure 4. 5j. In conclusion, these results confirm that specimens loaded at 0.5 wt.% manifest better performance in terms of piezoresistivity compared with other CNTs contents.

Unlike the tensile test, where a uniform ΔR_n trend in relation to the strain was obtained regardless of the CNT loadings, the ΔR_n trend versus displacement during fracture tests depends on the weight concentration. In other words, a linear pattern can be distinguished at CNTs content of 0.5 wt.%, whereas CNTs content of 0.25 and 0.75 wt.% manifest a nonlinear behaviour (Figure 4. 5j).

The linear trend at 0.5 wt.% can be attributed to simultaneous creation and breakage of electrical networks within the matrix in the compression and tension sides respectively [28]. These combined effects lead to linearity in piezoresistivity at CNTs content of 0.5 wt.% rather than nonlinearity observed during tensile test [149]. Nevertheless, it seems that positive change in ΔR_n arisen from breakage of electrical pathways at tension side dominates the negative change induced by formation of new electrical networks at compression side [111]. Therefore, in total, ΔR_n increases, though the trend is rather linear.

The nonlinear behaviour at 0.75 wt.% can be associated to high contents of CNTs, presence of CNTs clusters and formation of internal damages such as tiny cracks in the vicinity of the CNT clusters throughout the test. As it is shown in Figure 4. 1j-l, the presence of aggregates leads to formation of micro-cracks in their vicinity during fracture test. However, the CNT content is sufficiently high to avoid early failure

because of the higher fracture toughness of the specimen resulting from effective CNTs contribution in matrix reinforcement. In fact, as visible in Table 4. 1, specimens at 0.75 wt.% achieve the highest fracture toughness, although they also displayed the lowest tensile strength.

This contradicted behaviour of tensile and fracture tests at 0.75 wt.% can be explained by the different load configurations applied to the specimens throughout tensile and fracture toughness tests. In tensile tests, the whole bulk material is subject to the axial tension loading, whilst the SENB specimens undergo a localized stress concentration. Therefore, the presence of manufacturing defects may be less effective in deteriorating mechanical properties under fracture toughness tests, as there is less probability of having defects in the localized stress region. However, these internal damages contrast the formation of new electrical pathways in the compression side leading to non-linearity in ΔR_n, i.e. extensive breakage of electrically conductive pathways resulting from internal damages dominate the piezoresistivity of the material.

Table 4. 1. Fracture Toughness

CNT content	Specimen number	K_{IC} (MPa.m$^{0.5}$)
	1	1.08
0.25 wt.%	2	1.36
	3	0.44
	1	1.20
0.5 wt.%	2	1.06
	3	1.08
	1	1.34
0.75 wt.%	2	1.48
	3	1.34

The heterogeneous behaviors of specimens with CNT content of 0.25 wt.% hampers the comparison of its piezoresistive behaviour with other CNT contents. However, this data scatter can be attributed to inhomogeneous dispersion of CNTs as discussed before.

Before entering into the detailed description of the second phase's signals, the fracture toughness of each specimen is listed in Table 4. 1. It can be noticed that specimens with 0.25 wt.% CNT loading possess the lowest average fracture toughness, 0.94 $MPa\sqrt{m}$, compared with specimens loaded at 0.5 and 0.75 wt.% showing higher fracture toughness, in average of 1.11 and 1.39 $MPa\sqrt{m}$ respectively. The lowest fracture toughness at 0.25 wt.% can be attributed to improper dispersion of CNTs as well as existence of CNTs-poor regions in the matrix as discussed before, which is also reflected in the high scatter of fracture toughness results ranging from 0.44 to 1.36

$MPa\sqrt{m}$. On the other hand, less data scatter is obtained for 0.5 and 0.75 wt.%, due to a better dispersion of CNTs.

In general, three different macro-damage progressions take place depending on the fracture toughness of the specimen. When the specimens manifest a relatively high fracture toughness, an abrupt macroscopic brittle crack propagation takes place, as shown in Figure 4. 6a-b (0.25 wt.%), d (0. 5 wt.%), and g-i (0.75 wt.%). On the other hand, a gradual (Figure 4. 6c) and step (Figure 4. 6e-f) macro-damage evolution is typically associated with a minor fracture toughness. This is reflected in diverse ΔR_n signals as a function of mid-span displacement in Figure 4. 6, where the variation of ΔR_n is significantly higher than it was for the previous step, resulting in a horizontal line (green line in Figure 4. 6) for ΔR_n variation prior to macro-crack evolution.

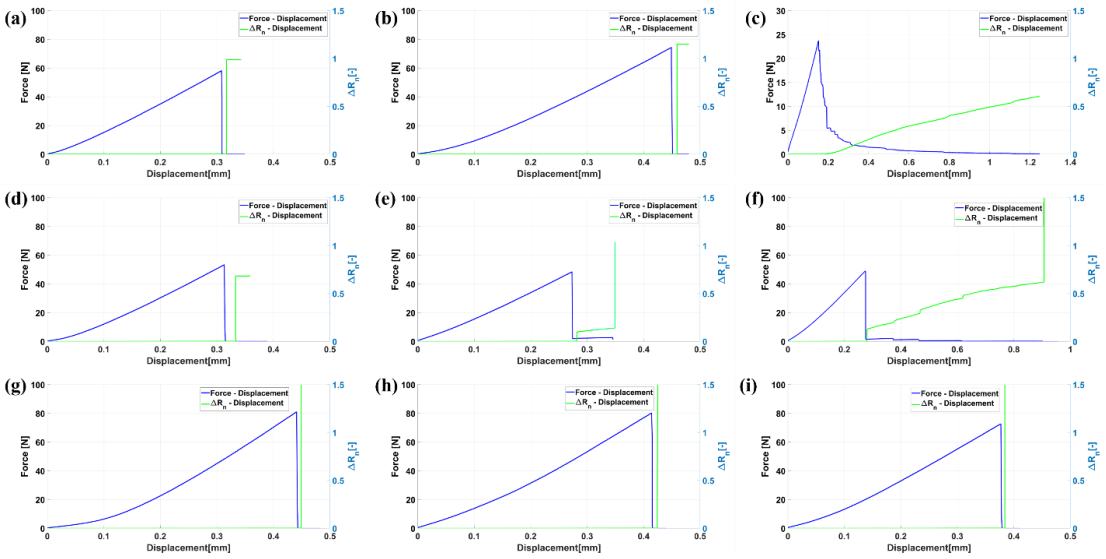

Figure 4. 6. Normalized resistance-displacment and force-displacment curve for three repetitions at each concentration before and upon crack failure: (a-c) 0.25 wt.%, (d-f) 0.5 wt.%, (g-i) 0.75 wt.% (Specimen 1 to 3 from left to right at each CNTs loading).

Figure 4. 7 shows a detailed analysis of ΔR_n change during crack propagation

for a specimen manifesting a gradual crack growth, as in Figure 4. 6c. To facilitate image visualization, green and blue arrows indicate the level of the ΔR_n and the force at different evolution steps respectively. An abrupt increase in normalized resistance around 0.02% can be seen in Figure 4. 7a (green arrow) with the onset of crack propagation (displacement < 0.165 mm), which might represent a novelty detection feature for the health assessment of a system.

Further increment in crack-extension results in higher increase in normalized resistance around 0.09 % as illustrated in Figure 4. 7b (0.165<displacement<0.175 mm). With the continuation of the crack extension, the ΔR_nincreases up to 0.28% at displacements between 0.175 and 0.194 mm as shown in Figure 4. 7c in which the crack extend up to 0.3 mm, corresponding to a residual minimal force of approximately 5N. This behavior progresses in Figure 4. 7d-h where the crack extends up to almost 3 mm resulting in a significant increase, approximately 40 %, of ΔR_n (0.194 <displacement< 0.77). Finally, at displacement of 1.2 mm, the specimen fails while ΔR_n increases up to 60 % (Figure 4. 7.i). In summary, it can be elucidated that any abrupt change in resistance is an indicator of crack initiation inside the system as shown in Figure 4. 7a, thus potentially enabling the health monitoring of structure subject to fatigue damage

progression.

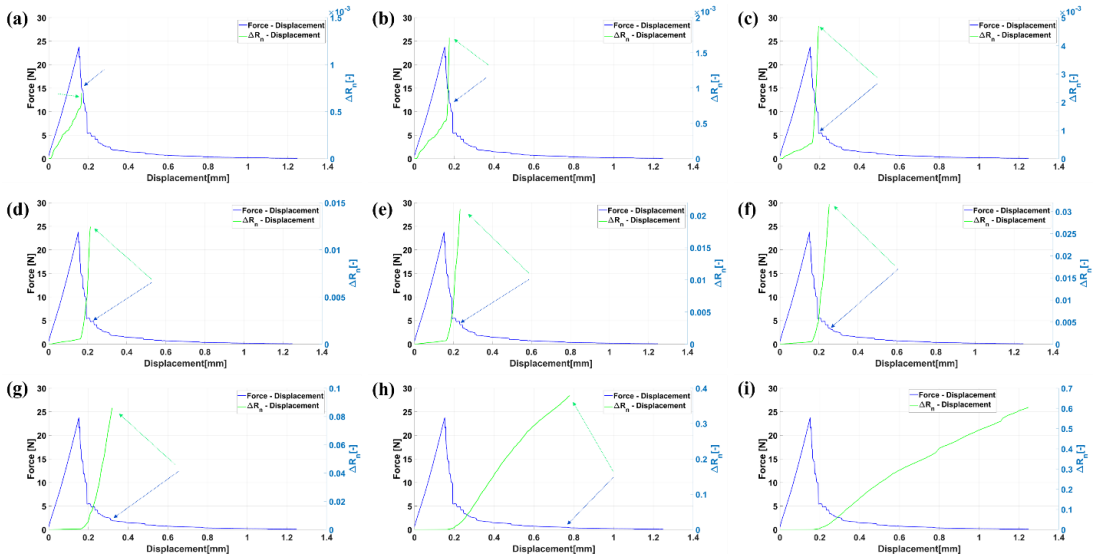

Figure 4. 7. Gradual extension of crack corresponding to Fig.9c: (a) displacement < 0.165, (b) 0.165 <displacement< 0.175, (c) 0.175 <displacement< 0.194, (d) 0.194 <displacement< 0.214, (e) 0.214 <displacement< 0.234, (f) 0.234 <displacement< 0.252, (g) 0.252 <displacement< 0.319, (h) 0.319 <displacement< 0.77, (i) 0.77 <displacement< 1.2.

ΔR_n as a function of crack propagation for a step damage evolution (Figure 4. 6f) is shown in Figure 4. 8. Before failure, at displacement of 0.27 mm, ΔR_n is approximately 0.15 % (Figure 4. 8a). With the onset of crack growth, ΔR_n increases abruptly up to 12 % (step 1) corresponding to 2 mm crack extension (Figure 4. 8b). However, the specimen did not fail completely, although the force reduced to a minimum. In fact, the next test phase (Figure 4. 8c) shows a minimal increase of the force resulting in the simultaneous increment of ΔR_n, up to the second step extension of the damage at 0.37 mm displacement. This stepped pattern continues up to the final specimen failure, happening at a 0.9mm displacement, when ΔR_n rises up to 170 %. As

a result, the developed nanocomposites can also monitor brittle fracture resulting from abrupt crack growth by showing remarkable increase in normalized resistance in a systematic manner.

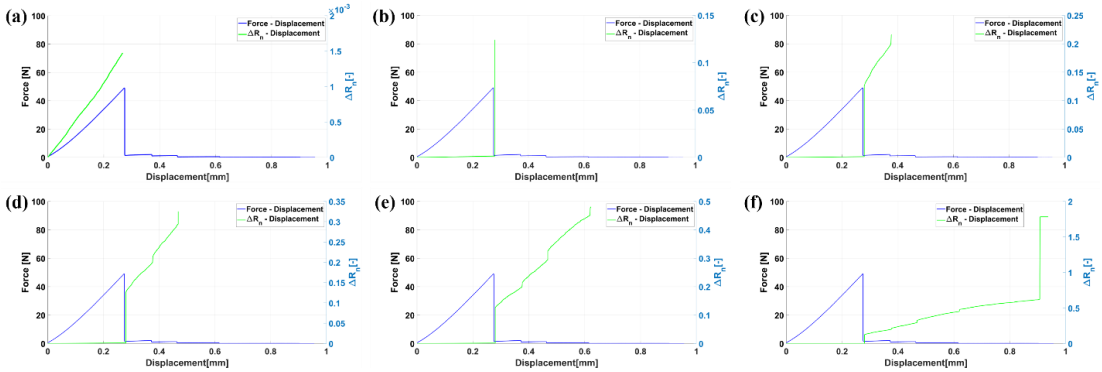

Figure 4. 8. Step extension of crack corresponding to Fig.9f: (a) displacement< 0.274, (b) 0.274 <displacement< 0.278, (c) 0.278 <displacement< 0.377, (d) 0.377 <displacement< 0.46, (e) 0.46 <displacement< 0.62, (f) 0.62 <displacement< 0.9.

4.4. Summary

Strain and damage sensing capability of epoxy reinforced with SWCNTs-DWCNTs were investigated under tensile and fracture toughness tests. Different CNT contents were analysed, each one leading to different microstructures depending on the manufacturing process, thus to different mechanical and electrical behaviours. In summary, the following outcomes were derived:

- State of CNTs dispersion and presence of CNTs clusters were strictly related to the CNTs content. CNTs content of 0.5 wt.% presented more homogeneous dispersion of CNTs along the epoxy matrix, whilst large clusters of CNTs were observed in the case of 0.75 wt.%. CNTs loading of 0.25 wt.% were

accompanied with CNT-poor regions inside the matrix due to low content of CNTs.

- The electrical conductivity increased up to 10 orders of magnitude at 0.25 wt.% (with respect to pure epoxy), while slight increase was noticed from 0.25 to 0.75 wt.%, suggesting the percolation threshold was exceeded. The maximum electrical conductivity (0.1 S/m) was achieved at 0.75 wt.% resulting from extensive amount of electrical networks within the matrix.
- For tensile tests, the normalized resistance change as a function of strain showed nonlinear trend while the nonlinearity decreased at high strain. Tunneling and contact resistances among CNTs were taken into consideration as the predominant mechanisms in driving the electromechanical properties of the sensors at low and high strains, respectively.
- Due to nonlinearity in ΔR_n – strain curves, sensitivity also showed a correlation with the strain, common to all the CNT contents, i.e. it enhanced by increasing strain, whereas its increment rate reduced at higher strains. CNT loading of 0.5 wt.% achieved the highest sensitivity (around 1.8) at strain of 0.06 [-]. The lower sensitivity observed at 0.25 and 0.75 wt % was attributed to occurrence of CNT-poor regions inside the matrix and presence of agglomerations and defects, respectively.
- In fracture tests, prior to crack failure, linear behavior was observed in normalized resistance change as a function of displacement for specimens containing 0.5 wt.% of CNTs which was attributed to simultaneous creation and breakage of electrical pathway within the matrix at tension and compression sides, respectively. However, a nonlinear trend was seen in the case of 0.75

wt.% due to formation of tiny cracks in the vicinity of large clusters of CNTs leading to more extensive destruction of electrical paths during deflection.

- In fracture tests, the nanocomposites were capable of self-monitoring crack initiation and extension inside the specimen, manifesting as abrupt increases in normalized resistance with the onset of first crack extension. Three different piezoresistive behaviors were noticed depending on the fracture toughness of the specimens including abrupt, gradual and step crack evolution. It was found out that any abrupt change in normalized resistance was a significant feature for monitoring the health of the specimen.

CHAPTER 5: COMPARISON OF SWCNTS AND DWCNTS/EPOXY

Throughout this chapter, tensile and impact strengths of the epoxy based nanocomposites loaded with different types of CNTs, specifically functionalized CNTs with a hydroxyl group i.e. SWCNTs-OH and SWCNTs-DWCNTs, the latter simply referred to as DWCNTs, at different weight concentrations including 0.5, and 0.75 wt.% will be examined. A detailed analysis of the microstructural characteristics of the nanocomposites using SEM and FESM characterization is provided to investigate presence of defects such as air bubbles, pores, agglomerations and entanglement on mechanical properties. Therefore, allowing a correlation of different CNT loadings with different microstructural defects, and highlighting their effects on the tensile and impact strengths as well as on the morphology of the fracture surfaces.

5.1. Microstructural characterization

One of the main challenges in CNT based nanocomposites is formation of air bubbles which can be even detected by visual inspection, as shown in Figure 5. 1a. It is worth noting that it is quite difficult to quantify the void content since their dispersion is not homogenous, especially at high CNT loading, thus, the analysis of the pore and void content are mostly carried out using SEM and optical microscopy. They can also be appeared in the form of porosities and voids (Figure 5. 1b-c) in the cross-section of the samples at smaller scale (micron) which, acting as a stress concentrator, significantly deteriorate mechanical properties of the specimen. Specifically, DWCNTs/epoxy mixture manifested higher amount of pores compared with SWCNTs/epoxy mixture due to lack of functionalization, thus, leading to difficulties in

efficient removal of the air bubbles. As a consequence, DWCNTs/epoxy samples present more defects than SWCNTs/epoxy, as shown in Figure 5. 1.

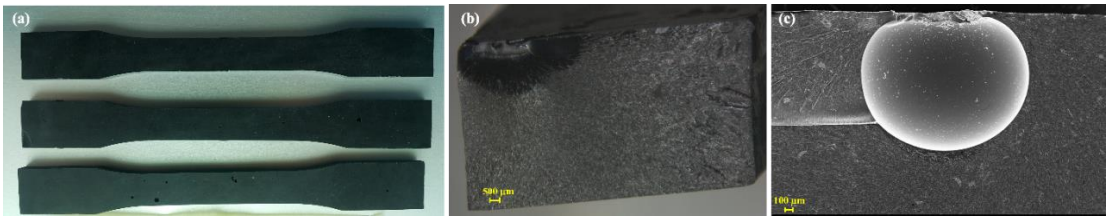

Figure 5. 1. Formation of bubbles and pores for DWCNT doped epoxy: (a) air bubbles visually evident on some dog-bone specimens, (b-c) presence of pores and voids within the cross-section of the dog-bone specimen.

Figure 5. 2 shows FESEM images of the cross section of dog-bone specimens after failure. A relatively good dispersion can be find out at SWCNTs and DWCNTs loading of 0.5 wt.% as shown in Figure 5. 2a and c for SWCNTs and DWCNTs respectively. On the other hand, high CNT content (0.75 wt.%) leads to presence of aggregates and formation of pores in their vicinity, as shown in Figure 5. 2b and d for SWCNTs and DWCNTs respectively. In fact, increasing CNTs content leads to more agglomeration which is accompanied with higher number of pores, marked with red arrows in Figure 5. 2b and d for SWCNTs/epoxy and DWCNTs/epoxy respectively, resulting from the high viscosity of the mixture at high CNTs content [67]. These CNTs-weak regions significantly reduce the mechanical properties of the CNT/epoxy nanocomposites as will be detailed later.

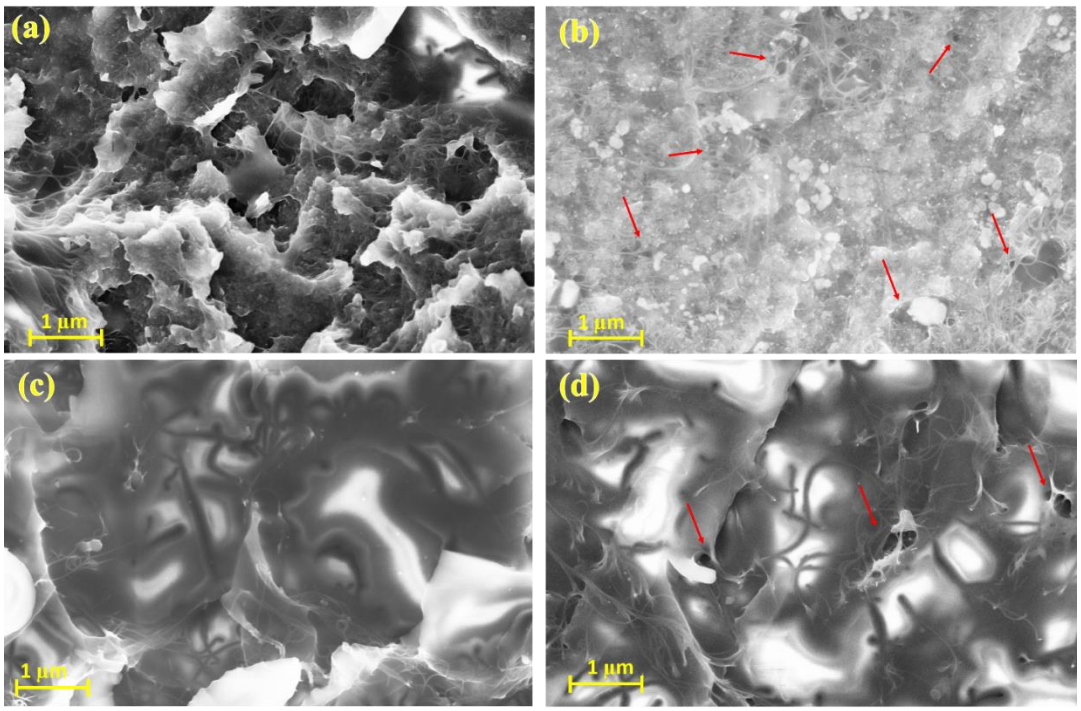

Figure 5. 2. FESEM images of the cross-section after tensile test failure: (a-b) SWCNTs/epoxy, (c-d) DWCNTs/epoxy (left to right indicate 0.5 and 0.75 wt.% respectively).

5.2. Mechanical properties

A detailed analysis of the obtained mechanical properties (tensile and impact strength), in relation with the microstructural characteristics, i.e. CNTs dispersion and manufacturing defects, is provided in the following sub-sections.

5.2.1. Tensile test

The average tensile strength of the nanocomposites and the pristine epoxy are shown in Figure 5. 3. The highest improvement in tensile strength (around 15 % increase) is obtained at SWCNT 0.5 wt.%, however, other nanocomposites manifest a

reduction with respect to the neat epoxy. The slight increase in tensile strength at 0.5 wt.% SWCNT can be attributed to more homogenous CNTs dispersion at this CNTs loading in comparison with other CNT loading. On the other hand, regardless of CNTs morphology used, SWCNTs and DWCNTs, tensile strength reduced at high CNTs loading (0.75 wt.%), resulting mainly from the agglomeration and subsequently presence of higher amount of pore as shown by red arrows in Figure 5. 2b and d.

It is worth noting that unlike the enhanced tensile strength for 0.5 wt.% SWCNTs, tensile strength reduced at 0.5 wt.% DWCNTs which can be ascribed to the lack of functionalization in the latter. In other words, the OH-functionalization used for SWCNTs could reach to better CNT/epoxy bonding, thus proper interfacial-shear bonding transfer takes place in the SWCNT in comparison with the DWCNT.

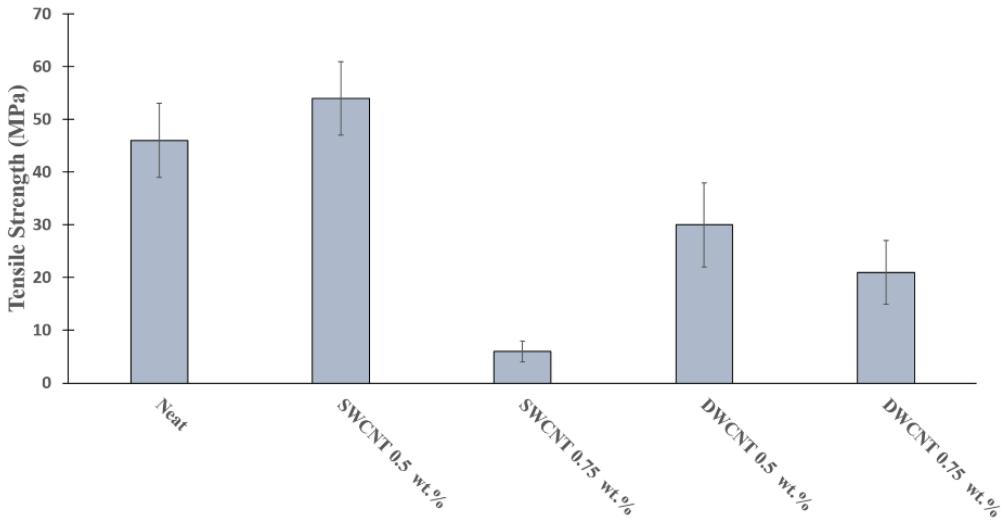

Figure 5. 3. Average tensile strength

In general, reduction of tensile strength at 0.75 wt.% SWCNTs, 0.5 and 0.75 wt.% DWCNTs can be related to presence of aggregates and pores mainly due to improper dispersion and degassing resulting from high viscosity of the CNT/epoxy

mixture, thus, hampering the evacuation of the air bubbles entrapped in the CNT/epoxy mixture. This induces defects, i.e. voids and tiny pores as well as aggregates, which severely deteriorate the tensile strength, due to susceptibility of the epoxy to defects resulting from brittleness of the epoxy. Generally, the high viscosity of the CNTs/epoxy mixture at high CNTs content, which does not allow proper degassing, causes these defects. Thus, viscosity establishes a limit for the CNTs content used.

Moreover, as it is shown in Figure 5. 3, at 0.75 wt.% loading, the reduction in tensile strength for SWCNTs is much larger than the DWCNTs. This can be attributed to higher amount of agglomeration in the former compared with the latter when high CNTs loading used. In general, formation of aggregates in SWCNTs is more prevalent than for DWCNTs, due to the larger surface area and aspect ratio of the former[43]. This induces the mechanical properties at high CNT content (0.75 wt.%) to be more affected by the agglomeration for SWCNTs doped nanocomposites, in fact the lowest tensile strength (6 MPa) is obtained for 0.75 wt.% SWCNTs/epoxy. However, SWCNTs manifested better tensile strength compared with DWCNTs at low CNT contents i.e. at 0.5 wt.%. This can be attributed to the OH-functionalization of SWCNTs resulting in improvement of interfacial load transfer between SWCNTs and epoxy [73], though the effect of functionalization may not be prevalent when excessive SWCNTs content (0.75 wt.%) is selected, due to formation of agglomerates.

Figure 5. 4 shows SEM images of the fracture surface of the tensile specimens. Depending on the tensile strength of the specimen, the fracture surfaces highlight two main features, including a river-like or cleavage pattern characterized by higher surface roughness (Figure 5. 4a, c, and i) and a flat or smooth surface (Figure 5. 4g and k). Specifically, the specimens with higher tensile strength demonstrate river-like patterns with higher surface roughness whereas an almost flat surface can be seen in the case of

specimens with lower tensile strength. Accordingly, the highest surface roughness is obtained for the 0.5 wt.% SWCNTs (Figure 5. 4c-d) and the neat epoxy (Figure 5. 4a-b), manifesting the highest tensile strength (among all specimens. On the other hand, the fracture surface becomes almost smooth at 0.75 wt.% loading for both SWCNTs (Figure 5. 4g-h) and DWCNT(Figure 5. 4 k-l) respectively.

SEM images of the fracture surface of the specimens manifested a relatively good tensile strength i.e. neat epoxy and 0.5 wt.% SWCNTs (Figure 5. 4a and c respectively) reveal two different regions as follow: (i) a flat region where initial fracture takes place and propagates abruptly as highlighted by the green dashed line in Fig.5a and c, (ii) a river-like pattern representing the evolution of several micro-cracks throughout the cross-section.

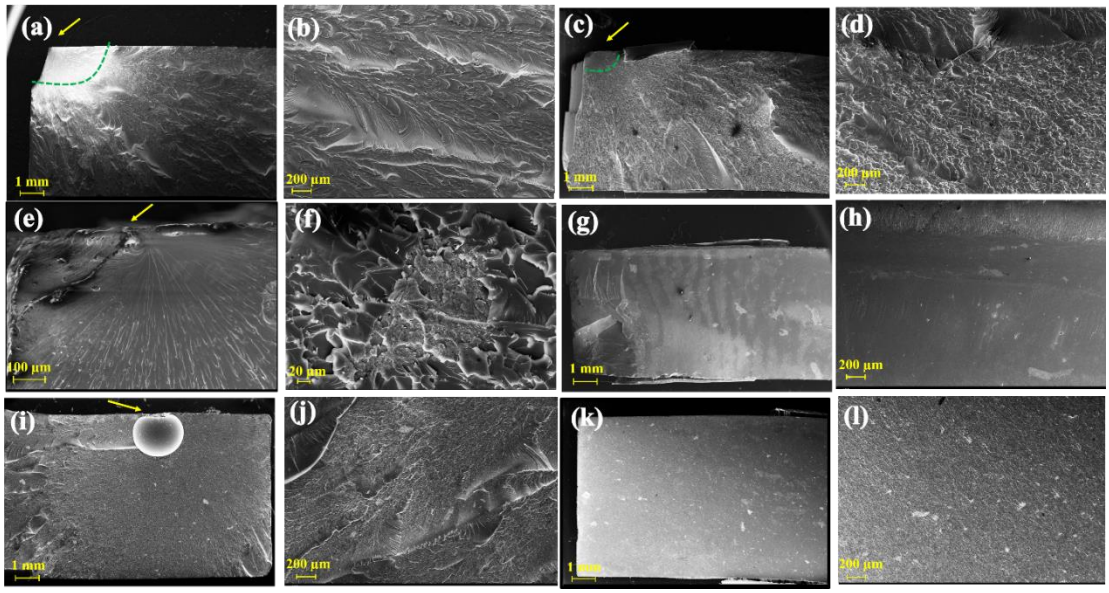

Figure 5. 4. SEM image of the fracture surface upon tensile test: (a-b) neat epoxy, (c-f) 0.5 wt.% SWCNTs, (g-h) 0.75 wt.% SWCNTs, (i-j) 0.5 wt.% DWCNTs, (k-l) 0.75 wt.% DWCNTs (dash green line and yellow arrow represent the initial flat region and the fracture initiation point respectively).

5.2.2. Impact strength

The effect of adding CNTs on impact strength of the nanocomposite is studied hereinafter. As shown in Figure 5. 5, incorporation of CNTs results in significant increase in Izod impact strength compared with the pristine epoxy, when relatively low CNT content is used (0.5 wt.%). In contrast, high CNTs content (0.75 wt.%) leads to a reduction which is attributed to the presence of defects, including aggregates and pores as discussed before. It is worth noting that, similarly to tensile test, the reduction in impact strength from 0.5 to 0.75 wt.% for SWCNT is much larger than DWCNT, which again can be attributed to higher amount of aggregates in the former than the latter.

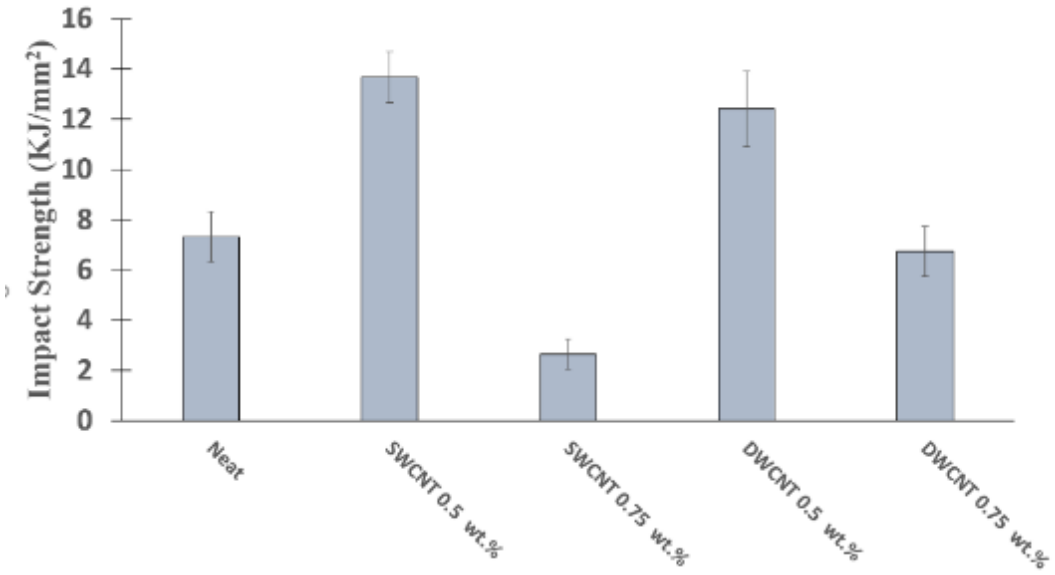

Figure 5. 5. Impact strength for different material configurations (average)

The lower impact strength for 0.5 wt.% DWCNT with respect to 0.5 wt.% SWCNT can be attributed to the presence of more defects such as pores as shown in Figure 5. 6, resulting from lack of functionalization used in the former. In general, Izod impact strength increases by 87 % and 70 % at 0.5 wt.% SWCNTs and 0.5 wt.%

DWCNTs respectively.

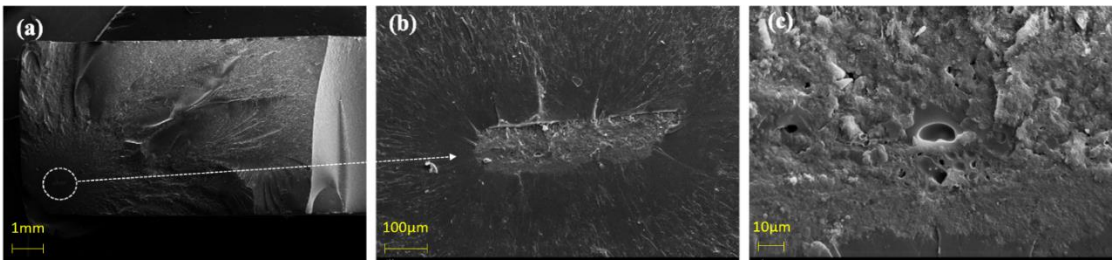

Figure 5. 6. (a-c) Presence of tiny pores within the cross-section of the impact specimen for DWCNTs doped epoxy at different magnifications.

An example of the fracture edge shaped after impact test is shown in Figure 5. 7 (side view). Arrows number 1 to 3 indicate starting and ending points of the fracture respectively. It should be mentioned that the majority of the impact energy is absorbed at stages 1 to 2, while stage 3 consumes the minimum amount of impact energy. This is confirmed based on the analysis of surface roughness, as shown in the following.

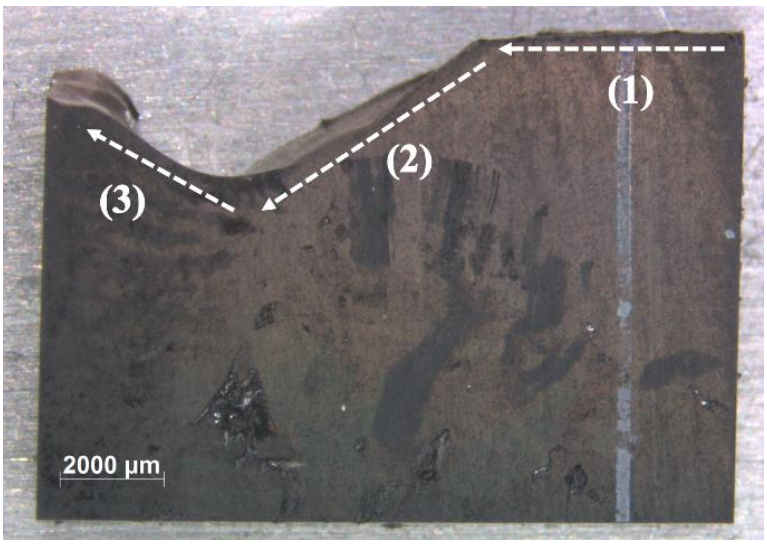

Figure 5. 7. Side view of the impact specimen showing different stage of fracture throughout the impact test.

SEM images of the specimen's cross section after impact tests are shown in Figure 5. 8. Morphology of the impact surfaces is similar as for the tensile tests, i.e. more surface roughness indicates higher impact strength and vice versa. Accordingly, the highest surface roughness can be seen at 0.5 wt.% SWCNTs (Figure 5. 8b) whereas an almost a flat surface is observed at 0.75 wt.% SWCNTs (Figure 5. 8c), which manifested the highest and lowest impact strengths respectively.

Two different regions can be identified at all CNTs contents, as shown by the blue dash line: (i) a rough surface region and (ii) a flat mirror-like region. Left and right sides with respect to the blue dashed line correspond to the stages 1-2 and 3 shown in Figure 5. 7, respectively. In fact, just after impact failure initiation indicated by yellow arrows in Figure 5. 8, in steps 1 and 2, the material provides resistance against crack propagation failure, and higher surface roughness is obtained.

In the last failure step, due to shortening of the cross section, crack propagates rapidly (brittle fracture) and a flat mirror-like pattern is achieved. It is worth mentioning that despite of appearance of two surface patterns for all the specimens, only one pattern i.e. a fine flat region can be noticed at 0.75 wt.% SWCNTs due to its low impact strength

which is again in agreement with tensile test results.

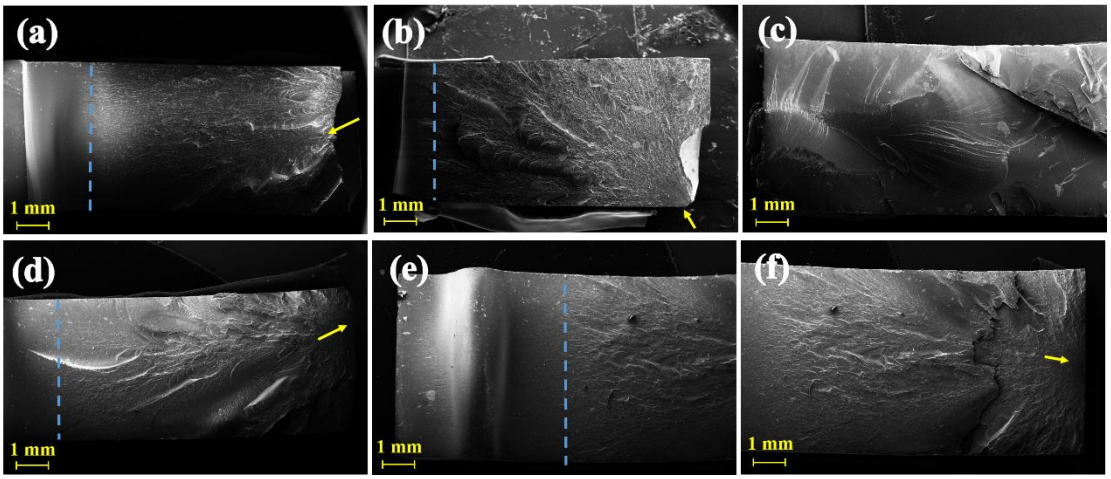

Figure 5. 8. SEM images of the specimens fracture surface after Izod tests: (a) pristine epoxy, (b) 0. 5 wt.% SWCNTs, (c) 0.75 wt.% SWCNTs, (d) 0. 5 wt.% DWCNTs, (e-f) 0. 75 wt.% DWCNTs.

5.3. Results comparison

In general, due to the presence of manufacturing defects such as agglomeration, the tensile test results showed a slight increase around 15% for 0.5 wt.% SWCNTs loading whist for other nanocomposites, a reduction appeared. For the impact test, a significant increase up to 87 % and 70 % was observed for 0.5 wt.% of SWCNTs and DWCNTs loadings respectively, followed by a reduction of the impact strength at 0.75 wt.% for both SWCNT and DWCNTs. The diverse behavior can be ascribed to the different load configuration, and stress distribution, the specimen undergoes during the tests.

The axial load during tensile test generates a homogeneously distributed stress which causes the test result to be very susceptible to any possible defect in the dog-

bone specimen, such as porosity and CNT aggregates, thus deteriorating tensile strength. The localized stress condition during impact reduces the probability of having a defect in the most stressed location. Therefore, a significant enhancement can be noticed in the impact strength CNT doped specimens. Further increase of impact strength can potentially be related to the activation of crack bridging mechanism (white dashed arrows in Figure 5. 9) and CNT pullout as shown in Figure 5. 9 [70].

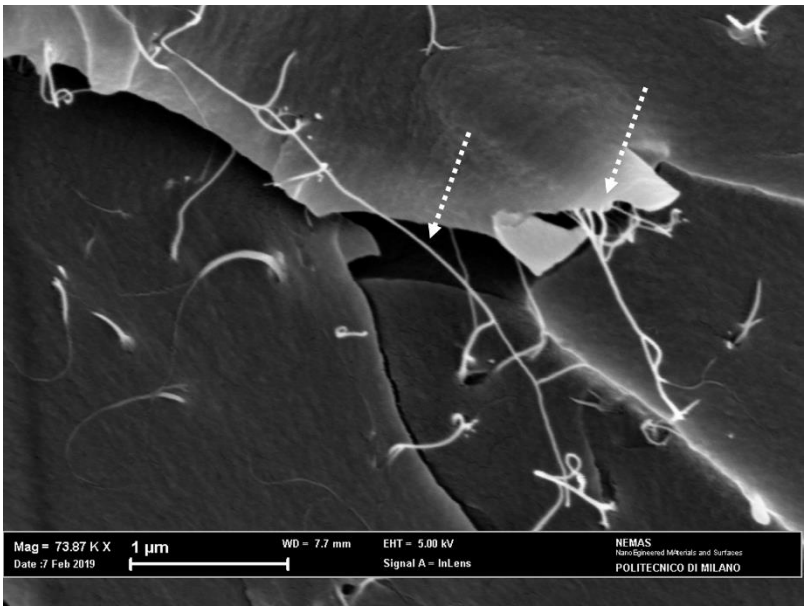

Figure 5. 9. Crack bridging mechanism shown by white dashed arrows.

5.4. Summary

Tensile and impact Izod tests on epoxy specimens loaded with SWCNTs and DWCNTs have been performed in this study. Although the presence of manufacturing defects such as air bubbles and tiny pores as well as CNT agglomerations resulted in heterogeneous behaviors in tensile and impact strengths, some outcomes were drawn in the attempt to correlate different CNT loadings with different microstructural defects, and highlight their effects on the tensile and impact strengths as well as on the

morphology of the fracture surfaces. In summary, the following conclusions emerged:

- A relatively good CNTs dispersion was obtained at low CNTs content i.e. 0.5 wt.%. Defects at 0.75 wt.% were attributed to improper degassing and dispersion procedures during manufacturing due to high viscosity of the nanocomposites mixture after addition of CNTs. Thus, higher CNT content (0.75 wt.%) has been established as a limit due to manufacturing restrictions. The presence of degasification defects were more noticeable in DWCNTs/epoxy with respect to SWCNTs due to lack of functionalization, whereas the latter displayed higher entanglements at 0.75 wt.% compared with the former.
- Tensile strength slightly improve up to 15 % for 0.5 wt.% SWCNT, whereas for other nanocomposites it reduced compared with the neat epoxy mainly due to presence of defects. In overall, SWCNTs/ epoxy achieved better tensile strength rather than DWCNTs/epoxy, though the lowest tensile strength was obtained at 0.75 wt.% SWCNTs, which was ascribed to the excessive amount of CNTs entanglements resulting in appearance of CNTs-weak region within the matrix.
- Impact strength was significantly improved by 87% and 70% at 0.5 wt.% SWCNTs, and 0.5 wt.% DWCNTs respectively, whereas higher CNTs loading leaded to a reduction of impact strength. Considering both impact and tensile strength, 0.5 wt.% was considered as the best weight concentration in terms of achieving compromise mechanical properties.
- The diverse influence of the addition of CNTs on tensile and impact strength was ascribed to the stress condition within the specimen, in presence of manufacturing defects: (i) global uniform stress distribution in tensile tests caused remarkable reduction of tensile strength due to susceptibility of the

epoxy to any possible defect in the specimen; (ii) localized stress in impact tests resulted in less detrimental effect by defects on impact strength, due to the minor probability of having a defect in the most stressed location.

- Flat mirror-like pattern and rough surface were seen for the specimens presenting low and high strength respectively (for both tensile and impact test). Higher surface roughness indicated higher strength while a flat surface indicated poor mechanical properties.
- Crack-bridging and CNTs pull-out mechanisms were the main toughening mechanisms resulting in improvement of impact strength of the CNTs based nanocomposites.

CHAPTER 6: HYBRID DWCNTS AND NANOCLAY/EPOXY

In this chapter, a comprehsive examination of the synergetic effects of the addition of CNTs and nanoclay on not only the mechanical properties, but also on the electrical conductivity and piezoresistive sensitivity performance has been performed. The nanocomposites were prepared in two different states i.e. binary (DWCNTs/epoxy) and ternary (DWCNTs-NC/epoxy) in order to compare the effect of the addition of nanoclay into CNTs doped epoxy in terms of microstructural, electrical, mechanical and electromechanical characteristics. For the hybrid state, the CNTs loading was kept constant at 0.1 wt.% while two different nanoclay contents including 0.5 wt.% and 1 wt.% were used. Theses nanoclay contents were used based on the ease of manufacturing procedure due to higher viscosity of the nanofillers/epoxy mixture at hybrid stats, thus, higher nanoclay loading was avoided. Tensile and mode I fracture tests were carried out for mechanical and piezoresistive characterization. XRD, SEM and FESEM analyses were used for the microstructural characterizations and the analysis of dispersion states of nanofillers. Finally, the mechanical property and piezoresistivity performance of the developed nanocomposites at hybrid states is compared with the binary state. It is worth noting that the nanoclay powder was preheated at 100 C˚ for one hour in order to dry them before dispersing them into the epoxy.

In the following sections, the microstructural properties of the nanocomposites along with the mechanical and electromechanical characteristics are investigated for both binary and ternary states in detail. Initially, the effect of the addition of nanoclay on CNTs dispersion is studied. Then, the associated electrical conductivity, tensile strength, fracture toughness and electromechanical properties in terms of sensitivity of

the CNTs doped epoxy is compared.

6.1. Microstructural characterization

6.1.1. FESEM analysis

FESEM images of the fracture surface of the tensile specimen are presented in Figure 6. 1a-c, d-f, and g-i to compare the dispersion state of the nanofillers at 0.1 wt.% DWCNT, 0.1 wt.% DWCNT - 0.5 wt.% NC, and 0.1 wt.% DWCNT – 1 wt.% NC, respectively. It is worth mentioning that higher magnification images corresponding to the dashed yellow rectangles in the left column figures (Figure 6. 1) are presented in the middles and right column figures for each nanocomposites. CNT content of 0.1 wt.% (Figure 6. 1a-c) manifests relatively good CNT dispersion, though the presence of CNT-rich and CNT-poor (agglomeration) regions are also noticeable as highlighted by white dashed rectangle and arrows in Figure 6. 1a respectively.

The presence of tiny CNT-aggregates is an inevitable phenomenon resulting from high surface areas and large aspect ratio of the CNTs as well as the CNT re-agglomeration due to high temperature (60 ˚C) used during manufacturing. Using high temperature during manufacturing is important to guarantee efficient removal of the entrapped air from the CNT/epoxy mixture, but this also allows some CNTs to bundle together as shown in Figure 6. 1b-c. It is worth noting that the agglomerated-CNTs are not severely twisted and entangled together, thus, reducing their detrimental effect on the final mechanical and electromechanical properties, as discussed below in detail. The absence of pores and voids in Figure 6. 1a-c thoroughly indicates that the degassing system used in this study is effective in the evacuation of the entrapped air.

A comparison of Figure 6. 1a-c with Figure 6. 1d-f proves that the addition of 0.5 wt.% nanoclay to DWCNT doped epoxy improves the CNT dispersion as no CNT-aggregates can be identified in the cross section image (Figure 6. 1d-f). This can also be proven in the higher magnification images provided in Figure 6. 1e-f, where red dashed arrows highlight presence of nanoclay. It is worth noting that it is quite difficult to see nanoclay dispersion at low magnification images due to their plate morphology (dashed red arrow in Figure 6. 1d), however, a clear image accentuated by dashed red arrows is clearly visible at high magnification in Figure 6. 1e-f. In addition, Figure 6. 1e-f show that, in addition to DWCNT manifesting good dispersion assisted by nanoclay, the dispersion state of nanoclay itself shows homogeneity. Thus, a proper dispersion was achieved for 0.1 wt.% DWCNT-0.5 wt.% NC/epoxy composite.

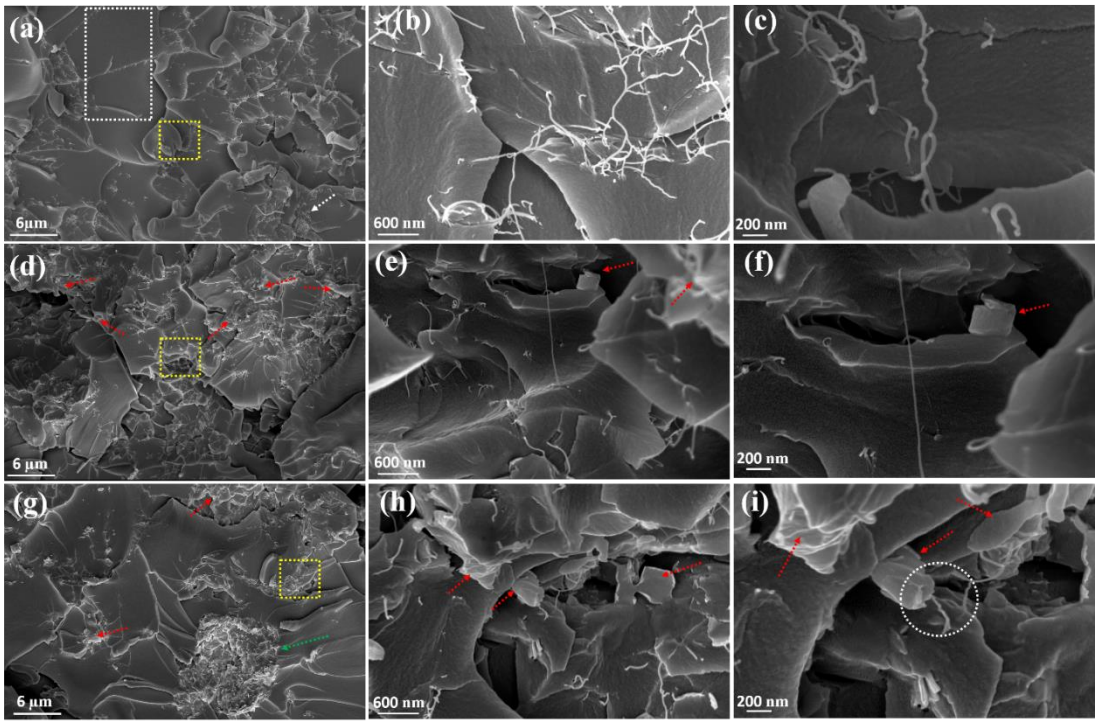

Figure 6. 1. FESEM images taken from the fracture surface of the tensile specimens: (a-c) 0.1 wt.% DWCNT/epoxy, (d-f) 0.1 wt.% DWCNT-0.5 wt.% NC/epoxy, (g-i) 0.1

wt.% DWCNT-1 wt.% NC/epoxy. Yellow dashed rectangles represent the regions magnified in the middle and right sides images.

The dispersion state of the nanofillers at higher nanoclay loading i.e. 0.1 wt.% DWCNT- 1 wt.% NC/epoxy is displayed in Figure 6. 1g-i. A homogenous CNT dispersion is obtained as no aggregated CNTs are visible in the cross-section images. Again, this indicates beneficial impact of the nanoclay in improving CNT dispersion, even though a higher nanoclay loading (1 wt.%) was used. An increase of the nanoclay content from 0.5 wt.% to 1 wt.%, therefore, does not possess a detrimental effect on CNT dispersion. On the other hand, it results in the presence of some nanoclay aggregates as shown by the dashed green arrow in Figure 6. 1g.

Nevertheless, the conclusion obtained from Figure 6. 1g-i is a combination of nanoclay-rich and -poor regions are achieved while DWCNT shows relatively good dispersion. Of notice is that, although some nanoclays tend to agglomerate, the agglomerate size is not critical to deteriorate the mechanical properties as a good interfacial bonding with the epoxy was achieved, i.e. no region with poor-wettability is noticeable in the vicinity of the agglomerated nanoclay (Figure 6. 1g). Finally, a proper interaction between the nanoclay, DWCNT and epoxy is also obtained as shown by a white dashed circle in Figure 6. 1i, indicating that not only a homogenous nanofiller dispersion is obtained, but also an appropriate mutual interaction between the nanofillers and the epoxy is achieved.

FESEM images of the fracture surface of the SENB specimens are also presented in Figure 6. 2 to guarantee the dispersion analysis of the nanofillers in this study are authentic regardless of the specimen types, being both the tensile and SENB specimens cut from the same plate. Similar to tensile specimen, the presence of CNT-

rich and CNT-poor regions are considerable for 0.1 wt.% DWCNT/epoxy (Figure 6. 2a-b), though the aggregated CNTs manifest quite proper interfacial bonding to the epoxy as no poor-wettability can be noticed from Figure 6. 2b. This indicates that although there are some aggregates formed in the binary state, they are not particularly critical to the mechanical properties.

On the other hand, regardless of the nanoclay content (0.5 wt.% and 1 wt.%), more homogenous DWCNT dispersions are achieved in ternary states as shown in Figure 6. 2c-d and Figure 6. 2e-f for 0.1 wt.% DWCNT-0.5 wt.% NC and 0.1 wt.% DWCNT-1 wt.% NC, respectively. This confirms nanoclay can successfully improve CNTs dispersion since it avoids re-agglomeration of CNTs arisen from elevated temperature employed during manufacturing i.e. it acts as an obstacle against CNT re-agglomeration.

In addition, increasing nanoclay loading form 0.5 wt.% to 1 wt.% results in the formation of nanoclay aggregates as marked by the yellow dashed arrow in Figure 6. 2e. Finally, as marked by white dashed circles in Figure 6. 2d and f, DWCNT, nanoclay and epoxy properly mutually interact, as proven by the stretching state of the DWCNT marked by the green dashed arrow in Figure 6. 2f, the straightness of the CNTs indicating that a successful shear-loading transfer occurs.

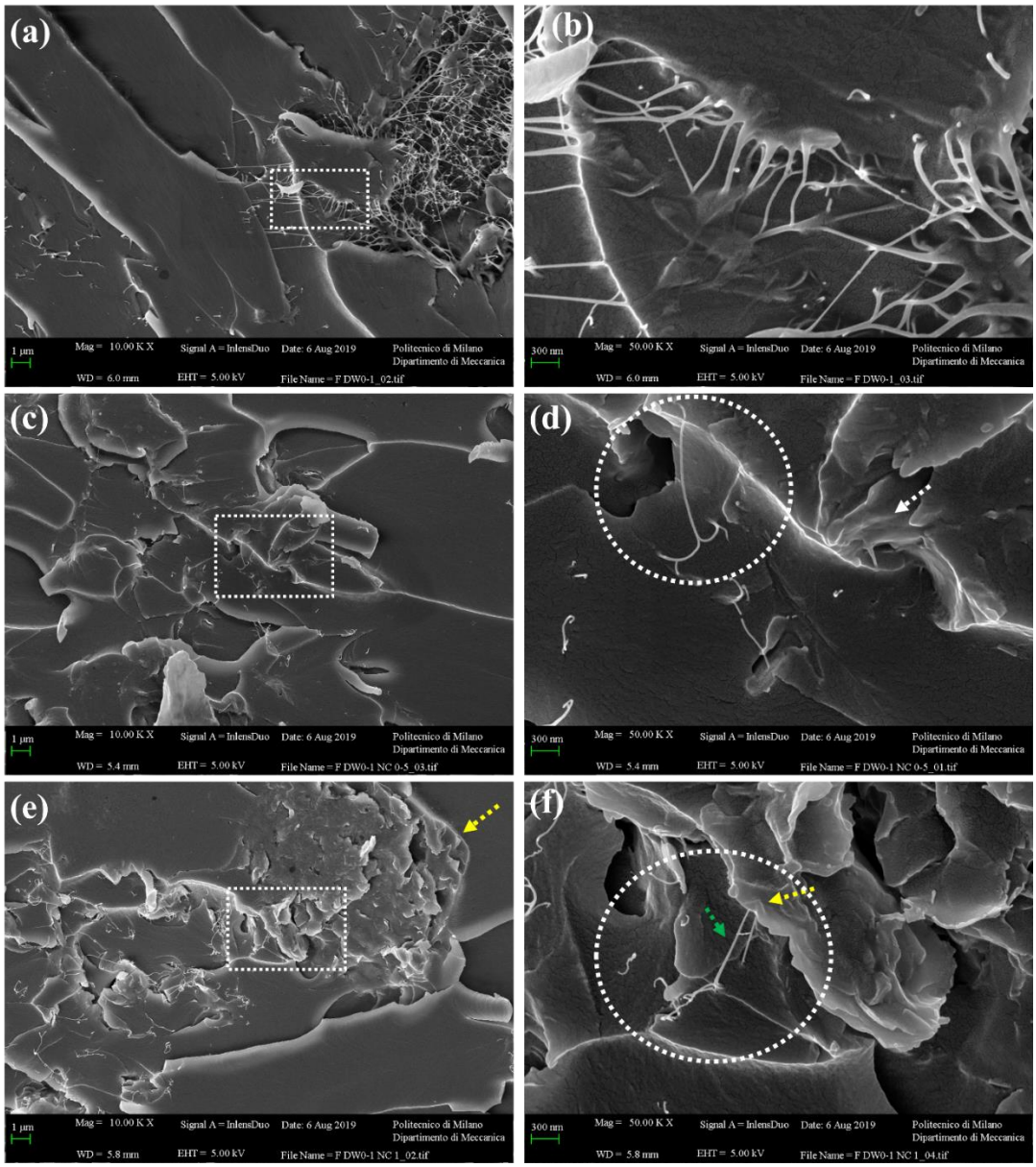

Figure 6. 2. FESEM images taken from the fracture surface of the SENB specimens: (a-b) 0.1 wt.% DWCNT/epoxy, (c-d) 0.1 wt.% DWCNT-0.5 wt.% NC/epoxy, (e-f) 0.1 wt.% DWCNT-1 wt.% NC/epoxy. White dashed circle represents the mutual interaction between DWCNT, nanoclay and epoxy.

6.1.2. XRD analysis

Polymers reinforced by nanoclay are divided into three groups depending on the

nanoclay gallery configuration including phase-separated, intercalated and exfoliated, as shown in Figure 6. 3a-c respectively [49]. The phase-separated configuration (Figure 6. 3a) exhibits a pattern in which the nanoclay sheets appear in their primary states (as received) i.e. without any resin penetration between the layers. Thus, they show the same d-spacing or basal spacing, the distance between clay galleries, which is detectable by XRD as a peak in correspondence of a specific 2θ angle, typical for nanoclay. The intercalated structure (Figure 6. 3b) is similar to the first one, but the distance between the clay galleries is expanded due to minimal penetration of the resin. This expansion is also detectable by XRD, exhibiting a peak at a smaller 2θ angle. Concerning the exfoliated structure (Figure 6. 3c), the individual nanoclay interlayers are completely separated, manifesting no specific peak by XRD.

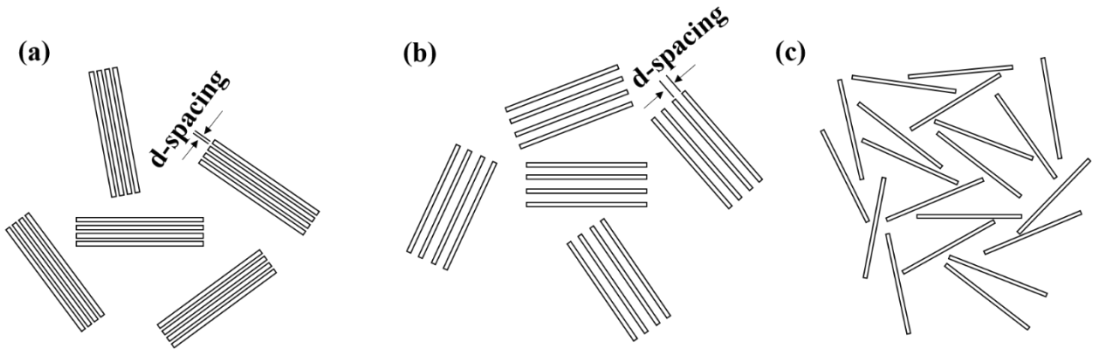

Figure 6. 3. Different nanoclay structures: (a) as-received nanofiller, (b) intercalated structure, (c) exfoliated structure.

Figure 6. 4a illustrates the XRD analysis performed for the DWCNTs and NC powders, the neat epoxy and the nanocomposites in binary and ternary states. The neat epoxy and the DWCNTs present a smooth and sharp peak at 2θ=18˚ and 2θ=26˚, respectively. The peak for the original nanoclay is at 2θ=7˚, indicating intercalated clay galleries. On the other hand, no peak is observed for the nanocomposites at ternary

states, indicating an exfoliated nanoclay configuration is obtained for the hybrid nanocomposites i.e. the stacks of the layered-nanoclays are separated as shown in Figure 6. 4b. As a result, nanoclay not only manifests an exfoliated structure in hybrid states, but it also enhances DWCNTs dispersion as illustrated in Figure 6. 4b. The effective exploitation of nanoclay in terms of enhancing mechanical, electrical and piezoresistive-sensitivity can thus be obtained as discussed below in detail.

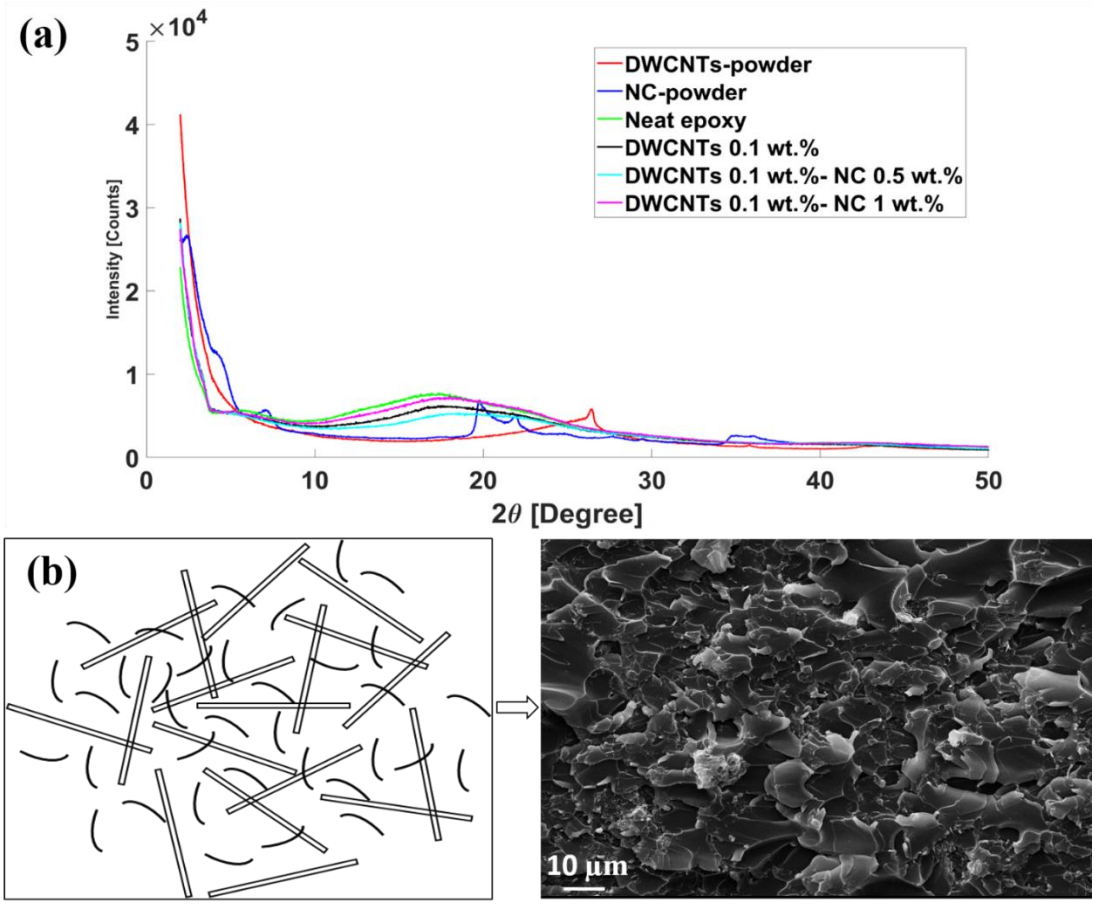

Figure 6. 4. (a) XRD analysis,(b) schematic illustration of the exfoliated nanoclay along with homogenous DWCNTs dispersion at hybrid state.

6.2. Mechanical properties

6.2.1. Tensile test

Figure 6. 5a shows the tensile strength of the neat epoxy and the nanocomposites. The tensile strength is visibly improved for all nanocomposites but the highest improvement of 20 % is achieved for the binary state (0.1 wt.% DWCNT) compared to the neat epoxy. The ternary state nanocomposites manifest a slight reduction in the tensile strength with respect to the binary state, even though their tensile strength is still higher than the neat epoxy. This can be attributed to the possible presence of manufacturing defects such as voids left in the cured plate, due to higher viscosity of the mixture in the ternary state compared with the binary state [46]. In fact, these voids act as stress concentrators, thus, resulting in the deterioration of tensile strength. It is worth noting that although effective degassing was performed in this study, most of the remaining bubbles are formed upon addition of the hardener to the mixture and cannot be timely removed as the mixture abruptly becomes rigid [69].

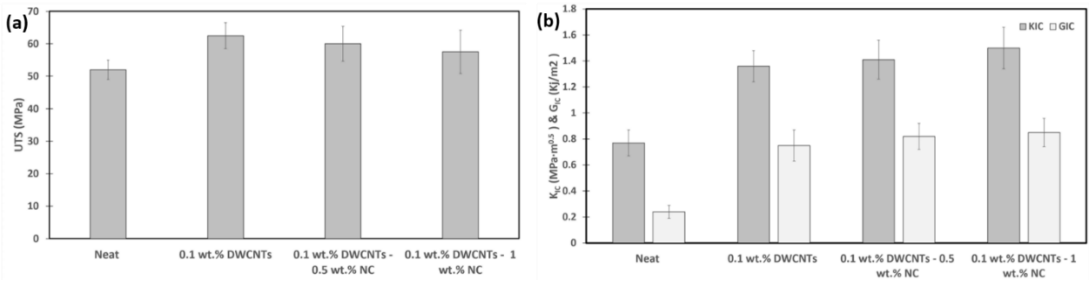

Figure 6. 5. Mechanical properties: (a) UTS, (b) K_{IC} and G_{IC}.

6.2.2. Fracture test

Figure 6. 5b displays the fracture toughness properties of the neat epoxy as well

as the nanocomposites. The K_{IC} and G_{IC} obtained for the neat epoxy are 0.77 MPa.m$^{0.5}$ and 0.24 KJ/m2 respectively. The incorporation of a small amount of DWCNTs (0.1 wt.%) leads to a substantial increase of K_{IC} and G_{IC} of up to 77 % and 212 %, respectively, compared to neat epoxy. The addition of nanoclay to CNTs doped epoxy results in a further increase of K_{IC} and G_{IC} while the highest increase of 94 % and 254 % is obtained for 0.1 wt.% DWCNT-1 wt.% NC.

Depending on the nanofiller morphology, several toughening mechanisms have been addressed in the literature for fracture toughness reinforcement of the epoxy based nanocomposite such as crack bridging, crack deflection, and crack pinning [146]. Specifically, while crack bridging is a common mechanism for CNTs doped materials, crack deflection and crack pinning are typical reinforcement mechanisms for nanoclay and graphene nanoplatelets as well as in the case of clustered nanofillers [146].

Figure 6. 6 shows different toughening mechanisms for the binary and ternary state nanocomposites produced in this study. For the binary state (Figure 6. 6a-c), a combination of crack deflection and crack bridging are the dominant reinforcement mechanisms. The former is likely to take place when the crack front reaches clustered CNTs as marked by the white dashed lines in Figure 6. 6a. The latter contributes to fracture toughness enhancement when the individual CNTs limit the opening of the crack front as shown in Figure 6. 6c. It is worth noting that crack bridging also has an effect at the interface between the aggregates and the matrix as marked by the yellow arrows in Figure 6. 6b. Consequently, for the binary state, the toughening mechanisms is the results of a combination effect of crack bridging and crack deflection with crack deflection being the main contributor in the vicinity of aggregates.

For the hybrid nanocomposites, crack deflection and crack bridging are the reinforcing mechanisms induced by nanoclay galleries and DWCNTs respectively

(Figure 6. 6d-f), the former acting as the predominant mechanism since nanoclay loading is higher than DWCNTs. The effect of crack deflection, with the crack front dividing into many tiny cracks and dissipating around the nanoclay, is clearly visible as marked by the white arrows in Figure 6. 6d-f. This deflection causes further dissipation of energy resulting in an increase of the fracture energy, i.e. the crack-front requires further energy to propagate. Finally, the higher fracture toughness properties of the hybrid nanocomposites compared to the binary one can be attributed to better dispersion of the nanoreinforcements in the former (as discussed above) in addition to the concurrence effect of both nanoclay and DWCNTs in toughening the epoxy.

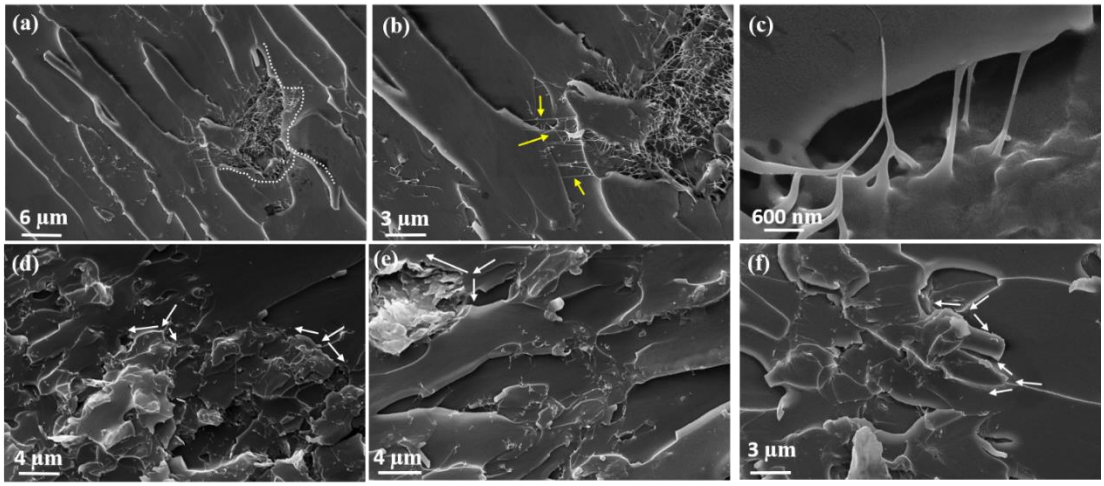

Figure 6. 6. Toughening mechanism: (a-c) crack deflection and crack bridging for DWCNT doped epoxy, (d-f) crack deflection for DWCNT/nanoclay doped epoxy. Crack propagation took place from right to left in all panels.

6.3. Electrical conductivity

Figure 6. 7a displays the electrical conductivity of the neat epoxy and nanocomposites. Addition of only small amount of DWCNTs (0.1 wt.%) results in a

substantial increase of the electrical conductivity of up to 9 orders of magnitude. This finding is in line with the literature indicating that a low percolation threshold can be obtained for CNTs doped epoxy material [25]. Specifically, tunneling effect and electrical contacts between neighbouring CNTs account for the formation of electrical networks throughout the matrix resulting in remarkable increase in electrical conductivity [46].

Interestingly, the electrical conductivity of the nanocomposite is further increased in hybrid states compared with the binary structure (Figure 6. 7a). Electrical conductivity of 0.01 S/m is achieved for DWCNT/epoxy whereas conductivity values of 0.08 S/m (+700 %) and 0.05 S/m (+400 %) are obtained for the ternary states loaded with 0.5 wt.% and 1 wt.% of nanoclay, respectively, due to the improvement of DWCNT dispersion after addition of nanoclay (Figure 6. 1d-i and Figure 6. 2c-f). The detrimental effect of agglomerated CNTs on the electrical conductivity in the binary state is explained in Figure 6. 7b-c where the electrical pathways formed in the matrix are highlighted by red dashed lines.

It is clear that, due to the better CNT dispersion in presence of nanoclay at ternary state, the number of electrical networks formed in the binary state (Figure 6. 7b) is lower than its content at the ternary state (Figure 6. 7c). The reduction of electrical conductivity at 1 wt.% nanoclay content compared to 0.5 wt.% can be related to a higher amount of non-conductive filler, which reduces the number of electrical networks formed throughout the matrix.

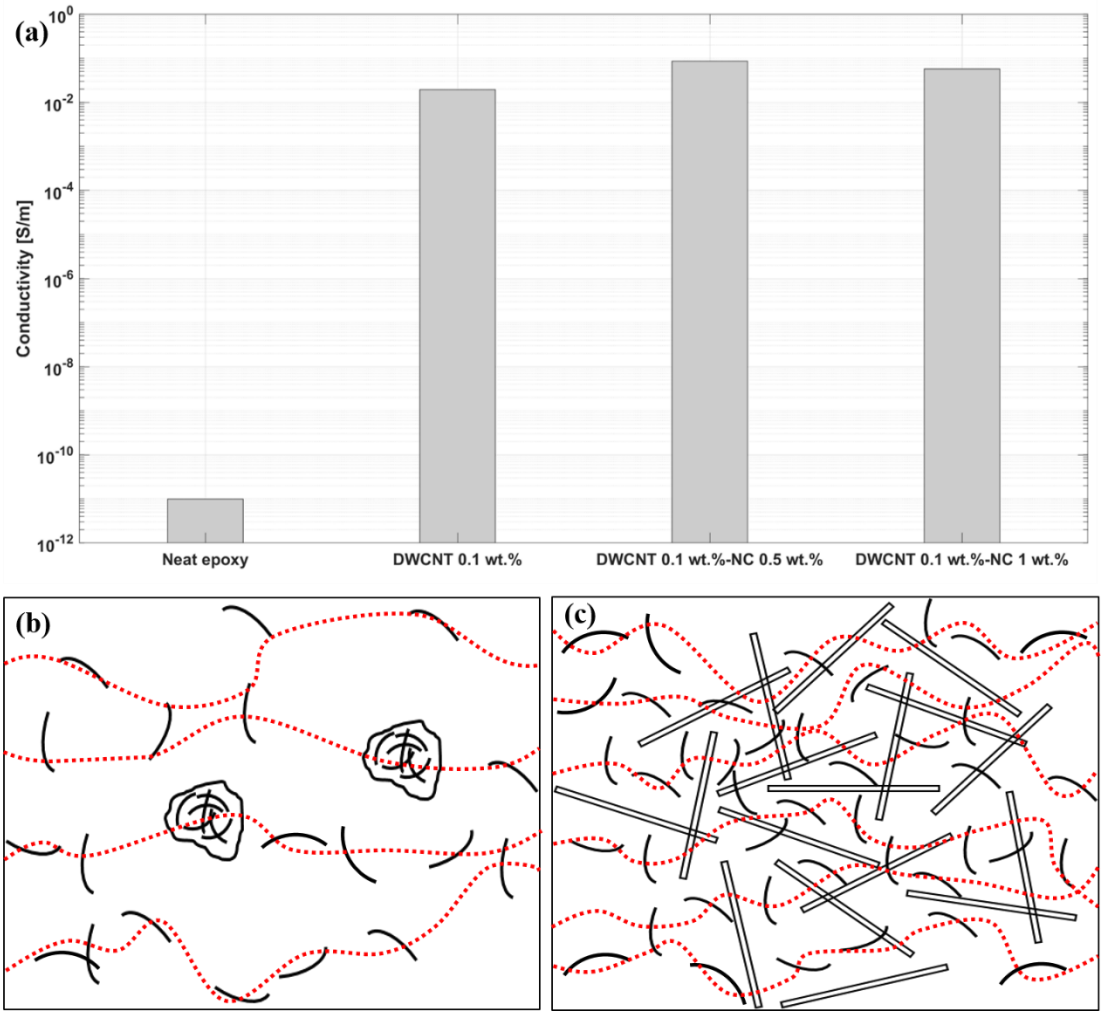

Figure 6. 7. (a) Electrical conductivity, (b-c) schematic illustration of the formation of electrical networks throughout the matrix in DWCNTs/epoxy and DWCNT-nanoclay/epoxy respectively.

6.4. Piezoresistivity performance

The self-sensing capability of the nanocomposites in tensile and mode I fracture tests are examined hereinafter. For the tensile test, the change in normalized resistance versus applied strain is monitored while for the fracture test, the normalized resistance change as a function of displacement is investigated. The normalized resistance change (ΔR_n) is expressed based on equation (6.1) :

$$\Delta R_n = \frac{\Delta R}{R_0} = \frac{R_t - R_0}{R_0} = \frac{I_0 - I_t}{I_t} \qquad (6.1)$$

Where ΔR is the relative resistance (Ω), R_0 the initial resistance (Ω), R_t the instantaneous resistance (Ω), I_0 the initial current (mA), and I_t the time dependent current (mA). Proportionality between electrical resistance and current is assured by constant voltage streaming into the specimen. Specifically for tensile tests, the strain sensitivity of the developed sensors, called Gauge Factor (GF), is expressed according to equation (6.2):

$$GF = \frac{\Delta R_n}{\varepsilon} \qquad (6.2)$$

Where ε is the applied axial strain corresponding to ΔR_n. In practice, the GF can be identified as the instantaneous slope of the $\Delta R_n - strain$ curve in tensile test if a nonlinear sensitivity is observed.

6.4.1. Tensile test

Figure 6. 8 shows the normalized resistance change as a function of the applied strain for the DWCNT/epoxy and DWCNT-nanoclay/epoxy during the tensile test. The $\Delta R_n - \varepsilon$ curves for all nanocomposites are plotted together in Figure 6. 8d to facilitate comparison. Regardless of the nanofillers loading and the surface morphology, all nanocomposites manifest a simultaneous increase in normalized resistance in response to strain increase i.e. they can successfully monitor any deformation and strain induced in the system. The apparent change in normalized resistance can be attributed to the breakage of electrical networks within the matrix as a result of the strain increase [30]. The applied strain causes neighbouring CNTs to gradually become farther away from each other and, thus, the number of effective electrical pathways contributing in

piezoresistivity of the system is gradually reduced.

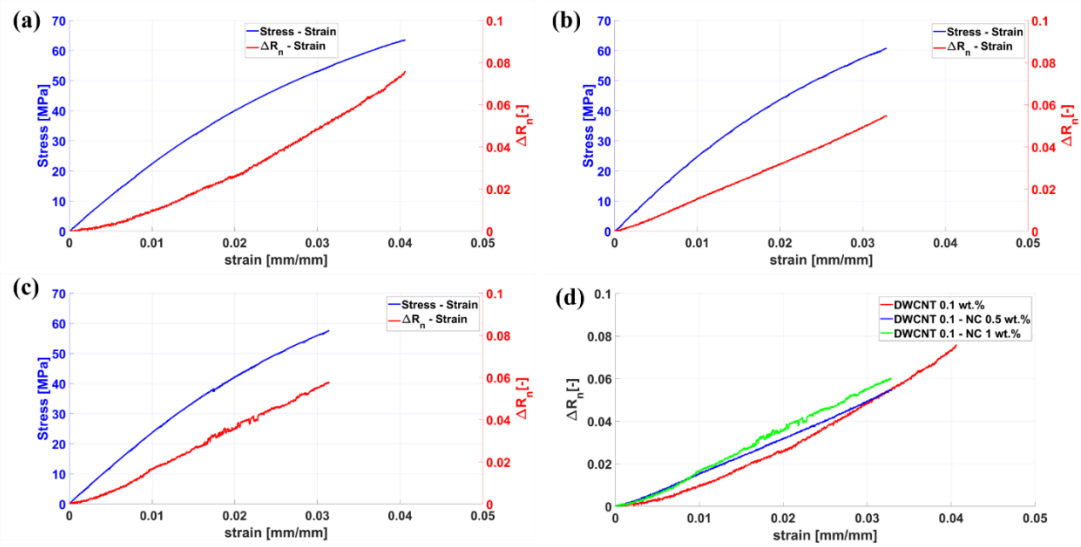

Figure 6. 8. Piezoresistive performance of the nanocomposites in tensile tests: (a) 0.1 wt.% DWCNTs/epoxy, (b) 0.1 wt.% DWCNTs- 0.5 wt.% NC, (c)0.1 wt.% DWCNTs-1 wt.% NC, (d) combined piezoresistivity for all samples.

In addition, the trend in normalized resistance versus strain for the binary and hybrid states are quite different as shown in Figure 6. 8. In fact, binary state shows a nonlinear trend whereas hybrid states show an almost linear trend. This can be attributed to different mechanisms governing the piezoresistivity, i.e. tunneling effects and loss of electrical contacts. For the binary state, the nonlinear trend indicates that the tunneling effect is the predominant mechanism that rules the electromechanical properties of the nanocomposite. This can be explained as the relationship between the tunneling resistance and the tunneling distance is nonlinear (equation 6.3) [44]:

$$R_{tunnel} = \frac{V}{AJ} = \frac{h^2 d}{Ae^2\sqrt{2m\lambda}} exp\left(\frac{4\pi d}{h}\sqrt{2m\lambda}\right) \qquad (6.3)$$

Where λ is the potential barrier height at almost 0.5 to 2.5 eV for the epoxy, m the electron mass, d the tunneling distance, less than 1.8 nm, h the Plank's constant, e

the quantum of electricity, A the cross section, J the tunneling current density, and V the electrical potential difference.

Focusing on the piezoresistive behaviours of ternary states (Figure 6. 8b-c), the linear trend in $\Delta R_n - \varepsilon$ curves indicates that the tunneling resistance may not act as the prevalent mechanism in piezoresistive behaviour. Potentially, loss of electrical contacts amongst adjacent CNTs or breakage of electrical networks formed in the matrix as a result of strain increase are the main mechanisms driving the piezoresistive behaviour in ternary states, manifesting as a linear trend in the $\Delta R_n - strain$ curve [45]. The latter can be explained by a higher number of conductive paths in the hybrid nanocomposites (Figure 6. 7), due to a more homogeneous CNT dispersion, which increases the possibility for contact electrical transfers among adjacent CNTs.

Figure 6. 8 shows that the addition of nanoclay not only improves the mechanical properties and electrical conductivity, but also increases the sensitivity, as expressed in equation (6.2). At least, at lower strain magnitudes, where ΔR_n for the hybrid nanocomposites is slightly higher than for the binary state, as summarized in Table 6. 1, where the mean value and the associated 95 % confidence boundary have been reported. A sensitivity of 1.53 is achieved for the binary composites at $\varepsilon \sim 0.01$ whilst the sensitivity of the nanocomposite increases by 13 % and 30 % for hybrid nanocomposites loaded at 0.5 wt.% and 1 wt.% respectively.

Table 6. 1. Average Sensitivity and 95 %-Confidence Bounds at Different Strain Levels

Nanocomposites	Sensitivity			
	$\varepsilon\sim0.005$	$\varepsilon\sim0.01$	$\varepsilon\sim0.015$	$\varepsilon\sim0.02$
0.1 wt.% DWCNTs	1.21±0.20	1.53±0.18	1.76±0.19	1.89±0.09
0.1 wt.% DWCNT-0.5 wt.% NC	1.71±0.15	1.74±0.15	1.69±0.12	1.71±0.13
0.1wt.% DWCNT-1 wt.% NC	1.56±0.27	1.99±0.20	1.72±0.28	1.78±0.20

6.4.2. Fracture test

The normalized resistance change during fracture tests is shown in Figure 6. 9, with the inset figures representing the piezoresistivity throughout the fracture test, where a significant increase in ΔR_n with the onset of crack growth can be identified. The piezoresistive behavior before crack extension is more complicated. In fact, in both binary and hybrid nanocomposites, the ΔR_n shows an oscillating trend i.e. a positive and negative variation can be seen for all samples. This can be attributed to formation and destruction of the conductive paths in the compression and tension sides respectively [46].

In fact, during fracture test, the SENB specimen is subject to a localized stress and strain magnification at the notch and a generalized state of combined tension-compression throughout the specimen, which causes the oscillatory behavior in the ΔR_n versus displacement curves. Furthermore, the range of ΔR_n variation is noticeably lower than for tensile tests, due to the sensibly lower general strain magnitudes and the

localized nature of the stress, thus highlighting the less predictable piezoresistive behaviour.

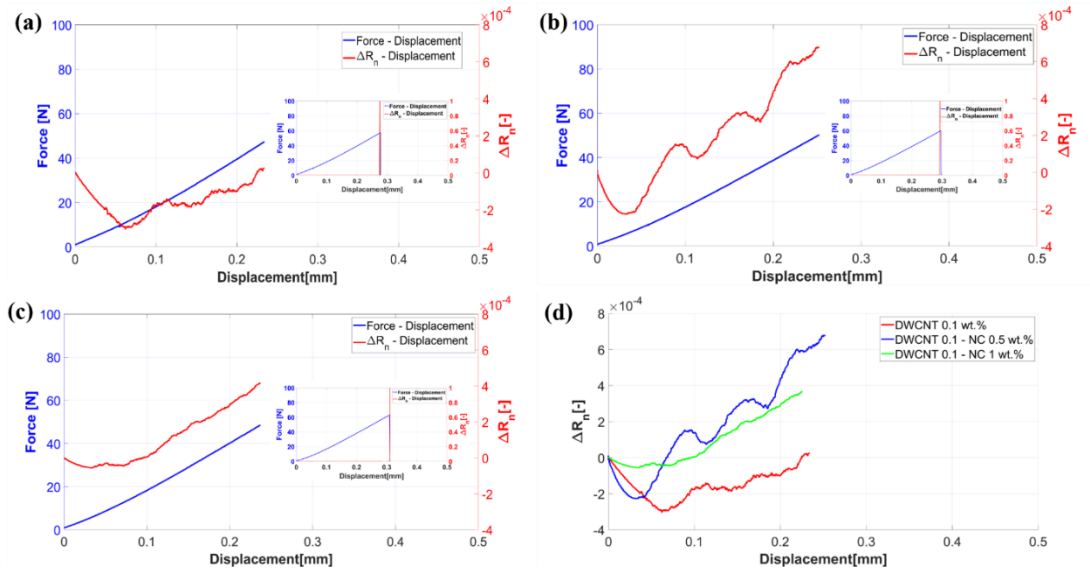

Figure 6. 9. Piezoresistive performance of the nanocomposites in fracture tests: (a) 0.1 wt.% DWCNTs/epoxy, (b) 0.1 wt.% DWCNTs- 0.5 wt.% NC, (c) 0.1 wt.% DWCNTs- 1 wt.% NC, (d) combined piezoresistivity for all samples. The insets show the piezoresistivity during whole fracture test.

However, a general decrease of ΔR_n can be noticed for all the nanocomposites at lower displacements, indicating the predominant effect of the localized compressive strain at the notch, followed by a general increase of the ΔR_n curve at higher displacements, characterized by an oscillatory behavior and including the effect of the distributed strain field. The gradual increase in ΔR_n versus displacement is more noticeable for the hybrid nanocomposites where a higher increase in ΔR_n with respect to the binary composite is measured.

Interestingly, a reduced oscillation in the signal is measured for the ternary state nanocomposite with 1 wt.% nanoclay loading, supposingly due to the nanoclay limiting

the formation of new electrical pathways at the compression sides, due to the fact that the CNTs are quite far from each other and thus, a steady state increase in ΔR_n can be achieved. This behavior is confirmed by a reduced decrement of ΔR_n at lower displacements when the localized compression at the notch drives the piezoresistive output.

6.5. Fractography

Figure 6. 10a-d and e-f display fracture surface images of the tensile and SENB specimens respectively. Two different regions can be distinguished for tensile specimens i.e. a mirror-like surface corresponding to the initial fracture region, which is highlighted by white dashed arrows in Figure 6. 10a-d, followed by a cleavage surface, referred to as a river-like pattern, where the main plastic deformation takes place.The SENB specimen (Figure 6. 10e-h) exhibits a flatter surface, which can be attributed to the brittleness of the epoxy. Two different morphologies can be detected i.e. the initial fracture region highlighted by white dashed arrows and the river-like morphology corresponding to the crack growth.

For both tensile and SENB specimens, the surface roughness of the specimens reflects their mechanical properties, i.e. a higher surface roughness demonstrates higher mechanical properties and vice versa [46]. This can be clearly seen by comparing fracture surface of the neat epoxy (Figure 6. 10a and e) with the nanocomposites (Figure 6. 10b-d and f-h). In fact, the neat epoxy manifests quite a low density cleavage pattern whereas higher numbers of cleavage morphologies can be seen in the nanocomposites. The higher surface roughness of the nanocomposites with respect to the neat epoxy can also be attributed to crack-deflection and crack bridging mechanisms which render the

crack growth harder, thus, the initial crack deviates further to propagate, resulting in a higher surface roughness of the nanocomposites.

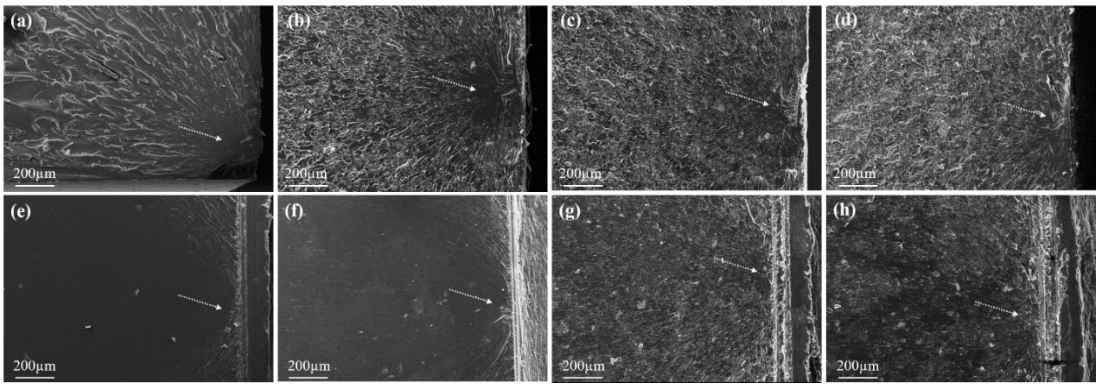

Figure 6. 10. Fracture morphology: (a-d) tensile specimen, (e-h) SENB specimen. Left to right images represent SEM images for the neat, 0.1 wt.% DWCNT, 0.1 wt.% DWCNT-0.5 wt.% NC, and 0.1 wt.% DWCNT-1 wt.% NC respectively.

6.6. Summary

Multifunctional properties of the epoxy based nanocomposites reinforced with DWCNTs and nanoclay were investigated throughout this study. Three different epoxy-based nanocomposites were prepared for comparison, including 0.1 wt.% DWCNTs, 0.1 wt.% DWCNTs - 0.5 wt.% NC and 0.1 wt.% DWCNTs – 1 wt.% NC. Tensile and fracture tests were carried out for mechanical and piezoresistive characterization while SEM, FESEM, XRD were employed for the microstructural analysis. The following conclusions were drawn:

- The hybrid nanocomposites (DWCNTs-NC/epoxy) showed a more uniform nanofiller dispersion in comparison with the binary composite (DWCNTs/epoxy). At binary state, the presence of CNTs-rich and CNTs-poor regions were considerable, resulting from CNT bundling during

manufacturing. The addition of nanoclay improved CNT dispersion because nanoclay galleries acted as an obstacle, thus, avoiding CNT re-agglomeration during manufacturing. In addition, XRD analysis revealed that an exfoliated structure was obtained for the nanoclay resulting from the appropriate manufacturing procedure used in this study. Finally, a proper mutual interaction took place between DWCNT, nanoclay and epoxy at ternary state nanocomposites where the stretching state of the DWCNT between epoxy and nanoclay manifested successful shear-loading transfer from the epoxy to the nanoclay and vice versa.

- Both binary and ternary nanocomposites manifested higher tensile strength compared to neat epoxy. The maximum increase of up to 20 % was obtained for the DWCNT/epoxy, while a slight reduction was observed in the ternary states. The reduction was attributed to the presence of manufacturing defects such as voids left inside the specimens resulting from higher viscosity of the mixture in the ternary state compared with the binary state.
- For the fracture toughness, a substantial increase in K_{IC} and G_{IC} was obtained for the nanocomposites compared to the neat epoxy. The highest enhancement around 94 % and 254 %, in K_{IC} and G_{IC} respectively, was achieved for 0.1 wt.% DWCNTs – 1 wt.% NC. A combination effect of crack bridging and crack deflection accounted for the significant increase in the fracture toughness properties of the nanocomposites.
- The electrical conductivity of the DWCNTs/epoxy substantially increased up to 9 orders of magnitude by the addition of only 0.1 wt.% DWCNTs. As a consequence of the improved CNTs dispersion, the electrical conductivity of

the ternary state materials increased by 700 % and 400 % with respect to the binary nanocomposite, for 0.5 wt.% and 1 wt.% NC loadings, respectively.

- For the piezoresistivity performance during tensile test, the hybrid nanocomposites showed better performance with respect to the binary state in monitoring strain increase. A nonlinear trend in the piezoresistivity test was observed for the binary composite whereas the hybrid nanocomposites showed an almost a linear behaviour. Tunneling resistance and loss of electrical contacts amongst neighbouring CNTs accounted for the nonlinearity and linearity that appeared for the binary and hybrid nanocomposites, respectively. The highest sensitivity of 1.99 was obtained for the hybrid nanocomposite loaded at 1 wt.% nanoclay at $\varepsilon \sim 0.01$ while a sensitivity of 1.74 and 1.53 was achieved for the 0.1 wt.% DWCNTs - 0.5 wt.% NC and the 0.1 wt.% DWCNTs doped materials, respectively.
- Different piezoresistive behaviors were distinguished in the fracture test, i.e. an oscillating trend was noticed at lower displacement (before crack extension), attributed to the simultaneous formation and destruction of conductive pathways in the compression and tension sides, respectively, and a more stable increase of resistance at higher displacement. Similar to the tensile test, 0.1 wt.% DWCNTs- 1 wt.% NC demonstrated better piezoresistive performance. Finally, with the onset of crack growth, all nanocomposites showed an abrupt increase in the normalized resistance.
- Based on the analysis of the fracture surface, two different regions were distinguished for the tensile specimens, i.e. a mirror-like surface corresponding to the initial fracture region, followed by a cleavage surface referred to as a river-like pattern, where the main plastic deformation took place. For the SENB

specimen, a flat surface was identified which was attributed to the brittleness of the epoxy, although, similarly to tensile specimens, two different morphologies were detected i.e. the initial tiny flat region followed by the river-like morphology corresponding to the crack growth. Finally, higher surface roughness corresponded to higher mechanical properties and vice versa.

To summarize, based on the mechanical and electromechanical performances of the hybrid nanocomposites in tensile and fracture tests, the addition of nanoclay to CNTs doped epoxy not only improves the mechanical properties, but it also leads to a better piezoresistive sensitivity performance resulting from better CNTs dispersion states at hybrid states in comparison to the binary nanocomposite. Taking into account the low cost of the nanoclay compared with CNTs, the hybrid nanocomposites developed in this study can be considered as a high value product since better multifunctional properties were achieved at a negligibly higher cost compared with the binary state material.

CHAPTER 7: HYBRID SWCNTS AND NANOCLAY/EPOXY

This chapter examines the positive effect of nanoclay addition as an aid to improve CNTs dispersion i.e. a novel method for enhancing CNTs dispersion will be analyzed throughout this study. This will create some advantageous over traditional dispersion methods where CNTs damage and CNTs-waste were the most drawback of sonication (high frequency and time) and calendaring methods respectively. A combination of sonication and toroidal methods were used for the nanofiller dispersion where nanoclay added to the CNTs doped epoxy as an auxiliary filler. In fact, the idea is to find a way to prevent CNTs re-agglomeration which is a typical problem during nanocomposite production [43]. SEM and FESEM were used for microstructural characterization while tensile and mode I fracture tests were employed for mechanical and electromechanical analysis (using two probe-techniques). In the end, the advantage of nanoclay not only as auxiliary filler but also on improving electrical and piezoresistive-sensitivity performance of the epoxy nanocomposites will be discussed.

7.1. Microstructural analysis

Figure 7. 1 shows the macroscopic and microscopic images of the CNTs dispersion state in binary and ternary states. For the binary composite, it is clear that CNTs are severely entangled which can be even detected by naked eyes (Figure 7. 1a). It can be concluded that for the binary composite, due to severe agglomeration of CNTs, the specimen is semi-transparent, so, bundles of CNTs can be easily seen as shown in Figure 7. 1a. Presence of aggregates can be related to the elevated temperature used during manufacturing as well as final curing of the nanocomposites resulted in severe CNT re-agglomeration [144]. It should be mentioned that high temperature usage

during production is an important step to achieve sound samples in terms i.e. no voids and pores. However, this would create CNT aggregates, thus, to avoid this phenomenon, nanoclay was added to CNT doped epoxy. As a result, by combination of nanoclay and elevated temperature in phase 2, high quality samples were achieved compared to the one produced in phase 1. Fig.4b-d display FESEM images of the cross section of binary composite, corresponding to Fig.4a, where poor-wettability of the agglomerated CNTs are noticeable. These aggregates drastically hamper electrical, mechanical and electromechanical properties of the nanocomposite [103]. It is worth noting that using high temperature is quite important for efficient removal of the entrapped air in the mixture. On other hand, it has also opposite effect in terms of CNTs reagglomration. As a result, this depends on the end user to find an optimum condition in terms of the desired properties. This part will be discussed in detail at the end of this paper after evaluating all mechanical and electromechanical properties.

For the hybrid composites (Figure 7. 1e-h), it can be seen that addition of nanoclay into CNTs doped epoxy improve CNTs dispersion as no CNTs aggregate can be thoroughly identified. Since same manufacturing method was used for both binary and ternary nanocomposites, one can say that introduction of nanoclay into CNTs doped epoxy can successfully avoid CNTs re-agglomeration i.e. they act as an obstacle against CNTs clustering, thus, more homogenous CNTs dispersion is achieved. Excluding the CNTs dispersion in hybrid nanocomposites, a combination of intercalated (red dashed arrows in Figure 7. 1) and exfoliated structures (yellow dashed arrows in Figure 7. 1) can be detected for the nanoclay structure in both hybrid states, though the presence of aggregates at 1 wt.% nanoclay loading is more prevalent. This can be attributed to higher viscosity of the mixture at 1 wt.% nanoclay with respect to 0.5 wt.% loading , thus, making more difficulties in effective dispersion of nanoclay. Presence of defects

in terms of voids and pores in vicinity of the intercalated nanoclay, in particular at 1wt.% nanoclay loading (Figure 7. 1h), are also noticeable, manifesting itself in mechanical properties degradation which will be discussed later.

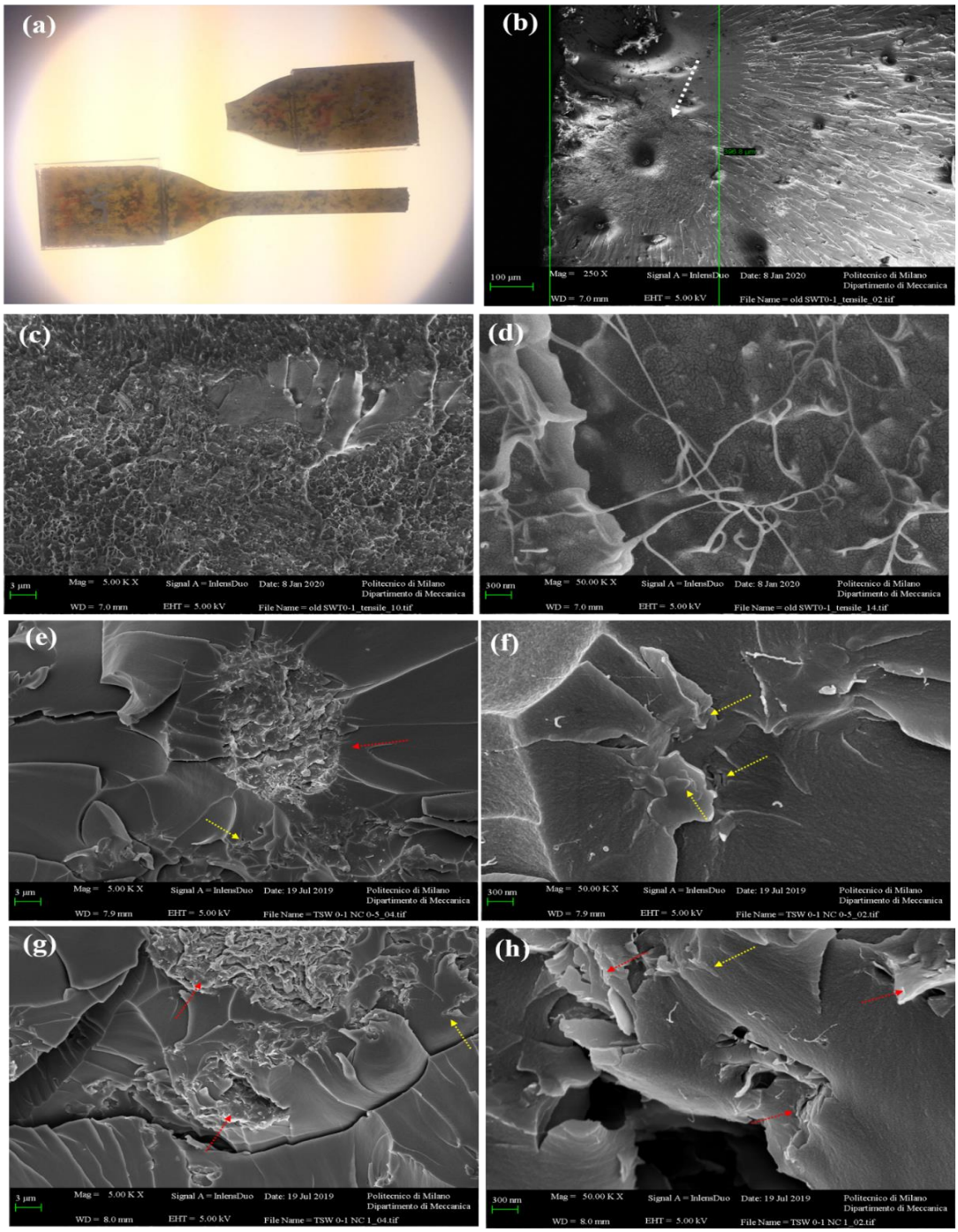

Figure 7. 1. Dispersion state: (a-d) 0.1wt.% SWCNTs, (e-f) 0.1wt%. SWCNTs-0.5wt.% nanoclay, (g-h) 0.1wt%. SWCNTs-1wt.% nanoclay. The FESEM images were taken from the fracture surface of the tensile specimens.

Figure 7. 2 shows the XRD analysis performed on the nanoclay powder and

ternary nanocomposites. For the nanoclay powder, a peak at $2\theta = 7$ is achieved indicating an intercalated nanoclay structure which is a typical structure for the nanoclay powder before applying any dispersion methods. On the other hand, no particular peak can be seen for the ternary nanocomposites manifesting an exfoliated structure. This means that the intercalated structure for as-received nanoclay was successfully transformed to exfoliated structure i.e. the d-spacing between interclay galleries were expanded, thus, homogenously dispersed in the matrix. This indicates that the dispersion method used in this study, combined iterative of sonication and toroidal methods, can successfully break the nanoclay aggregates, thus, an effective exploitation of the nanoclay in tailoring mechanical properties of the epoxy can be achieved. Taking into account the FESEM images (Figure 7. 1e-h) and the XRD analysis (Figure 7. 2), it can be stated out that a combination of intercalated and exfoliated structures is achieved for the nanoclay structure in both ternary state nanocomposites.

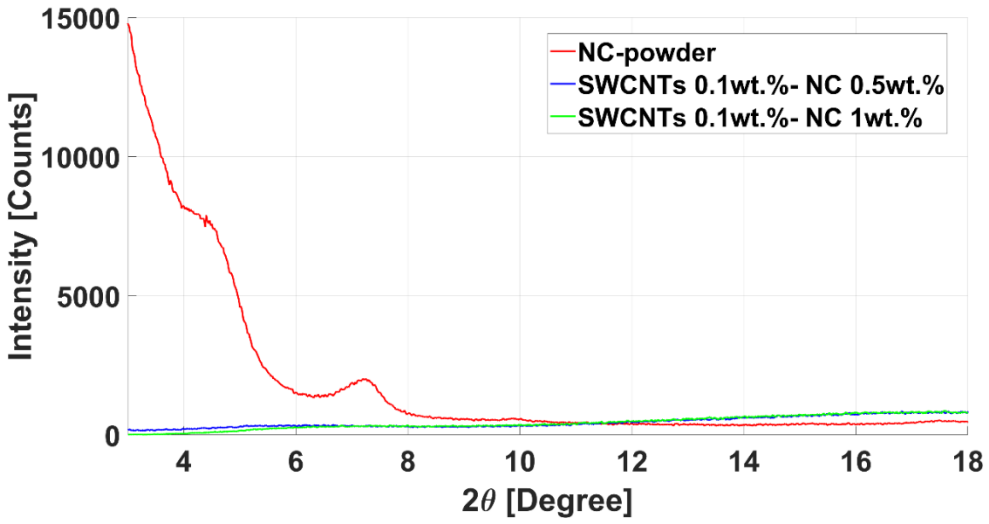

Figure 7. 2. XRD analysis.

7.2. Electrical conductivity

Figure 7. 3 shows the electrical conductivity of the nanocomposites and neat epoxy. The electrical conductivity of the binary nanocomoiste increases by 4 orders of magnitude with respect to the neat epoxy. On the other hand, significant increase in electrical conductivity (compared to the binary composite) around 6 orders of magnitude is achieved by addition of nanoclay. The low enhancement of the electrical conductivity at binary state can be related to CNT agglomeration as shown in Figure 7. 1a-b. It can be concluded that nanoclay addition acts as an auxiliary filler in CNT dispersion enhancement i.e. preventing of CNT re-agglomeration during manufacturing, thus electrical conductivity improves in ternary states compared to the binary composite. In addition, small reduction of electrical conductivity at 1 wt.% nanoclay loading can be seen with respect to 0.5 wt.% nanoclay. This can be attributed to the predominant effect of intercalated structure for the nanoclay in the former with respect to the intercalated and exfoliated structures obtained in the latter.

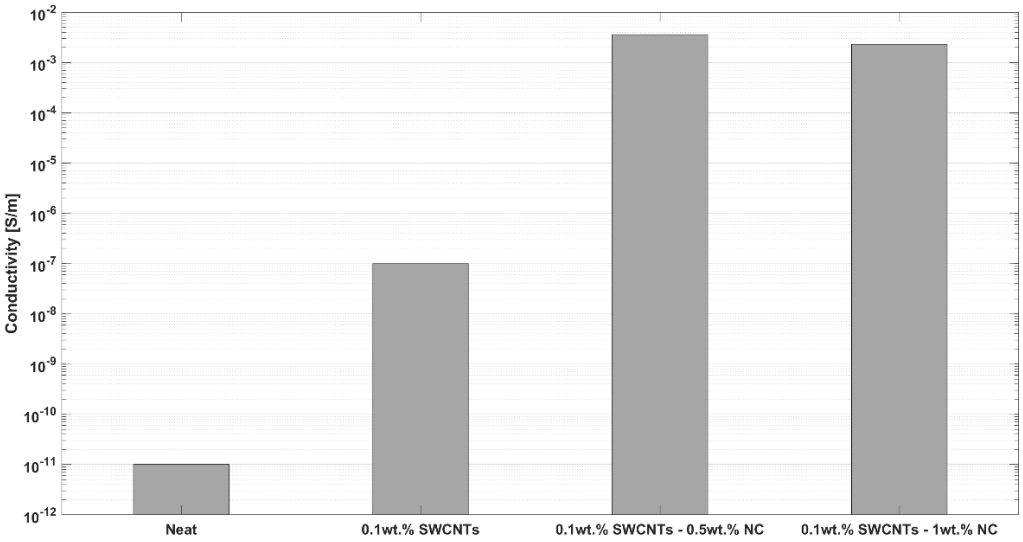

Figure 7. 3. Electrical conductivity.

7.3. Mechanical properties

7.3.1. Tensile strength

Figure 7. 4a-b display the average Young's modulus and UTS, respectively, for the neat epoxy and nanocomposites. In binary state, Young's modulus and tensile strength reduces by 6 % and 19 %, respectively, compared to the neat epoxy. This can be again attributed to CNT agglomeration resulting from poor-wettability of the agglomerated CNTs which acts as stress concentration [69]. On the other hand, addition of nanoclay into CNTs doped epoxy i.e. in hybrid states enhance tensile strength of the epoxy by 13 % and 17 % for 0.5 wt.% and 1 wt.% nanoclay contents. This can be related to better dispersion states of the CNTs and nanoclay as shown in Figure 7. 4e-f. In other words, nanoclay can be successfully employed as an auxiliary filler to improve CNT dispersion which accounts for increasing electrical and mechanical properties of the nanocomoiste in ternary states compared with the binary one.

In addition, although tensile strength slightly increase at 1 wt.% nanoclay content compared with 0.5 wt.% nanoclay, stiffness reduces which can be related to higher amount of intercalated nanoclay structure in the former, showing weak interfacial bonding with epoxy as shown in Figure 7. 4g-h. It is worth noting that a proper bonding between nanoreinforcement and matrix is critical in order to thoroughly enhance stiffness [150]. Considering the manufacturing procedure used in this study, one can say that at high nanoclay loading (1 wt.%), nanoclay cannot be properly separated compared with 0.5 wt.% nanoclay content, thus, this lead to reduction of Young's modulus at high concentration [47].

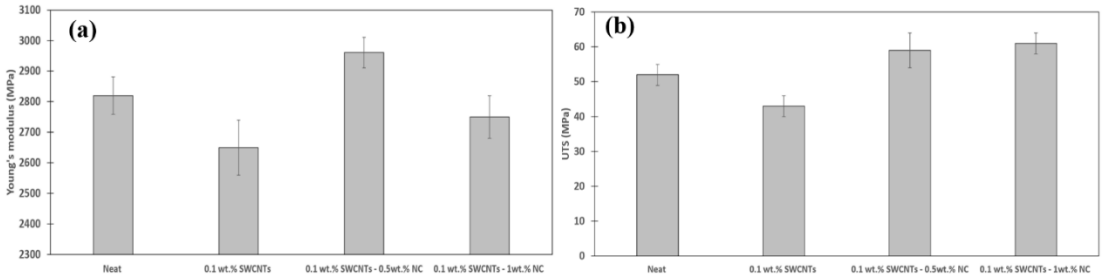

Figure 7. 4. Tensile properties: (a) Young's modulus, (b) UTS.

Figure 7. 5 shows the SEM image of the fracture surface of the tensile specimen for the pristine epoxy and nanocomposites. The fracture surface for all specimens can be divided into two different regions including the initial fracture region (highlighted by white dashed arrows), showing a flat and mirror-like surface morphology, followed by a rougher surface, manifesting a river-like pattern (for the neat epoxy and binary composite) and cores/cavities (for the hybrid composites).

Apart from that, specimen with higher tensile strength manifests higher surface roughness and vice versa. This can be clearly identified for the ternary nanocomposites (Figure 7. 5f and h for 0.5 wt.% and 1 wt.% nanoclay loadings), manifesting higher

surface roughness and cavities compared with the neat epoxy (Figure 7. 5b) and binary composite (Figure 7. 5d) which is in agreement with the tensile strength results obtained in this study. Presence of cavities in hybrid nanocomposites (Figure 7. 5f and h) can be related to failure of the nanoclay aggregates during shear-loading transfer in tensile test [80] peeling off the aggregates, thus, leaving a core and cavity in their seat which results in increasing surface roughness.

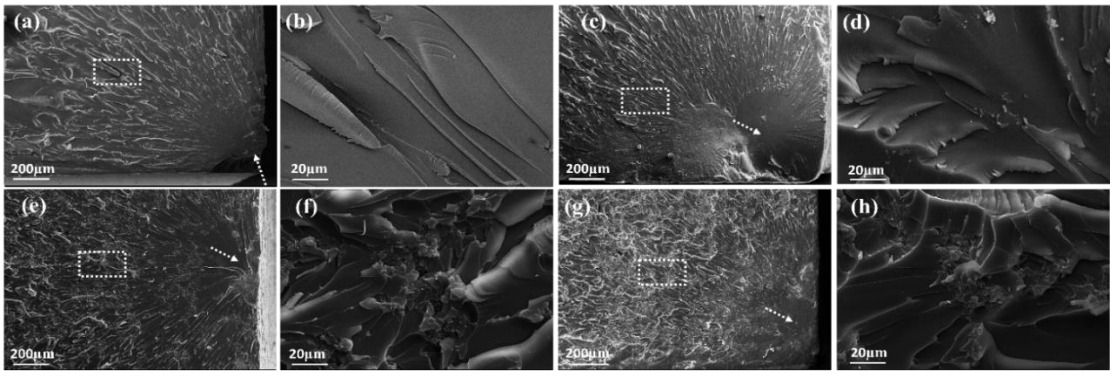

Figure 7. 5. SEM image of the fracture surface of the tensile specimen: (a-b) pristine epoxy, (c-d) 0.1 wt.% SWCNTs/epoxy, (e-f) 0.1 wt.% SWCNTs-0.5 wt.% nanoclay/epoxy, (g-h) 0.1 wt.% SWCNTs-1 wt.% nanoclay/epoxy. The dashed white rectangle indicate the area that highlighted in the next image.

7.3.2. Fracture toughness

Figure 7. 6 shows the fracture toughness properties of the near epoxy and the nanocomposites. For the binary composite, K_{IC} and G_{IC} enhance by 28 % and 4 %, respectively, with respect to the neat epoxy. In fact, unlike tensile test results where clustered CNTs manifest harmful impact on tensile strength properties, they can slightly increase fracture toughness properties i.e. no detrimental effects on fracture toughness properties can be identified. Incorporation of 0.5 wt.% nanoclay into CNTs doped

epoxy causes further increase in K_{IC} and G_{IC} around 72 % and 175 %, respectively, (compared to the neat epoxy), and 34 % and 64 %, respectively, (compared to the binary composite). Higher nanoclay loading (1 wt.%) results in small reduction in K_{IC} and G_{IC} compared to 0.5 wt.% nanoclay loading, but still higher than binary composite and neat epoxy.

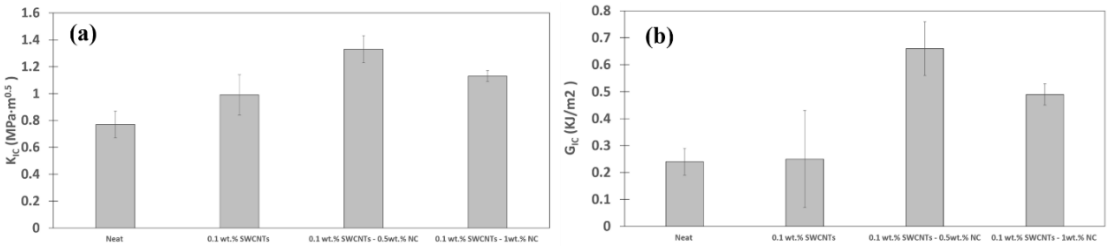

Figure 7. 6. Fracture toughness properties: (a) K_{IC}, (b) G_{IC}.

In order to better understand the toughening mechanism for both binary and ternary states, the SEM image of the fracture surface of the SENB specimen are shown in Figure 7. 7. The white arrows indicate the crack-opening direction. For the pristine epoxy (Figure 7. 7a), a smooth surface can be seen representing a brittle fracture. Figure 7. 7b shows the toughening mechanism for the binary composite where the agglomerated CNTs can act as an obstacle against crack propagation, thus, increasing fracture toughness properties. This can be also proved by formation of many tiny crack after crack-front confronts the agglomerated CNTS (red arrows in Figure 7. 7b) which is known as crack-tailing [75].

It is worth mentioning that crack-bridging mechanism may not thoroughly toughen the epoxy since it is most likely to take place where CNTs are well dispersed. Crack-pinning and crack deflection [151] are accounted for the significant increase in fracture toughness for ternary composites as shown in Figure 7. 7c-d. This can be

related to higher young's modulus of the nanoclay and their large surface areas, thus, when crack front reaches the nanoclay sites, they will be either pinned or deviated. This results in dissipating more energy for the initial crack to propagate. It is worth mentioning that the crack-bridging mechanism resulting from well-dispersed CNTs in ternary states can be another reason for the enhanced fracture toughness, though their effect might be less significant due to larger amount of nanoclay platelet compared with CNTs. In addition, surface roughness of the hybrid nanocomposites are quite higher than the binary nanocomposite and neat epoxy i.e. similar to tensile test results, the higher fracture toughness manifests itself in higher surface roughness.

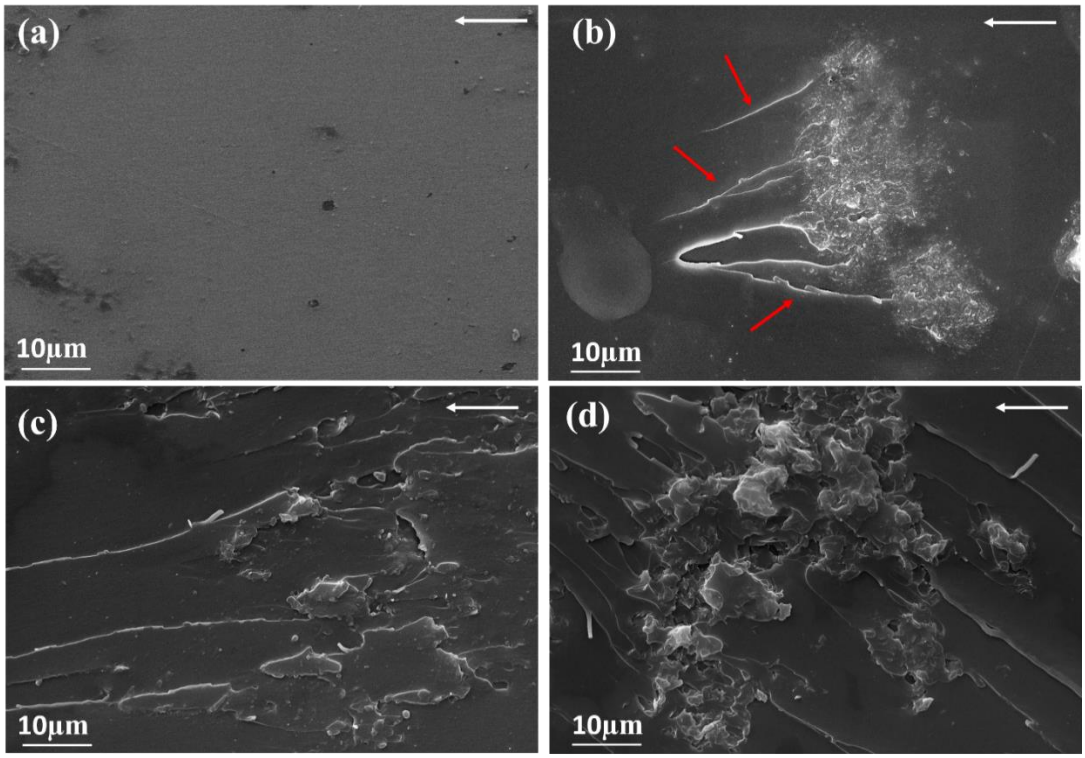

Figure 7. 7. SEM image of the fracture surface of the SENB specimens: (a) neat epoxy, (b) 0.1 wt.% SWCNTs/epoxy, (c) 0.1 wt.% SWCNTs-0.5 wt.% nanoclay/epoxy, (d) 0.1 wt.% SWCNTs-1 wt.% nanoclay/epoxy.

7.4. Piezoresistivity

Piezoresistive performance of the binary nanocomposite during tensile and fracture tests is shown in Figure 7. 8a and b respectively. No piezoresistivity is found for the binary nanocomposite, instead, high amount of noise and oscillation in the output signals (normalized resistance) can be seen. This can be attributed to the low electrical conductivity of the binary nanocomposite itself resulting from severe agglomeration of CNTs, thus, no piezoresistivty can be achieved for the binary nanocomposites. It can be concluded that the agglomerated CNTs not only hamper electrical and mechanical properties, but also lead to sever degradation of electromechanical properties.

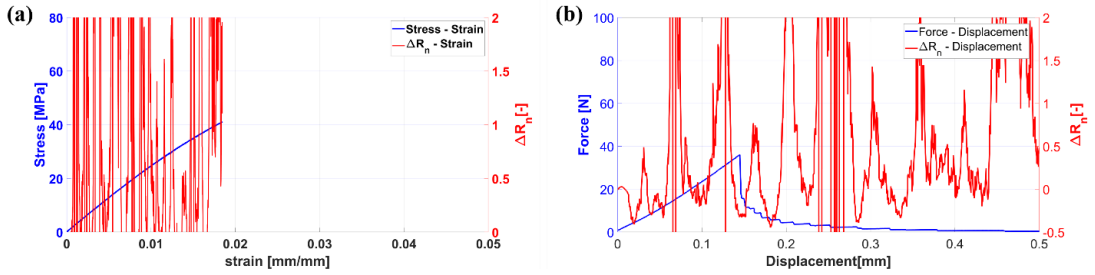

Figure 7. 8. Piezoresistivity behaviour for the binary nanocomposite: (a) tensile test, (b) fracture test.

Figure 7. 9a-b shows the piezoresistivity behaviour as a function of strain increase during tensile test for the 0.5wt.% and 1wt.% nanoclay loadings doped into CNTs/epoxy respectively. To ease the comparison, the piezoresistive-sensitivity for both nanoclay loadings are also plotted together (Figure 7. 9c).

Regardless of the nanoclay content used, both hybrid nanocomposites manifest appropriate self-sensing capabilities in monitoring strain increase i.e. the normalized

resistance increases as a function of strain increase. This indicates that addition of nanoclay into CNTs doped epoxy leads to significant enhance in piezoresistivity which can be attributed to homogenous CNTs dispersion in the hybrid states (Figure 7. 9e-h) compared with poor CNTs dispersing obtained in the binary states (Figure 7. 9a-d).

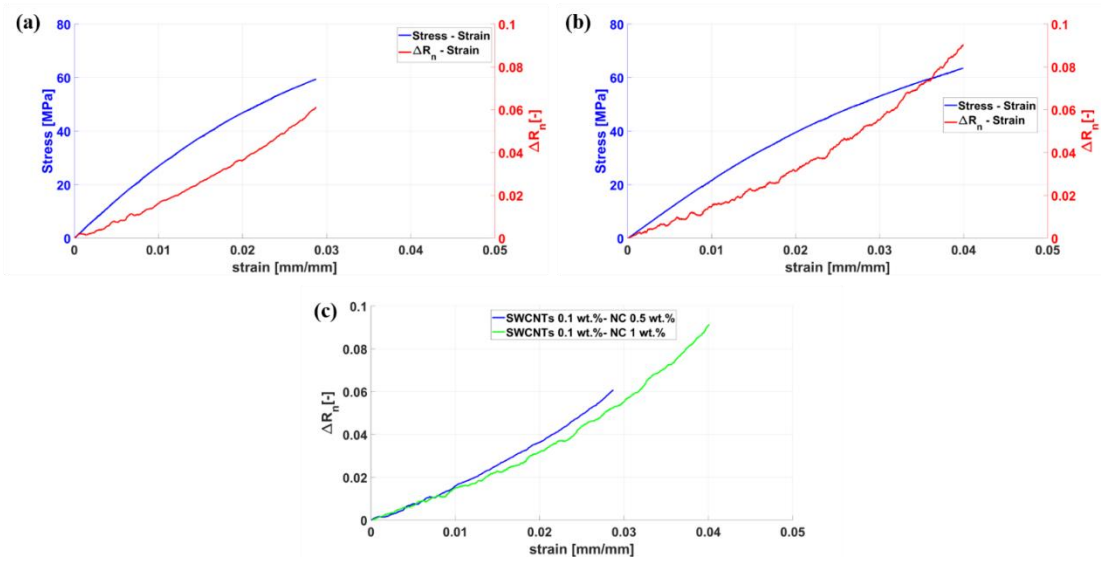

Figure 7. 9. Stress-strain and ΔR_n-strain curves for the ternary nanocomposites during tensile test: (a) 0.1wt.% SWCNTs-0.5wt.% nanoclay, (b) 0.1wt.% SWCNTs-1wt.% nanoclay, (c) ΔR_n versus strain curves for all ternary states together.

In addition, a nonlinear trend in piezoresistivity can be identified for both ternary nanocomposites (Figure 7. 9c). This can be related to the predominate effect of tunneling resistance in ruling piezoresistivity [103]. It is worth noting that tunneling resistance is nonlinearly and exponentially proportional to the tunneling distance, (equation 6.3), thus, the nonlinear piezoresistiviity observed in hybrid nanocomposites can be thoroughly related to the tunneling effect [44]. The average G.Fs at different stain values are summarized in Table 7. 1. No significant difference in sensitivity can be distinguished for 0.5wt.% and 1wt.% nanoclay loading. Apart from the nanoclay

loading, the sensitivity increases in response of strain increase resulting from tunneling effect which dominates the piezoresistivitiy [103]. A sensitivity of 2.1 and 2 at strain of 0.01 mm, corresponding to the approximate yielding point, are obtained for 0.5wt.% and 1wt.% nanoclay contents respectively.

Table 7. 1. Sensitivity at Different Strain Values

Nanocomposites	Sensitivity [-]			
	$\varepsilon \sim 0.005$	$\varepsilon \sim 0.01$	$\varepsilon \sim 0.015$	$\varepsilon \sim 0.02$
0.1wt.%SWCNT-0.5wt.%NC	1.44±0.1	2.10±0.1	2.30±0.08	2.35±0.1
0.1wt.% SWCNT-1wt.%NC	1.46±0.2	2.00±0.15	2.15±0.20	2.34±0.20

Figure 7. 10 shows the piezoresistivity performance of the ternary nanocomposites during fracture test. Due to significant difference observed in normalized resistance before and after crack growth, the piezoresistivity behaviour is divided into two plots i.e. before crack extension (Figure 7. 10a, c and e) and upon failure (Figure 7. 10b and d). The piezoresistivity performance of the nanocomposites at displacment < 0.1mm manifest slight positive and negative change in normalized resistance, followed by a slight decrease at 0.1mm< displacement <0.2mm.

In fact, at the beginning of the test, the simultaneous formation and breakage of conductive networks in the compression and tension sides of SENB specimen, respectively, neutralize their effects on piezoresistivity [103], thus no specific trend can be seen. At 0.1mm < displacement < 0.2mm, it seems that negative effect of new electrical networks formed in the compression side dominate the piezoresistivity behaviour. This along with the higher area of the compression sides compared with the

tension side (due to the fact notch is located mostly in the tension sides) account for the decreasing trend appeared at 0.1mm < displacement < 0.2mm.

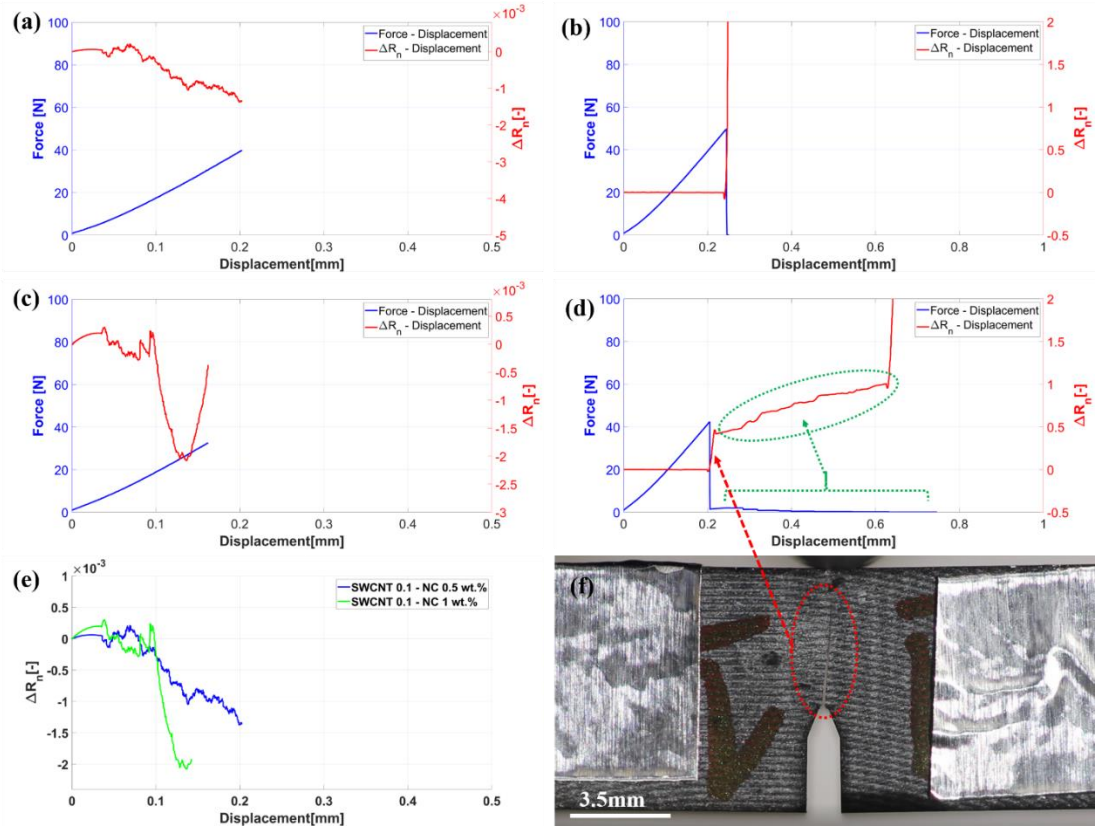

Figure 7. 10. Force-displacment and ΔR_n-displacment curves during fracture tests: (a-b) 0.1wt.% SWCNTs-0.5wt.% nanoclay, (c-d) 0.1wt.% SWCNTs-1wt.% nanoclay fracture test, (e) ΔR_n versus displacement for all ternary states together, (f) crack extension.

However, with the onset of crack propagation, the normalized resistance dramatically increase as shown in Figure 7. 10b and d. Unlike the 0.5wt.% nanoclay loading where the specimen manifested abrupt and complete failure (Figure 7. 10b), the 1wt.% nanoclay loading did not break completely upon first failure (Figure 7. 10d). Hence, the force-displacment curve and subsequently ΔR_n-displacement curve show

step by step patterns (after first failure) till complete fracture as illustrated by green dashed lines in Figure 7. 10d). With the onset of crack growth i.e. at first step as shown in Figure 7. 10d and f, the initial crack is extended up to 3.6mm while the normalized resistance dramatically increases by 50%, indicating that the developed sensor can successfully trace any crack growth in the system.

7.4. Summary

The effect of nanoclay platelets addition in tailoring mechanical and electromechanical properties of SWCNTs doped epoxy were investigated throughout this study. Two different types of nanocomposites including binary (SWCNT/epoxy) and hybrid (SWCNTs-NC/epoxy) states were prepared for the examination. The following outcomes can be made from this study:

- In the binary state, poor CNTs dispersions was seen resulting from their re-agglomeration during manufacturing process whereas addition of nanoclay into CNTs doped epoxy could enhance the CNTs dispersion at ternary states. In addition, a combination of intercalated and exfoliated structure for the nanoclay in ternary states was achieved.
- The electrical conductivity substantially increased by 4 orders of magnitudes for the ternary composites containing 0.5wt.% nanoclay compared with the binary states. This was related to better CNTs dispersion in the former with respect to the latter. In addition, at higher nanoclay loading (1wt.%), the electrical conductivity was slightly reduced resulting from the intercalated/exfoliated structures of the nanoclay.

- The binary nanocomposites showed lower UTS and stiffness with respect to the neat epoxy resulting from poor bonding between CNTs aggregates and epoxy, whereas an increase of 13% and 17% in UTS at 0.5wt.% and 1wt.% nanoclay loadings were achieved with respect to the neat epoxy arisen from better dispersion of the both nanoreinforcement. Young's modulus did not show significant change, though slightly increased at 0.5wt.% nanoclay content in comparison with the pristine epoxy.
- Two different regions were distinguished from the fracture morphology including the initial fracture region, showing a flat and mirror-like surface morphology, followed by a rougher surface, manifesting a river-like pattern (for the neat epoxy and binary composite) and cores/cavities (for the hybrid composites). Apart from that, surface toughness increased by increasing tensile strength specimen.
- For the binary composite, K_{IC} and G_{IC} enhanced by 28% and 4%, respectively, with respect to the neat epoxy where crack-tailing was accounted for the enhancement. For the hybrid nanocomposite containing 0.5wt.% nanoclay, further increase in K_{IC} and G_{IC} around 72% and 175%, respectively, (compared with the neat epoxy), and 34% and 64%, respectively, (compared with the binary composite) were achieved. Nanoclay loading of 1wt.% manifested small reduction in K_{IC} and G_{IC} compared with 0.5wt.% nanoclay loading, but still higher than binary composite and neat epoxy. Crack-pinning and crack deflection were accounted for the significant increase in fracture toughness for ternary composites.
- No piezoresistivity was found for the binary nanocomposite resulting from poor CNTs dispersion. It was concluded that the CNTs aggregates not only

hampered electrical and mechanical properties, but also lead to sever degradation of electromechanical properties. On the other hand, appropriate self-sensing capabilities in monitoring strain increase were achieved for hybrid nanocomposites during tensile test. This indicated that addition of nanoclay into CNTs doped epoxy caused significant enhance in piezoresistivity which was attributed to homogenous CNTs dispersion in the hybrid states.

- A nonlinear trend in piezoresistivity was identified for the hybrid nanocomposites resulting from the predominate effect of tunneling resistance in ruling piezoresistivity. A sensitivity of 2.1 and 2 at strain of 0.01 mm, corresponding to the approximate yielding point, were found for 0.5wt.% and 1wt.% nanoclay contents respectively. The piezoresistivity performance of the ternary nanocomposite showed negligible reduction before failure resulting from the negative effect of new electrical networks formed in the compression side which dominated the piezoresistivity behaviour. However, the normalized resistance manifested significant increase with the onset of crack growth, indicating that the developed sensor could thoroughly trace any damage extension in the system.

CHAPTER 8: GLOBAL DATA

In this chapter, all outcomes are combined and compared together in order to better interpret the nanocomposites performance at different loadings as well as the composite types i.e. binary and ternary states. The results are compared in terms of tensile strength, fracture toughness, electrical conductivity and piezoresistive-sensitivity obtained from tensile test. In addition, the Izod impact strength at binary state is also plotted for the comparison. Finally, to ease the comparison, this chapter is divided into three subsections including phase 1, phase 2 and combination of phase 1&2.

8.1. Phase 1

Figure 8. 1 shows the global results in binary states. Regardless of the CNT morphology, SWCNTs or DWCNTs, 0.5wt.% manifests better performance in terms of mechanical properties i.e. the highest tensile strength, Izod impact strength, and fracture toughness are obtained at 0.5wt.% for both SWCNTs and DWCNTs doped epoxy as shown in Figure 8. 1a-c respectively. It is worth noting that fracture toughness at 0.75wt.% for both SWCNTs and DWCNTs are not validated because they cannot met equation 2.7 resulting from low tensile strength of the nanocomposites at such concentration. In addition, tensile and impact strengths are reduced at 0.75wt.% compared with the neat epoxy which was attributed to presence of CNTs aggregates and voids.

Excluding 0.5wt.% SWCNTs which manifested slight increase (15%) in tensile strength, other nanocomposites possessed lower tensile strength compared to the neat epoxy. This was related to detrimental effect of voids and pores, left in the specimen

due to improper degassing, on tensile strength whereas fracture toughness and impact strength did not significantly affected by such defects. DWCNTs/epoxy manifest lower tensile and impact strengths compared with the SWCNTs/epoxy due to higher void contents. This was attributed to OH-functionalization of SWCNTs which improved interfacial bonding of epoxy and nanofiller.

For the electrical conductivity, both SWCNTs and DWCNTs manifested significant increase in electrical conductivity i.e. 9 orders of magnitude (Figure 8. 1d-e). In addition, DWCNTs demonstrated a relatively higher conductivity with respect to SWCNTs which was attributed to higher amount of CNT agglomeration in the latter compared to the former. It is worth noting that SWCNTs possessed higher SSA and aspect ratio compared to DWCNTs, thus, they most likely to agglomerate with respect to DWCNTs. Apart from CNT morphology, a low percolation threshold region was identified for both SWCNTs and WCNTs i.e. in the range of 0.1-0.3wt.% as shown in Figure 8. 1d.

For the piezoresistive-sensitivity, similar to electrical conductivity, DWCNTs manifested better performance in strain monitoring (Figure 8. 1f). In fact, the highest sensitivity around 2.4 was obtained at 0.5wt.% DWCNTs whereas the maximum sensitivity of 1.97 was identified for 0.25wt,% SWCNTs. Sensitivity was decreased by increasing weight concentration for SWCNTs/epoxy which was in line with the literature indicating that the highest gauge factor was obtained near percolation threshold region. On the other hand, lower sensitivity was distinguished at 0.25wt.% DWCNTs with respect to 0.5wt.% DWCNTs which was related to poor CNTs dispersion in the former.

In overall, taking into account the mechanical and electromechanical properties of the nanocomposite, 0.5wt.% SWCNTs demonstrated better performance in the

binary state at phase 1. Although 0.5wt.% DWCNTs also manifested proper performance in terms of fracture toughness , impact strength, electrical conductivity and sensitivity, its low tensile strength with respect to 0.5wt.% SWCNTs and the neat epoxy has led to some uncertainty. It is worth noting that these performances are based on the manufacturing method used in phase 1, thus, one might get different outcomes by using different manufacturing methodology.

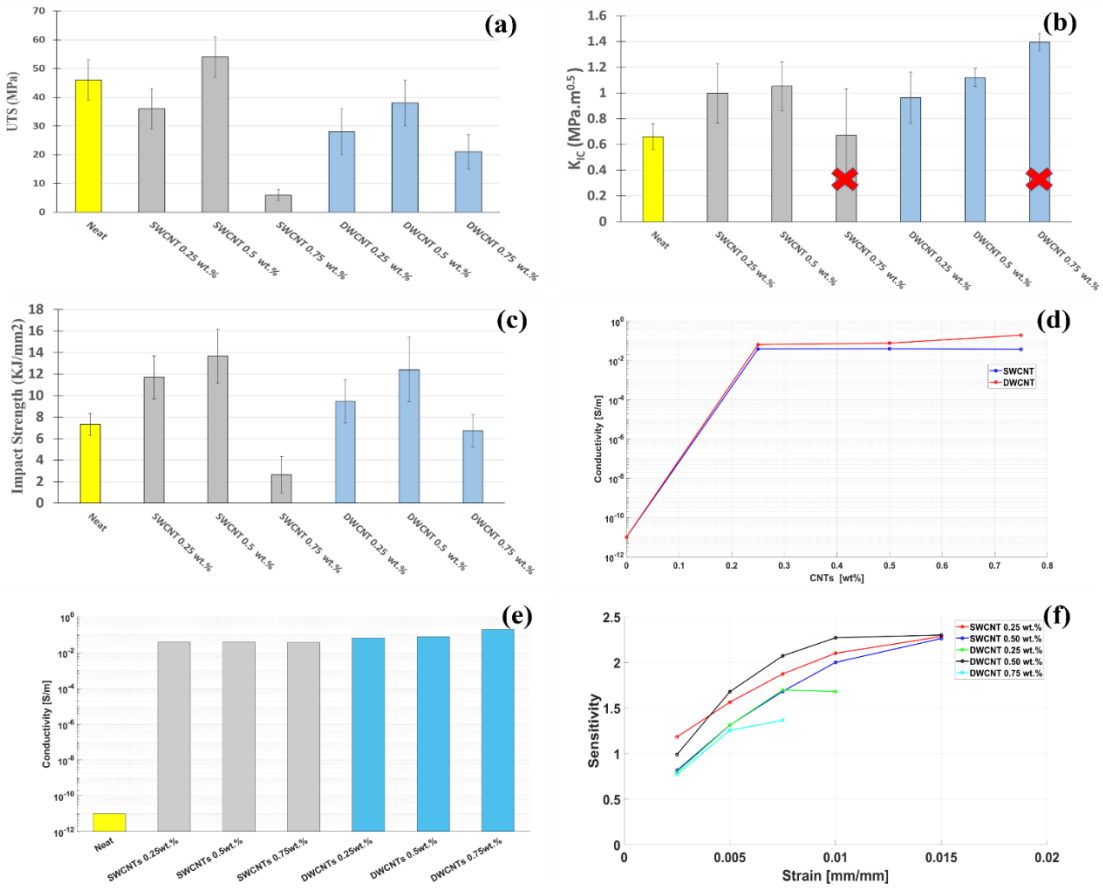

Figure 8. 1. Global results in phase 1: (a) tensile strength, (b) K_{IC}, (c) Impact strength, (d-e) electrical conductivity, (f) sensitivity.

8.2. Phase 2

Figure 8. 2 displays the mechanical, electrical and electromechanical

performance of the nanocomposites produced in phase 2. Different behaviours were observed when nanoclay introduced to the SWCNTs and DWCNTs doped epoxies. In fact, the tensile strength of the ternary SWCNTs-nanoclay/epoxy was improved compared to binary SWCNTs/epoxy in which binary composite showed lower tensile strength with respect to the neat epoxy resulting from CNT re-agglomeration throughout manufacturing. Similarly, fracture toughness of ternary SWNTs-nanoclay/epoxy was also higher than binary SWCNTs/epoxy (Figure 8. 2b). This indicates that nanoclay could improve SWCNTs dispersion, thus, resulting in enhanced mechanical properties.

Unlike SWCNTs based nanocomposites in which its ternary states manifested higher tensile strength compared to its binary state, ternary DWCNTs-nanoclay/epoxy showed slight reduction in tensile strength with respect to the its binary state (Figure 8. 2a). This was attributed to higher void contents and poor interfacial bonding of nanoclay/epoxy in the former with respect to the latter. On the other hand, for the fracture toughness, both ternary DWCNTs-nanoclay and SWCNTs-nanoclay possessed higher toughness compared with their binary state (Figure 8. 2b).

Apart from CNT morphology, both ternary nanocomposites i.e. SWCNTs-nanoclay/epoxy and DWCNTs-nanoclay/epoxy manifested higher electrical conductivity in their ternary states with respect to their binary states (Figure 8. 2c-d). In fact, for the SWCNTs based nanocomposites, almost no conductivity was detected whereas addition of nanoclay to SWCNTs/epoxy resulted in substantial increase up to 4 orders of magnitude in electrical conductivity. For the DWCNTs based nanocomposite, addition of nanoclay to DWCNTs/epoxy was led to 700% increase in electrical conductivity in the ternary state. This again indicates that nanoclay addition to CNTs doped epoxy could successfully enhance their dispersions, thus, improving

formation of electrical networks throughout the ternary nanocomposites.

For the piezoresistivity performance, all ternary nanocomposites manifested higher sensitivity with respect to their binary states (Figure 8. 2e). For the SWCNTs based epoxy, no sensitivity was identified due to lack of electrical conductivity whereas a sensitivity of 2.1 was identified for the ternary SWCNTs nanocomposite loaded at 0.5wt.% nanoclay. Similarly, for the DWCNTs based nanocomposites, higher sensitivity around 2 was achieved for its ternary state whilst a sensitivity of 1.5 was seen for the binary composite.

In overall, hybrid SWCNTs-nanoclay/epoxy showed higher sensitivity with respect to the hybrid DWCNTs-nanoclay/epoxy (at strain of 0.01 mm/mm) resulting from further damage evaluations during loading, at macro-scale, thus, higher breakage of electrical networks. On the other hand, ternary DWCNTs based epoxy manifested a relatively higher sensitivity at low strain (0.005mm/mm) compared to ternary SWCNTs based epoxy which can be attributed to better dispersion of DWCNTs with respect to SWCNTs. Consequently, taking into account mechanical, electrical and electromechanical properties of the nanocomposites, hybrid DWCNTs-nanoclay showed better performance with respect to the ternary SWCNTs nanocomposites.

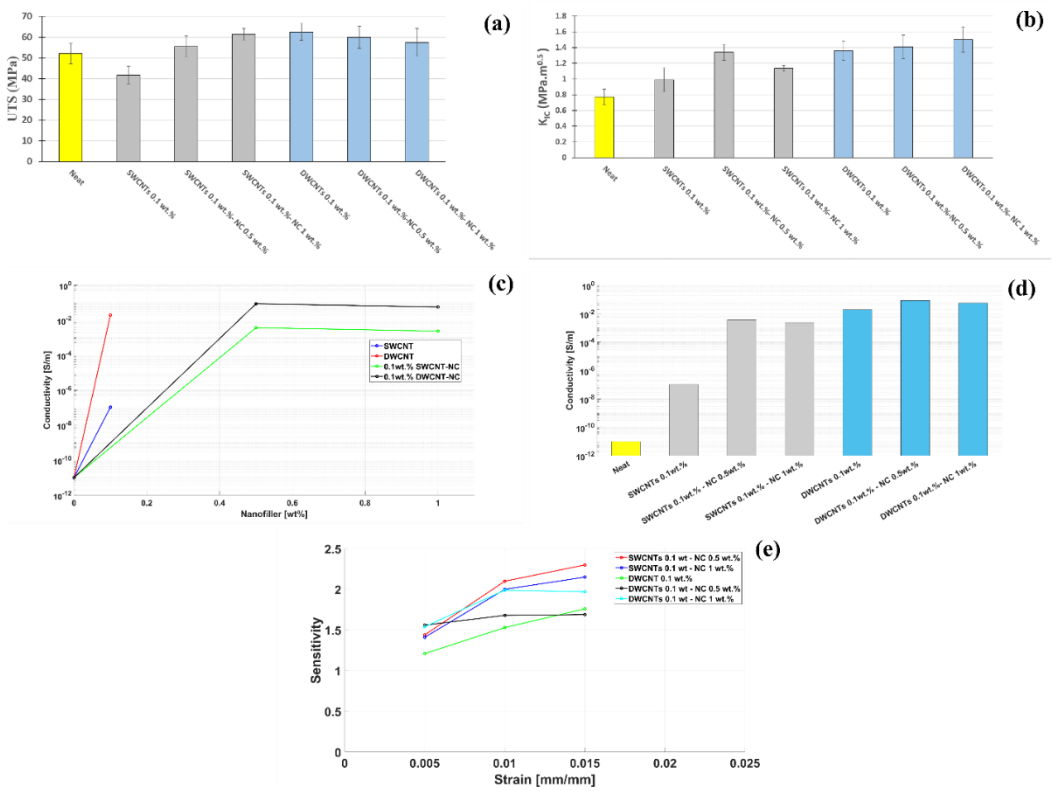

Figure 8. 2. Global results in phase 1: (a) tensile strength, (b) K_{IC}, (c-d) electrical conductivity, (e) sensitivity.

8.3. Combined data in phases 1&2

In this section, all data extracted in phase 1 and 2 are combined and interpreted together in order to better compare the multifunctional properties of the nanocomposites developed. In addition, samples produced in phase 1 and 2 were highlighted by green and blue bars in Figure 8. 3 while the neat epoxy was shown by yellow bar. Comparing Figure 8. 3a-b clearly indicate higher performance of the nanocomposites developed in phase 2 compared with the ones in phase 1. In other words, higher tensile strength with less variation in phase 2 with respect to lower tensile strength and higher deviation in phase 1 can be seen. Similar behaviour can be also noticed for fracture toughness in samples developed at phase 2 with respect to phase 1.

For the electrical conductivity, no significant change can be seen in phase 1 and 2, though the former demonstrated a relatively higher electrical conductivity (Figure 8. 3c). This can be attributed to higher amount of CNTs used in phase 1 i.e. 0.25-0.75wt.% whilst less CNT content, 0.1wt.%, was used in phase 2. Nevertheless, with much less CNT content used in phase 2, appropriate electrical conductivity was obtained in ternary nanocomposites. For the piezoresistivity performance, it seems that sample produced in phase 1, in particular, manifested a relatively higher sensitivity with respect to the ternary nanocomposites produced in phase 2 (at strain of 0.01 mm/mm), though the variations are in the range of 0.2-0.4 (Figure 8. 3d).

In overall, by taking into consideration of multifunctional properties including tensile strength, fracture toughness, electrical conductivity and sensitivity, it can be pointed out that the ternary nanocomposites developed in phase 2 demonstrated better performance compared to the ones produced in phase 1. In fact, low tensile strength along with high variations observed in phase1, raised questions for the effective exploitation of CNTs in multifunctional properties enhancement. In other words, highly monotonous outcomes especially for tensile strength without sacrificing other properties indicates the effective performance of nanofiller in phase 2 of the project. This means that the modified manufacturing methodology used in phase 2 along with using nanoclay as an auxiliary dispersing agent could achieve better CNT dispersion, thus, better performance.

It should be noted that less amount of CNTs was used in phase 2 while nanoclay are cheap. Thus, highly added-value product with cost effectiveness was produced in phase 2 compared with expensive and low quality composites in phase 1.

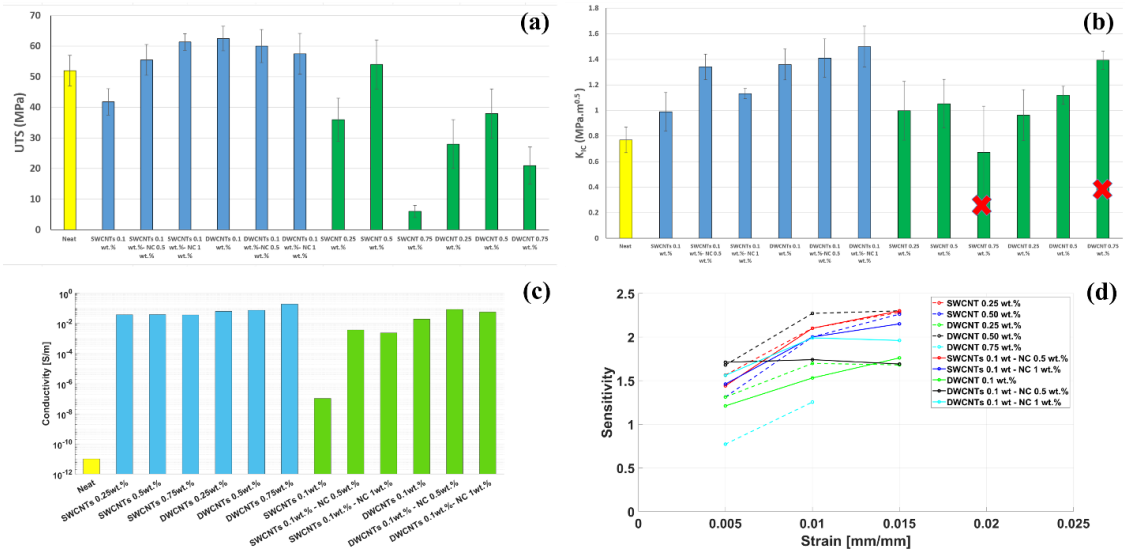

Figure 8. 3. Combined global results in phase 1 and 2: (a) tensile strength, (b) K_{IC}, (c) Impact strength, (d-e) electrical conductivity, (f) sensitivity

9. CONCLUSION AND FUTURE WORKS

9.1. Conclusion

The current thesis was aimed to investigate multifunctional properties of epoxy based nanocomposites reinforced with CNTs and nanoclay. The thesis was divided into two main phase including phase 1 and 2. In the first phase, different types of CNTs, SWCNTs and DWCNTs, with various weight concentration were used in order to find out the optimum CNTs contents as well as manufacturing methodology to be used for phase 2. In the second phase, nanoclay was added to CNTs doped epoxy i.e. (ternary states) while the manufacturing methodology was also modified based the phase 1 outcomes. Finally, the performance of the nanocomposites was compared in terms of tensile strength, fracture toughness, electrical conductivity and piezoresistive-sensitivity. In the following, the main outcomes of this thesis were summarized.

Phase1: binary SWCNTs/epoxy

- The electrical conductivity was increased up to 9 orders of magnitude with the addition of 0.25 wt.% of CNTs
- Higher sensitivity was achieved in the case of the CNT content of 0.25 wt.% compared with 0.5 wt.% at lower strain.
- Bridging mechanism was considered as the main toughening mechanism in SWCNTs reinforced epoxy at CNT content of 0.25 and 0.5 wt.% whereas the weak interfacial bonding between CNTs aggregates and the epoxy resulted in

alignment of CNTs parallel to shear loading transfer, inducing the degradation of mechanical properties at 0.75 wt.% .

Phase1: DWCNTs/epoxy

- The electrical conductivity increased up to 10 orders of magnitude at 0.5 wt.% (with respect to pure epoxy).
- CNT loading of 0.5 wt.% achieved the highest sensitivity (around 1.8) at strain of 0.06 [-]. The lower sensitivity observed at 0.75 wt.% was attributed to presence of agglomerations and defects.

Phase 2: ternary DWCNTs-nanoclay

- The hybrid nanocomposites (DWCNTs-NC/epoxy) showed a more uniform nanofiller dispersion in comparison with the binary composite (DWCNTs/epoxy). At binary state, the presence of CNTs-rich and CNTs-poor regions were considerable.
- The addition of nanoclay improved CNTs dispersion because nanoclay galleries acted as an obstacle, thus, avoiding CNTs re-agglomeration during manufacturing.
- An exfoliated structure was obtained for the nanoclay resulting from the appropriate manufacturing procedure used in this study.
- Both binary and ternary nanocomposites manifested higher tensile strength compared to neat epoxy. The maximum increase of up to 20% was obtained for the DWCNT/epoxy, while a slight reduction was observed in the ternary states.

- For the fracture toughness, a substantial increase in K_{IC} and G_{IC} was obtained for the nanocomposites compared to the neat epoxy. The highest enhancement around 94 % and 254 %, in K_{IC} and G_{IC} respectively, was achieved for 0.1 wt.% DWCNTs – 1 wt.% NC.
- A combination effect of crack bridging and crack deflection accounted for the significant increase in the fracture toughness properties of the nanocomposites.
- The electrical conductivity of the DWCNTs/epoxy substantially increased up to 9 orders of magnitude by the addition of only 0.1wt.% DWCNTs. As a consequence of the improved CNTs dispersion, the electrical conductivity of the ternary state materials increased by 700% and 400% with respect to the binary nanocomposite, for 0.5wt.% and 1wt.% NC loadings, respectively.
- For the piezoresistivity performance during tensile test, the hybrid nanocomposites showed better performance with respect to the binary state in monitoring strain increase. The highest sensitivity of 1.99 was obtained for the hybrid nanocomposite loaded at 1wt.% nanoclay at $\varepsilon \sim 0.01$ while a sensitivity of 1.74 and 1.53 was achieved for the 0.1wt.% DWCNTs - 0.5wt.% NC and the 0.1wt.% DWCNTs doped materials, respectively.

Phase 2: ternary SWCNTs-nanoclay

- In the binary state, poor CNTs dispersions was seen resulting from their re-agglomeration during manufacturing process whereas addition of nanoclay into CNTs doped epoxy could enhance the CNTs dispersion at ternary states. In addition, a combination of intercalated and exfoliated structure for the nanoclay in ternary states was achieved.

- The electrical conductivity substantially increased by 4 orders of magnitudes for the ternary composites containing 0.5wt.% nanoclay compared to the binary states. This was related to better CNTs dispersion in the former with respect to the latter.
- The binary nanocomposites showed lower UTS and stiffness with respect to the neat epoxy resulting from poor bonding between CNTs aggregates and epoxy, whereas an increase of 13% and 17% in UTS at 0.5wt.% and 1wt.% nanoclay loadings were achieved with respect to the neat epoxy arisen from better dispersion of the both nanoreinforcement.
- For the hybrid nanocomposite containing 0.5wt.% nanoclay, further increase in K_{IC} and G_{IC} around 72% and 175%, respectively, (compared with the neat epoxy), and 34% and 64%, respectively, (compared with the binary composite) were achieved. Crack-pinning and crack deflection were accounted for the significant increase in fracture toughness for ternary composites.
- No piezoresistivity was found for the binary nanocomposite resulting from poor CNTs dispersion. On the other hand, appropriate self-sensing capabilities in monitoring strain increase were achieved for hybrid nanocomposites during tensile test.
- A sensitivity of 2.1 and 2 at strain of 0.01 mm, corresponding to the approximate yielding point, were found for 0.5wt.% and 1wt.% nanoclay contents respectively.

9.2. Suggestion for future works

As discussed in this thesis, unlike fracture toughness which substantially increased in both binary and ternary states, tensile strength did not improve sufficiently. In addition, slight variation in piezoresisitivity trend is another concern about the reliability of the results. In this context, the following research area are recommended:

1- Investigation of the effect of using various solvent and different manufacturing temperature ranges on improving degassing and reducing void content
2- The effect of aspect ratio and surface finctionlaztion on piezoresistivity performance using same CNTs morphology
3- The effect of CNTs aggregates distribution and size on electromechanical performance
4- Investigation of the effect of using different dispersion techniques on mechanical and electromechanical performance in both binary and ternary composites
5- Nanoclay addition into CNTs doped epoxy or CNTs addition into nanoclay doped epoxy? which one lead to better multifunctional properties

REFERENCE

[1] Quilter A. Composites in Aerospace Applications. Inf Handl Serv Inc 2004:1–5.

[2] Soutis C. Carbon fiber reinforced plastics in aircraft construction 2005;412:171–6. doi:10.1016/j.msea.2005.08.064.

[3] Peters ST (Ed. . Handbook of Composites. Springer, Boston, MA; n.d.

[4] Lubineau G, Rahaman A. A review of strategies for improving the degradation properties of laminated continuous-fiber/epoxy composites with carbon-based nanoreinforcements. Carbon N Y 2012;50:2377–95. doi:10.1016/j.carbon.2012.01.059.

[5] Forintos N, Czigany T. Multifunctional application of carbon fiber reinforced polymer composites: Electrical properties of the reinforcing carbon fibers – A short review. Compos Part B Eng 2019;162:331–43. doi:10.1016/j.compositesb.2018.10.098.

[6] Domun N, Hadavinia H, Zhang T, Sainsbury T, Liaghat GH, Vahid S. Improving the fracture toughness and the strength of epoxy using nanomaterials-a review of the current status. Nanoscale 2015;7:10294–329. doi:10.1039/c5nr01354b.

[7] Bachmann J, Hidalgo C, Bricout S. Environmental analysis of innovative sustainable composites with potential use in aviation sector—A life cycle assessment review. Sci China Technol Sci 2017;60:1301–17. doi:10.1007/s11431-016-9094-y.

[8] Piquet B. A350XWB Special Edition. Airbus Tech Mag 2013:25.

[9] Liu S, Chevali VS, Xu Z, Hui D, Wang H. A review of extending performance of epoxy resins using carbon nanomaterials. Compos Part B Eng 2018;136:197–214. doi:10.1016/j.compositesb.2017.08.020.

[10] Chung DDL. A review of multifunctional polymer-matrix structural composites. Compos Part B Eng 2019;160:644–60. doi:10.1016/j.compositesb.2018.12.117.

[11] Ma D, Esmaeili A, Manes A, Sbarufatti C, Jiménez-Suárez A, Giglio M, et al. Numerical study of static and dynamic fracture behaviours of neat epoxy resin. Mech Mater 2020;140:103214. doi:10.1016/j.mechmat.2019.103214.

[12] Guadagno L, Raimondo M, Vittoria V, Vertuccio L, Naddeo C, Russo S, et al. Development of epoxy mixtures for application in aeronautics and aerospace. RSC Adv 2014;4:15474–88. doi:10.1039/c3ra48031c.

[13] Han S, Meng Q, Araby S, Liu T, Demiral M. Mechanical and electrical properties of graphene and carbon nanotube reinforced epoxy adhesives: Experimental and numerical analysis. Compos Part A Appl Sci Manuf 2019;120:116–26. doi:10.1016/j.compositesa.2019.02.027.

[14] Singh AK, Panda BP, Mohanty S, Nayak SK, Gupta MK. Recent Developments on Epoxy-Based Thermally Conductive Adhesives (TCA): A Review. Polym - Plast Technol Eng 2018;57:903–34. doi:10.1080/03602559.2017.1354253.

[15] Kinloch AJ. Toughening epoxy adhesives to meet today's challenges. MRS Bull 2003;28:445–8. doi:10.1557/mrs2003.126.

[16] Hollaway LC. A review of the present and future utilisation of FRP composites in the civil infrastructure with reference to their important in-service properties. Constr Build Mater 2010;24:2419–45. doi:10.1016/j.conbuildmat.2010.04.062.

[17] Petrie EM. Epoxy Adhesive Formulations. 2006.

[18] Paluvai NR, Mohanty S, Nayak SK. Synthesis and Modifications of Epoxy Resins and Their Composites: A Review. Polym - Plast Technol Eng 2014;53:1723–58. doi:10.1080/03602559.2014.919658.

[19] Ueki T, Nishijima S, Izumi Y. Designing of epoxy resin systems for cryogenic

use. Cryogenics (Guildf) 2005;45:141–8. doi:https://doi.org/10.1016/j.cryogenics.2004.07.002.

[20] Garg AC, Mai Y-W. Failure mechanisms in toughened epoxy resins—A review. Compos Sci Technol 1988;31:179–223. doi:https://doi.org/10.1016/0266-3538(88)90009-7.

[21] Pandey G, Thostenson ET. Carbon nanotube-based multifunctional polymer nanocomposites. Polym Rev 2012;52:355–416. doi:10.1080/15583724.2012.703747.

[22] Liu S, Chevali VS, Xu Z, Hui D, Wang H. A review of extending performance of epoxy resins using carbon nanomaterials. Compos Part B Eng 2018;136:197–214. doi:10.1016/j.compositesb.2017.08.020.

[23] Sánchez-romate XF, Artigas J, Jiménez-suárez A, Sánchez M, Güemes A, Ureña A. Critical parameters of carbon nanotube reinforced composites for structural health monitoring applications : Empirical results versus theoretical predictions. Compos Sci Technol 2019;171:44–53. doi:10.1016/j.compscitech.2018.12.010.

[24] Tuloup C, Harizi W, Aboura Z, Meyer Y, Khellil K, Lachat R. On the use of in-situ piezoelectric sensors for the manufacturing and structural health monitoring of polymer-matrix composites: A literature review. Compos Struct 2019;215:127–49. doi:10.1016/J.COMPSTRUCT.2019.02.046.

[25] Bauhofer W, Kovacs JZ. A review and analysis of electrical percolation in carbon nanotube polymer composites. Compos Sci Technol 2009;69:1486–98. doi:10.1016/j.compscitech.2008.06.018.

[26] Zheng Q, Han B, Ou J. 11 - NanoComposites for structural health monitoring. In: Pacheco-Torgal F, Diamanti MV, Nazari A, Granqvist CG, Pruna A, Amirkhanian S, editors. Nanotechnol. Eco-efficient Constr. (Second Ed. Second

Edi, Woodhead Publishing; 2019, p. 227–59. doi:https://doi.org/10.1016/B978-0-08-102641-0.00011-6.

[27] Kwon DJ, Wang ZJ, Choi JY, Shin PS, Devries KL, Park JM. Damage sensing and fracture detection of CNT paste using electrical resistance measurements. Compos Part B Eng 2016;90:386–91. doi:10.1016/j.compositesb.2016.01.020.

[28] Moriche R, Sánchez M, Jiménez-Suárez A, Prolongo SG, Ureña A. Strain monitoring mechanisms of sensors based on the addition of graphene nanoplatelets into an epoxy matrix. Compos Sci Technol 2016;123:65–70. doi:10.1016/j.compscitech.2015.12.002.

[29] De la Vega A, Kinloch IA, Young RJ, Bauhofer W, Schulte K. Simultaneous global and local strain sensing in SWCNT-epoxy composites by Raman and impedance spectroscopy. Compos Sci Technol 2011;71:160–6. doi:10.1016/j.compscitech.2010.11.004.

[30] Sanli A, Müller C, Kanoun O, Elibol C, Wagner MFX. Piezoresistive characterization of multi-walled carbon nanotube-epoxy based flexible strain sensitive films by impedance spectroscopy. Compos Sci Technol 2016;122:18–26. doi:10.1016/j.compscitech.2015.11.012.

[31] Takeda T, Narita F. Fracture behavior and crack sensing capability of bonded carbon fi ber composite joints with carbon nanotube-based polymer adhesive layer under Mode I loading. Compos Sci Technol 2017;146:26–33. doi:10.1016/j.compscitech.2017.04.014.

[32] Li J, Ma PC, Chow WS, To CK, Tang BZ, Kim JK. Correlations between percolation threshold, dispersion state, and aspect ratio of carbon nanotubes. Adv Funct Mater 2007;17:3207–15. doi:10.1002/adfm.200700065.

[33] Obitayo W, Liu T. A review: Carbon nanotube-based piezoresistive strain

sensors. J Sensors 2012;2012. doi:10.1155/2012/652438.

[34] Kulakov V, Aniskevich A, Ivanov S, Poltimae T, Starkova O. Effective electrical conductivity of carbon nanotube–epoxy nanocomposites. J Compos Mater 2017;51:2979–88. doi:10.1177/0021998316678304.

[35] Li C, Thostenson ET, Chou TW. Dominant role of tunneling resistance in the electrical conductivity of carbon nanotube-based composites. Appl Phys Lett 2007;91. doi:10.1063/1.2819690.

[36] Oskouyi AB, Sundararaj U, Mertiny P. Tunneling conductivity and piezoresistivity of composites containing randomly dispersed conductive nano-platelets. Materials (Basel) 2014;7:2501–21. doi:10.3390/ma7042501.

[37] Hu N, Karube Y, Yan C, Masuda Z, Fukunaga H. Tunneling effect in a polymer / carbon nanotube nanocomposite strain sensor 2008;56:2929–36. doi:10.1016/j.actamat.2008.02.030.

[38] Aqel A, El-Nour KMMA, Ammar RAA, Al-Warthan A. Carbon nanotubes, science and technology part (I) structure, synthesis and characterisation. Arab J Chem 2012;5:1–23. doi:10.1016/j.arabjc.2010.08.022.

[39] Kroto HW, Heath JR, O'Brien SC, Curl RF, Smalley RE. C60: Buckminsterfullerene. Nature 1985;318:162–3. doi:10.1038/318162a0.

[40] Iijima S. Helical microtubules of graphitic carbon. Nature 1991;354:56–8. doi:10.1038/354056a0.

[41] Li W. The self-sensing, electrical and mechanical properties of the epoxy composites reinforced with carbon nanotubes-micro reinforcement nano/micro hybrids 2013.

[42] Jacobsen NR, Møller P, Clausen PA, Saber AT, Micheletti C, Jensen KA, et al. Biodistribution of Carbon Nanotubes in Animal Models. Basic Clin Pharmacol

Toxicol 2017;121:30–43. doi:10.1111/bcpt.12705.

[43] Gojny FH, Wichmann MHG, Fiedler B, Schulte K. Influence of different carbon nanotubes on the mechanical properties of epoxy matrix composites - A comparative study. Compos Sci Technol 2005;65:2300–13. doi:10.1016/j.compscitech.2005.04.021.

[44] Simmons JG. Generalized Formula for the Electric Tunnel Effect between Similar Electrodes Separated by a Thin Insulating Film. J Appl Phys 1963;34:1793–803. doi:10.1063/1.1702682.

[45] Cao X, Wei X, Li G, Hu C, Dai K, Guo J, et al. Strain sensing behaviors of epoxy nanocomposites with carbon nanotubes under cyclic deformation. Polym (United Kingdom) 2017;112:1–9. doi:10.1016/j.polymer.2017.01.068.

[46] Esmaeili A, Sbarufatti C, Ma D, Manes A, Jiménez-Suárez A, Ureña A, et al. Strain and crack growth sensing capability of SWCNT reinforced epoxy in tensile and mode I fracture tests. Compos Sci Technol 2019;186:107918. doi:10.1016/J.COMPSCITECH.2019.107918.

[47] Paluvai NR, Mohanty S, Nayak SK. Effect of nanoclay on the mechanical, thermal, and water absorption properties of an UP-toughened epoxy network. J Adhes 2015;92:840–61. doi:10.1080/00218464.2015.1047828.

[48] Anh NT, Tung NQ, Canh NX, Hoan N Van. Eco-friendly flame retardant additives for epoxy resin nanocomposites 2019;332:323–32.

[49] Zabihi O, Ahmadi M, Nikafshar S. A technical review on epoxy-clay nanocomposites : Structure , properties , and their applications in fi ber reinforced composites. Compos Part B 2018;135:1–24. doi:10.1016/j.compositesb.2017.09.066.

[50] Liu J, Boo W, Clearfield A, Sue H, Liu J, Boo W, et al. Intercalation and

Exfoliation : A Review on Morphology of Polymer Nanocomposites Reinforced by Inorganic Layer Structures Intercalation and Exfoliation : A Review on Morphology of Polymer Nanocomposites Reinforced by Inorganic Layer Structures 2007;6914. doi:10.1081/AMP-200068646.

[51] Wang L, Wang K, Chen L, Zhang Y, He C. Preparation, morphology and thermal/mechanical properties of epoxy/nanoclay composite. Compos Part A Appl Sci Manuf 2006;37:1890–6. doi:10.1016/j.compositesa.2005.12.020.

[52] Abdul A, Yop K, Jin S, Hui D. Composites : Part B Epoxy clay nanocomposites – processing , properties and applications : A review. Compos Part B 2013;45:308–20. doi:10.1016/j.compositesb.2012.04.012.

[53] Zabihi O, Ahmadi M, Nikafshar S, Chandrakumar Preyeswary K, Naebe M. A technical review on epoxy-clay nanocomposites: Structure, properties, and their applications in fiber reinforced composites. Compos Part B Eng 2018;135:1–24. doi:10.1016/j.compositesb.2017.09.066.

[54] Aradhana R, Mohanty S, Nayak SK. High performance epoxy nanocomposite adhesive: Effect of nanofillers on adhesive strength, curing and degradation kinetics. Int J Adhes Adhes 2018;84:238–49. doi:10.1016/j.ijadhadh.2018.03.013.

[55] Fukushima Y, Inagaki S. Synthesis of an Intercalated Compound of Montmorillonite and 6-Polyamide. In: Atwood JL, Davies JED, editors. Incl. Phenom. Inorganic, Org. Organomet. Hosts, Dordrecht: Springer Netherlands; 1987, p. 365–74.

[56] Usuki A, Kojima Y, Kawasumi M, Okada A, Fukushima Y, Kurauchi T, et al. Synthesis of nylon 6-clay hybrid. J Mater Res 1993;8:1179–84. doi:DOI: 10.1557/JMR.1993.1179.

[57] Ke YC, Stroeve PBT-P-LS and SN, editors. Preface, Amsterdam: Elsevier Science; 2005, p. vii–viii. doi:https://doi.org/10.1016/B978-044451570-4/50000-8.

[58] Sun J, Kyu S, Jin S, Lee Y. Journal of Analytical and Applied Pyrolysis Improved flame retardant properties of epoxy resin by fluorinated MMT / MWCNT additives. J Anal Appl Pyrolysis 2010;89:225–32. doi:10.1016/j.jaap.2010.08.003.

[59] Kyu S, Chol B, Sun J, Jin S, Lee Y. Journal of Industrial and Engineering Chemistry Flame retardant epoxy complex produced by addition of montmorillonite and carbon nanotube. J Ind Eng Chem 2010;16:891–5. doi:10.1016/j.jiec.2010.09.014.

[60] Kiliaris P, Papaspyrides CD. Polymer/layered silicate (clay) nanocomposites: An overview of flame retardancy. Prog Polym Sci 2010;35:902–58. doi:https://doi.org/10.1016/j.progpolymsci.2010.03.001.

[61] Zabihi O, Ahmadi M, Khayyam H, Naebe M. Fish DNA-modified clays: Towards highly flame retardant polymer nanocomposite with improved interfacial and mechanical performance. Sci Rep 2016;6:1–17. doi:10.1038/srep38194.

[62] Viet N V., Wang Q, Kuo WS. Effective Young's modulus of carbon nanotube/epoxy composites. Compos Part B Eng 2016;94:160–6. doi:10.1016/j.compositesb.2016.03.060.

[63] Faleh H, Al-Mahaidi R, Shen L. Fabrication and characterization of nano-particles-enhanced epoxy. Compos Part B Eng 2012;43:3076–80. doi:10.1016/j.compositesb.2012.04.055.

[64] Montazeri A, Javadpour J, Khavandi A, Tcharkhtchi A, Mohajeri A. Mechanical

properties of multi-walled carbon nanotube/epoxy composites. Mater Des 2010;31:4202–8. doi:10.1016/j.matdes.2010.04.018.

[65] Allaoui A, Bai S, Cheng HM, Bai JB. Mechanical and electrical properties of a MWNT / epoxy composite. Compos Sci Technol 2002;62:1993–8.

[66] Wang Q, Dai J, Li W, Wei Z, Jiang J. The effects of CNT alignment on electrical conductivity and mechanical properties of SWNT/epoxy nanocomposites. Compos Sci Technol 2008;68:1644–8. doi:10.1016/j.compscitech.2008.02.024.

[67] Wernik JM, Meguid SA. On the mechanical characterization of carbon nanotube reinforced epoxy adhesives. Mater Des 2014;59:19–32. doi:10.1016/j.matdes.2014.02.034.

[68] Cha J, Jun GH, Park JK, Kim JC, Ryu HJ, Hong SH. Improvement of modulus, strength and fracture toughness of CNT/Epoxy nanocomposites through the functionalization of carbon nanotubes. Compos Part B Eng 2017;129:169–79. doi:10.1016/j.compositesb.2017.07.070.

[69] Gojny FH, Wichmann MHG, Köpke U, Fiedler B, Schulte K. Carbon nanotube-reinforced epoxy-composites: Enhanced stiffness and fracture toughness at low nanotube content. Compos Sci Technol 2004;64:2363–71. doi:10.1016/j.compscitech.2004.04.002.

[70] Opelt C V., Becker D, Lepienski CM, Coelho LAF. Reinforcement and toughening mechanisms in polymer nanocomposites - Carbon nanotubes and aluminum oxide. Compos Part B Eng 2015;75:119–26. doi:10.1016/j.compositesb.2015.01.019.

[71] Wang Q, Wen G, Chen J, Su DS. Reinforcing epoxy resin with nitrogen doped carbon nanotube: A potential lightweight structure material. J Mater Sci Technol 2018. doi:10.1016/j.jmst.2018.02.021.

[72] Quan D, Urdániz JL, Ivanković A. Enhancing mode-I and mode-II fracture toughness of epoxy and carbon fibre reinforced epoxy composites using multi-walled carbon nanotubes. Mater Des 2018;143:81–92. doi:10.1016/j.matdes.2018.01.051.

[73] Cha J, Kim J, Ryu S, Hong SH. Comparison to mechanical properties of epoxy nanocomposites reinforced by functionalized carbon nanotubes and graphene nanoplatelets. Compos Part B Eng 2019;162:283–8. doi:10.1016/j.compositesb.2018.11.011.

[74] Zheng N, Sun W, Liu H, Huang Y, Gao J. Effects of carboxylated carbon nanotubes on the phase separation behaviour and fracture-mechanical properties of an epoxy / polysulfone blend. Compos Sci Technol 2018;159:180–8. doi:10.1016/j.compscitech.2018.02.039.

[75] Shokrian MD, Shelesh-nezhad K, Najjar R. Toughening e ff ect of nanocomposite-wall microcapsules on the fracture behavior of epoxy. Polymer (Guildf) 2019;168:104–15. doi:10.1016/j.polymer.2019.02.027.

[76] Ayatollahi MR, Shadlou S, Shokrieh MM. Fracture toughness of epoxy/multi-walled carbon nanotube nano-composites under bending and shear loading conditions. Mater Des 2011;32:2115–24. doi:10.1016/j.matdes.2010.11.034.

[77] Geng Y, Liu MY, Li J, Shi XM, Kim JK. Effects of surfactant treatment on mechanical and electrical properties of CNT/epoxy nanocomposites. Compos Part A Appl Sci Manuf 2008;39:1876–83. doi:10.1016/j.compositesa.2008.09.009.

[78] Subhani T, Latif M, Ahmad I, Rakha SA, Ali N, Khurram AA. Mechanical performance of epoxy matrix hybrid nanocomposites containing carbon nanotubes and nanodiamonds. Mater Des 2015;87:436–44.

doi:10.1016/j.matdes.2015.08.059.

[79] Hernández-Pérez A, Avilés F, May-Pat A, Valadez-González A, Herrera-Franco PJ, Bartolo-Pérez P. Effective properties of multiwalled carbon nanotube/epoxy composites using two different tubes. Compos Sci Technol 2008;68:1422–31. doi:10.1016/j.compscitech.2007.11.001.

[80] Qi B, Zhang QX, Bannister M, Mai YW. Investigation of the mechanical properties of DGEBA-based epoxy resin with nanoclay additives. Compos Struct 2006;75:514–9. doi:10.1016/j.compstruct.2006.04.032.

[81] Wang K, Chen L, Wu J, Toh ML, He C, Yee AF. Epoxy nanocomposites with highly exfoliated clay: Mechanical properties and fracture mechanisms. Macromolecules 2005;38:788–800. doi:10.1021/ma048465n.

[82] Lu HJ, Liang GZ, Ma XY, Zhang BY, Chen XB. Epoxy/clay nanocomposites: Further exfoliation of newly modified clay induced by shearing force of ball milling. Polym Int 2004;53:1545–53. doi:10.1002/pi.1596.

[83] Zaman I, Le QH, Kuan HC, Kawashima N, Luong L, Gerson A, et al. Interface-tuned epoxy/clay nanocomposites. Polymer (Guildf) 2011;52:497–504. doi:10.1016/j.polymer.2010.12.007.

[84] Nguyen TA, Nguyen QT, Bach TP. Mechanical Properties and Flame Retardancy of Epoxy Resin / Nanoclay / Multiwalled Carbon Nanotube Nanocomposites 2019;2019.

[85] Zeng S, Shen M, Xue Y, Zheng Y, Zhang K, Han Y, et al. Controllable mechanical properties of epoxy composites by incorporating self-assembled carbon nanotube – montmorillonite. Compos Part B 2019;164:368–76. doi:10.1016/j.compositesb.2018.12.028.

[86] Thakur AK, Kumar P, Srinivas J. Studies on Effective Elastic Properties of

CNT/Nano-Clay Reinforced Polymer Hybrid Composite. IOP Conf Ser Mater Sci Eng 2016;115. doi:10.1088/1757-899X/115/1/012007.

[87] Wang Z, Xu C, Zhao Y, Zhao D, Wang Z, Li H, et al. Fabrication and mechanical properties of exfoliated clay – CNTs / epoxy nanocomposites 2008;490:481–7. doi:10.1016/j.msea.2008.01.040.

[88] Diamanti K, Soutis C. Structural health monitoring techniques for aircraft composite structures. Prog Aerosp Sci 2010;46:342–52. doi:10.1016/j.paerosci.2010.05.001.

[89] Zhang H, Bilotti E, Peijs T. The use of carbon nanotubes for damage sensing and structural health monitoring in laminated composites: a review. Nanocomposites 2015;1:167–84. doi:10.1080/20550324.2015.1113639.

[90] Gigliotti M, Pannier Y, Gonzalez RA, Lafarie-Frenot MC, Lomov S V. X-ray micro-computed-tomography characterization of cracks induced by thermal cycling in non-crimp 3D orthogonal woven composite materials with porosity. Compos Part A Appl Sci Manuf 2018;112:100–10. doi:10.1016/j.compositesa.2018.05.020.

[91] Sadeghi MZ, Nienheysen P, Arslan S, Dafnis A, Silva Marció B, Schmitt RH, et al. Damage detection by double-sided ultrasonic assessment in low-velocity impacted CFRP plates. Compos Struct 2019;208:646–55. doi:10.1016/j.compstruct.2018.10.025.

[92] Machado MA, Antin K-N, Rosado LS, Vilaça P, Santos TG. Contactless high-speed eddy current inspection of unidirectional carbon fiber reinforced polymer. Compos Part B Eng 2018;168:226–35. doi:10.1016/J.COMPOSITESB.2018.12.021.

[93] Dziendzikowski M, Kurnyta A, Dragan K, Klysz S, Leski A. In situ Barely

Visible Impact Damage detection and localization for composite structures using surface mounted and embedded PZT transducers: A comparative study. Mech Syst Signal Process 2016;78:91–106. doi:10.1016/j.ymssp.2015.09.021.

[94] Dharap P, Li Z, Nagarajaiah S, Barrera E V. Nanotube film based on single-wall carbon nanotubes for strain sensing. Nanotechnology 2004;15:379–82. doi:10.1088/0957-4484/15/3/026.

[95] Bennett G. Probability Inequalities for the Sum of Independent Random Variables. J Am Stat Assoc 1962;57:33–45. doi:10.1016/j.sna.2017.10.047.

[96] Shohag MAS, Okoli OI. Nonparasitic behavior of embedded triboluminescent sensor in multifunctional composites. Compos Part A Appl Sci Manuf 2019;116:114–25. doi:10.1016/j.compositesa.2018.10.029.

[97] Kang I, Schulz MJ, Kim JH, Shanov V, Shi D. A carbon nanotube strain sensor for structural health monitoring. Smart Mater Struct 2006;15:737–48. doi:10.1088/0964-1726/15/3/009.

[98] Burton AR, Lynch JP, Kurata M, Law KH. Fully integrated carbon nanotube composite thin film strain sensors on flexible substrates for structural health monitoring. Smart Mater Struct 2017;26. doi:10.1088/1361-665X/aa8105.

[99] Li A, Bogdanovich AE, Bradford PD. Aligned carbon nanotube sheet piezoresistive strain sensors. Smart Mater Struct 2015;24. doi:10.1088/0964-1726/24/9/095004.

[100] García-Macías E, Rodríguez-Tembleque L, Sáez A, Ubertini F. Crack detection and localization in RC beams through smart MWCNT/epoxy strip-like strain sensors. Smart Mater Struct 2018;27. doi:10.1088/1361-665X/aae668.

[101] Yang G, Liu L, Wu Z. Improved strain sensing capability of nano-carbon free-standing buckypapers based strain gauges. Smart Mater Struct 2019;28:65009.

doi:10.1088/1361-665x/ab147e.

[102] Aly K, Bradford PD. Real-time impact damage sensing and localization in composites through embedded aligned carbon nanotube sheets. Compos Part B Eng 2019;162:522–31. doi:10.1016/j.compositesb.2018.12.104.

[103] Esmaeili A, Sbarufatti C, Ma D, Manes A, Jiménez-Suárez A, Ureña A, et al. Strain and crack growth sensing capability of SWCNT reinforced epoxy in tensile and mode I fracture tests. Compos Sci Technol 2019;186:107918. doi:10.1016/J.COMPSCITECH.2019.107918.

[104] Vertuccio L, Guadagno L, Spinelli G, Lamberti P, Tucci V, Russo S. Piezoresistive properties of resin reinforced with carbon nanotubes for health-monitoring of aircraft primary structures. Compos Part B Eng 2016;107:192–202. doi:10.1016/j.compositesb.2016.09.061.

[105] Vertuccio L, Guadagno L, Spinelli G, Lamberti P, Zarrelli M, Russo S, et al. Smart coatings of epoxy based CNTs designed to meet practical expectations in aeronautics. Compos Part B Eng 2018;147:42–6. doi:10.1016/j.compositesb.2018.04.027.

[106] Sánchez-Romate XF, Moriche R, Jiménez-Suárez A, Sánchez M, Prolongo SG, Güemes A, et al. Highly sensitive strain gauges with carbon nanotubes: From bulk nanocomposites to multifunctional coatings for damage sensing. Appl Surf Sci 2017;424:213–21. doi:10.1016/j.apsusc.2017.03.234.

[107] Rams J, Sánchez M, Ureña A, Jiménez-Suárez A, Campo M, Gemes A. Use of carbon nanotubes for strain and damage sensing of epoxy-based composites. Int J Smart Nano Mater 2012;3:152–61. doi:10.1080/19475411.2011.651508.

[108] Wang Y, Wang Y, Wan B, Han B, Cai G, Li Z. Properties and mechanisms of self-sensing carbon nano fi bers / epoxy composites for structural health

monitoring. Compos Struct 2018;200:669–78. doi:10.1016/j.compstruct.2018.05.151.

[109] Khalid HR, Nam IW, Choudhry I, Zheng L, Lee HK. Piezoresistive characteristics of CNT fiber-incorporated GFRP composites prepared with diversified fabrication schemes. Compos Struct 2018;203:835–43. doi:10.1016/j.compstruct.2018.08.003.

[110] Wang G, Wang Y, Zhang P, Zhai Y, Luo Y, Li L, et al. Structure dependent properties of carbon nanomaterials enabled fiber sensors for in situ monitoring of composites. Compos Struct 2018;195:36–44. doi:10.1016/j.compstruct.2018.04.052.

[111] Spinelli G, Lamberti P, Tucci V, Vertuccio L, Guadagno L. Experimental and theoretical study on piezoresistive properties of a structural resin reinforced with carbon nanotubes for strain sensing and damage monitoring. Compos Part B Eng 2018;145:90–9. doi:10.1016/j.compositesb.2018.03.025.

[112] Sanli A, Benchirouf A, Müller C, Kanoun O. Piezoresistive performance characterization of strain sensitive multi-walled carbon nanotube-epoxy nanocomposites. Sensors Actuators, A Phys 2017;254:61–8. doi:10.1016/j.sna.2016.12.011.

[113] Wang X, Zhang L, Zhao C, Ma K, Du K, Bai Y, et al. In situ monitoring the manufacturing process of polymer composites with highly flexible and sensitive GNP/ MWCNT film sensors. Sensors Actuators A Phys 2018;285:127–33. doi:10.1016/j.sna.2018.11.016.

[114] Tanner JL, Mousadakos D, Broutas P, Chatzandroulis S, Raptis YS, Tsoukalas D. Nanoparticle strain sensor. Procedia Eng 2011;25:635–8. doi:10.1016/j.proeng.2011.12.158.

[115] Knite M, Teteris V, Kiploka A, Kaupuzs J. Polyisoprene-carbon black nanocomposites as tensile strain and pressure sensor materials. Sensors Actuators, A Phys 2004;110:142–9. doi:10.1016/j.sna.2003.08.006.

[116] Han H, Martinez V, Forró C, Polesel-Maris J, Vörös J, Zambelli T. Integration of silver nanowires into SU-8 hollow cantilevers for piezoresistive-based sensing. Sensors Actuators, A Phys 2020;301. doi:10.1016/j.sna.2019.111748.

[117] Stauffer D, Bunde A. Introduction to Percolation Theory . Phys Today 1987;40:122–3. doi:10.1063/1.2820231.

[118] Mansor MR, Fadzullah SHSM, Masripan NAB, Omar G, Akop MZ. Comparison Between Functionalized Graphene and Carbon Nanotubes. Elsevier Inc.; 2019. doi:10.1016/b978-0-12-814548-7.00009-x.

[119] Wichmann MHG, Buschhorn ST, Gehrmann J, Schulte K. Piezoresistive response of epoxy composites with carbon nanoparticles under tensile load. Phys Rev B - Condens Matter Mater Phys 2009;80:1–8. doi:10.1103/PhysRevB.80.245437.

[120] Oliva-Avilés AI, Avilés F, Sosa V. Electrical and piezoresistive properties of multi-walled carbon nanotube/polymer composite films aligned by an electric field. Carbon N Y 2011;49:2989–97. doi:10.1016/j.carbon.2011.03.017.

[121] Tanabi H, Erdal M. Effect of CNTs dispersion on electrical, mechanical and strain sensing properties of CNT/epoxy nanocomposites. Results Phys 2019;12:486–503. doi:10.1016/j.rinp.2018.11.081.

[122] Aly K, Li A, Bradford PD. Strain sensing in composites using aligned carbon nanotube sheets embedded in the interlaminar region. Compos Part A Appl Sci Manuf 2016;90:536–48. doi:10.1016/j.compositesa.2016.08.003.

[123] Hu N, Karube Y, Arai M, Watanabe T, Yan C. Investigation on sensitivity of a

polymer / carbon nanotube composite strain sensor. Carbon N Y 2009;48:680–7. doi:10.1016/j.carbon.2009.10.012.

[124] Gong S, Zhu ZH, Meguid SA. Carbon nanotube agglomeration effect on piezoresistivity of polymer nanocomposites. Polymer (Guildf) 2014;55:5488–99. doi:10.1016/j.polymer.2014.08.054.

[125] Ayatollahi MR, Shokrieh MM, Shadlou S, Kefayati AR, Chitsazzadeh M. Mechanical and Electrical Properties of Epoxy/ Multi-walled Carbon Nanotube/Nanoclay Nanocomposites. Polym J 2011;c:835–43.

[126] Liu L, Grunlan JC. Clay assisted dispersion of carbon nanotubes in conductive epoxy nanocomposites. Adv Funct Mater 2007;17:2343–8. doi:10.1002/adfm.200600785.

[127] Lu KL, Lago RM, Chen YK, Green MLH, Harris PJF, Tsang SC. Mechanical damage of carbon nanotubes by ultrasound. Carbon N Y 1996;34:814–6.

[128] Montazeri A, Chitsazzadeh M. Effect of sonication parameters on the mechanical properties of multi-walled carbon nanotube/epoxy composites. Mater Des 2014;56:500–8. doi:10.1016/j.matdes.2013.11.013.

[129] Ma PC, Siddiqui NA, Marom G, Kim JK. Dispersion and functionalization of carbon nanotubes for polymer-based nanocomposites: A review. Compos Part A Appl Sci Manuf 2010;41:1345–67. doi:10.1016/j.compositesa.2010.07.003.

[130] Li YB, Wei BQ, Liang J, Yu Q, Wu DH. Transformation of carbon nanotubes to nanoparticles by ball milling process. Carbon N Y 1999;37:493–7. doi:10.1016/S0008-6223(98)00218-8.

[131] Balakrishnan A, Saha MC. Tensile fracture and thermal conductivity characterization of toughened epoxy/CNT nanocomposites. Mater Sci Eng A 2011;528:906–13. doi:10.1016/j.msea.2010.09.064.

[132] Wang Q, Wen G, Chen J, Su DS. Reinforcing epoxy resin with nitrogen doped carbon nanotube: A potential lightweight structure material. J Mater Sci Technol 2018;34:2205–11. doi:10.1016/j.jmst.2018.02.021.

[133] Quan D, Urdániz JL, Ivanković A. Enhancing mode-I and mode-II fracture toughness of epoxy and carbon fibre reinforced epoxy composites using multi-walled carbon nanotubes. Mater Des 2018;143:81–92. doi:10.1016/j.matdes.2018.01.051.

[134] Mehdikhani M, Gorbatikh L, Verpoest I, Lomov S V. Voids in fiber-reinforced polymer composites: A review on their formation, characteristics, and effects on mechanical performance. J Compos Mater 2019;53:1579–669. doi:10.1177/0021998318772152.

[135] Ashir M, Nocke A, Bulavinov A, Pinchuk R, Cherif C. Influence of defined amount of voids on the mechanical properties of carbon fiber-reinforced plastics. Polym Compos 2019;40:E1049–56. doi:10.1002/pc.24820.

[136] Li Y, Li Q, Ma H. The voids formation mechanisms and their effects on the mechanical properties of flax fiber reinforced epoxy composites. Compos Part A Appl Sci Manuf 2015;72:40–8. doi:10.1016/j.compositesa.2015.01.029.

[137] Hashemi SA, Mousavi SM. Effect of bubble based degradation on the physical properties of Single Wall Carbon Nanotube/Epoxy Resin composite and new approach in bubbles reduction. Compos Part A Appl Sci Manuf 2016;90:457–69. doi:10.1016/j.compositesa.2016.08.015.

[138] Liu L, Zhang BM, Wang DF, Wu ZJ. Effects of cure cycles on void content and mechanical properties of composite laminates. Compos Struct 2006;73:303–9. doi:10.1016/j.compstruct.2005.02.001.

[139] Vietri U, Guadagno L, Raimondo M, Vertuccio L, Lafdi K. Nanofilled epoxy

adhesive for structural aeronautic materials. Compos Part B Eng 2014;61:73–83. doi:https://doi.org/10.1016/j.compositesb.2014.01.032.

[140] Luo S, Obitayo W, Liu T. SWCNT-thin-film-enabled fiber sensors for lifelong structural health monitoring of polymeric composites - From manufacturing to utilization to failure. Carbon N Y 2014;76:321–9. doi:10.1016/j.carbon.2014.04.083.

[141] Zemen Y, Schulz SC, Trommler H, Buschhorn ST, Bauhofer W, Schulte K. Comparison of new conductive adhesives based on silver and carbon nanotubes for solar cells interconnection. Sol Energy Mater Sol Cells 2013;109:155–9. doi:10.1016/j.solmat.2012.10.020.

[142] Wang L, Loh KJ. Wearable carbon nanotube-based fabric sensors for monitoring human physiological performance. Smart Mater Struct 2017;26. doi:10.1088/1361-665X/aa6849.

[143] Kausar A, Rafique I, Muhammad B. Review of Applications of Polymer/Carbon Nanotubes and Epoxy/CNT Composites. Polym - Plast Technol Eng 2016;55:1167–91. doi:10.1080/03602559.2016.1163588.

[144] Jiménez-Suárez A, Campo M, Gaztelumendi I, Markaide N, Sánchez M, Ureña A. The influence of mechanical dispersion of MWCNT in epoxy matrix by calendering method: Batch method versus time controlled. Compos Part B Eng 2013;48:88–94. doi:10.1016/j.compositesb.2012.12.011.

[145] Nag-Chowdhury S, Bellegou H, Pillin I, Castro M, Longrais P, Feller JF. Non-intrusive health monitoring of infused composites with embedded carbon quantum piezo-resistive sensors. Compos Sci Technol 2016;123:286–94. doi:10.1016/j.compscitech.2016.01.004.

[146] Quaresimin M, Schulte K, Zappalorto M, Chandrasekaran S. Toughening

mechanisms in polymer nanocomposites: From experiments to modelling. Compos Sci Technol 2016;123:187–204. doi:10.1016/j.compscitech.2015.11.027.

[147] Alian AR, Meguid SA. Multiscale modeling of the coupled electromechanical behavior of multifunctional nanocomposites. Compos Struct 2019;208:826–35. doi:10.1016/j.compstruct.2018.10.066.

[148] Sensors S. Flexible Carbon Nanotube Films for High Performance Strain Sensors 2014:10042–71. doi:10.3390/s140610042.

[149] Wichmann MHG, Buschhorn ST, Lars B. Direction sensitive bending sensors based on multi-wall carbon nanotube / epoxy nanocomposites 2008. doi:10.1088/0957-4484/19/47/475503.

[150] Bisht A, Dasgupta K, Lahiri D. Effect of graphene and CNT reinforcement on mechanical and thermomechanical behavior of epoxy—A comparative study. J Appl Polym Sci 2018;135:1–11. doi:10.1002/app.46101.

[151] Kim BC, Park SW, Lee DG. Fracture toughness of the nano-particle reinforced epoxy composite. Compos Struct 2008;86:69–77. doi:10.1016/j.compstruct.2008.03.005.

APPENDIX: LIST OF PUBLICATIONS

Published

- Esmaeili A, Sbarufatti C, Ma D, Manes A, Jiménez-Suárez A, Ureña A, et al. Strain and crack growth sensing capability of SWCNT reinforced epoxy in tensile and mode I fracture tests. Compos Sci Technol 2019;186:107918. doi:10.1016/J.COMPSCITECH.2019.107918. https://doi.org/10.1016/j.compscitech.2019.107918.
- Ma D, Esmaeili A, Manes A, Sbarufatti C, Jiménez-Suárez A, Giglio M, et al. Numerical study of static and dynamic fracture behaviours of neat epoxy resin. Mech Mater 2020;140:103214. doi:10.1016/j.mechmat.2019.103214. https://doi.org/10.1016/j.mechmat.2019.103214.
- Esmaeili A, Sbarufatti C, Hamouda AMS. Characteristics of Intermetallic Compounds in Dissimilar Friction Stir Welding: A Review. Metallogr Microstruct Anal 2019;8:445–61. doi:10.1007/s13632-019-00557-w. https://doi.org/10.1007/s13632-019-00557-w.
- Esmaeili A, Urena A, Hamouda AM. Piezoresistive characterization of epoxy based nanocomposites loaded with SWCNTs-DWCNTs in tensile and fracture tests 2020:1–12. doi:10.1002/pc.25558. https://doi.org/10.1002/pc.25558.
- Esmaeili A, Hamouda AMS. Evaluation of Thermal History and Defect in Friction Stir Processing of As-Cast Magnesium AZ91. Nano Eng. Mater. Technol. II, vol. 916, Trans Tech Publications; 2018, p. 239–43.

doi:10.4028/www.scientific.net/MSF.916.239.

https://doi.org/10.4028/www.scientific.net/MSF.916.239.

- Esmaeili A, Hamouda AMS. The role of intermetallic compounds and composite-like structure development during dissimilar friction stir welding of aluminum to brass on metallurgical and flexural characteristics. Proc 2016 7th Int Conf Mech Aerosp Eng ICMAE 2016 2016:64–7. doi:10.1109/ICMAE.2016.7549509. 10.1109/ICMAE.2016.7549509.

In production

- Esmaeili A, Sbarufatti C, Hamouda AMS. Investigation of Mechanical Properties of MWCNTs Doped Epoxy Nanocomposites in Tensile , Fracture and Impact Tests 2020;990:239–43. Materials Science Forum ISSN: 1662-9752, Vol. 990, pp 239-243. Kyoto, Japan. October 2019.(Conference).
- Esmaeili A, Sbarufatti C, Hamouda AMS.Hybrid effect of MWCNTs and nanoclay in tailoring tensile strength and fracture toughness of the epoxy based nanocomposites. Submitted into “Composites B”. The 10th International Conference on Key Engineering Materials. Madrid, spain.

Revised

- A. Esmaeili, C. Sbarufatti, A. Jiménez-Suárez, A. Ureña, A.M.S. Hamouda. A comparative study of the tensile and impact strengths of the SWCNTs-OH and DWCNTs doped epoxy nanocomposites. Submitted into “Polymer research”.

Under review

- A. Esmaeili, C. Sbarufatti, A. Jiménez-Suárez, A.M.S. Hamouda, L.Rovatti, A. Ureña. Synergistic effects of double-walled carbon nanotubes and montmorillonite (Shelsite 30B) platelets in enhancement of tensile strength, fracture toughness, electrical conductivity, and piezoresistive-sensitivity of epoxy based nanocomposites. Submitted into “Composites Sceince and technology ”.
- A. Esmaeili, D, MA, C. Sbarufatti, A.Manes, T. Oggioni A. Jiménez-Suárez, A. Ureña, A.M.S. Hamouda. An experimental and numerical investigation of highly tough epoxy-based nanocomposite by addition of MWCNTs: Tensile and mode I fracture test Submitted into “Composites Structures”.
- A. Esmaeili, C. Sbarufatti, A. Jiménez-Suárez, A.M.S. Hamouda, L.Rovatti, A. Ureña. Nanoclay platelets addition as an auxiliary dispersing agent in tailoring electrical, mechanical, and piezoresisitve properties of SWCNTs doped epoxy nanocomposites. Submitted into “Composites B”.